
**Pacific Northwest
National Laboratory**

Operated by Battelle for the
U.S. Department of Energy

Characterization of Vadose Zone Sediment: Slant Borehole SX-108 in the S-SX Waste Management Area

R. J. Serne	R. E. Clayton	I. V. Kutnyakov
G. V. Last	V. L. LeGore	T. C. Wilson
H. T. Schaefer	M. J. O'Hara	K. B. Wagnon
D. C. Lanigan	C. F. Brown	B. A. Williams
C. W. Lindenmeier	R. D. Orr	D. S. Burke
C. C. Ainsworth		

February 2002

Prepared for CH2M HILL Hanford Group, Inc., and
the U.S. Department of Energy
under Contract DE-AC06-76RL01830



DISCLAIMER

This report was prepared as an account of work sponsored by an agency of the United States Government. Neither the United States Government nor any agency thereof, nor Battelle Memorial Institute, nor any of their employees, makes **any warranty, express or implied, or assumes any legal liability or responsibility for the accuracy, completeness, or usefulness of any information, apparatus, product, or process disclosed, or represents that its use would not infringe privately owned rights.** Reference herein to any specific commercial product, process, or service by trade name, trademark, manufacturer, or otherwise does not necessarily constitute or imply its endorsement, recommendation, or favoring by the United States Government or any agency thereof, or Battelle Memorial Institute. The views and opinions of authors expressed herein do not necessarily state or reflect those of the United States Government or any agency thereof.

PACIFIC NORTHWEST NATIONAL LABORATORY

operated by

BATTELLE

for the

UNITED STATES DEPARTMENT OF ENERGY

under Contract DE-AC06-76RL01830



This document was printed on recycled paper.

(8/00)

**Characterization of Vadose Zone
Sediment: Slant Borehole SX-108
in the S-SX Waste Management Area**

R. J. Serne	R. E. Clayton	I. V. Kutnyakov
G. V. Last	V. L. LeGore	T. C. Wilson
H. T. Schaef	M. J. O'Hara	K. B. Wagnon
D. C. Lanigan	C. F. Brown	B. A. Williams
C. W. Lindenmeier	R. D. Orr	D. S. Burke
C. C. Ainsworth		

February 2002

Prepared for CH2M HILL Hanford Group, Inc., and
the U.S. Department of Energy
under Contract DE-AC06-76RL01830

Pacific Northwest National Laboratory
Richland, Washington 99352

Executive Summary

The overall goal of the of the Tank Farm Vadose Zone Project, led by CH2M HILL Hanford Group, Inc., is to define risks from past and future single-shell tank farm activities. To meet this goal, CH2M HILL Hanford Group, Inc., asked scientists from Pacific Northwest National Laboratory to perform detailed analyses on vadose zone sediment from within the S-SX Waste Management Area. This report is the fourth in a series of four reports to present the results of these analyses. Specifically, this report contains all the geologic, geochemical, and selected physical characterization data collected on vadose zone sediment recovered from a slant borehole installed beneath tank SX-108 (or simply SX-108 slant borehole).

This report also presents our interpretation of the data in the context of the sediment lithologies, the vertical extent of contamination, the migration potential of the contaminants, and the correspondence of the contaminant distribution to groundwater. The information presented in this report supports the S-SX field investigation report to be prepared by CH2M HILL Hanford Group, Inc.^(a)

Overall, our analyses identified common ion exchange and heterogeneous (solid phase-liquid solute) redox reactions as two mechanisms that influence the distribution of contaminants within that portion of the vadose zone affected by tank liquor. We did not observe significant indications of caustic alteration of the sediment mineralogy or porosity, but we did observe slightly elevated pH values and faint indications of caustic reactions with the sediment within 9.1 meters (30 feet) of the tank bottom. X-ray diffraction measurements indicate no evidence of mineral alteration or precipitation resulting from the interaction of the tank liquor with the sediment. However, scans of some of the samples by scanning electron microscopy suggest that there is evidence of caustic attack on the sample obtained just under the SX-108 tank shadow and ~3.7 meters (~12 feet) deeper than the tank bottom.^(a)

Our analyses found it unlikely that the source of the contamination in the groundwater under SX Tank Farm is the pore fluids in the vadose zone directly beneath tank SX-108. A more plausible source of the contamination reaching the groundwater is the fluid originally lost from tank SX-115 (Serne et al. 2002b). Pore fluids proximate to the SX-115 tank show a technetium-99 to nitrate ratio closer to that present in the groundwater than the leaked fluid from tank SX-108. However, the ratios for the porewaters in the slant borehole are not constant, possibly caused by irregular mixing between the plumes of two separate leak events and/or dynamic convection currents driven by the time varying head load under the tank. Temperature measurements at the wall of the slant borehole casing, previous in-tank temperature measurements, and thermal modeling^(a) suggest that complicated convection cells of water vapor and liquid water were active under tank SX-108.

The near horizontally bedded, southwesterly dipping sediment likely caused anisotropic flow of the migrating contaminants. The vertical distribution of cesium-137 at both the slant borehole under tank

(a) *Draft Field Investigation Report for Waste Management Area S-SX*. RPP-7884, Draft, Volume 2, Appendix D, CH2M HILL Hanford Group, Inc., Richland, Washington.

SX-108 and at the adjacent 41-09-39 borehole (Serne et al. 2002a) suggest that much of the tank fluid that leaked from surrounding tanks traveled to the southwest within the coarse-grained Hanford formation H1 unit. At the slant borehole under tank SX-108, there is also a large mass of cesium-137 in the fine sand of the Hanford formation H2 unit that lies below the H1 unit. At the slant borehole, there is a fine-grained lens within the H2 unit at 32.2 meters (105.6 feet) below ground surface (bgs) that was not affected much by the hypersaline tank liquors. The migrating plume of cesium-137 seems to have bypassed this sample area under the tank, making it difficult to fully interpret the vertical distribution of contaminants under SX-108. Compared to the cesium-137 distributions, there is very little strontium-90 in the sediment suggesting that strontium-90 is not mobile in the redox fluid that leaked from the SX tanks.

The main controls on sediment pH do not appear to be sensitive to the distance tank liquor traveled, but instead may be more sensitive to time of reaction. At the SX-108 slant borehole, the H1a sediment shows high pH and elevated electrical conductivity. However, the pH values in the sediment below tank SX-108 are not nearly as high as would be expected if tank liquor completely saturated the sediment. The closest sample obtained below tank SX-108 was ~3.7 meters (~12 feet) below the tank bottom. Therefore, it would appear that any zone of highly altered pH occurs in a zone that is less than 3.7 meters (12 feet) thick. Beneath this depth, the pH is slightly elevated down to at least 25.6 vertical meters (84 vertical feet) bgs. At 26.8 meters (88 feet) bgs to the final depth of the borehole, the slant borehole sediment pH is normal.

The electrical conductivity results suggest that the tank leak fluid dominates the porewater at the slant borehole to a depth of 39.3 meters (129 feet) bgs, about 1.5 meters (5 feet) into the Plio-Pleistocene mud (PPlz) sediment. The electrical conductivity of the two deeper samples does not drop to natural background levels, but the electrical conductivity is significantly lower than all the shallow samples in the profile. Thus, the leading edge of the contaminant plume is below the total depth sampled, but the bulk of the salt is still above 39.3 meters (129 feet) bgs. Based on the nitrate profile at borehole 41-09-39, which does show the whole extent of the plume, we estimate that the leading edge of the plume beneath tank SX-108 may have stopped at the contact of the PPlz and Plio-Pleistocene carbonate (PPlc) units near 45.7 meters (150 feet) bgs. This estimate does not consider any complications from the convection cells that may have transported water vapor and recondensed water under tank SX-108.

The technetium-99 data show that there are significant concentrations of technetium-99 between the depths of 25.9 to 42.1 meters (85 to 138 feet) bgs. The leading edge of the technetium-99 plume appears to reach 42.1 meters (138 feet) bgs, though even the deepest sample at 44 meters (144.5 feet) bgs is slightly elevated in technetium-99.

Porewaters from the cores in the three Hanford formation units (H1a, H1, and H2) were dominated by sodium and nitrate. At the slant borehole, the most concentrated porewater was in the H2 unit and was essentially 16 to 17 M sodium nitrate with 1 M concentration of calcium, 0.5 M chromate, and several tenths molar sulfate, chloride, potassium, and magnesium. This extremely hypersaline composition is about three times higher in all constituents as found in the H2 porewater at borehole 41-09-39 but the increase is caused more by sediment dessication than different leak chemical compositions. The species present in the contaminated porewaters at both boreholes are remarkably similar.

The water leachable chromium profiles suggest that chromium is not as mobile as technetium-99. This is true also at the other boreholes within the SX Tank Farm. Researchers^(a) identified a caustic catalyzed reaction where ferrous-bearing minerals are dissolved, and the iron(II) released to the pore fluids reduces chromium(VI) to chromium(III) that coprecipitates to form ferric(chromic) hydroxides.

The water extractable cations suggest that an ion-exchange process dominates the porewater/sediment interactions in the slant borehole zone where tank fluid passed by or currently exists. The leading edge of the tank leak plume is enriched in alkaline earth cations that were displaced from the native sediment exchange sites. There appears to be two ion exchange fronts present in the slant borehole profile but the fact that the hole is slanted and the presence of the bypassed sediment at about 32 meters (105 feet) bgs complicates the premise that these two ion exchange fronts in fact represent two separate plumes caused by two different leaks.

We conclude that in the future, if natural recharge remains the driving force, that cesium-137 will be adequately retarded once it is completely separated from the high sodium porewater plume. We found that the in situ desorption K_d for cesium-137 is highly variable from a low of 2.3 to a high of 307 mL/g. In the sediment where the estimated porewater composition was >10 M sodium nitrate (between 24.4 and 29.6 meters [80 and 97 feet] bgs), the in situ desorption K_d varied between 2 and 10 mL/g. Much of the variability can be correlated to the major cation composition of the porewater, especially the sodium concentration. Above 24.4 meters (80 feet) bgs and below 29.6 meters (97 feet) bgs, cesium-137 in situ desorption K_d is larger because the pore fluids do not contain high sodium concentrations that compete for adsorption sites.

Based on comparing the depth of penetration of various contaminants and comparing the percentages that are water leachable, we can state that chromium and molybdenum migrate faster than cesium-137 but slower than technetium-99, selenium, and nitrate. The technetium-99 desorption data are consistently near zero, meaning that the technetium-99 is not interacting with the sediment. Despite the findings that approximately one-third of the chromium appears to get reduced via caustic dissolution of ferrous containing minerals, the chromium desorption K_d values are still <1 mL/g in the entire zone where the bulk of the tank fluid currently resides.^(a)

(a) *Draft Field Investigation Report for Waste Management Area S-SX*. RPP-7884, Draft, Volume 2, Appendix D, CH2M HILL Hanford Group, Inc., Richland, Washington.

Acknowledgments

This work was conducted as part of the Tank Farm Vadose Zone Project led by CH2M HILL Hanford Group, Inc., in support of the U.S. Department of Energy's Office of River Protection. The authors wish to thank Anthony J. Knepp, Fredrick M. Mann, David A. Myers, Thomas E. Jones, and Harold A. Sydnor with CH2M HILL Hanford Group, Inc., and Marc I. Wood with Fluor Hanford for their support of this work. We would also like to express our gratitude to Robert Yasek with DOE's Office of River Protection.

We would especially like to thank Kent D. Reynolds (Duratek Federal Services, Inc.) for his efforts in design and construction of the sampler breakdown table and core extruder, and Kevin A. Lindsey (Kennedy Jenkes Consultants, Inc.) for his insights on the geologic nature of the materials penetrated by this borehole.

Finally, we would like to thank Bruce J. Bjornstad and Duane G. Horton for their technical review of this document, Launa F. Morasch, Janet Tarantino, Barbara Wilson, and Jo Lynn Draper for editorial and document production support, and Kathy Neiderhiser, Rose Urbina, and Rose M. Watt for publication design support.

Acronyms and Abbreviations

ASA	American Society of Agronomy
ASTM	American Society for Testing and Materials
bgs	below ground surface
IC	ion chromatography
ICP	inductively coupled plasma
ICP-MS	inductively coupled plasma mass spectrometer
ICP-OES	inductively coupled plasma – optical emission spectroscopy
PNNL	Pacific Northwest National Laboratory
PPlc	Plio-Pleistocene carbonate
PPlz	Plio-Pleistocene mud
RCRA	Resource Conservation and Recovery Act
REDOX	Reduction Oxidation Plant
SEM	scanning electron microscope
TEM	transmission electron microscopy
UFA	unsaturated flow apparatus

Contents

Executive Summary	iii
Acknowledgments.....	vii
Acronyms and Abbreviations	ix
1.0 Introduction	1.1
2.0 Geology	2.1
2.1 Geologic Setting of the SX Tank Farm.....	2.1
2.2 Drilling and Sampling of the SX-108 Slant Borehole.....	2.7
2.3 Geophysical Logging	2.9
2.4 Sample Breakdown and Recovery	2.12
2.5 Subsampling and Geologic Description.....	2.13
2.6 Geology of the SX-108 Slant Borehole.....	2.14
2.6.1 Backfill.....	2.15
2.6.2 Hanford Formation.....	2.15
2.6.3 Plio-Pleistocene Unit.....	2.20
3.0 Geochemical Method and Materials.....	3.1
3.1 Sample Inventory	3.1
3.2 Tiered Approach.....	3.1
3.3 Materials and Methods	3.2
3.3.1 Moisture Content.....	3.2
3.3.2 1:1 Sediment-to-Water Extract.....	3.2
3.3.3 Pore Water Composition	3.4
3.3.4 Radioanalytical Analysis.....	3.4
3.3.5 Carbon Content of Sediment.....	3.5
3.3.6 8 M Nitric Acid Extract.....	3.6
3.3.7 Elemental Analysis.....	3.6
3.3.8 Particle Size Distribution	3.6
3.3.9 Particle Density	3.7
3.3.10 Mineralogy	3.7
4.0 Results and Discussion	4.1
4.1 Moisture Content.....	4.1
4.2 1:1 Sediment-to-Water Extracts	4.1
4.2.1 pH and Electrical Conductivity.....	4.3
4.2.2 Water Extract and Porewater Compositions.....	4.6

4.2.3	Radionuclide Content in Vadose Zone Sediment.....	4.23
4.2.4	Total Carbon, Calcium Carbonate, and Organic Carbon Content of Vadose Zone Sediment	4.32
4.2.5	8 M Nitric Acid Extractable Amounts of Selected Elements.....	4.33
4.2.6	Sediment Total Oxide Composition.....	4.38
4.2.7	Particle Size Measurements on Vadose Zone Sediment	4.43
4.2.8	Particle Density of Bulk Sediment.....	4.46
4.2.9	Mineralogy	4.47
5.0	Contaminant Migration Potential and Comparison of Contaminant Contents at the SX-108 Slant Borehole to Borehole 41-09-39.....	5.1
5.1	Quantification of Desorption Potential for Major Contaminants in Slant Borehole	5.1
5.2	Comparison of Porewater Composition in Boreholes 41-09-39 and 299-W23-19	5.4
6.0	Summary and Conclusions	6.1
6.1	Conceptual Model of the Geology at the Slant Borehole.....	6.1
6.2	Vertical Extent of Contamination.....	6.3
6.3	Controlling Geochemical Processes Based on Characterization.....	6.7
6.4	Estimates of Sorption-Desorption Values	6.11
6.5	Other Characterization Observations	6.14
7.0	References	7.1
	Appendix A – Core Descriptions.....	A.1
	Appendix B – Additional Core Photos.....	B.1
	Appendix C – Comparison of Water Extractable and 8 M Nitric Acid Extractable Concentrations	C.1
	Appendix D – X-Ray Diffraction Patterns for Selected Core Samples	D.1

Figures

2.1 Generalized, Composite Stratigraphy for the Late Cenozoic Sediment Overlying the Columbia River Basalt Group on the Hanford Site	2.2
2.2 SX Tank Farm Under Construction in 1953	2.3
2.3 The SX Tanks Under Construction and the Native Hanford Formation Sediment	2.3
2.4 Location of SX-108 Slant Borehole, Other Pertinent Wells, and Cross Sections	2.5
2.5 Geologic Cross Section A-A'	2.6
2.6 Borehole Location	2.7
2.7 Schematic of Shielded Split-Spoon Sampler	2.8
2.8 Location of Split-Spoon Samples	2.8
2.9 Detailed Lithology and Analytical Values of Split-Spoon Samples from the SX-108 Slant Borehole	2.10
2.10 Shielded Split-Spoon Sampler on Breakdown Table Inside Fume Hood	2.13
2.11 Sediment Classification Scheme and Grain Size Nomenclature	2.14
2.12 Disaggregated Core from the Hanford Formation H1a Unit	2.15
2.13 Disaggregated Core (Sample 3A) from the Hanford Formation H1 Unit	2.17
2.14 Disaggregated Core (Sample 4A) from the Hanford Formation H1 Unit	2.17
2.15 Sample 7A from the Upper Portion of the Lower Fine Sand and Mud Sequence of the Hanford Formation H2 Unit	2.19
2.16 Samples 13A and 14A from the Lower Portion of the Hanford Formation H2 Unit	2.20
2.17 Disaggregated Core Sample S0070-17A from the Upper Plio-Pleistocene Mud Unit	2.21
4.1 pH and Electrical Conductivity for Calculated and Actual Porewaters for Slant Borehole Sediment	4.4
4.2a Anions Calculated and Actual Porewaters from the Slant Borehole under SX-108	4.8
4.2b 1:1 Sediment-to-Water Extract Inorganic Carbon and Alkalinity Contents for the Slant Borehole Sediment under SX-108	4.9
4.3 Cations Calculated and Actual Porewaters for Slant Borehole Sediment	4.12
4.4 Pore Fluid Concentrations of Aluminum, Iron, Silicon, and Manganese, and Actual Porewaters for Slant Borehole Sediment	4.16
4.5a Trace Metals Pore Fluid and Actual Porewaters for Slant Borehole Sediment	4.19
4.5b Silver, Cadmium, and Lead Concentrations in Pore Fluid and Actual Porewaters for Slant Borehole Sediment	4.20
4.6 Cesium-137 in Vadose Sediment Plotted with Linear and Log Scale	4.27
4.7 Concentration of Technetium-99 in Slant Borehole Sediment that is Water or Acid Extractable	4.29
4.8 Concentration of Uranium in Slant Borehole Sediment that is Water or Acid Extractable	4.30
4.9 Comparison of Technetium-99 and Iodine-129 in Dilution-Corrected Porewaters	4.31
4.10 Particle Size Distribution of Slant Borehole Samples from H1a and H1 Units	4.45

4.11 Particle Size Distribution of Slant Borehole Samples from H2 Unit.....	4.45
4.12 Particle Size Distribution of Slant Borehole Samples from PPlz versus Range in H2 Unit	4.46
4.13 Typical Illite Particle from Sample 3A.....	4.50
4.14 Two Thin Platy Illites Surrounded by Smaller Particles of Feldspar, Quartz, and Amphibole	4.51
4.15 Typical Chlorite Grain from Sample 7A	4.52
4.16 Thick Delicate Smectite Laths Curled up to Appear Dense	4.53
4.17 Typical Dense Smectite Aggregate from Sample 15A.....	4.53
5.1 Comparison of Water-Extractable Sodium for the Two Contaminated SX Boreholes	5.16
5.2 Comparison of Water-Extractable Chromium for the Two Contaminated SX Boreholes.....	5.17
5.3 Comparison of Water-Extractable Calcium for the Two Contaminated SX Boreholes	5.18
5.4 Comparison of Cesium-137 Content in the Sediment from the Two SX Boreholes	5.20
5.5 Comparison of Technetium-99 Content in the Sediment from the Two SX Boreholes	5.21

Tables

2.1 Stratigraphic Terminology Used in this Report for the Vadose Zone Beneath the SX Tank Farm	2.4
2.2 Location of Split-Spoon Samples as Derived from a Gyroscopic Survey of the Borehole Casing	2.9
2.3 Sample Location, Retrieval Date, and Estimated Recovery	2.11
2.4 Summary of Core Sample Data for Hydrostratigraphic Subunits Within the Lower Fine Sand and Mud Sequence	2.18
4.1 Moisture Content of Sediment from Slant Borehole	4.2
4.2 Water Extract pH and Electrical Conductivity Values	4.3
4.3 Comparison of Actual Porewater pH and Electrical Conductivity with Dilution-Corrected 1:1 Water Extract Values	4.5
4.4 Anion Content of Water Extracts of Slant Borehole Sediment	4.7
4.5 Comparison of Calculated with Actual Porewater Anion Concentrations for Slant Borehole Vadose Zone Sediment	4.10
4.6 Calculated Porewater Cation Composition from Water Extracts of Vadose Zone Sediment from Slant Borehole.....	4.11
4.7 Comparison of Actual to Calculated Porewaters—Cations.....	4.14
4.8 Comparison of ICP Sulfur as Sulfate with IC Sulfate for Water Extracts and Porewaters	4.15
4.9 Calculated Porewater Trace Metal Composition for Water Extracts of Sediment from Slant Borehole	4.17

4.10 Comparison of Actual to Calculated Porewaters—Trace Metals	4.17
4.11 Ratio of Porewater Constituents to Mobile Species	4.21
4.12 Gamma Energy Analysis of Vadose Zone Sediment.....	4.24
4.13 Strontium-90 and Tritium Contents of Vadose Zone Sediment	4.25
4.14 Technetium-99 and Uranium-238 Content in Sediment and in Water Extracts	4.26
4.15 Iodine-129 Content in Dilution-Corrected Water Extracts for Selected Slant Borehole Sediment	4.31
4.16 Carbon Content in Vadose Sediment from Slant Borehole	4.32
4.17 Acid-Extractable Major Element Content of the Vadose Sediment from Slant Borehole	4.34
4.18 Acid-Extractable Trace Element Content of the Vadose Sediment from Slant Borehole	4.36
4.19 Total Composition of the Vadose Zone Sediment from Slant Borehole Percent Weight as Oxides	4.39
4.20 Total Composition of the Clay-Sized Fraction of Sediment from Slant Borehole Percent Weight as Oxides.....	4.40
4.21 Percentage of Elements Extracted by 8 M Nitric Acid.....	4.41
4.22 Particle Size Distribution Percent Weight	4.43
4.23 Folk-Wentworth Sediment Classification.....	4.44
4.24 Particle Size Distribution Based on Combined Wet Sieve/Hydrometer Methods.....	4.44
4.25 Particle Density of Bulk Sediment from Slant Borehole.....	4.47
4.26 Semiquantitative Mineral Composition for Bulk Samples	4.47
4.27 Semiquantitative Analysis of the Clay Fraction from Slant Borehole.....	4.48
5.1 In Situ K_d Values for Contaminants Desorbing from Slant Borehole Vadose Zone Sediment	5.2
5.2 Comparison of the pH and Electrical Conductivity in Porewaters from the Two Boreholes....	5.5
5.3 Comparison of the Anion Concentrations in Porewaters from the Two Boreholes	5.6
5.4 Comparison of the Cation Concentrations in Porewaters from the Two Boreholes.....	5.8
5.5 Comparison of the Metal Concentrations in Porewaters from the Two Boreholes	5.10
5.6 Comparison of the Maximum Concentration of Porewaters from Various Lithologies in the Two Boreholes.....	5.14
5.7 Comparison of the Radionuclide Content in Sediment from the Two Boreholes	5.19

1.0 Introduction

The overall goal of the of the Tank Farm Vadose Zone Project, led by CH2M HILL Hanford Group, Inc., is to define risks from past and future single-shell tank farm activities, to identify and evaluate the efficacy of interim measures, and to aid via collection of geotechnical information and data, the future decisions that must be made by the Department of Energy regarding the near-term operations, future waste retrieval, and final closure activities for the single-shell tank Waste Management Areas. For a more complete discussion of the goals of the Tank Farm Vadose Zone Project, see the overall work plan, *Phase I RCRA Facility Investigation/Corrective Measures Study Work Plan for the Single-Shell Tank Waste Management Areas* (DOE 1999).

To meet these goals, CH2M HILL Hanford Group, Inc., asked scientists from Pacific Northwest National Laboratory (PNNL) to perform detailed analyses of vadose zone sediment, both uncontaminated and contaminated, from within the S-SX Waste Management Area.

Specifically, this report contains all the geologic, geochemical, and selected physical characterization data collected on vadose zone sediment recovered from the SX-108 slant borehole. We also provide our interpretation of the data in the context of determining the appropriate lithologic model, the vertical extent of contamination, the migration potential of the contaminants that still reside in the vadose zone, and the correspondence of the contaminant distribution in the borehole sediment to groundwater plumes in the aquifer proximate and down gradient from the SX Tank Farm.

This report is one in a series of four reports to present recent data collected on vadose zone sediment, both uncontaminated and contaminated, from within the S-SX Waste Management Area. Three other PNNL reports discuss the characterization of 1) uncontaminated sediment from outcrop/large excavations and two Resource Conservation and Recovery Act (RCRA) boreholes, to provide a baseline against information from contaminated sediment; 2) contaminated sediment obtained from the 41-09-39 borehole east of tank SX-109, which has been decommissioned; and 3) contaminated sediment from borehole SX-115, which is now monitoring well 299-W23-19.

The documents contain preliminary interpretations to identify the distribution of key contaminants within the vadose zone and to determine what their future migration potential could be. The information will be incorporated in the S-SX field investigation report.^(a)

This report is divided into sections that describe the geology, the geochemical characterization methods employed, the geochemical results, the contaminant migration potential, as well as summary and conclusions, references cited, and four appendixes.

(a) *Draft Field Investigation Report for Waste Management Area S-SX*. RPP-7884, Draft, Volume 2, Appendix D, CH2M HILL Hanford Group, Inc., Richland, Washington.

2.0 Geology

The geology of the vadose zone underlying the SX Tank Farm forms the framework through which the contaminants move and the physical structure that along with geochemistry properties control the migration and distribution of contaminants. Of particular interest are the interrelationships between the coarser- and finer-grained sediments, and the degree of contrast in their physical and geochemical properties.

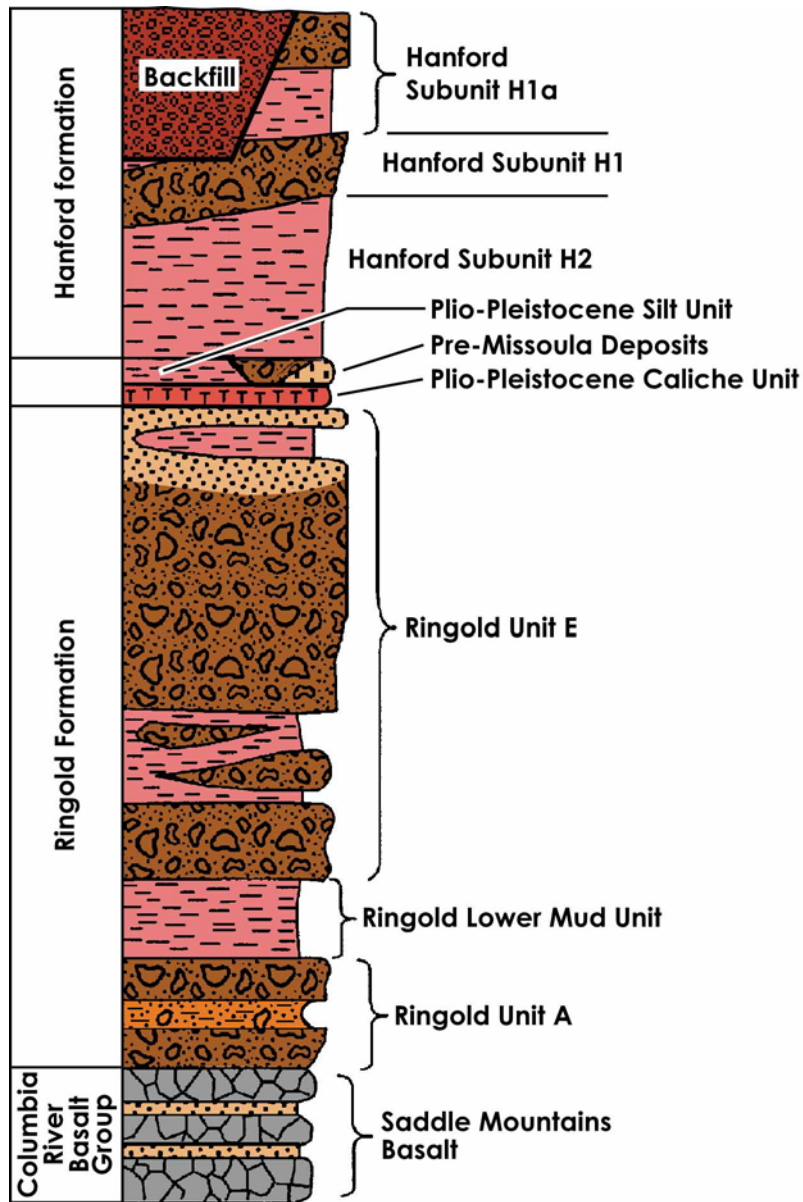
This section presents a brief discussion on the geologic setting of the tank farm; brief discussions of the drilling, sampling, and geophysical logging of the SX-108 slant borehole (borehole C3082); the laboratory methods used to extract, subsample, and visually describe the sampled materials; and a description of the materials penetrated by the SX-108 slant borehole.

2.1 Geologic Setting of the SX Tank Farm

The SX Tank Farm was constructed in 1953 and 1954 within Pleistocene Hanford formation and Holocene eolian deposits that mantle the southwestern extent of the Cold Creek flood bar (Johnson et al. 1999). The geology beneath the SX Tank Farm has been the subject of numerous reports, including the most recent ones by Johnson and Chou (1998, 1999), Johnson et al. (1999), Lindsey et al. (2000), Socbczyk (2000), and Serne et al. (2002a, b, c). The major stratigraphic units beneath the tank farm include (in descending order) the Hanford formation, the Plio-Pleistocene unit, and the Ringold Formation (Figure 2.1). The upper 16 meters (53 feet) of the Hanford formation was removed during construction of the tank farm (Figures 2.2 and 2.3) and the stockpiled sediment later was used as backfill around the underground storage tanks.

The stratigraphic terminology used in this report is summarized in Table 2.1. The general stratigraphic interpretation presented here is consistent with that provided in the 41-09-39 borehole report (Serne et al. 2002a), the Resource Conservation and Recovery Act borehole core sample and composite sample report (Serne et al. 2002c), and the 299-W23-19 borehole report (Serne et al. 2002b).

Figure 2.4 illustrates the location of the SX-108 slant borehole, and other wells used to create the cross section shown in Figure 2.5. Some slight discrepancies may occur between the depths of the geologic contacts presented here and those presented by others, because of various sources of uncertainty in the geologic data sets and the individual geologists' interpretations. Johnson et al. (1999) identified the principal sources of uncertainty as related to the drilling and sampling techniques, logging of the boreholes, and uncertainties in the geometric shape of the sedimentary units. They found that the stratigraphy beneath the S-SX Tank Farms is relatively consistent across the area and that the optimal depths for stratigraphic correlations between different data sets were typically accurate to within 1 to 3 meters (a few feet to 10 feet).



2002/DCL/SX-108/001

Figure 2.1. Generalized, Composite Stratigraphy for the Late Cenozoic Sediment Overlying the Columbia River Basalt Group on the Hanford Site (after Johnson and Chou 1998, 1999)



Figure 2.2. SX Tank Farm Under Construction in 1953 (looking northeast)



Figure 2.3. The SX Tanks Under Construction and the Native Hanford Formation Sediment (looking west, with the SX-101 tank in the foreground)

Table 2.1. Stratigraphic Terminology Used in this Report for the Vadose Zone Beneath the SX Tank Farm

Stratigraphic Symbol ^(a)	Formation	Facies/Subunit	Description	Genesis
Holocene/Fill	NA	Backfill	Poorly sorted gravel to medium sands and silt derived from the Hanford formation (Price and Fecht 1976)	Manmade
H1a	Hanford formation	Unit H1a - gravelly sand	Top coarse sand and gravel sequence equivalent to Johnson et al. (1999) Gravel Unit B	Cataclysmic Flood Deposits
		Unit H1a - slightly silty sand	Upper fine sand and silt sequence	
H1		Unit H1	Middle coarse sand and gravel sequence equivalent to Gravel Unit A described by Johnson et al. (1999) and Hanford Unit A described by Sobczyk (2000)	
H2		Unit H2	Lower fine sand and silt sequence	
PPlz and/or H/PP1	Plio-Pleistocene Unit	Upper	Very fine sand to clayey silt sequence. Interstratified silt to silty very fine sand and clay deposits at least partially correlative with the early Palouse soil described by Tallman et al. (1979) and DOE (1988) and the unnamed Hanford formation [?] or Plio-Pleistocene Deposits [?] described by Lindsey et al. (2000), and the H/PP deposits in Wood et al. (2001)	Fluvial and/or Eolian Deposits (with some weakly developed paleosols)
PPlc		Lower	Carbonate-rich sequence. Weathered and naturally altered sandy silt to sandy gravel, moderately to strongly cemented with secondary pedogenic calcium carbonate	Well-developed calcic paleosol or sequence of calcic soils
Rtf	Ringold Formation	Member of Taylor Flat	Interstratified sand and silt deposits, equivalent to the Upper Ringold unit described by Tallman et al. (1979) and DOE (1988)	Fluvial and Overbank-Paleosol Deposits
Rwi(e)		Member of Wooded Island, subunit E	Moderate to strongly cemented well-rounded gravel and sand deposits, and interstratified finer-grained deposits	Fluvial
(a) After Lindsey et al. (2000).				

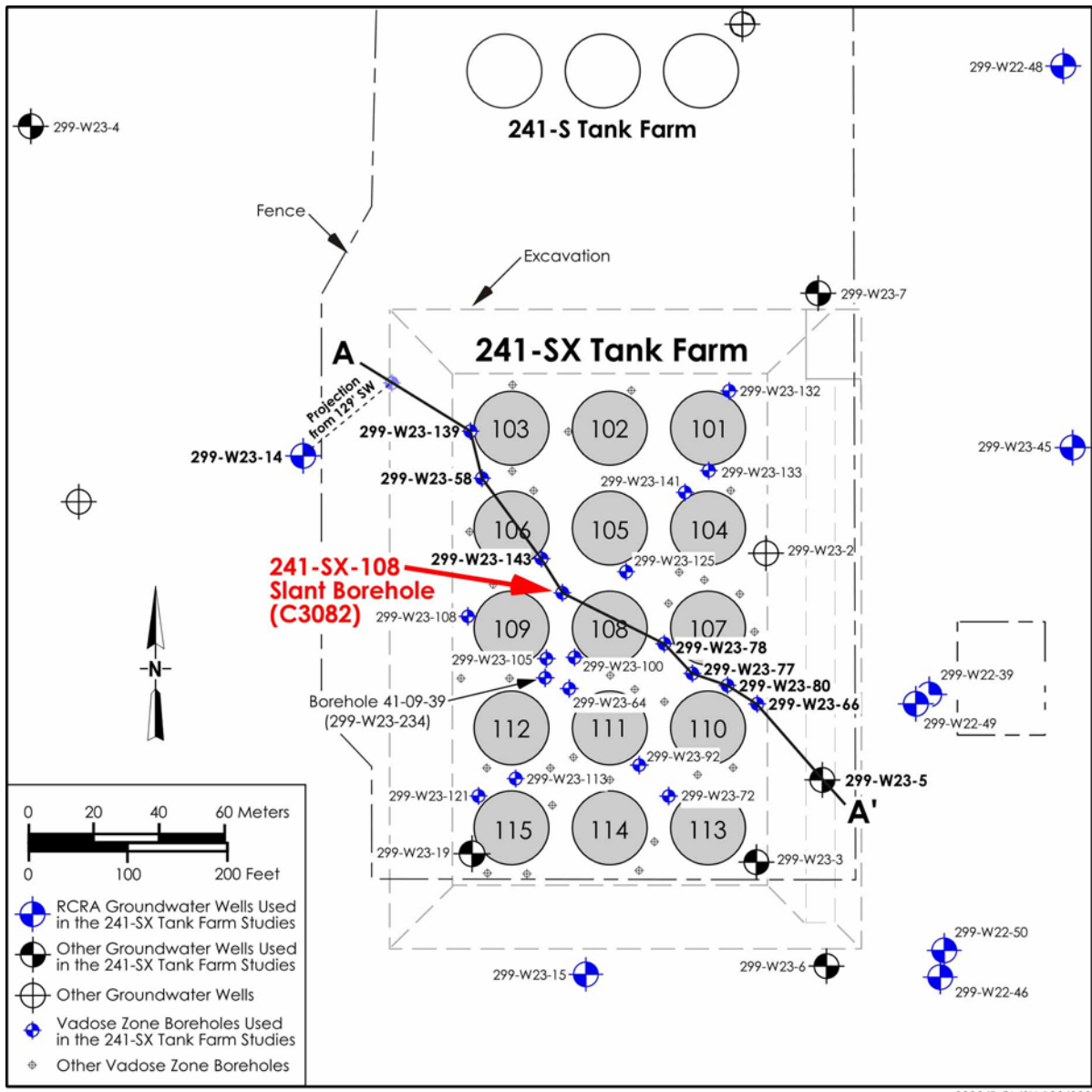


Figure 2.4. Location of SX-108 Slant Borehole (C3082), Other Pertinent Wells, and Cross Sections. A-A' is location of cross section depicted in Figure 2.5.

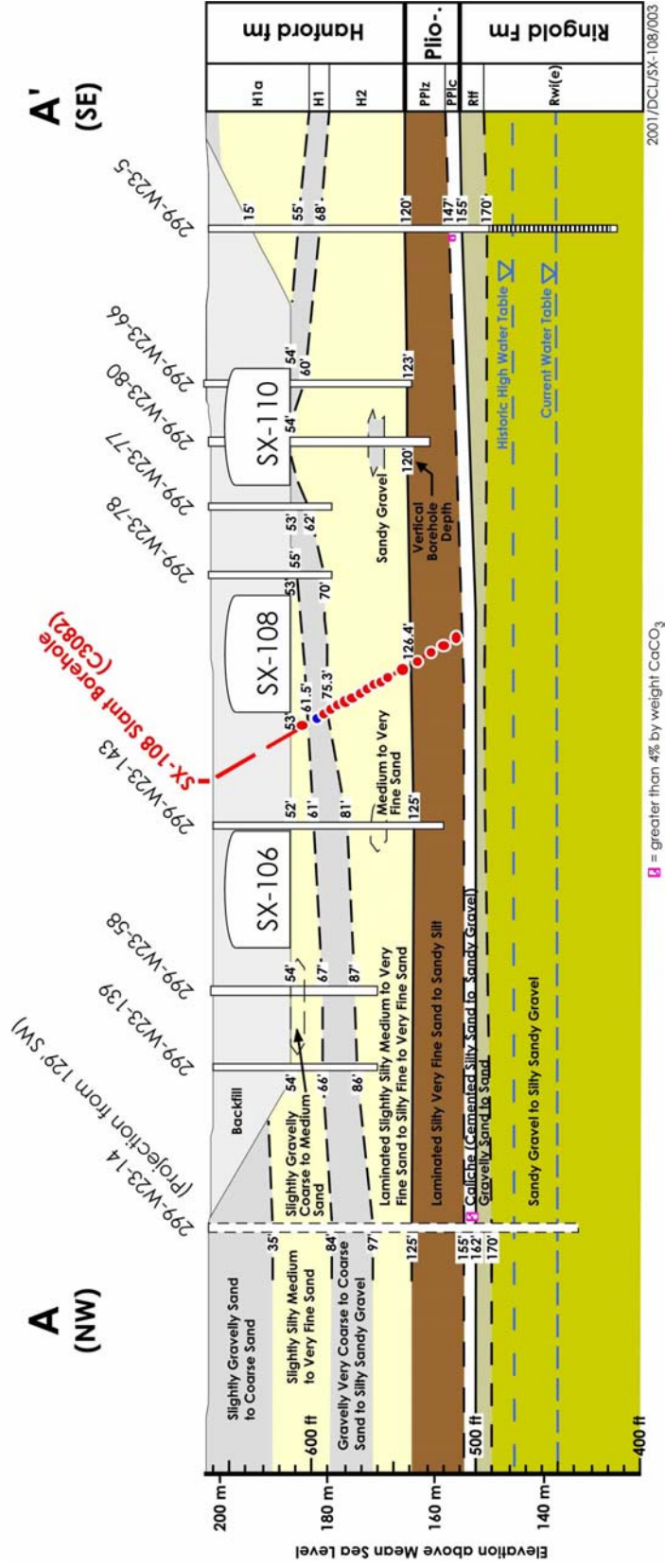


Figure 2.5. Geologic Cross Section A-A' (looking northeast). Lithologic contact depths in boreholes are measured in feet.

2.2 Drilling and Sampling of the SX-108 Slant Borehole

The SX-108 slant borehole (borehole C3082) was drilled and samples were collected between June 2 and July 27, 2000 (Gardner and Reynolds 2000). This borehole was installed approximately 12 meters (40 feet) from the edge of tank SX-108 on the northwest side (Figure 2.6).

The borehole was drilled at an angle of approximately 30 degrees from vertical and in a direction to pass beneath the center of the tank to a total pipe run length of 52.2 meters (171.2 feet) and a vertical depth of 43.9 meters (143.99 feet) (Gardner and Reynolds 2000). The borehole was advanced using a ResonantSonic^(a), International drill rig with pile driver to drive the closed-end casing with removable drive tip. The blow counts required to drive the casing were recorded for comparison to geologic units.

Core samples were taken ahead of the casing by removing the drive tip and pushing a specially designed split-spoon sampler into the undisturbed formations beneath the casing. The split-spoon sampler was designed specifically for this project and contained internal 1.9 centimeters (0.75 inch) thick lead shielding to reduce worker exposure during handling of the highly radioactive sediment samples (Figure 2.7). Detailed descriptions of the sampler design and sampling methods can be found in *Slant Borehole Demonstration Summary Report* (WMTS 2000b).

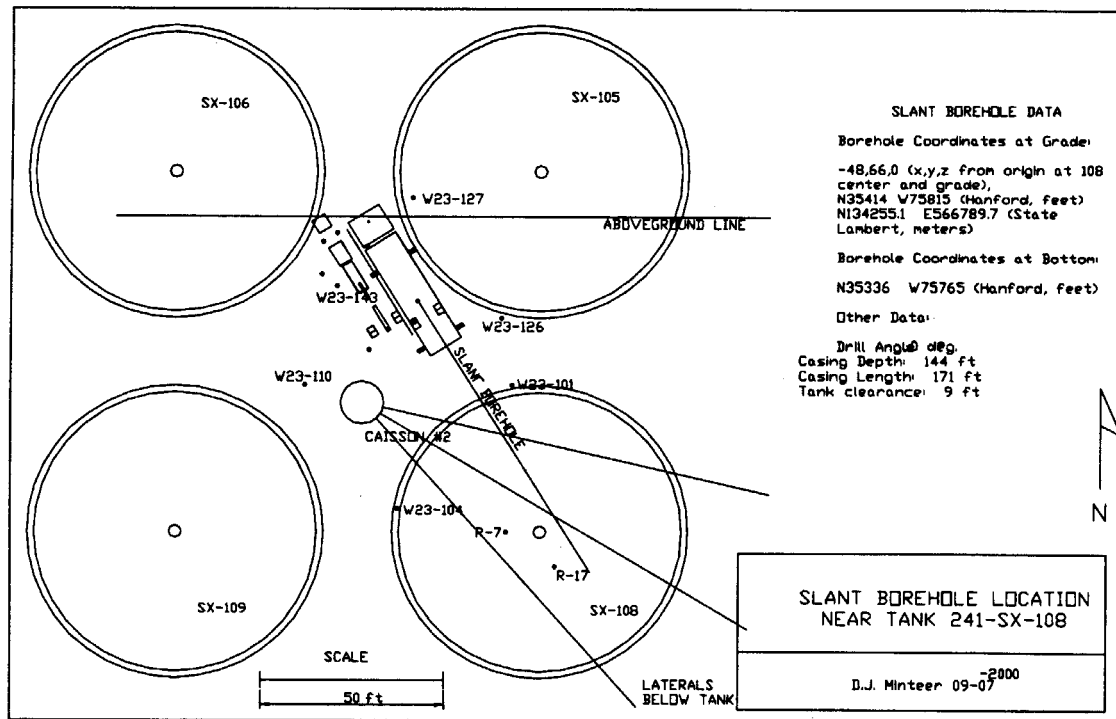


Figure 2.6. Borehole Location (after Gardner and Reynolds 2000)

(a) ResonantSonic is a trademark of ResonantSonic International, Woodland, California.

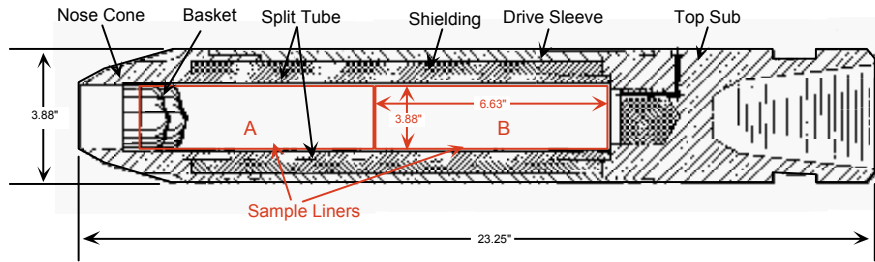


Figure 2.7. Schematic of Shielded Split-Spoon Sampler (after WMTS 2000a, b, c)

Seventeen sampling attempts were made and 16 samples were recovered at 1.5- and 3-meter (5- and 10-foot) intervals throughout that portion of the borehole extending from the base of the backfill to the total depth. Only one sample, 02, was lost in its entirety down the inside of the casing when the sampled materials fell out while breaking the connections between the drill pipe, down-hole air hammer, and sampler (Gardner and Reynolds 2000). Sample 02 was sampling a zone that consisted of coarse sand and small pebbles from one of the highest contamination zones (based on spectral gamma logging). The materials lost were subsequently smeared throughout the entire length of casing causing difficulty in meeting contamination control requirements and in interpreting the geophysical logging data (Gardner and Reynolds 2000).

Figure 2.8 illustrates the location of each sample, while Table 2.2 provides the three-dimensional location for each sample as calculated from the gyroscopic survey of the borehole casing. Following the

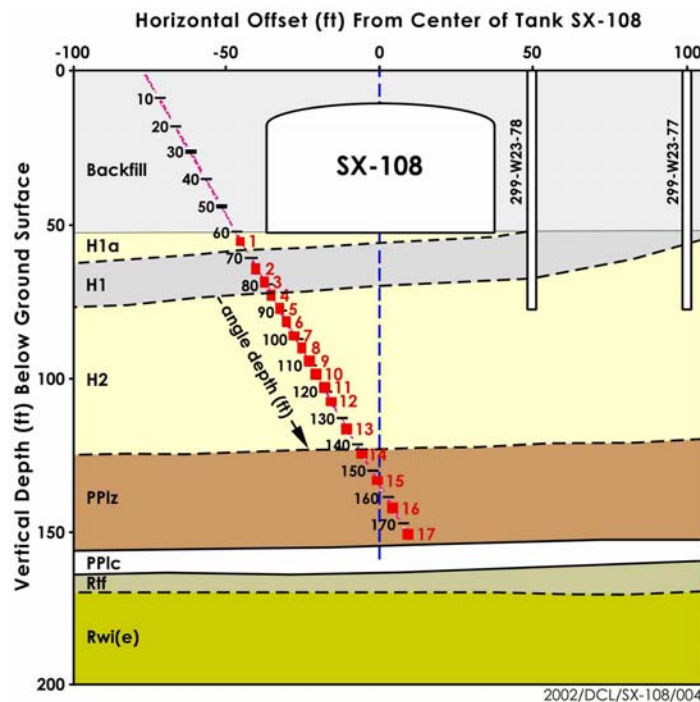


Figure 2.8. Location of Split-Spoon Samples

retrieval of each sampler, samples were (except for sample 06) immediately capped, packaged, and transported to PNNL's 3720 laboratory for breakdown, sample recovery, and analysis (Gardner and Reynolds 2000). Due to a range fire and general area evacuation, sample 06 was left in the SX Tank Farm for 7 days before being transported. Each sampler was surrounded by blue ice to maintain sample temperature between 2 to 4°C during transportation. The shipping containers were sealed with custody tape and maintained under chain-of-custody protocols (Gardner and Reynolds 2000).

Table 2.2. Location of Split-Spoon Samples as Derived from a Gyroscopic Survey of the Borehole Casing

Sample No.	Casing Length (Angle Depth) (ft) ^(a)	Gyro E (ft) ^(a)	Gyro N (ft) ^(a)	Gyro (Vertical) Depth (ft) ^(a)	Northing (m)	Easting (m)	Elevation (m)
Origin	0.00	0.00	0.00	0.00	134255.11	566789.73	201.84
S0070-01	63.20	18.69	-26.01	54.48	134247.18	566795.43	185.23
S0070-02	73.20	21.45	-30.43	63.02	134245.83	566796.27	182.63
S0070-03	78.20	22.82	-32.67	67.27	134245.15	566796.69	181.34
S0070-04	83.20	24.21	-34.93	71.51	134244.46	566797.11	180.04
S0070-05	88.20	25.62	-37.20	75.73	134243.77	566797.54	178.76
S0070-06	93.20	27.04	-39.49	79.94	134243.07	566797.97	177.47
S0070-07	98.20	28.46	-41.81	84.13	134242.37	566798.40	176.20
S0070-08	103.20	29.89	-44.15	88.32	134241.65	566798.84	174.92
S0070-09	108.20	31.34	-46.51	92.48	134240.93	566799.28	173.65
S0070-10	113.20	32.78	-48.88	96.64	134240.21	566799.72	172.38
S0070-11	118.50	34.32	-51.41	101.04	134239.44	566800.19	171.04
S0070-12	123.20	35.68	-53.67	104.92	134238.75	566800.61	169.86
S0070-13	133.20	38.63	-58.54	113.14	134237.27	566801.50	167.35
S0070-14	143.20	41.60	-63.49	121.30	134235.76	566802.41	164.87
S0070-15	153.20	44.60	-68.48	129.44	134234.24	566803.32	162.39
S0070-16	163.20	47.61	-73.52	137.54	134232.70	566804.24	159.92
S0070-17	171.20	50.01	-77.58	143.99	134231.46	566804.97	157.95

(a) Multiply by 0.3048 to convert to meters.

2.3 Geophysical Logging

Several geophysical logging techniques were used during and after installation of the SX-108 slant borehole. These techniques included gyroscopic borehole surveys, casing wall temperature logging, neutron-neutron moisture logging, high-purity germanium spectral gamma logging, and high-rate gamma logging. Detailed descriptions of the logging tools, data analysis, and general conclusions can be found in the *SX-108 Slant Borehole Completion Report* (Gardner and Reynolds 2000). A composite of the temperature, moisture, spectral gamma, and high-rate gamma logs is shown in Figure 2.9.

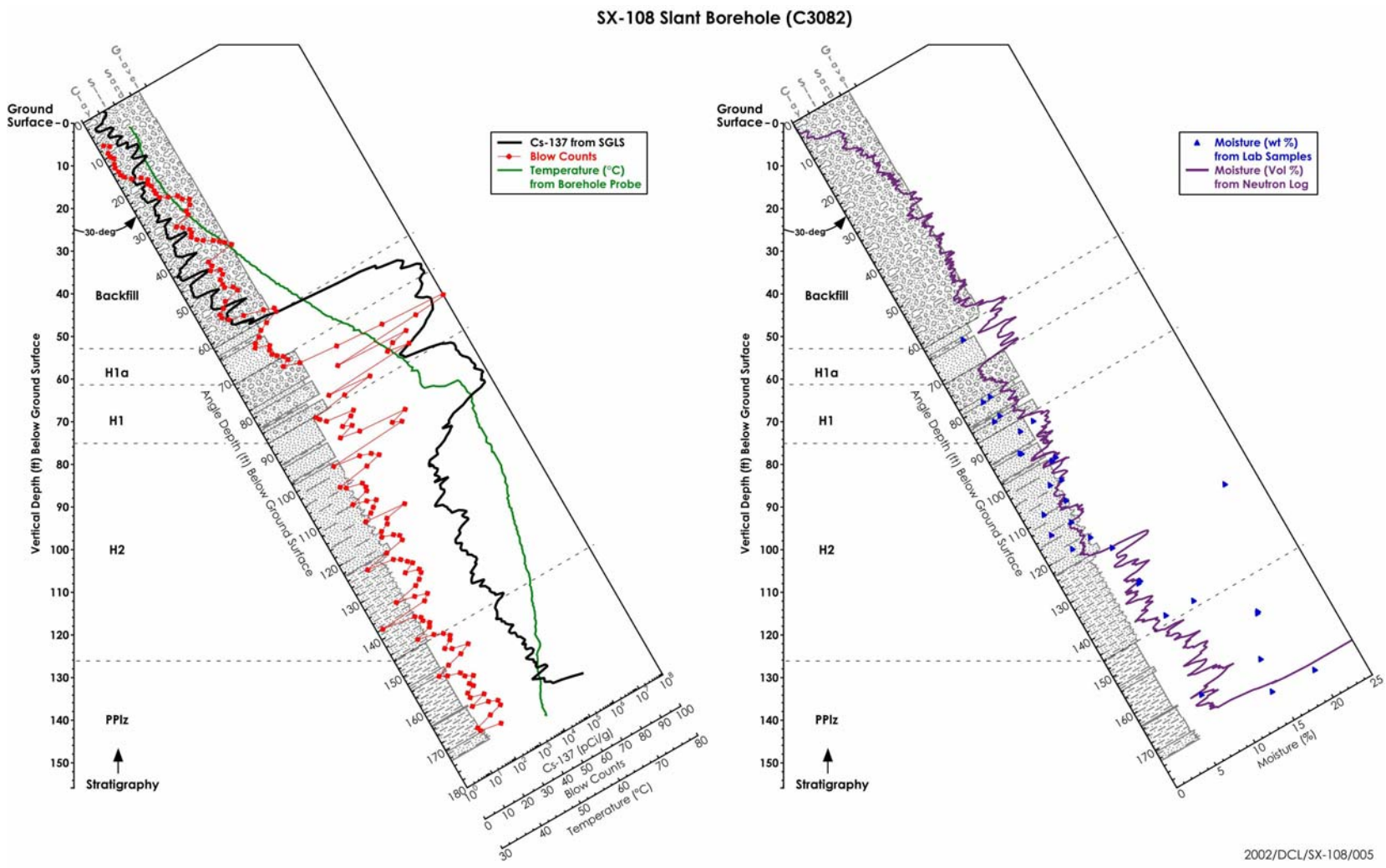


Figure 2.9. Detailed Lithology and Analytical Values of Split-Spoon Samples from the SX-108 Slant Borehole

The borehole gyroscope surveys were conducted to verify the actual location of the drive tip and casing and to provide the precise position of the sampling points (Table 2.3). An infrared temperature sensor was used to read the temperature of the steel-cased borehole wall and infer the formation temperatures.

Table 2.3. Sample Location, Retrieval Date, and Estimated Recovery

Sample No.		Sample Depth/Angle (ft) ^(a)	Sample Depth/Vertical ^(b) (ft) ^(a)	Midpoint Depth (ft) ^(a)	Date Collected	Date Opened	% Recovery
S0070-01	B	63.2 - 63.7	54.5 - 54.9	54.7	6/13/00	6/14/00	50-60
	A	63.7 - 64.2	54.9 - 55.3	55.1			100
S0070-02	B	73.2 - 73.7	63.0 - 63.5	63.2	6/14/00	NA	0
	A	73.7 - 74.0	63.5 - 63.7	63.6			0
S0070-03	B	78.2 - 78.7	67.3 - 67.7	67.5	6/19/00	7/20/00 ^(c)	NA
	A	78.7 - 79.2	67.7 - 68.1	67.9			NA
S0070-04	B	83.2 - 83.7	71.5 - 71.9	71.7	6/20/00	6/26/00	80-90
	A	83.7 - 84.2	71.9 - 72.4	72.2			100
S0070-05	B	88.2 - 88.7	75.7 - 76.2	75.9	6/21/00	6/22/00	75
	A	88.7 - 89.2	76.2 - 76.6	76.4			100
S0070-06	B	93.2 - 93.7	79.9 - 80.4	80.2	6/28/00 ^(d)	7/5/00	67
	A	93.7 - 94.2	80.4 - 80.8	80.6			100
S0070-07	B	98.2 - 98.7	84.1 - 84.6	84.3	7/6/00	7/11/00	100
	A	98.7 - 99.2	84.6 - 85.0	84.8			100
S0070-08	B	103.2 - 103.7	88.3 - 88.8	88.5	7/10/00	7/12/00	75-80
	A	103.7 - 104.2	88.8 - 89.2	89.0			100
S0070-09	B	108.2 - 108.7	92.5 - 92.9	92.7	7/12/00	7/13/00	70
	A	108.7 - 109.2	92.9 - 93.3	93.1			100
S0070-10	B	113.2 - 113.7	96.6 - 97.1	96.9	7/14/00	7/18/00	50
	A	113.7 - 114.2	97.1 - 97.5	97.3			100
S0070-11	B	118.2 - 118.7	101.0 - 101.5	101.3	7/17/00	7/18/00	75-80
	A	118.7 - 119.2	101.5 - 101.9	101.7			100
S0070-12	B	123.2 - 123.7	104.9 - 105.4	105.1	7/18/00	7/19/00	50
	A	123.7 - 124.2	105.4 - 105.8	105.6			100
S0070-13	B	133.2 - 133.7	113.1 - 113.6	113.4	7/20/00	7/25/00	40
	A	133.7 - 134.2	113.6 - 114.0	113.8			100
S0070-14	B	143.2 - 143.7	121.3 - 121.7	121.5	7/24/00	7/26/00	60
	A	143.7 - 144.2	121.7 - 122.2	121.9			100
S0070-15	B	153.2 - 153.7	129.4 - 129.9	129.7	7/25/00	7/27/00	100
	A	153.7 - 154.2	129.9 - 130.3	130.1			100
S0070-16	B	163.2 - 163.7	137.5 - 138.0	137.8	7/26/00	7/27/00	100
	A	163.7 - 164.2	138.0 - 138.4	138.2			100
S0070-17	B	171.2 - 171.7	144.0 - 144.4	144.2	7/27/00	7/28/00	100
	A	171.7 - 172.2	144.4 - 144.9	144.6			100

(a) Multiply by 0.3048 to convert to meters.
(b) Based on gyroscopic borehole survey (Gardner and Reynolds 2000).
(c) Could not open sampler - materials dug out by hand.
(d) Sampler not transported to the laboratory until July 5, 2000.

The neutron-neutron moisture log recorded the average volumetric moisture content within a 20- to 30-centimeter (8- to 12-inch) radius of the borehole. Slightly increased moisture content was noted between angle depths of 17.7 and 21.3 meters (58 to 70 feet), and second significant moisture content change noted at an angle depth of 37.8 meters (124 feet) (Gardner and Reynolds 2000). These moisture content changes correlate well with changes in the geologic materials (see Section 2.4).

Several spectral-gamma and high-rate gamma logging events were conducted using different logging systems and conditions. Cesium-137 was the only gamma-emitting contaminant detected. Above the angle depth of 18.3 meters (60 feet), cesium-137 concentrations were generally less than 20 pCi/g, and were attributed (most likely) to internal casing contamination (Gardner and Reynolds 2000). This internal casing contamination resulted from the loss of sample 02 down the borehole. Between angle depths of 18.9 and 31.7 meters (62 to 104 feet), very high concentrations of cesium-137 (on the order of 10^8 pCi/g) were measured. Internal contamination and/or drag down most likely dominate contamination detected below an angle depth of 31.7 meters (104 feet) (Gardner and Reynolds 2000).

2.4 Sample Breakdown and Recovery

After arrival at the laboratory, the split-spoon samplers were stored intact in a refrigerator to maintain the sample temperatures between 2 and 4°C. Upon retrieval from the refrigerator, each sampler was taken to a fume hood, where it was unpackaged and the outside of the sampler decontaminated. The sampler was then transferred to the breakdown table inside a second walk-in fume hood where the nose cone (shoe) and top sub were broken loose from the drive sleeve (sampler body) (Figure 2.10). The sampler was then transferred back to the first fume hood, where the sampler was completely disassembled and the sample liners recovered.

Each sampler contained two thin stainless steel sample liners or sleeves, each approximately 5 centimeters (2 inches) in diameter and 15.2 centimeters (6 inches) long. The lower most sample liner was designated A, and the upper liner was designated B. The approximate amount of sample material retained in each liner (percent recovery) was noted and the material removed and placed in separate containers for subsampling, geologic description, and photography. Table 2.3 lists the samples collected, when they were opened in the laboratory, and the estimated recovery.

All samples followed this same general procedure except sample 03. Several attempts were made to disassemble this sampler, but the sampler body and/or shoe threaded connection had apparently been damaged when driving of the sampler (Gardner and Reynolds 2000). Thus, the sample materials were recovered by extracting the material out of either end of the sampler and were eventually combined as sample A.



Figure 2.10. Shielded Split-Spoon Sampler on Breakdown Table Inside Fume Hood
(See Figure 2.7 for sampler detail)

2.5 Subsampling and Geologic Description

Immediately upon sample recovery, the sampled materials were quickly inspected. Moisture samples and gamma energy analysis samples then were collected from discrete portions of each sample liner. The intent was to sample the finer grained and/or wetter materials as well as distinct hydrogeologic units, while at the same time trying to avoid slough and/or unrepresentative portions. The remaining portions of the samples were then used for brief visual geologic evaluation.

The visual geologic evaluation was conducted in accordance with procedures ASTM D2488-93 (1993) and PNL-MA-567-DO-1 (PNL 1990) to describe and record the sampled materials. Throughout the subsampling and geologic evaluation activities, the geologist made continual visual observations regarding the sample's structure, grain size, grain shape, color, moisture, consistency, cementation, hardness, and reaction to hydrochloric acid. Particular attention was given to estimate the percentage (by weight) of gravel, sand, and mud (silt plus clay), and to classify the samples based on the modified Folk (1968) and Wentworth (1922) classification historically used at the Hanford Site and described by Fecht and Price (1977). This sediment classification scheme uses a tertiary diagram to categorize the sediment into 1 of 19 classes based on the relative proportions of gravel, sand, and mud (silt plus clay) (Figure 2.11). Geologic logs recording the visual observations made while opening, subsampling, and characterizing these materials are provided in Appendix A. Photographs were also taken of each sample and are included in Appendix B.

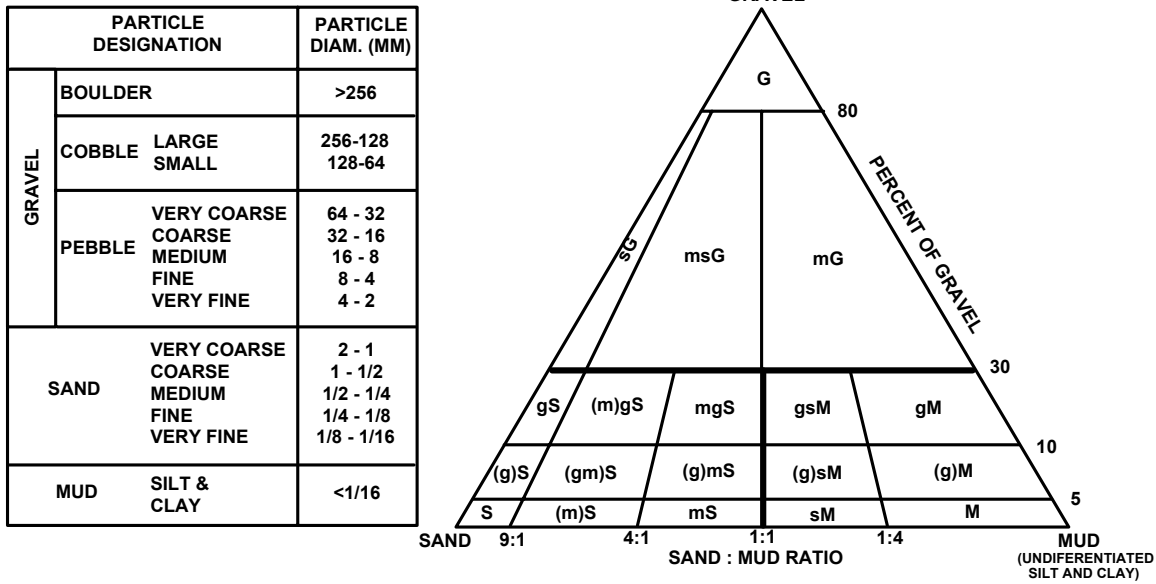


Figure 2.11. Sediment Classification Scheme (modified from Folk 1968) and Grain-Size Nomenclature (modified from Wentworth 1922)

2.6 Geology of the SX-108 Slant Borehole

Figure 2.9 presents a generalized hydrostratigraphic section for the borehole. Note that both the pipe run lengths (angle depth) and true vertical depth below ground surface are given. Note also that only about 30 centimeters (1 foot) of formation materials were recovered for each 1.5- to 3-meter (5- to 10-foot) interval from the base of the backfill to total depth. Because of worker safety and disposal logistics, continuous coring was not feasible. The hydrostratigraphy shown here is a synergistic interpretation of the geologic descriptions of the sample materials, laboratory analyses, and geophysical logs. Although the borehole was drilled at an angle of approximately 30 degrees from vertical, nearly all depths and/or thicknesses discussed below are from vertical, as feet below ground surface (feet bgs).

This borehole intersected three primary stratigraphic units: 1) backfill (not sampled), 2) the Hanford formation, and 3) the top of the Plio-Pleistocene unit. The backfill extends to a depth of about 16.2 meters (53 feet) where it contacts the Hanford formation. The next 2.6 meters (8 feet) are interpreted to correlate with the upper fine sand and mud sequence of the Hanford formation H1a unit. Below this lies the 4.2-meter (14-foot) thick middle coarse sand and gravel sequence (H1 unit). The contact between the Hanford formation and the Plio-Pleistocene unit is interpreted to occur at a depth of 38.5 meters (126 feet).

Descriptions summarizing the observations and physical soil properties for each of the major hydrostratigraphic units sampled by this borehole are presented below.

2.6.1 Backfill

The backfill was not sampled. However, engineering drawing H-2-37985, sheet 2 of 2 shows the elevation of the base of backfill beneath the SX-108 tank as being 185.65 meters (609.12 feet) above mean sea level. Given the elevation of the borehole origin as 201.84 meters (662.24 feet) (see Table 2.2), then the depth of the base of backfill should be at a vertical depth of approximately 16.2 meters (53.1 feet), which is equivalent to an angle depth of approximately 18.7 meters (61.3 feet). This contact depth is further supported by an increase in blow counts and an increase in moisture content (as indicated in the neutron-neutron moisture log); see Figure 2.12.

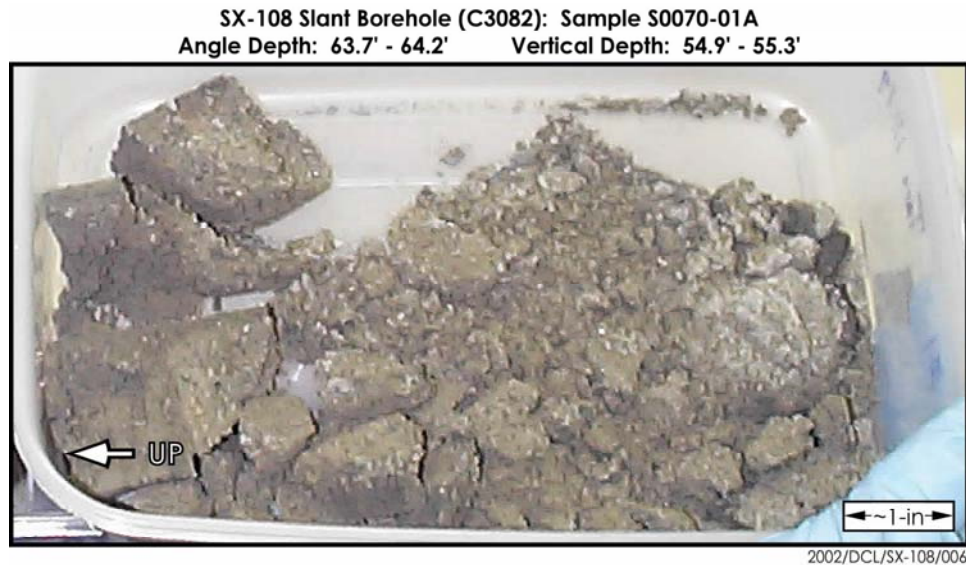


Figure 2.12. Disaggregated Core (Sample S0070-01A) from the Hanford Formation H1a Unit (Note change from dark olive brown muddy sand on the left [top of sample] to olive brown medium sand on the right side [bottom].)

2.6.2 Hanford Formation

Split-spoon core samples were collected from all three Hanford formation subunits (H1a, H1, and H2).

2.6.2.1 Upper Fine Sand and Mud Sequence (Hanford formation H1a unit)

The upper fine sand and mud sequence of the Hanford formation H1a unit is approximately 2.6 meters (8.4 feet) thick extending from the base of the backfill to a vertical depth of approximately 18.7 meters (61.5 feet). This vertical depth is equivalent to an angle depth of approximately 21.6 meters (71 feet). The location of this contact is supported by a slight increase in the blow counts and a sharp decrease in the neutron-neutron moisture log.

Only one split-spoon sample, 01, was collected from this upper fine sand and mud sequence. This sample was collected from a vertical depth of approximately 16.6 to 16.9 meters (54.5 to 55.3 feet), approximately 0.4 to 0.7 meters (1.4 to 2.2 feet) beneath the base of the backfill and about 2.4 meters (8 feet) away from the edge of the tank.

The upper portion of this sample (liner B) contained a thin (0.5 centimeters [1 inch] thick) layer of dry gray muddy (silty) sand containing some possible rock flour (ground up rock), overlying moist muddy sand. This muddy sand strata extended into the A liner where it was described as wet, dark olive brown (2.5Y3/3), and very strong (of hard consistency). It had only a weak reaction to the dilute hydrochloric acid. The total thickness of this stratum was approximately 12 centimeters (5 inches). A moist medium sand was recovered in the lower portion of the A liner and was described as friable (crumbled with handling), olive brown (2.5Y4/3), with a weak reaction to hydrochloric acid, and with a hint of horizontal laminations (sample came out in disks). The gravimetric moisture content was measured at 4.33 wt%. Figure 2.12 illustrates the disaggregated core from the A liner.

2.6.2.2 Middle Coarse Sand and Gravel Sequence (Hanford formation H1 unit)

The middle coarse sand and gravel sequence, the Hanford formation H1 unit, is estimated to be approximately 4.2 meters (13.8 feet) thick, extending to a vertical depth of approximately 22.9 meters (75.3 feet). The equivalent angle depth of this contact, 26.5 meters (87 feet), is supported by a sharp decrease in blow counts and an increase in the neutron-neutron moisture log, which is further substantiated by an increase in the gravimetric moisture content of samples collected below this contact.

Two split-spoon samples, 03 and 04, were recovered from this coarse unit. A third sample, 02, was attempted, but the sample fell out of the sampler during retrieval (Gardner and Reynolds 2000). Sample 03 was taken at a vertical depth of approximately 20.5 to 20.8 meters (67.3 to 68.1 feet), approximately 4.3 to 4.6 meters (14.2 to 15 feet) beneath the base of the backfill and directly beneath the edge of the tank. This sampler could not be disassembled and the sample liners individually recovered. Thus, the entire sample was recovered by extracting the sample out of the intact sampler and eventually combining sediment from both liners together as 03A. Sample 04 was taken at a vertical depth of approximately 21.8 to 22.1 meters (71.5 to 72.4 feet), approximately 5.8 meters (18.9 feet) beneath the base of the backfill and approximately 0.6 meters (2 feet) inside the edge of the tank.

The upper portion of sample 03 (taken from the B liner and the top of the A liner) was described as a dry grayish brown medium to fine sand with some mud (predominantly silt - with perhaps some rock flour) and some gravel fragments (up to medium pebble). The sample was very friable with a weak to strong reaction to hydrochloric acid. The materials at the bottom of the A liner were described as a dry grayish brown (2.5Y5/2) coarse to medium sand essentially free of mud (silt). The sample was highly compacted with a weak to strong reaction to hydrochloric acid.

Sample 04 contained some fine gray powder (rock flour) in the top of the B liner. The remainder of the sample was described as a salt and pepper textured medium (to fine) sand with an overall light brownish gray (2.5Y6/2) color and a strong reaction to hydrochloric acid.

The gravimetric moisture contents of these samples ranged from 3.76 to 2.76 wt%. Figure 2.13 and 2.14 illustrates the disaggregated core from the A liners.

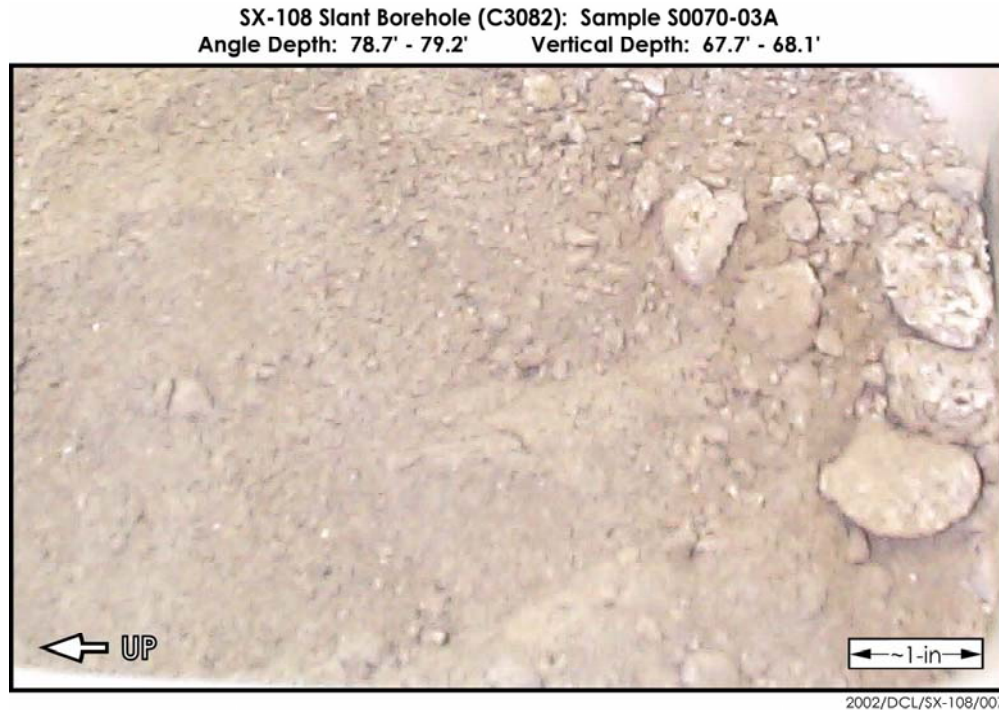


Figure 2.13. Disaggregated Core (Sample 3A) from the Hanford Formation H1 Unit

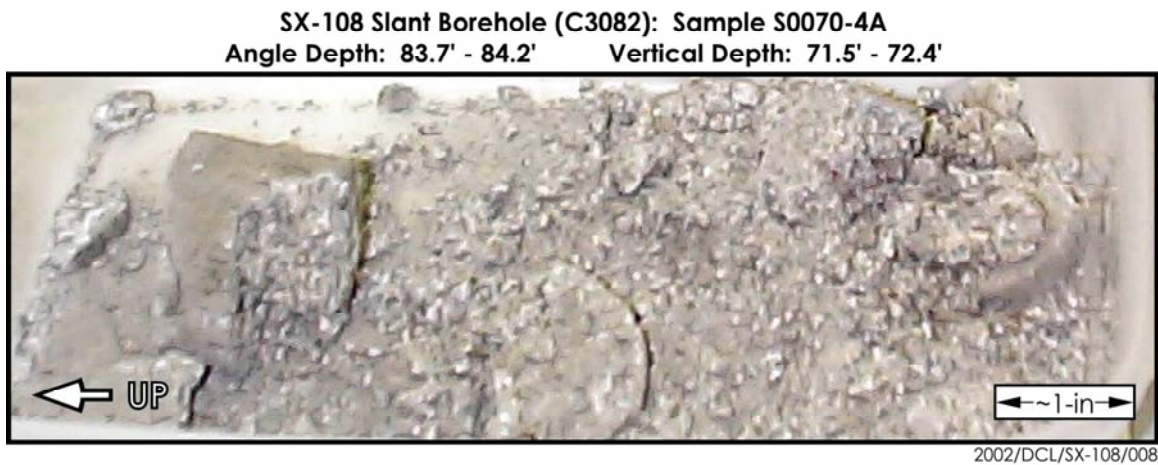


Figure 2.14. Disaggregated Core (Sample 4A) from the Hanford Formation H1 Unit

2.6.2.3 Lower Fine Sand and Mud Sequence (Hanford formation H2 unit)

The lower fine sand and mud sequence of the Hanford formation H2 unit is estimated to be approximately 15.6 meters (51.1 feet) thick, extending to a vertical depth of approximately 38.5 meters (126.4 feet). The equivalent angle depth of this contact, 44.5 meters (146 feet), is supported by a slight increase in the blow counts and a sharp increase in the neutron-neutron moisture log, which is further substantiated by an increase in the gravimetric moisture content of samples collected below this contact.

Ten split-spoon samples (S0070-5 through S0070-14) were collected throughout this horizon. These samples were collected from depths of approximately 6.9 to 21 meters (22.8 to 68.8 feet) directly beneath the SX-108 tank. The Hanford formation H2 unit represented by these samples is composed of stratified sand, muddy sand, and mud, and can be further broken down into three weakly defined subunits on the basis of texture (grain size), moisture content, blow counts, and gamma contamination. Table 2.4 summarizes the pertinent core sample data for each of these subunits.

Examination of the disaggregated core samples between the angle depths of 26.5 meters (87 feet) and 31.7 meters (104 feet) suggests that the upper portion of the Hanford formation H2 unit beneath the SX-108 tank is composed of mostly interstratified medium to fine sand with occasional muddy very fine sand and/or mud strata. These materials were described as dry, light brownish gray (2.5Y6/2) (sand) to dark olive brown (2.5Y3/3) (mud), and weakly cemented, with mostly weak to moderate (weak to strong) reaction to hydrochloric acid (Figure 2.15).

Table 2.4. Summary of Core Sample Data for Hydrostratigraphic Subunits Within the Lower Fine Sand and Mud Sequence (Hanford Formation H2 Unit)

Angle Depth (ft) ^(a)	Lithologic Description	Dominant Color	Dominant Reaction to HCl	Average Moisture Content (wt%)	Average Blow Counts	Average ¹³⁷ Cs Concentration (pCi/g)
78-104	Stratified deposits of mostly medium to fine sand, with minor muddy sand and mud laminations	Light olive brown to grayish brown (2.5Y5/3 - 5/2)	Weak to moderate (weak to strong)	5.21	36.4	1.62E+07
104-123	Stratified to finely laminated deposits of mostly fine to very fine sand some grading downward to medium sand. Some silt, particularly at the top of graded beds	Grayish brown to olive brown (2.5Y5/2 - 4/3)	Strong	3.81	25.7	4.49E+03
123-146	Stratified deposits of fine to very fine sand, muddy sand, and mud (very finely laminated)	Grayish brown to olive brown (2.5Y5/2 - 4/3)	Moderate (weak to strong) to strong	10.74	21.7	1.58E+03

(a) Multiply by 0.3048 to convert to meters.

SX-108 Slant Borehole (C3082): Sample S0070-7A
Angle Depth: 98.7' - 99.2' Vertical Depth: 84.6' - 85.0'



Figure 2.15. Sample 7A from the Upper Portion (angle depth of 25.9 meters [84.8 feet]) of the Lower Fine Sand and Mud Sequence of the Hanford Formation H2 Unit (Note the thin mud strata sandwiched between two medium to fine sand units.)

The middle portion of the H2 unit (angle depths of 31.7 to 37.5 meters [104 to 123 feet]) appears to be dominated by interstratified sand deposits often exhibiting an upward grading texture ranging from medium sand at the bottom to fine to very fine sand with some mud (silt) at the top. The finer-grained strata appear to be finely laminated, while the coarser-grained strata display no obvious internal structure. These samples were described as dry, but were more uniform in color (ranging from light olive brown [2.5Y6/2] to grayish brown [2.5Y5/2]) and with a strong reaction to hydrochloric acid.

Samples from the lower portion of the H2 unit (angle depths of 37.5 to 44.5 meters [123 to 146 feet]) suggest that these deposits are composed of highly stratified fine to very fine sand and mud to muddy very fine sand. These samples are dry, olive brown (2.5Y4/3) to light olive brown (2.5Y5/3), with a moderate (weak to strong) to strong reaction to hydrochloric acid (Figure 2.16).

The finer-grained strata are massive to very finely laminated and well compacted. The coarser-grained strata are friable with no obvious internal structure.

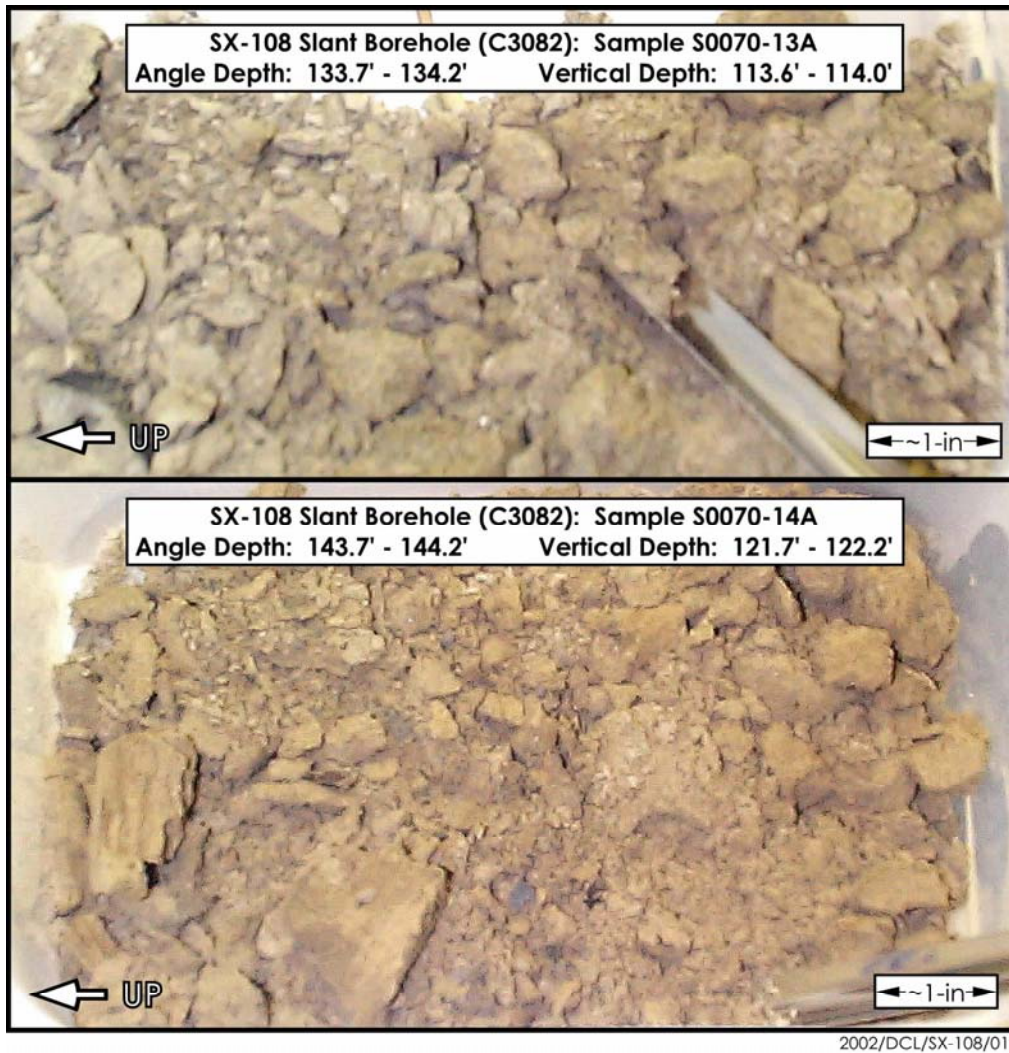


Figure 2.16. Samples 13A (top) and 14A (bottom) from the Lower Portion of the Hanford Formation H2 unit (note fine sand in 13A and the mud in 14A)

2.6.3 Plio-Pleistocene Unit

The Plio-Pleistocene unit includes all material overlying the Ringold Formation and underlying the Hanford formation (including the Early Palouse Soil, the Pre-Missoula Gravels [or equivalent], and the unnamed Hanford formation [?] or Plio-Pleistocene Deposits [?] described by Lindsey et al. 2000). This unit has generally been differentiated from overlying fine-grained Hanford formation sediment by greater calcium carbonate content, more massive structure in core, and high natural gamma response in geophysical logs (DOE 1988; Bjornstad 1990). The upper Plio-Pleistocene mud (PPlz) unit (silt) was penetrated in the SX-108 slant borehole between angle depths of 44.5 to 52.5 meters (146 to 172.2 feet). The lower Plio-Pleistocene carbonate (PPlc) unit lies deeper than the total depth of the borehole and was not encountered.

2.6.3.1 Upper Plio-Pleistocene Mud Unit

Approximately 8 meters (26.2 feet) of the upper PPlz unit was penetrated, yielding an estimated vertical thickness of at least 5.6 meters (18.5 feet). The lower contact of this unit was not encountered.

Three split-spoon samples (15 through 17) were collected from this horizon. Visual examination of these samples suggests that the upper portion of this sequence consists of interstratified mud and muddy very fine sand, with occasional very fine sand (Figure 2.17). These samples are dry to moist, light olive brown (2.5Y5/3) to olive brown (2.5Y4/3), with a generally moderate to strong reaction to hydrochloric acid. The sandier strata are friable and often finely laminated with muddier (siltier) lamina. The muddier strata are very finely laminated with some limonitic staining, fairly well compacted/cemented, and variable in clay content. The gravimetric moisture content ranged from 7.5 wt% in a very fine sand strata to 19.7 wt% in a mud (clayey) strata.



Figure 2.17. Disaggregated Core Sample 17A from the Upper Plio-Pleistocene Mud Unit

3.0 Geochemical Method and Materials

This chapter discusses the methods and philosophy used to determine which samples would be characterized and parameters that would be measured.

3.1 Sample Inventory

Samples were identified using a project-specific prefix, in this case S00070 followed by a specific sample identification suffix such as -01, for each split spoon. As noted in Section 2.0, the cores contained two sleeves identified by the letters A and B, where the A sleeve was always in the position closest to the drive shoe.

3.2 Tiered Approach

During the investigations at 41-09-39, changes in sediment type and contaminant concentrations were noted within a distance of a few inches within a given sleeve. It was concluded that a more methodical scoping approach would be necessary to provide the technical justification for selecting samples for detailed characterization as defined in the data quality objectives process. Subsequently, a tiered method was developed that considered depth, geology (e.g., lithology, grain-size composition, carbonate content, etc.), individual sleeve contaminant concentration (e.g., radionuclides, nitrate, etc.), moisture content, and overall sample quality. Inexpensive analyses and certain key parameters (i.e., moisture content, gamma energy analysis) were performed on sediment from each sleeve.

The objective of the tier 1 characterization was to quantify the extent of penetration of mobile contaminants into the vadose zone sediment. The tier 1 analyses in general showed the same pattern as 41-09-39 where the B sleeve contained more cesium-137 contamination than the A sleeve, reflecting the fact that some sediment from shallower depths (containing more contaminants) was pushed in front of the drive point. The shallower material pushed ahead of the drive point was the first material that was collected in the subsequent sampling event and ended up in the top portion of the B sleeve. Upon homogenization of the B sleeve, the net result was a bias toward higher cesium-137 activities. Because a bimodal distribution of several contaminants was found, this biasing trend in the B sleeves was not followed when the sampler was pushing through the leading edge of the shallower lobe of the bimodal plume. We analyzed only the sediment from the A Sleeve for most constituents except moisture and gamma energy. We did not notice measurable or significant drag-down effects for contaminants that are mainly within the porewater and not concentrated on the sediment sorption sites.

Immediately following the geologic examination, the sleeve contents were subsampled for moisture content, gamma-emission radiocounting (for these samples, effectively cesium-137, potassium-40, uranium-238, and thorium-232 data), one-to-one water extracts (which provide soil pH, electrical conductivity, cation, and nitrate data), total carbon and inorganic carbon content, and 8 M nitric acid extracts (which provide a measure of the total sediment content of contaminants). The remaining sediment from each sleeve was then sealed and placed in cold storage. Later additional aliquots of

selected A sleeves were removed to measure particle size distribution and mineralogy and to squeeze porewater.

3.3 Materials and Methods

During subsampling of the sleeve sample, every effort was made to minimize moisture loss and prevent cross contamination between sleeve samples. Depending on the sample matrix, very coarse pebble and larger material (>32 millimeter) was avoided during subsampling. Larger substrate was excluded to provide moisture contents representative of counting and 1:1 sediment-to-water extract samples. Results from subsample measurements should then take into consideration a possible bias toward higher concentrations for some analytes that would be considered associated with smaller size sediment fractions. The sediment in the Plio-Pleistocene formation contained no large pebbles or cobbles.

Procedures ASTM D2488-93 (1993) and PNL-MA-567-DO-1 (PNL 1990) were followed for visual descriptions and recording of all split-spoon samples. The sediment classification scheme used for geologic identification of the sediment types is based on the modified Folk/Wentworth classification scheme described earlier (see Figure 2.2). However, the mineralogic and geochemical characterization relied on further separation of the mud into discrete silt and clay sizes.

3.3.1 Moisture Content

Gravimetric water contents of the sediment samples from each sleeve were determined using PNNL procedure PNL-MA-567-DO-1 (PNL 1990). This procedure is based on the American Society for Testing and Materials procedure *Test Method for Laboratory Determination of Water (Moisture) Content of Soil and Rock* (ASTM D2216-98 1998). One representative subsample of at least 6 to 40 grams was taken from each sleeve. Sediment samples were placed in tared containers, weighed, and dried in an oven at 105°C until constant weight was achieved, which took at least 24 hours. The containers then were removed from the oven, sealed, cooled, and weighed. At least two weighings, after 24-hour heatings, were performed to ensure that all moisture was removed. All moisture content activities were performed using a calibrated balance. A calibrated weight set was used to verify balance performance before weighing samples. The gravimetric water content was computed as percentage change in soil weight before and after oven drying.

3.3.2 1:1 Sediment-to-Water Extract

The soluble inorganic constituents were determined using a 1:1 sediment-to-deionized-water extract method. This method was chosen because the sediment was too dry to easily extract vadose zone porewater. The extracts were prepared by adding an equal weight of deionized water to approximately 80 grams of sediment subsampled from each sleeve. The weight of deionized water needed was calculated based on the weight of the field-moist samples and their previously determined moisture contents. The appropriate amount of deionized water was added to screw cap jars containing the sediment samples. The jars were sealed and briefly shaken by hand, then placed on a mechanical orbital shaker for 1 hour. The samples were allowed to settle until the supernatant liquid was fairly clear. The

supernatant was carefully decanted and separated into unfiltered aliquots for conductivity and pH determinations, and filtered aliquots (passed through 0.45 μm membranes) for anion, cation, carbon, and radionuclide analyses. More details can be found in Rhoades (1996) within *Methods of Soils Analysis Part 3* (ASA 1996a).

3.3.2.1 pH and Conductivity

Two approximately 3-milliliter aliquots of the unfiltered 1:1 sediment-to-water extract supernatant were used for pH and conductivity measurements. The pHs for the extracts were measured with a solid-state pH electrode and a pH meter calibrated with buffers 4, 7, and 10. Conductivity was measured and compared to potassium chloride standards with a range of 0.001 M to 1.0 M.

3.3.2.2 Anions

The 1:1 sediment-to-water extracts were analyzed for anions using an ion chromatograph. Fluoride, chloride, nitrite, phosphate, sulfate, and oxalate were separated on a Dionex AS4A column with an eluent of 1.75 mM NaHCO_3 /1.85 mM Na_2CO_3 and measured using a conductivity detector following PNL-ALO-212, Rev. 1, which is based on U.S. Environmental Protection Agency (EPA) Method 300.0A (EPA 1984).

3.3.2.3 Cations and Trace Metals

Major cation analysis was performed using an inductively coupled plasma (ICP) unit using high-purity calibration standards to generate calibration curves and verify continuing calibration during the analysis run. Dilutions of 100x, 50x, 10x, and 5x were made of each sample for analysis to investigate and correct for matrix interferences. Details are found in EPA Method 6010B (EPA 2000b). The second instrument used to analyze trace metals, including technetium-99, iodine-129, and uranium-238, was an inductively coupled plasma mass spectrometer (ICP-MS) using the PNNL-AGG-415 method (PNNL 1998). This method is quite similar to EPA Method 6020 (EPA 2000c).

3.3.2.4 Alkalinity and Carbon

The alkalinity and inorganic/organic carbon content of several of the 1:1 sediment-to-water extracts were measured using standard titration with acid and a carbon analyzer respectively. The alkalinity procedure is equivalent to the U.S. Geological Survey Method Field Manual (USGS 2001) <http://water.usgs.gov/owq>. Inorganic and organic carbon on the water extracts were determined using a carbon analyzer and ASTM Method D4129-88 (1988) "Standard Test Method for Total and Organic Carbon in Water by High Temperature Oxidation and by Coulometric Detection."

3.3.3 Porewater Composition

Three samples (12A, 15A, and 17A) were packed in drainable cells that were inserted into an ultracentrifuge. The samples were centrifuged for up to 8 hours and several thousand gs to squeeze the porewater out of the sediment. The pH, electrical conductivity, cation, trace metals, and anions were measured using the same techniques as used for the 1:1 sediment-to-water extracts.

3.3.4 Radioanalytical Analysis

3.3.4.1 Gamma Energy Analysis

Gamma energy analysis was performed on sediment from all sleeves. Gamma energy analysis was performed on water and acid extracts and the three UFA™ (UFA Venture, Richland, Washington) squeezings.

All samples for gamma energy analysis were analyzed using 60%-efficient intrinsic germanium gamma detectors. All germanium counters were efficiency calibrated for distinct geometries using mixed gamma standards traceable to the National Institute of Standards and Technology. Samples analyzed varied from 5 to 80 grams in a fixed geometry. All spectra were background subtracted. Spectral analysis was conducted using libraries containing most mixed fission products, activation products, and natural decay products. Control samples were run throughout the analysis to ensure correct operation of the detectors. The controls contained isotopes with photo peaks spanning the full detector range and were monitored for peak position, counting rate, and full-width half-maximum. Details are found in *Gamma Energy Analysis, Operation, and Instrument Verification using Genie2000 Support Software* (PNNL 1997).

3.3.4.2 Strontium-90

Sediment aliquots were weighed and spiked with strontium-85. Sediment samples were leached overnight with concentrated nitric acid, then an aliquot of the leachate was diluted 50% with deionized water. Leachate aliquots were first passed through the SrSpec columns with 8 M nitric acid to capture strontium, then the resins were washed with 10 column volumes of 8 M nitric acid. The strontium was eluted from the SrSpec column using deionized water. The water extract was evaporated to dryness in a liquid scintillation vial and was ready for counting after adding the cocktail. The purified strontium samples were analyzed by gamma spectroscopy to determine chemical yield from the added tracer and to quantify any contamination from cesium-137. Samples were analyzed by liquid scintillation counting to determine the amount of strontium-90. A matrix spike, a blank spike, a duplicate, and blanks were run with each sample set to determine the efficiency of the separation procedure as well as the purity of reagents. For the most part, the separation procedure was straightforward. Chemical yields were generally good with some explainable exceptions. Matrix and blank spike yields were good, bias was consistent, and blanks were below detection limits.

3.3.4.3 Tritium

The tritium content of selected sediment samples was determined by distillation from 1-gram samples using method PNL-ALO-418 and a Lachat Microdistillation apparatus. The tritium was condensed on special GORE-TEX collectors that were analyzed by liquid scintillation.

3.3.5 Carbon Content of Sediment

The carbon content of borehole sediment samples was determined using ASTM Method D4129-88, *Standard Methods for Total and Organic Carbon in Water Oxidation by High Temperature Oxidation and by Coulometric Detection* (ASTM 1988). Total carbon in all samples was determined using a Coulometrics Inc. Model 5051 Carbon Dioxide Coulometer with combustion at approximately 980°C. Ultrapure oxygen was used to sweep the combustion products through a barium chromate catalyst tube for conversion to carbon dioxide. Evolved carbon dioxide was quantified through coulometric titration following absorption in a solution containing ethanolamine. Equipment output reported carbon content values in micrograms per sample. Soil samples for determining total carbon content were placed into precombusted, tared platinum combustion boats and weighed on a four-place analytical balance. After the combustion boats were placed into the furnace introduction tube, a 1-minute waiting period was allowed so that the ultrapure oxygen carrier gas could remove any carbon dioxide introduced to the system from the atmosphere during sample placement. After this system sparge, the sample was moved into the combustion furnace and titration begun. Sample titration readings were performed at 3 minutes after combustion began and again once stability was reached, usually within the next 2 minutes. The system background was determined by performing the entire process using an empty, precombusted platinum boat. Adequate system performance was confirmed by analyzing for known quantities of a calcium carbonate standard.

Inorganic carbon contents for borehole sediment samples were determined using a Coulometrics, Inc., Model 5051 Carbon Dioxide Coulometer. Soil samples were weighed on a four-place analytical balance, then placed into acid-treated glass tubes. Following placement of sample tubes into the system, a 1-minute waiting period allowed the ultrapure oxygen carrier gas to remove any carbon dioxide introduced to the system from the atmosphere. Inorganic carbon was released through acid-assisted evolution (50% hydrochloric acid) with heating to 200°C. Samples were completely covered by the acid to allow full reaction to occur. Ultrapure oxygen gas swept the resultant carbon dioxide through the equipment to determine inorganic carbon content by coulometric titration. Sample titration readings were performed 5 minutes following acid addition and again once stability was reached, usually within 10 minutes. Known quantities of calcium carbonate standards were analyzed to verify that the equipment was operating properly. Background values were determined. Inorganic carbon content was determined through calculations performed using the microgram-per-sample output data and sample weights. Organic carbon was calculated by subtracting inorganic carbon from total carbon and using the remainder.

3.3.6 8 M Nitric Acid Extract

Approximately 20 grams of oven-dried sediment was contacted with 8 M nitric acid at a ratio of ~5 parts acid to 1 part sediment. The slurries were heated to ~80°C for several hours and then the fluid was separated by centrifugation and filtration through 0.2 µm membranes. The acid extracts were analyzed for major cations and trace metals using ICP and ICP-MS techniques, respectively. The acid digestion procedure is based on EPA SW-846 Method 3050B (EPA 2000a) that can be accessed on-line at <http://www.epa.gov/epaoswer/hazwaste/test/sw846.htm>.

3.3.7 Elemental Analysis

The elemental composition of the bulk sediment and clay fractions was determined by a combination of energy and wavelength dispersive x-ray fluorescence using methods developed at PNNL. Samples analyzed by the energy dispersive x-ray fluorescence method follow the KLM Procedure XRF-01, which utilizes a KEVEX 0810A commercial x-ray fluorescence excitation and detection subsystem. Sample preparation involved mixing the sample in a Coors high-density alumina (Al_2O_3) mortar and pestle. Six hundred milligrams of the mixed sample were removed and further ground to ~300 mesh size, placed between two sheets of stretched para-film, and loaded into the 0810A x-ray fluorescence unit. Acquisition times ranged between 600 and 3,000 seconds, depending on the targets (iron, gadolinium, silver, zirconium). Forty-one elements (aluminum, antimony, arsenic, barium, bromine, cadmium, calcium, cerium, cesium, chlorine, chromium, copper, gallium, indium, iodine, iron, lanthanum, lead, manganese, molybdenum, nickel, niobium, palladium, phosphorous, potassium, rhodium, rubidium, ruthenium, selenium, silicon, silver, strontium, sulfur, tellurium, thorium, tin, titanium, uranium, vanadium, yttrium, and zinc) were analyzed on each sample and the spectrum interpretation was by the backscatter fundamental parameter approach (described in KLM-01, pages 2 and 3). Sample analysis by the wavelength method was accomplished using a Siemens Spectra 3000 instrument, equipped with both a flow counter detector to detect soft radiation of the low Z elements and a scintillation counter detector for the harder radiation of the higher Z elements. Bulk solid samples were prepared by taking 180 to 1,500 milligrams of ~300 mesh ground sample and pressing it into a 3.2-centimeter diameter pellet, using a 27,000-kilogram laboratory press. Standard addition and similar matrix methods were used to generate calibration curves for sodium and magnesium, which were then used to process the data. Additional discussion of x-ray fluorescence techniques for quantitative analysis of sediment are found in Chapter 7 “Elemental Analysis by X-Ray Fluorescence Spectroscopy” of ASA (1996b), part 3, pages 161–223 and in the Siemens Spectra 3000 Reference Manual.

3.3.8 Particle Size Distribution

Both dry sieving and wet sieving/hydrometer methods were used to determine the particle size distribution. For the dry sieving, an aliquot of the oven-dried sediment was sieved through the following sequence of sieves: 4, 2, 1, 0.5, 0.25, 0.212, 0.125, 0.063 millimeters, and pan. Between 120 and 210 grams of oven-dried sediment were used and total mass recovery was measured. An auto shaker, either Rotap Model RX-29 or Gilson SS-8R was used. The method is similar to that in ASTM Method 422-63, *Standard Method for Particle-Size Analysis of Soils* (ASTM 1986).

The second particle-size measurement technique used the wet sieve/hydrometer method (ASA [1986a], part 1; method 15-5 Hydrometer Method [pages 404–408]) and concentrated on quantifying the silt and clay distribution. The silt and clay separates were saved for mineralogical analyses. Samples from the borehole that were used for the hydrometer method were never air or oven dried to minimize the effects of particle aggregation that can affect the separation of clay grains from the coarser material.

3.3.9 Particle Density

The particle density of bulk grains was determined using pycnometers (see ASA 1986b, part 1; method 14-3 Pycnometer Method [pages 378–379]) and oven-dried material. The particle density is needed to determine the particle size when using the hydrometer method.

3.3.10 Mineralogy

The mineralogy of the bulk sample and silt- and clay-size fractions of selected sediment samples were determined by x-ray diffraction techniques. Bulk sediment samples were dispersed by transferring 100 grams of sediment into a 1-liter bottle and mixing with 1 liter of 0.001 M solution of sodium hexametaphosphate. The suspensions were allowed to shake over night to ensure complete dispersion. The sand fraction was separated from the dispersed sample by wet sieving through a #230 sieve. The silt fractions were separated from the clay fractions by using Stoke's settling law described in Jackson (1969). The lower limit of the fraction was taken at >2 microns. Sand and silt fractions were oven dried at 110°C and prepared for x-ray diffraction and x-ray fluorescence analysis.

Each clay suspension was concentrated to an approximate volume of 10 milliliters by adding a few drops of 10N magnesium chloride to the dispersing solution. Concentrations of the clay in the concentrated suspensions were determined by drying known volumes and weighing the dried sediment. The density of the slurry was calculated from the volume pipetted and the final weight of dried sediment. Volumes of slurry equaling 250 milligrams of clay were transferred into centrifuge tubes and treated to remove carbonates following the procedure described by Jackson (1969). The carbonate free clay was then saturated with either magnesium (Mg^{2+}) or potassium (K^+) cations. Clay samples were prepared using the Drever (1973) method and placed onto an aluminum slide for x-ray diffraction analysis. Due to the tendency of the clay film to peel and curl, the magnesium (Mg^{2+})-saturated specimens were solvated with a few drops of a 10% solution of ethylene glycol in ethanol and placed into a desiccator containing excess ethylene glycol for a minimum of 24 hours. Potassium-saturated slides were air dried and analyzed, then heated to 575°C and reanalyzed.

All samples were analyzed on a Scintag x-ray diffraction unit equipped with a Pelter thermoelectrically cooled detector and a copper x-ray tube. Slides of preferentially oriented clay were scanned from 2 to 45 degrees 2θ , and randomly oriented powder mounts were scanned from 2 to 75 degrees 2θ . The bulk samples were prepared by crushing approximately 0.5 gram of sample to a fine powder that was then packed into a small circular holder. After air-drying approximately 0.5 gram of the clay slurry, a random mount was prepared and analyzed from 2 to 75 degrees 2θ .

Semiquantification of mineral phases by x-ray diffraction was performed according to Brindley and Brown (1980). The relationship of intensity and mass absorption to the weight fraction of an unknown phase is expressed as:

$$I/I_p = \mu_p / \mu (wf)$$

where:

I is the intensity of the unknown phase

I_p is the intensity of the pure phase

μ_p is the mass absorption of the pure phase

μ is the average mass absorption of the unknown mixture

wf is the weight fraction of the unknown.

Pure mineral phases of illite, smectite, kaolinite, and chlorite were obtained from the Clay Mineral Society's source clays repository (operated from the University of Missouri in Columbia), and analyzed under the same conditions as the sediment samples. Quartz, feldspars, and calcite standards were purchased from the Excalibur Mineral Company (Peekskill, New York), ground and analyzed on the diffractometer to obtain intensities for pure nonclay phases.

The mass attenuation coefficients of selected samples were measured according to Brindley and Brown (1980). Ground bulk powders and air-dried clays were packed into a 2.39-centimeter (0.94-inch) thick circular holder with no backing. The holder was placed in front of the detector and positioned to allow the x-ray beam, diffracted from pure quartz, to pass through the sample and into the detector. The scan was analyzed from 26 to 27 degrees 2θ . The mass attenuation coefficients were measured directly using the following equation:

$$\mu = (1/\rho x) \ln(I_0/I_x)$$

where:

$1/\rho x$ is the mass per unit area as the sample is prepared

I_0 is the intensity of the incident beam

I_x is the intensity of the transmitted beam through sample thickness x .

In addition to x-ray diffraction, transmission electron microscopy (TEM) characterization of selected samples was conducted on a JEOL 1200X electron microscope equipped with a Link detector system. Samples were prepared for TEM by transferring a small aliquot of a dilute clay slurry onto a formvar carbon coated 3-millimeter copper support grid. The clay solution contained 0.15% tert-butylamine to reduce the surface tension of water.

Structural formulas were derived from data collected from the TEM analysis. On average, an energy dispersive x-ray spectra was collected from a minimum of five particles from the same mineral phase common to the sample. The x-ray spectra were collected and processed using the Cliff-Lorimer Ratio Thin Section method and then converted to a structural formula [based on half-unit cell ($O_{10}(OH)_2$) by the method described in Reynolds and Reynolds (1989) and Newman (1987)].

4.0 Results and Discussion

This section presents the geochemical and physical characterization data collected on sediment from the slant borehole. The tier 1 phase emphasized tests that were inexpensive or that were key to determining the vertical distribution of contaminants. Information on the borehole sediment presented in this section includes moisture content, pH and electrical conductivity of 1:1 water extracts, and measurements of major cations, anions, trace metals, and radionuclides. The particle size and mineralogy of selected samples also were measured to aid in selecting contacts between major geologic units. We also were looking for geochemical and mineralogic changes caused by interaction with the caustic fluids leaking from the tanks.

4.1 Moisture Content

The moisture content of the sediment from each sleeve is listed in Table 4.1 and presented as a graph in Figure 2.9. Figure 2.9 shows both the field volumetric moisture obtained via neutron logging and the gravimetric moisture content of small aliquots of sediment taken during the geologic description activities. The moisture content profile shows one higher moisture region in the Hanford formation H2 laminated sand facies where a silt stringer exists at a vertical depth of 32 meters (105 feet) below ground surface (bgs). At a vertical depth of ~37.2 meters (~122 feet) bgs to the bottom of the borehole at ~43.9 meters (~144 feet) bgs within the Plio-Pleistocene (PPlz) mud, the moisture content increases from 11.95% to 19.70%. There is one sleeve, 16A within the PPlz unit with a lower moisture content of 7.5% by weight. Compared to the other vertical borehole drilled in the SX Tank Farm, the moisture content in the slant borehole sediment from the Hanford formation is notably drier suggesting that the heat and rain shadow from tank SX-108 have kept the sediment drier than other boreholes.

The laboratory-generated data show gravimetric moisture content (wt%) and the field data are related to volumetric water content (vol%). If the field tool was calibrated accurately and the vadose zone bulk density profiles were known, one could convert the field data to gravimetric data by dividing by the bulk density. For our needs, we merely compare the two logs qualitatively to see if the moisture peaks correspond depthwise.

4.2 1:1 Sediment-to-Water Extracts

The main objectives for placing the slant borehole under tank SX-108 were to investigate whether we could find a zone of highly altered sediment from reactions of caustic, high salinity redox tank liquor and to explore the vertical extent of contamination under the suspected worst leaking tank in the SX Tank Farm. In addition to determining the vertical extent of cesium-137 so that comparisons could be made to distributions in the vertical dry wells surrounding the tanks, there was interest in determining whether the mobile contaminants that have reached the groundwater in the southwest corner of SX Tank Farm could be traced all the way to the bottom of the slant borehole. The most economical method of determining

Table 4.1. Moisture Content of Sediment from Slant Borehole

Lithologic Unit	Sample No.	Sample Depth (Vertical ft) ^(a)	% Moisture
H1A	01B	54.5-54.9	ND
H1A	01A	54.9-55.3	4.33
H1	02B	63.0-63.5	NS
H1	02A	63.5-63.7	NS
H1	03B	67.3-67.7	3.76
H1	03A	67.7-68.1	2.76
H1	04B	71.5-71.9	3.55
H1	04A	71.9-72.4	2.77
H2	05B	75.7-76.2	6.48
H2	05A	76.2-76.6	4.69
H2	06B	79.9-80.4	3.50
H2	06A	80.4-80.8	3.68
H2	07B	84.1-84.6	6.60
H2	07A	84.6-85.0	6.18
H2	08B	88.3-88.8	4.52
H2	08A	88.8-89.2	6.02
H2	09B	92.5-92.9	5.32
H2	09A	92.9-93.3	2.35
H2	10B	96.6-97.1	4.62
H2	10A	97.1-97.5	1.91
H2	11B	101.0-101.5	5.50
H2	11A	101.5-101.9	3.15
H2	12B	104.9-105.4	7.02
H2	12A	105.4-105.8	21.35
H2	13B	113.1-113.6	7.95
H2	13A	113.6-114.0	7.64
H2	14B	121.3-121.7	8.51
H2	14A	121.7-122.2	11.95
PPlz	15B	129.4-129.9	17.50
PPlz	15A	129.9-130.3	17.42
PPlz	16B	137.5-138.0	15.13
PPlz	16A	138.0-138.4	7.50
PPlz	17B	144.0-144.4	14.49
PPlz	17A	144.4-144.9	19.70
(a) Multiply by 0.3048 to convert to meters. ND = Not determined. NS = No sample.			

the distribution of the mobile contaminants in the vadose zone sediment is to use the water extracts because most of the sediment is too dry to readily extract porewater. The following sections discuss the results of the analysis done in the water extracts.

4.2.1 pH and Electrical Conductivity

The pH and electrical conductivity for the water extracts are shown in Table 4.2 and Figure 4.1. The electrical conductivity has been corrected for the dilution with deionized water, but the pH is plotted as measured.

The pH profile shows that between 16.8 and 25.9 meters (55 and 85 feet) bgs (in the Hanford formation H1a, H1, and top of the H2), there are elevated values suggesting the presence of caustic waste interaction. One sample within this interval, 6A, had a water extract pH of only 8, which causes the vertical profile to appear bimodal.

Table 4.2. Water Extract pH and Electrical Conductivity Values

Sample ID	Vertical Depth (ft) ^(a)	Dilution Factor	1:1 pH	1:1 EC mS/cm	Pore EC mS/cm
01A	55.1	23.13	9.16	0.404	9.34
02A	63.02	NS	NS	NS	NS
03AB	67.9	36.88	9.58	0.701	25.85
04A	72.2	36.15	9.54	0.576	9.57
05A	76.4	21.36	9.78	0.877	14.21
06A	80.6	27.18	8.00	16.71	454.2
07A	84.8	16.20	9.55	54.62	1166.5
08A	89.0	16.61	7.83	49.01	1771.6
09A	93.1	42.56	7.88	31.76	1009.3
10A	97.3	52.34	8.23	25.56	1337.7
11A	101.7	31.78	8.38	13.93	592.8
12A	105.6	4.69	8.02	2.36	11.04
13A	113.8	13.38	7.99	29.78	398.4
14A	122.0	8.69	7.82	30.24	262.8
15A	130.1	5.74	7.45	40.01	229.7
16A	138.2	13.31	7.24	5.80	77.16
17A	144.6	5.08	7.22	3.47	17.63

(a) Multiply by 0.3048 to convert to meters.
 EC = Electrical conductivity.
 NS = No sample was available.

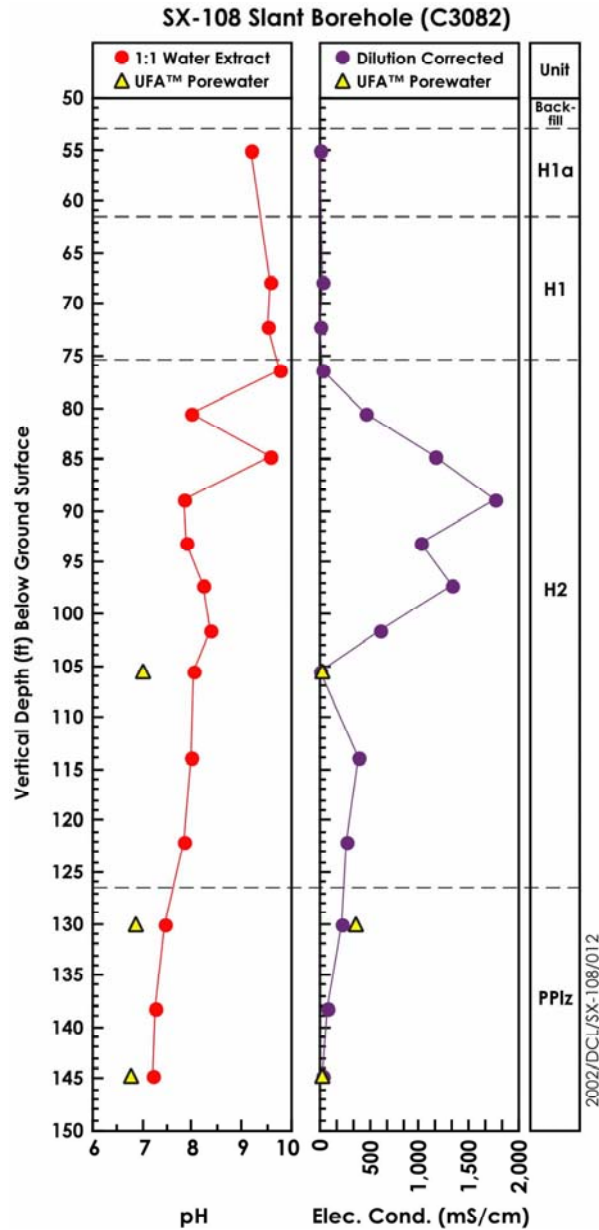


Figure 4.1. pH and Electrical Conductivity for Calculated (from sediment-to-water extracts) and Actual Porewaters for Slant Borehole Sediment

The elevated pH values range from 9.16 to 9.78 in the shallower zone and reach 9.55 in the deeper zone. These two elevated pH zones are within the lower portion of the Hanford formation H1a, Hanford formation H1 coarse unit, and within the upper portion of the Hanford formation H2 laminated sand. If the value for sample 6A is accurate, the pH profile is rather variable and not easy to interpret. Because so many chemical reactions can affect the pH, it is not possible to determine whether the tank leak fluid traveled mainly in a vertical direction or spread horizontally resulting in a complicated vertical profile at this borehole. The simplest description would place less weight on the 6A sample, then the elevated pH

plume would occur from the tank bottom 15.5 meters (~51 feet) bgs to 25.9 meters (85 feet) bgs. The elevated pH region would be ~10.4 meters (~34 feet) thick and include the H1a, H1, and the upper 2.7 meters (9 feet) of the H2 unit.

The porewater electrical conductivity (calculated by multiplying the water extract electrical conductivity by the dilution factor) shows a two-lobed elevated plume between 24.6 and 31 meters (80.6 and 101.7 feet) bgs and a much smaller and deeper third lobe between 34.7 and 42.1 meters (113.8 and 138.2 feet) bgs. It would appear that the leaking fluid traveled through the three Hanford facies such that the leading edge of the plume now resides in the fine-grained Plio-Pleistocene sediment. There appears to be a thin lens of sediment that has not been contacted with much of the tank liquor at 32.2 meters (105.6 feet) bgs. This sample is a fine-grained lens within the Hanford formation H2 laminated sand. It has high moisture content but relatively low salt content and little indication of tank liquor impact. Perhaps this sample represents a fine-grained lens that has very low permeability such that it was bypassed by the tank liquor. If we ignore the sample at 32.2 meters (105.6 feet) bgs, then the electrical conductivity plume simplifies to a plume with a peak at 27.1 meters (89 feet) bgs and a leading edge that reaches the vertical extent of the borehole.

The three porewaters that were extracted from the sediment using an ultracentrifuge are compared with equivalent dilution-corrected 1:1 water extracts from the same depth in Table 4.3. The three UFA™ squeezings were performed on one sample from the bottom of the H2 unit and two samples from the PPlz unit below the zone where the water extracts suggest that there is evidence of caustic reactions, thus all the pH values are within the normal range. The actual porewater electrical conductivity is somewhat higher than the dilution-corrected 1:1 water extracts. Aside from the fact that the aliquots used from each sleeve were different, there is no chemical explanation as to why the UFA extracts would have a higher electrical conductivity value than the dilution-corrected 1:1 water extracts. In many cases for

Table 4.3. Comparison of Actual Porewater pH and Electrical Conductivity with Dilution-Corrected 1:1 Water Extract Values

Sample ID	Depth (ft) ^(a)	Dil. Fac.	pH	1:1 EC $\mu\text{S/cm}$	Pore EC $\mu\text{S/cm}$
12A	105.6	4.69	8.02	2.36	11.0
12A-ufa		-	7.03	-	14.0
15A	130.1	5.74	7.45	40.0	230
15A-ufa		-	6.89	-	352
17A	144.6	5.08	7.22	3.47	17.6
17A-ufa		-	6.79	-	35.2
(a) Multiply by 0.3048 to convert to meters. EC = Electrical conductivity. ufa represents the actual porewater obtained by ultracentrifugation.					

uncontaminated and slightly contaminated sediment, the UFA extracts show lower electrical conductivity values than the dilution-corrected 1:1 water extracts because the 1:1 sediment-to-water extracts often dissolve material not present in the vadose zone porewater.

4.2.2 Water Extract and Porewater Compositions

The 1:1 sediment-to-water extracts and the calculated porewater anion composition are shown in Table 4.4 and Figures 4.2a and 4.2b. There is obvious nitrate contamination starting at about 20.7 meters (67.9 feet) bgs and extending down into the sediment of the fine-grained PPLz all the way to the bottom of the borehole at 44.1 meters (144.6 feet) bgs. The majority of the nitrate contamination resides between 24.6 and 39.7 meters (80.6 and 130.1 feet) bgs with values reaching as high as 994 g/L or 16 M at 29.7 meters (97.3 feet) bgs. The vertical extent of the nitrate plume is greater than the deepest sample analyzed, 44.1 meters (144.6 feet) bgs, PPLz. The nitrite and chloride profiles show elevated (compared to sediment from clean boreholes) concentrations between 23.3 meters (76.4 feet) bgs and the bottom of the borehole. Both show the highest concentrations at 29.6 meters (97.2 feet) bgs with values of 3.1 and 6.7 g/L. The sulfate profile is a bit different. There is elevated sulfate between 24.6 and 39.7 meters (80.6 and 130 feet) bgs. The maximum concentration is found at 28.4 meters (93 feet) bgs (all the others peak at 29.6 meters [97 feet] bgs) with a value of 24 g/L. All the anion profiles show that the sample at 32.2 meters (105.6 feet) bgs has a local minimum in anion concentrations similar to the electrical conductivity profile. We believe that this sample is an isolated low-permeability zone that did not have much tank liquor advect through the sediment.

Figure 4.2b shows the profiles for inorganic carbon and alkalinity (both converted to bicarbonate concentrations) for the 1:1 sediment-to-water extracts. We did not make dilution corrections back to vadose zone porewater concentrations because carbonate dissolution is occurring during the extraction. Compared to uncontaminated porewaters, there is elevated inorganic carbon/alkalinity in most of the profile. The alkalinity values in general are larger than the inorganic carbon suggesting that some other constituents in the extracts are consuming H^+ . We have not determined what geochemical significance to place on the dissolved inorganic carbon and alkalinity data.

Therefore, it appears that the anion data, which are generally good indicators of all mobile contaminants, show that tank fluids have contacted the sediment at this borehole from the bottom of the tank to the bottom of the borehole. The bulk of the tank liquor still resides in the vadose zone within the Hanford formation H2 laminated sand. The highest concentrations are found between 28.3 and 29.6 meters (93 and 97 feet) bgs within the H2 unit. The leading edge of the plume has reached or gone beyond the total depth of the slant borehole at 44.1 meters (144.6 feet) bgs.

Compared to borehole 41-09-39, the tank liquor plume has traveled deeper. As discussed in Serne et al. (2002a), the majority of the 41-09-39 plume still resides in the shallower coarse-grained H1 unit. Compared to the SX-115 leak plume that predominately resides in the PPLz unit (see Serne et al. 2002b), the SX-108 plume center of mass did not travel as far below the tank. As found at 41-09-39 and SX-115, sulfate is more reactive with the sediment and does not travel as deeply as nitrate, nitrite, and chloride.

Table 4.4. Anion Content of Water Extracts of Slant Borehole Sediment

ID	Depth	Dil. Fac.	water:soil Ratio	1:1 Extracts in mg/L							Dilution Corrected Porewater mg/L						
				Nitrate	Fluoride	Nitrite	Chloride	Sulfate	Phosphate	Alk ^(a)	Nitrate	Nitrite	Chloride	Sulfate	Phosphate	Fluoride	Alk ^(a)
1A	55.1	23.13	1.00	6.95	1.94	<0.1	1.76	20.0	<0.5	211	161	<2.31	40.7	462	<11.6	44.7	4,884
1A-Dup	55.1	23.13	1.00	6.07	1.71	<0.1	1.27	17.5	<0.5	519	140	<2.31	29.4	405	<11.6	39.6	12,007
3AB	67.9	36.88	1.02	29.1	3.69	0.36	3.38	21.7	0.87	382	1,072	13.1	125	801	0.88	136	14,105
4A	72.2	36.15	1.00	23.5	2.27	0.31	1.51	11.5	0.68	387	851	11.2	54.7	415	0.68	81.9	13,977
5A	76.4	21.36	1.00	92.9	3.24	0.34	3.92	27.3	1.06	407	1,984	7.30	83.8	584	1.06	69.3	8,701
6A	80.6	27.18	1.00	11,743	ND	ND	<10	70.9	<5	587	319,225	ND	<272	1,926	<136	ND	15,945
7A	84.8	16.20	1.00	46,645	<10	ND	26.0	607	<50	1,702	755,649	ND	421	9,833	<810	<162	27,577
8A	89.0	16.61	1.00	39,713	<10	87.5	83.3	566	<50	886	659,796	1453	1,383	9,412	<831	<166	14,725
9A	93.1	42.56	1.00	22,852	<10	57.1	123	566	<50	504	972,499	2429	5,213	24,092	<2,128	<426	21,439
10A	97.3	52.34	1.00	18,994	<10	59.0	128	276	<50	484	994,113	3088	6,713	14,465	<2,617	<523	25,335
11A	101.7	31.78	1.00	9,524	<1	<10	130	46.8	<50	130	302,677	318	4,121	1,486	<1,589	<31.8	4,130
12A	105.6	4.69	1.00	1,535	<1	<1	23.3	31.4	<5	100	7,191	<46.9	109	147	<23.4	<4.69	467
13A	113.8	13.38	1.02	22,223	<10	72.5	213	293	<50	704	297,334	970	2,846	3,923	<669	<134	9,418
14A	122.0	8.69	1.04	21,496	<10	46.3	187	339	<50	389	186,815	402	1,624	2,945	<435	<86.9	3,381
14A-Dup	122.0	8.38	1.00	24,084	<10	31.9	212	387	<50	436	201,786	267	1,773	3,246	<419	<83.8	3,650
15A	130.1	5.74	1.00	34,574	<10	34.4	331	507	<50	541	198,485	198	1,903	2,908	<287	<57.4	3,104
16A	138.2	13.31	1.00	4,193	<1	<10	56.2	11.4	<5	219	55,822	<133	749	151	<66.6	<13.3	2,914
17A	144.6	5.08	1.00	2,395	<1	<1	34.7	11.6	<5	123	12,155	<5.08	176	59.1	<25.4	<5.08	622

(a) Alk = Alkalinity as mg/L of calcium CO₃.
 ND = Not determined.
 Depths represent vertical depth in feet below ground surface (multiply by 0.3048 to convert to meters).

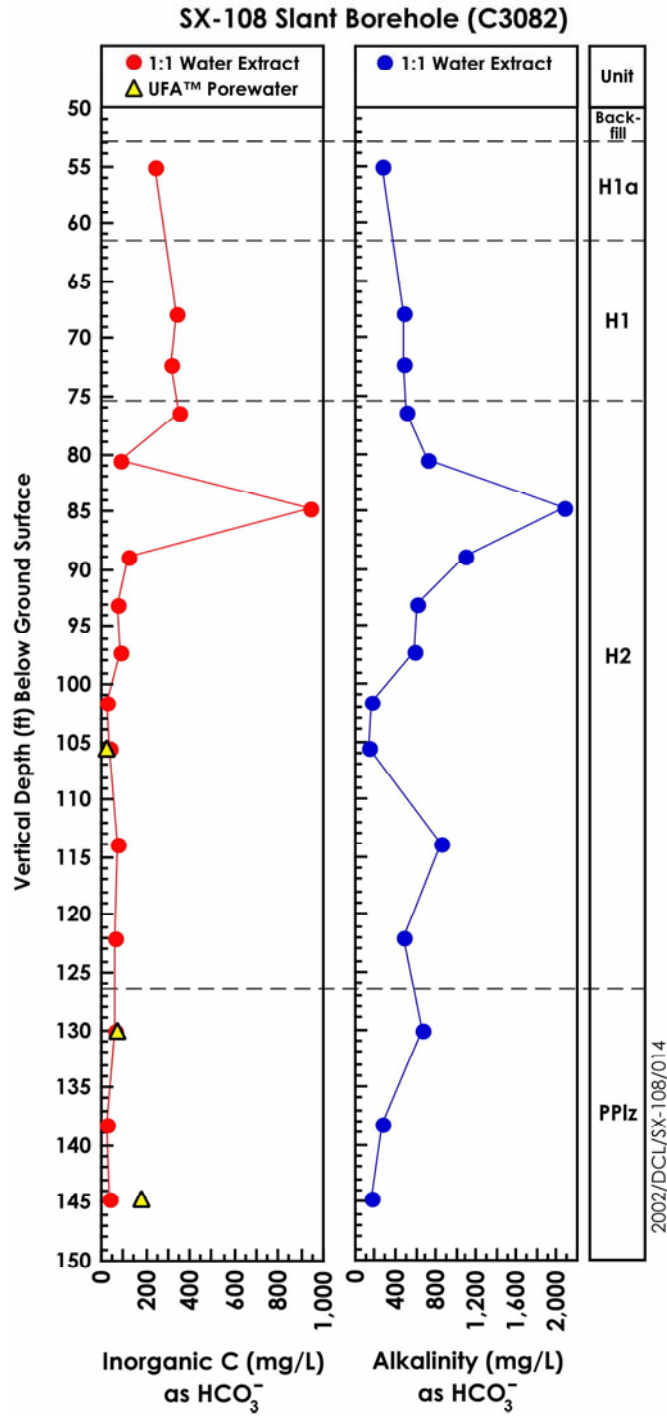


Figure 4.2b. 1:1 Sediment-to-Water Extract Inorganic Carbon and Alkalinity Contents for the Slant Borehole Sediment under SX-108

There also is a fine-grained lens at 32.2 meters (105.6 feet) bgs within the H2 unit that has not been in contact with as much of the concentrated tank liquor as the surrounding sediment both above and below.

Table 4.5 shows the comparison of the calculated porewater composition (from the sediment to water extracts) with the actual porewaters. The comparison is hampered by our inability to meticulously homogenize the sediment samples (because of worker dose and need to minimize the potential for airborne contamination from the very dry fine-grained fractions of silt/clay within the samples). Thus, some of the variation could be sample heterogeneity.

As found for the electrical conductivity comparison, the actual porewater anion composition has slightly larger concentrations of anions (all three cases for nitrate and chloride and in one case for sulfate) than the calculated porewaters from water extracts. There are plausible explanations for the dilution-corrected water extracts (i.e., calculated porewaters) having larger concentrations, but we cannot offer an explanation for the observed opposite trend found for the slant borehole analyses.

All-in-all, based on the profiles shown in Figure 4.2a, the anion data for porewater in the vadose zone sediment, either calculated from water extracts or directly measured, give a good indication of the vertical extent of penetration of the bulk of the leaked fluid. All the anion profiles show rapidly decreasing concentrations at the vertical extent of the borehole.

Table 4.6 shows the calculated concentrations of cations in the porewater from the vadose zone sediment at the slant borehole obtained by dilution correction of the 1:1 sediment-to-water extracts. The distributions of several of the cations versus depth are shown in Figure 4.3. The depth profiles for the divalent alkaline earth cations barium, calcium, magnesium, and strontium show remarkable similarities as do the monovalent alkali cations sodium and potassium. Each of the divalent cations shows a large

Table 4.5. Comparison of Calculated with Actual Porewater Anion Concentrations for Slant Borehole Vadose Zone Sediment

Sample ID	Depth (ft) ^(a)	Dil. Fac.	Dilution Corrected Porewater mg/L						
			Nitrate	Nitrite	Chloride	Sulfate	Phosphate	Fluoride	Alk ^(b)
12A	104.92	4.69	7,191	<47	109	147	<23.4	<4.69	467
12A-ufa			9,348	<5	152	60	<25	<2.5	NA
15A	129.44	5.74	198,485	198	1,903	2,908	<287	<57.4	3104
15A-ufa			230,227	<200	2,364	3,481	<100	<5	NA
17A	143.99	5.08	12,155	<5.08	176	59	<25.4	<5.1	622
17A-ufa			23,171	<17	364	27	<83	<8.3	NA

(a) Multiply by 0.3048 to convert to meters.
(b) Reported as mg/L of calcium CO₃
ID notes: ufa represents the actual porewater obtained by ultracentrifugation
NA = Not analyzed.

Table 4.6. Calculated Porewater Cation Composition from Water Extracts of Vadose Zone Sediment from Slant Borehole

ID	Depth (ft bgs) ^(a)	Dil. Fac.	water:soil Ratio	Al $\mu\text{g/L}$	Ba $\mu\text{g/L}$	Ca mg/L	Fe $\mu\text{g/L}$	K mg/L	Mg mg/L	Na mg/L	Si mg/L	Sr $\mu\text{g/L}$	SO ₄ mg/L	Mn $\mu\text{g/L}$
1A	55.1	23.13	1.00	16,351	(375)	28.23	16,197	(77)	(5.7)	2,378	420	(259)	451	(585)
1A-Dup	55.1	23.13	1.00	15,702	(409)	25.51	14,623	(82)	(5.3)	2,344	398	57.4	427	(526)
3A	67.9	36.88	1.02	66,585	1,073	(34.97)	67,342	(131)	27.18	6,829	734	(265)	855	(1,349)
4A	72.2	36.15	1.00	50,399	(819)	(32.95)	56,108	(86)	(16.9)	7,195	865	692	526	(882)
5A	76.4	21.36	1.00	26,641	(468)	(17.97)	29,374	(43)	(4.8)	5,716	367	5,340	657	(375)
6A	80.6	27.18	1.00	10,769	(223)	1,647.9	9,997	703	101	153,069	(193)	8,131	2,329	<1,359
7A	84.8	16.20	1.00	8,598	2,809	39.59	8,481	1,339	(3.3)	345,472	170	2,794	10,402	<810
8A	89.0	16.61	1.00	(3,405)	(207)	1,966	(3,397)	2,961	118	305,019	(99)	31,612	10,320	<831
9A	93.1	42.56	1.00	(4,924)	(527)	4,303	(5,271)	4,388	151	370,034	(225)	45,684	22,196	<2,128
10A	97.3	52.34	1.00	(11,869)	1,695	1,821.3	(12,356)	3,604	128	391,103	(295)	36,890	13,276	<2,617
11A	101.7	31.78	1.00	<7,945	29,778	37,905	<7,945	1,358	3,143	65,257	(285)	421,747	1,902	1,813
12A	105.6	4.69	1.00	(929)	1,739	1,309	(929)	87	213	691	66	7,485	113	(91)
13A	113.8	13.38	1.02	(2,006)	548	1,583	(2,124)	1,001	137	110,749	(102)	23,332	3,600	<669
14A	122.0	8.69	1.04	(1,297)	653	1,678	(1,297)	566	163	68,587	(74)	27,027	2,836	<435
14A-Dup	122.0	8.38	1.00	(1,146)	587	1,855	(1,125)	611	175	73,859	(71)	29,976	3,042	<419
15A	130.1	5.74	1.00	(370)	507	2,555	(357)	555	270	70,723	82	37,277	2,891	<287
16A	138.2	13.31	1.00	(577)	18,286	10,030	(577)	348	2,259	4,404	164	64,992	147	2,287
17A	144.6	5.08	1.00	(412)	3,519	2,169	(412)	113	593	649	60	11,816	59	541

(a) Multiply by 0.3048 to convert to meters.
 ID notes: Dup represents a duplicate water extract on a separate aliquot of sediment. Note that some analytes are reported as $\mu\text{g/L}$ and others as mg/L . Depth represents the vertical depth in feet; the sulfur values have been converted to sulfate to allow comparison to the anion data in Table 4.4.

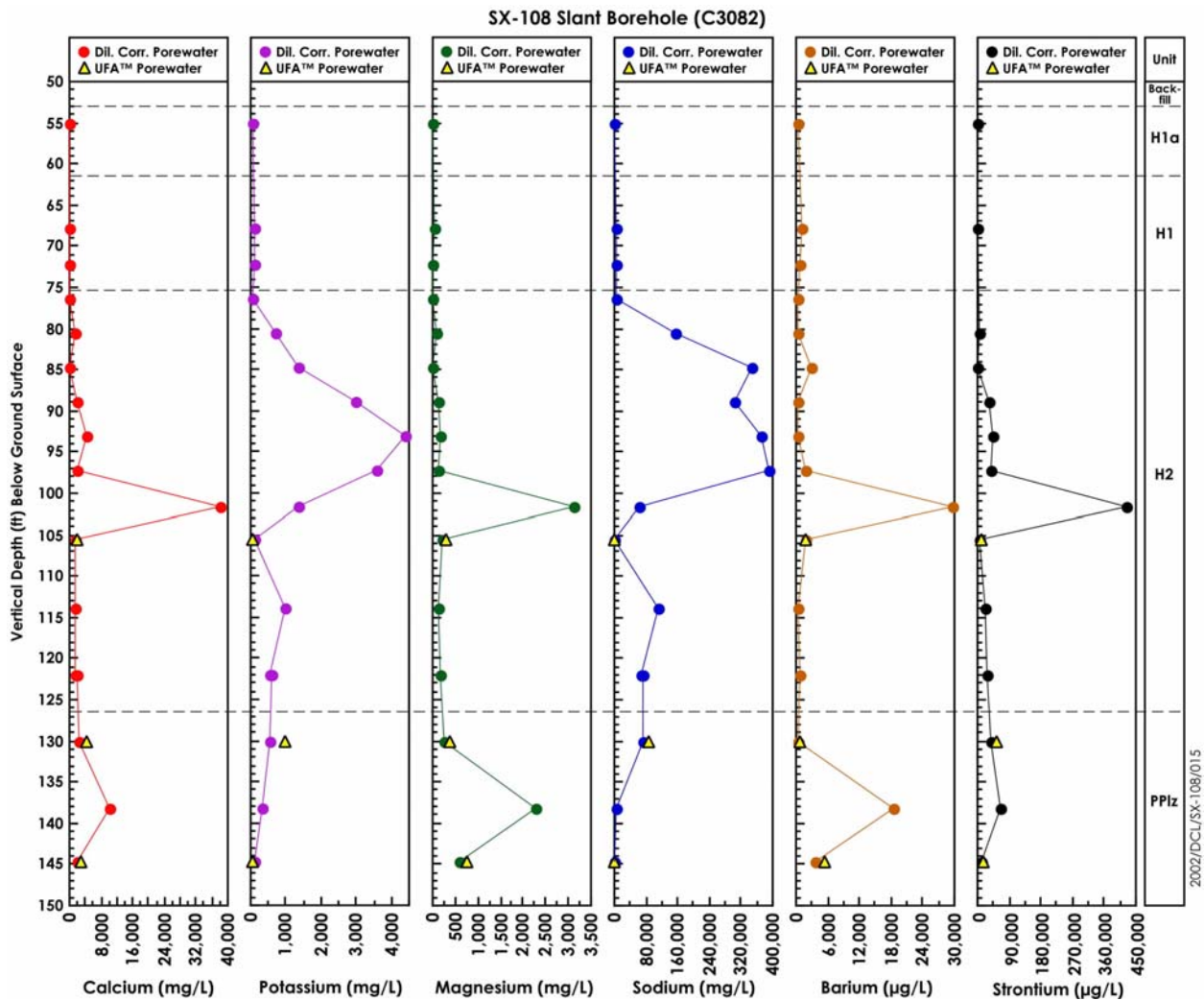


Figure 4.3. Cations Calculated (from sediment-to-water extracts) and Actual Porewaters for Slant Borehole Sediment

increase in the amount that is water extractable for the sample at 31 meters (101.7 feet) bgs within the H2 unit. Peak concentrations range from 30 mg/L for barium, 38 g/L for calcium, 3 g/L for magnesium, and 421 mg/L for strontium. The concentrations then drop rapidly at 32 meters (105 feet) bgs before rising again to form a second smaller peak at 42.1 meters (138.2 feet) bgs. This second peak has 18 mg/L barium, 10 g/L calcium, 2.3 g/L magnesium, and 65 mg/L strontium. Below 42.1 meters (138.2 feet) bgs, the concentrations of the divalent cations again drop and remain low to the bottom of the borehole. However, the concentrations in the deepest sediment sample are still greatly elevated compared to uncontaminated sediment. The bimodal distribution appears to be real, suggesting two leak events, with the first being of lower concentration and perhaps larger volume. The bimodal distribution is not caused solely by the apparent lens of less permeable sediment at 32.2 meters (105.6 feet) bgs that was discussed above while describing the anion distributions. There are also other plausible explanations for the bimodal distribution of water-leachable cations such as complicated evaporation-condensation water cycles caused

by the heat load from the tanks (see the science and technology modeling efforts discussed in the field investigation report).^(a)

The sodium water extractable/calculated porewater composition shows a distribution that differs from the divalent cations. Elevated concentrations of sodium in porewater start at 23.3 meters (76.4 feet) bgs but the first peak occurs at 29.7 meters (97.3 feet) bgs with a concentration of 391 g/L. The sodium peak concentration is 1.3 meters (4.4 feet) shallower than the divalent cation peaks. We suggest that the sodium in the tank liquor is exchanging for the divalent cations that constitute ~90 to 95% of the exchange sites on natural Hanford sediment (see Serne et al. 2002c). The ion exchange reactions push the divalent cations out in front of the sodium tank liquor plume.

The second deeper plume for monovalent cations occurs at 34.7 meters (113.8 feet) bgs for both potassium and sodium. The concentration maxima for the second smaller peaks are 1.1 g/L and 111 g/L for the potassium and sodium, respectively. The second peak for the monovalent cations is 7.4 meters (24.4 feet) shallower than the depth for the second peak in the divalent cations. The ion exchange reactions, especially for the borehole 299-W23-19 near SX-115, have been modeled by the Science and Technology Program, which was funded by the Vadose Zone/Groundwater/Columbia River Integration program. They have shown that the separation between the peaks of the divalent and monovalent cations increases as the concentration of the monovalent cations in the invading tank liquor decreases. Thus, the greater separation in the peaks for the deeper plume agrees with the hypothesis that the first leak was more dilute than the second leak. This could occur if the amount of concentration in the tank from self-boiling was significantly different prior to the separate leak events. Again, there are other plausible scenarios that could be the cause of the bimodal distribution of water-leachable cations in the slant borehole vadose zone sediment.

Assuming that the slant borehole penetrated almost the entire zone of contamination, the bulk of the leaked fluid under tank SX-108 currently resides in H2 fine-grained laminated sand. The leading edge is within the PPlz unit; we did not find the maximum vertical extent. The maximum sodium concentration in the porewater is calculated to be 17 M in agreement with the maximum nitrate concentration. This concentration is above the solubility of nitrate at the temperatures that the extractions and ultracentrifugations were performed. Thus, the identification of sodium nitrate solids in the bulk sediment (discussed below in the mineralogy section) is consistent with the water extracts. Based on thermodynamic modeling performed by the Science and Technology Program, the solubility of sodium nitrate at the temperature in the formation sediment (see Figure 2.9) 17 M is very close to saturation. Therefore, we cannot state that the sediment in the formation contains solid sodium nitrate at the current elevated temperatures. It is plausible that solid sodium nitrate may exist in the dry sediment below the tank from the complicated and time varying heat source that can cause water-water vapor convection cells to occur.

The comparison of the actual porewaters, obtained by ultracentrifugation, with the dilution-corrected water extracts is shown on Figure 4.3 and Table 4.7. We did not attempt to obtain vadose zone porewaters out of the most contaminated samples because of worker dose concerns and concerns that the

(a) *Draft Field Investigation Report for Waste Management Area S-SX*. RPP-7884, Draft, Volume 2, Appendix D, CH2M HILL Hanford Group, Inc., Richland, Washington.

expensive ultracentrifuge could get contaminated and thus restricted from other uses. As found for the anions, the actual porewaters have higher concentrations of most of the cations than the dilution-corrected water extracts. We have no explanation for this discrepancy. However, as shown in Figure 4.3, the comparison of the actual porewaters with the dilution-corrected water extracts agrees adequately to define the vertical distribution of the vadose zone pore fluids that suggest a bimodal distribution is present.

The agreement between the total sulfur measured by inductively coupled plasma (ICP), converted to sulfate, with the direct determination of sulfate in the water extracts by ion chromatography is shown in Table 4.8 and Figure 4.2a. In general, the agreement is excellent, thus showing that all the water-extractable sulfur is in fact sulfate.

The sulfate plume maximum occurs at 28.4 meters (93.1 feet) bgs with a value of 22 g/L. The second plume maximum is at 34.7 meters (113.8 feet) bgs with 3.6 g/L. Sulfate concentrations drop to background levels in sample 17A, 44.1 meters (144.6 feet) bgs.

Tables 4.6 and 4.7 and Figure 4.4 show the porewater concentration of aluminum, iron, silicon, and manganese. The shallow sediment shows that higher concentrations of aluminum and iron are water extractable, perhaps signifying the presence of more amorphous aluminum and iron compounds from the reaction of the native sediment with the caustic tank fluids with subsequent precipitation of solids.

Tables 4.9 and 4.10 show the dilution-corrected 1:1 sediment-to-water extract trace metal concentrations and comparison of the calculated porewater versus the actual porewater trace metal composition, respectively. The vertical distributions of several trace metal porewater concentrations are shown in Figures 4.5a and 4.5b. Table 4.9 and Figure 4.5a show that there are extremely elevated

Table 4.7. Comparison of Actual to Calculated (from 1:1 water extracts) Porewaters—Cations

ID	Depth (ft bgs) ^(a)	Dil. Fac.	water:soil Ratio	Dilution Corrected Porewater										
				Al μg/L	Ba μg/L	Ca mg/L	Fe μg/L	K mg/L	Mg mg/L	Na mg/L	Si mg/L	Sr μg/L	SO4 mg/L	Mn μg/L
12A	104.92	4.69	1.00	(929)	1,739	1,309	(929)	87.2	213	691	66.4	7,485	113	(91)
12A-ufa				(204)	1,847	1,957	<500	56	284	741	28.4	10,611	60	231
15A	129.44	5.74	1.00	(370)	507	2,555	(357)	555	270	70,723	82.5	37,277	2,891	<287
15A-ufa				416	775	4,356	2,162	969	372	85,160	14.5	54,366	3,330	<125
17A	143.99	5.08	1.00	(412)	3,519	2,169	(412)	113	593	649	59.9	11,816	59	541
17A-ufa				413	5,275	3,127	(92)	60.7	762	599	24.7	17,203	27	706

(a) Multiply by 0.3048 to convert to meters.
 ID notes: ufa represents the actual porewater obtained by ultracentrifugation. Note that some analytes are reported as μg/L and others mg/L. Analytes in parentheses are below the limit of quantification, but the value is still believed to be reliable.

Table 4.8. Comparison of ICP Sulfur as Sulfate with IC Sulfate for Water Extracts and Porewaters

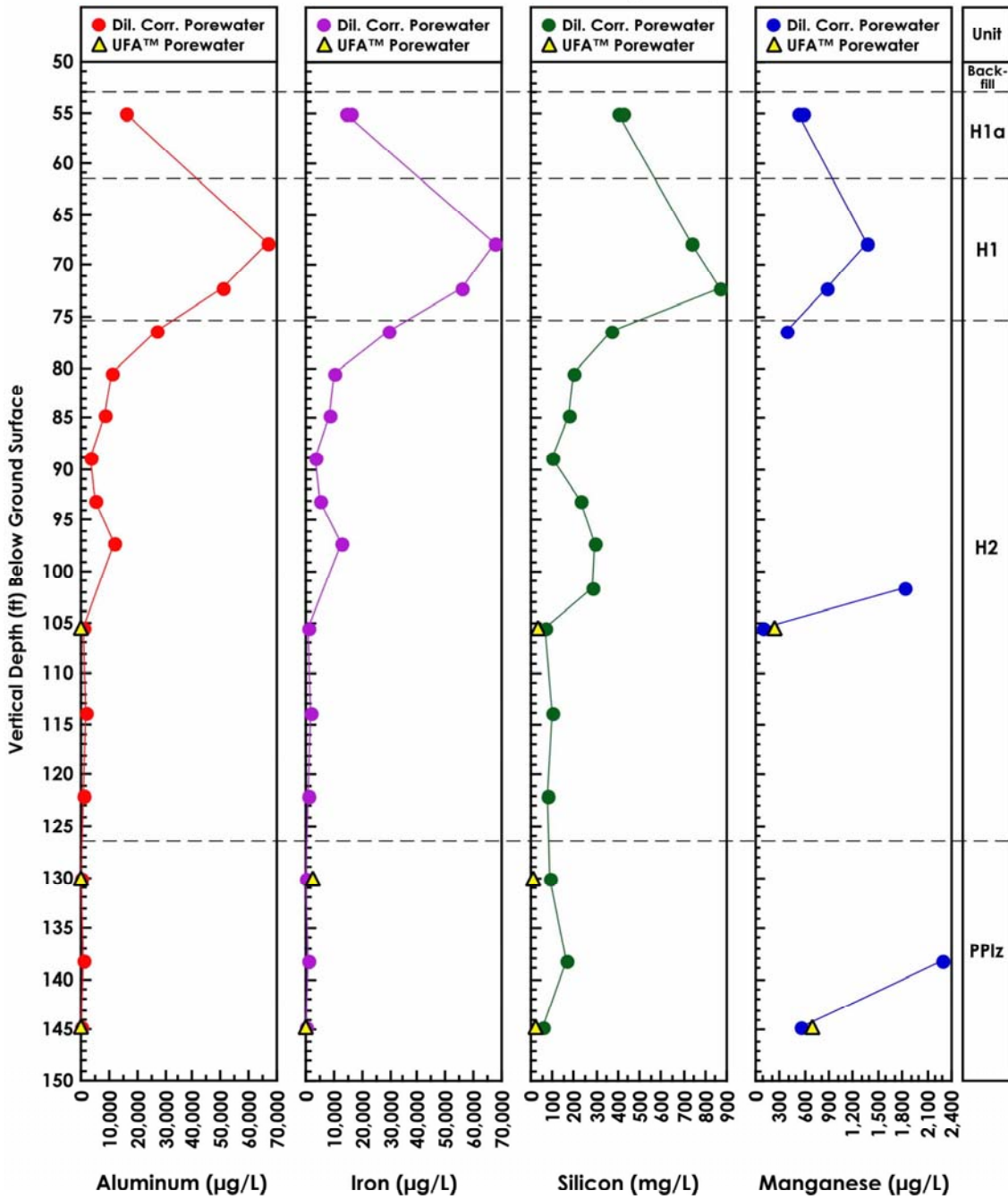
Sample ID	Depth (ft bgs) ^(a)	Strata	Sulfate		
			ICP ^(b) mg/L	IC mg/L	Difference %
1A	55.1	H1a	451	462	2.4
1A-Dup	55.1	H1a	427	405	5.2
3A	67.9	H1	855	801	6.5
4A	72.2	H1	526	415	23.7
5A	76.4	H2	657	584	11.8
6A	80.6	H2	2,329	1,926	18.9
7A	84.8	H2	10,402	9,833	5.6
8A	89	H2	10,320	9,412	9.2
9A	93.1	H2	22,196	24,092	8.2
10A	97.3	H2	13,276	14,465	8.6
11A	101.7	H2	1,902	1,486	24.6
12A	105.6	H2	113	147	25.8
12A-ufa	105.6	H2	60	60	0
13A	113.8	H2	3,600	3,923	8.6
14A	122	H2	2,836	2,945	3.8
14A-Dup	122	H2	3,042	3,246	6.4
15A	130.1	PPlz	2,891	2,908	5.9
15A-ufa	130.1	PPlz	3,330	3,481	4.4
16A	138.2	PPlz	147	151	2.7
17A	144.6	PPlz	59	59.1	0.8
17A-ufa	144.6	PPlz	27	<83.5	"---"

(a) Multiply by 0.3048 to convert to meters.
(b) Sulfur is measured and converted to sulfate by the following equation: $(96.066/32.066) \times \text{ICP measured sulfur value (mg/L)}$.

ID notes: ufa represents the actual porewater obtained by ultracentrifugation.

concentrations of chromium, selenium, and technetium-99 in the vadose zone porewater. There is also elevated molybdenum and perhaps arsenic in the sediment. The elevated concentrations of most of these trace constituents starts at 20.7 meters (67.9 feet) bgs. The chromium, molybdenum, and arsenic porewater vertical distributions are distinctly different, but the vertical distribution of technetium-99 and selenium is very similar. The chromium and molybdenum both show a peak at 24.6 meters (80.6 feet) bgs. The chromium shows an even larger peak at 28.4 meters (93.1 feet) bgs and a third smaller peak at 34.7 meters (113.8 feet) bgs. The maximum porewater concentration of chromium in the three peaks is 13.6, 21.8, and 5.8 g/L, respectively. There does not appear to be elevated chromium concentrations in the porewater for samples below 42.1 meters (138.2 feet) bgs. Thus, the slant borehole may have captured the entire chromium plume.

SX-108 Slant Borehole (C3082)



2002/DCL/SX-108/016

Figure 4.4. Pore Fluid Concentrations of Aluminum, Iron, Silicon, and Manganese (calculated from sediment-to-water extracts) and Actual Porewaters for Slant Borehole Sediment

Table 4.9. Calculated Porewater Trace Metal Composition for Water Extracts of Sediment from Slant Borehole

Sample ID	Depth ^(a)	Dil. Fac.	water:soil Ratio	⁹⁹ Tc pCi/mL	U µg/L	Cr ^(b) mg/L	As ^(c) µg/L	Se µg/L	Mo µg/L	Ag µg/L	Cd µg/L	Pb µg/L
1A	55.1	23.13	1.00	<392	(35.9)	(0.21)	875	<1,157	305	(2.31)	(30.1)	253,389
1A-Dup	55.1	23.13	1.00	<392	(28.9)	(0.22)	798	<1,157	347	<57.8	<57.8	4,196
3A	67.9	36.88	1.02	(125)	140	29.1	1,239	<1,844	11,446	<92.2	(3.69)	(679)
4A	72.2	36.15	1.00	(61)	210	27.8	3,687	<1,808	2,176	<90.4	<90.4	(95.8)
5A	76.4	21.36	1.00	(217)	98.3	75.1	1,772	(145)	3,036	(32.0)	<53.4	(334)
6A	80.6	27.18	1.00	1,106	32.6	13,150 ^(b)	266	1,298	127,610	(216)	279	(78.8)
7A	84.8	16.20	1.00	16,485	1434	5,018 ^(b)	2,019	984.2	90,874	(183)	211	(953)
8A	89.0	16.61	1.00	47,439	43.2	13,782 ^(b)	507	2,477	40,238	(276)	105	(74.7)
9A	93.1	42.56	1.00	168,400	46.8	21,817 ^(b)	1,290	5,612	7,510	(12.8)	(4.26)	(1,221)
10A	97.3	52.34	1.00	237,279	55.0	20,838 ^(b)	1,675	8,615	871	(15.7)	<131	(325)
11A	101.7	31.78	1.00	144,287	(6.36)	28.1	753	3,849	184	<79.5	<79.5	(89.0)
12A	105.6	4.69	1.00	2,792	(2.35)	0.98	23.5	(37.5)	56.7	<11.7	<11.7	(9.8)
13A	113.8	13.38	1.02	96,874	13.4	5,766 ^(b)	561	3,182	3,180	(8.03)	(14.7)	(33.5)
14A	122.0	8.69	1.04	58,820	(5.65)	2,588 ^(b)	422	1,954	258	(5.21)	(0.87)	(45.2)
14A-Dup	122.0	8.38	1.00	64,773	(7.12)	2,913 ^(b)	440	2,249	231	(5.03)	<21.0	(21.8)
15A	130.1	5.74	1.00	66,072	6.89	1,931 ^(b)	443	2,360	78.6	(3.44)	(0.00)	(12.6)
16A	138.2	13.31	1.00	19,255	18.6	(0.26)	82.5	(419)	181	<33.3	(2.66)	(58.6)
17A	144.6	5.08	1.00	2,800	5.08	(0.02)	20.8	(69.1)	100	(0.51)	<12.7	(26.9)

(a) Depth is vertical feet bgs (multiply by 0.3048 to convert to meters).
(b) Higher chromium values are from ICP-Optical Emission Spectroscopy (OES), not ICP-MS. Note chromium values are in mg/L.
(c) Arsenic values are suspect due to possible mass interferences during the ICP-MS analysis.
Parentheses indicate value is below limit of quantification.

Table 4.10. Comparison of Actual to Calculated (from 1:1 water extracts) Porewaters—Trace Metals

Sample ID	Depth (ft) ^(a)	Dil. Fac.	water:soil Ratio	⁹⁹ Tc pCi/mL	µg/L							
					U	Cr	As	Se	Mo	Ag	Cd	Pb
12A	104.92	4.69	1.00	2,792	(2.35)	980	(23.5)	(37.5)	56.7	<11.7	<11.7	(9.8)
12A-ufa				3,570	12.1	709	(9.7)	47.8	9.09	(0.1)	(0.1)	(1.0)
15A	129.44	5.74	1.00	66,072	6.89	1,931,500 ^(b)	(443)	2,360	78.6	(3.44)	(0.00)	(12.6)
15A-ufa				69,451	1.44	2,115,298 ^(b)	293	(1,567)	42.1	(1.0)	(4.2)	(4.0)
17A	143.99	5.08	1.00	2,800	5.08	(17.3)	(20.8)	(69.1)	100	(0.51)	<12.7	(26.9)
17A-ufa				4,950	8.56	(10)	12.4	60.6	12.1	<2.5	(1.1)	<25

(a) Multiply by 0.3048 to convert to meters
(b) High chromium values are from ICP-OES.
ID notes: ufa represents the actual porewater obtained by ultracentrifugation.

Although molybdenum has its first concentration peak at the same depth as chromium, there is no second larger molybdenum peak at 28.4 meters (93.1 feet) bgs. There is a small molybdenum peak at

34.7 meters (113.8 feet) bgs at the same depth as the deepest chromium peak. Based on the water extract data, it appears that the chromium mass traveled deeper than molybdenum.

The technetium-99 and selenium porewater concentrations both show a three-lobed vertical distribution. The largest concentration is found at 29.7 meters (97.3 feet) bgs and a second slightly smaller peak is found at 34.7 meters (113.8 feet) bgs. Finally, both constituents show a small peak at 39.6 meters (130 feet) bgs. The maximum concentration of technetium-99 in the three peaks is as the profile deepens: 2.4×10^8 , 9.6×10^7 , and 6.6×10^7 pCi/L, respectively. The selenium maximum concentrations for the same peaks are 8.6, 3.2, and 2.4 mg/L.

The arsenic concentrations in the water extracts may not be real. The inductively coupled plasma-mass spectrometer (ICP-MS) results might be affected by mass interferences, although we did not find positive proof. The vertical distribution of arsenic shows a four-lobed shape with the maximum concentrations slightly decreasing with depth. The maxima for the four peaks, found at depths 22, 25.8 and 29.7 meters (72.2, 84.8, and 97.3 feet) bgs, and the latter diffused over the 34.4 to 39.6 meters (113 to 130 feet) bgs, are 3.7, 2.0, 1.7, 0.45 mg/L.

The other trace constituents, shown in Table 4.9 and Figures 4.5a and 4.5b; in particular uranium, silver, cadmium, and lead do not show any distinct plumes. Further, except for lead in sample 1A, the porewater concentrations are not significantly elevated above values found in uncontaminated sediment. The water extractable lead in sample 1A is elevated. As will be discussed, the acid extract for this sample also suggests elevated lead is present. It is quite plausible that lead in the tank liquor has percolated a small distance into the sediment where it readily becomes sequestered. There are faint hints of sporadically elevated concentrations of some trace metals in additional water extracts but no obvious trends are noted. Given the extreme salinity (16 to 17 M sodium nitrate) of the pore fluid, getting accurate analyses of trace constituents is difficult.

There are obvious elevated concentrations of technetium-99 and selenium in the PPlz unit as far as the borehole reached. We cannot assess whether the molybdenum and arsenic water-extractable plumes have been entirely captured in the slant borehole samples. We believe that the borehole penetrated the entire chromium plume and that very little if any chromium has entered the PPlz at the location of this borehole. Almost all of the mass of these trace constituents is captured in the Hanford formation H2 Fine Sand unit.

Table 4.10 shows the comparison of the trace constituents porewater concentrations obtained by ultracentrifugation with the calculated porewater concentrations from the dilution-corrected 1:1 sediment-to-water extracts. For the arsenic, molybdenum, and selenium, the calculated porewater values are slightly higher than the actual porewaters as would be expected if some mass were dissolved or desorbed from the sediment during the extraction. In general, the three chromium comparisons show

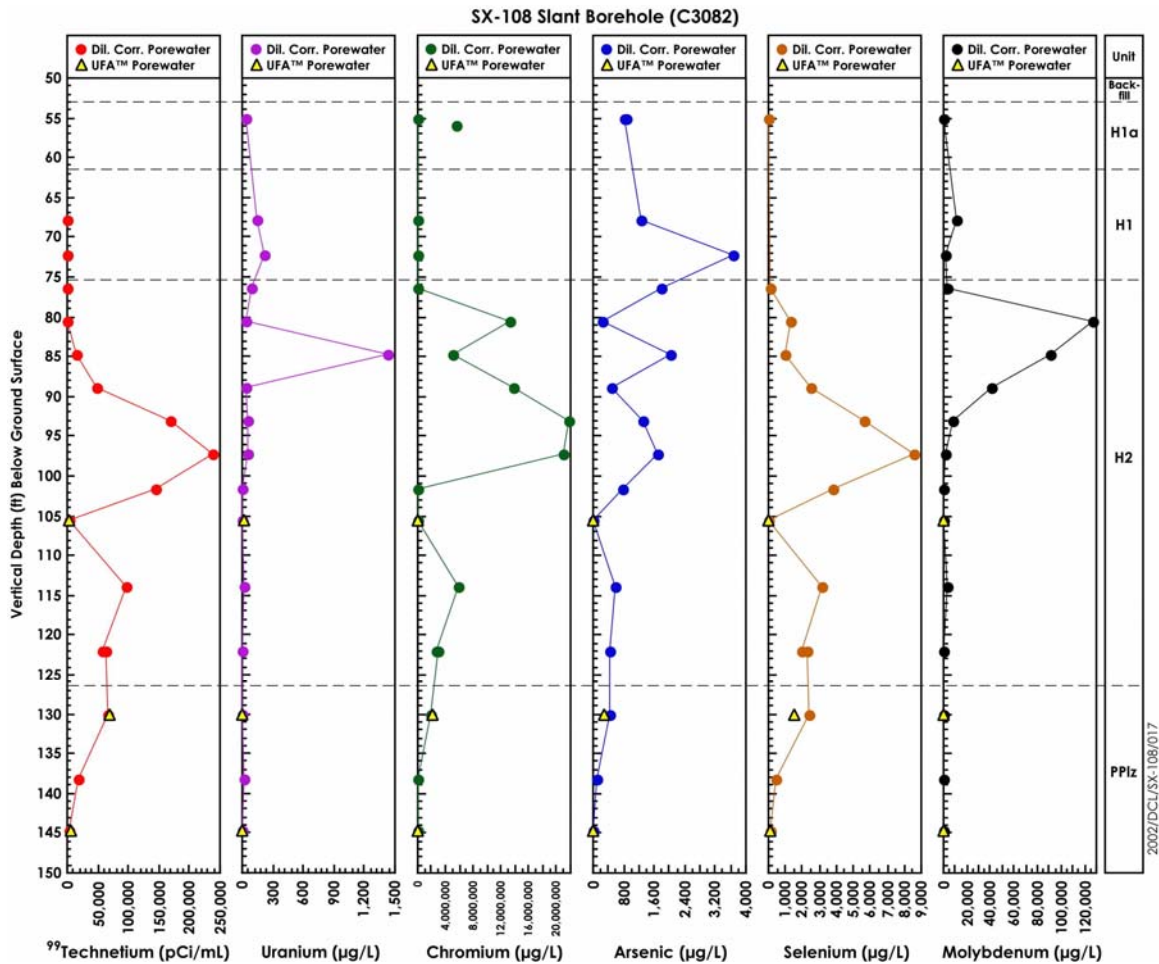


Figure 4.5a. Trace Metals Pore Fluid (calculated from sediment-to-water extracts) and Actual Porewaters for Slant Borehole Sediment

that there is no difference between the values. For the technetium-99 porewater concentrations, the ultracentrifuged values are consistently higher than the dilution-corrected values. This was the same trend observed for many of the major cations and anions, but we have no explanation for the differences. In some cases, the differences are within analytical error; in other cases the differences appear to be real.

As previously mentioned, we did not attempt ultracentrifugation of the samples that contained the highest concentrations of sodium and nitrate because they also contained high concentrations of cesium-137 that was a concern for worker safety and equipment contamination. We did ultracentrifuge sample 12A that was peculiarly low in contamination. The ultracentrifuged porewater confirms that this sediment does not contain a chemical signature that indicates the contamination comes from tank liquor. The actual porewater obtained from sample 17A, the deepest sample collected does confirm that the technetium-99 is still elevated, but the chromium has returned to background levels.

SX-108 Slant Borehole (C3082)

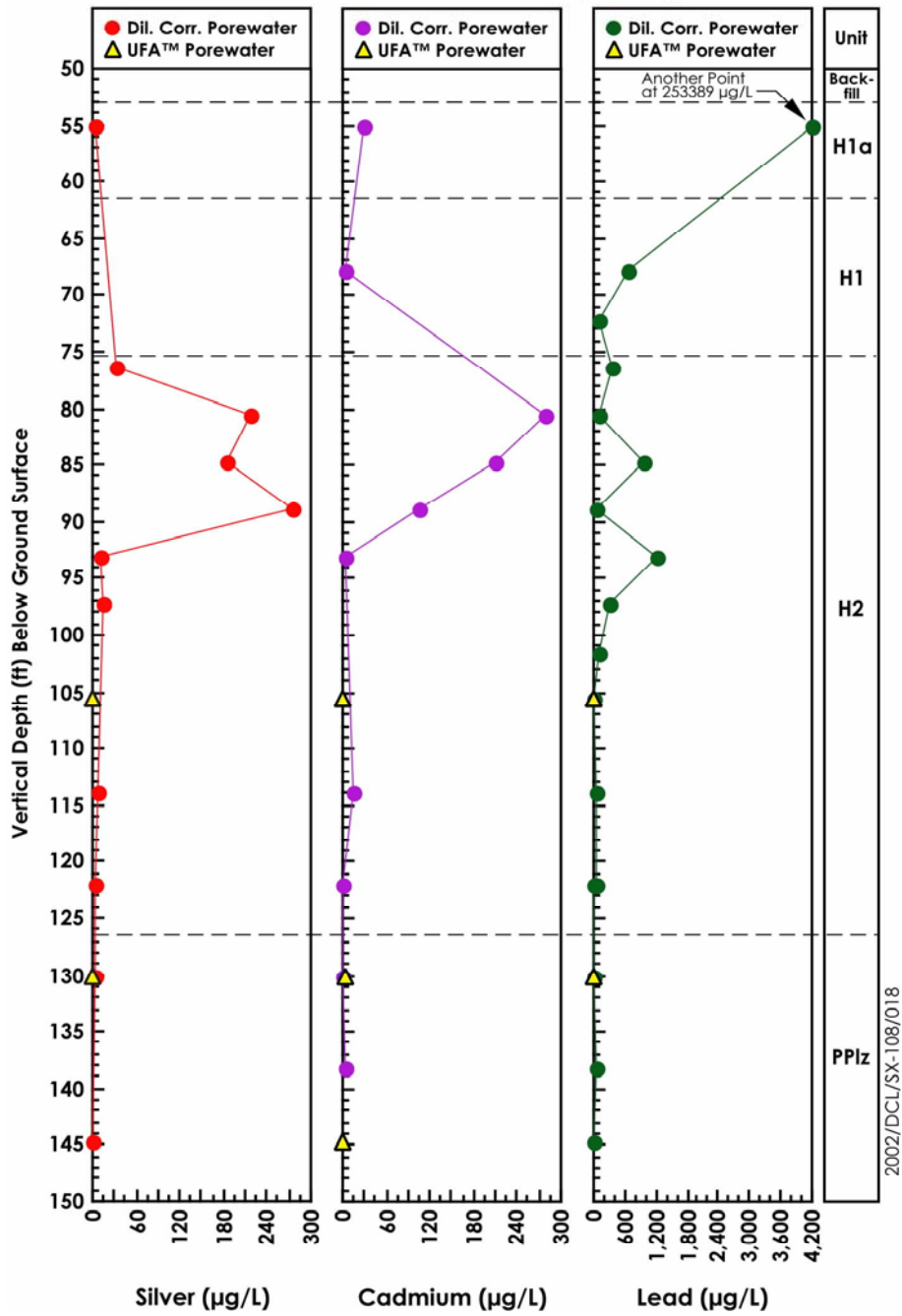


Figure 4.5b. Silver, Cadmium, and Lead Concentrations in Pore Fluid (calculated from sediment-to-water extracts) and Actual Porewaters for Slant Borehole Sediment

A more sophisticated method to evaluate the vertical migration of the trace metals would be to plot ratios of the trace metals versus nitrate. If tank liquor dilution with extant porewater were the only reason for the decrease in concentrations for all the mobile constituents, then the ratios of one to another should remain constant.

The ratios of the porewater constituents versus nitrate and versus technetium-99 are shown in Table 4.11. These ratios have the units of pCi/mg for the technetium-99 to nitrate and $\mu\text{g}/\text{mg}$ for the trace

Table 4.11. Ratio of Porewater Constituents to Mobile Species (nitrate and technetium-99)

ID	Depth ^(a)	⁹⁹ Tc	Cr	Mo	Na	Cl	U	Cr	As	Se	Mo	Na	Cl
		NO ₃	NO ₃	NO ₃	NO ₃	NO ₃	⁹⁹ Tc						
Hanford Formation H1a Sand Unit													
1A	55.1	<2.44	1.31	1.90	14.8	0.25	0.09	>0.54	>2.23	“---”	“---”	“---”	“---”
1A-Dup	55.1	<2.80	1.57	2.48	16.7	0.21	0.07	>0.56	>2.03	“---”	“---”	“---”	“---”
Hanford Formation H1 Coarse Sand/Gravel Unit													
3A	67.9	0.12	27.2	10.68	6.4	0.12	1.12	233	9.91	<14.7	91.5	54.59	1.00
4A	72.2	0.07	32.7	2.56	8.5	0.06	3.42	454	60.1	<29.5	35.5	117	0.89
Hanford Formation H2 Fine Laminated Sand Unit													
5A	76.4	0.11	37.8	1.53	2.9	0.04	0.45	345	8.15	0.67	13.97	26.30	0.39
6A	80.6	0.00	41.2	0.40	0.48	0.00	0.03	11886	0.24	1.17	115	138	0.25
7A	84.8	0.02	6.64	0.12	0.46	0.00	0.09	304	0.12	0.06	5.51	20.96	0.03
8A	89	0.07	20.9	0.06	0.46	0.00	0.00	291	0.01	0.05	0.85	6.43	0.03
9A	93.1	0.17	22.4	0.01	0.38	0.01	0.00	130	0.01	0.03	0.04	2.20	0.03
10A	97.3	0.24	21.0	0.00	0.39	0.01	0.00	87.82	0.01	0.04	0.00	1.65	0.03
11A	101.7	0.48	0.09	0.00	0.22	0.01	0.00	0.19	0.01	0.03	0.00	0.45	0.03
12A	105.6	0.39	0.14	0.01	0.10	0.02	0.00	0.35	0.01	0.01	0.02	0.25	0.04
13A	113.8	0.33	19.4	0.01	0.37	0.01	0.00	59.52	0.01	0.03	0.03	1.14	0.03
14A	122	0.31	13.9	0.00	0.37	0.01	0.00	44.00	0.01	0.03	0.00	1.17	0.03
14A-Dup	122	0.32	14.4	0.00	0.37	0.01	0.00	44.97	0.01	0.03	0.00	1.14	0.03
Plio-Pleistocene Fine-Grained Mud Unit (PPlz)													
15A	130.1	0.33	9.73	0.00	0.36	0.01	0.00	29.23	0.01	0.04	0.00	1.07	0.03
16A	138.2	0.34	0.00	0.00	0.08	0.01	0.00	0.01	0.00	0.02	0.01	0.23	0.04
17A	144.6	0.23	0.00	0.01	0.05	0.01	0.00	0.01	0.01	0.02	0.04	0.23	0.06
(a) Depth is vertical feet (multiply by 0.3048 to convert to meters). Sample 12A is highlighted in red because it has not been in contact with as much tank liquor as the other samples below 20.4 meters (67 feet) bgs.													

metals ratioed versus nitrate, and $\mu\text{g/pCi}$ for trace metal versus technetium-99. Chloride versus nitrate and sodium versus nitrate are both dimensionless. For the ratio carbon or sodium versus technetium, the units are mg/picocurie.

The technetium-99 to nitrate ratio suggests that the two constituents maintain a near constant ratio of about 0.3 pCi/mg from 34.7 meters (113.8 feet) bgs to the bottom of the borehole. Above this depth, the ratio is lower (varies from 0.02 to 0.24 pCi/mg). It is not clear whether this signifies two leak events with different compositions or complications with the presence of nitrate solids in the sediment that are not completely dissolving from all samples during the water extraction.

The chromium to nitrate ratio below 20.4 meters (67 feet) bgs, where the contamination begins, shows a very complicated distribution with three waves that start with a high ratio in the shallow portion of each wave and end with a low ratio. As discussed in the science and technology portion of the field investigation report,^(a) the chromium in the tank liquor interacts with iron (II) that is released when caustic fluid attacks certain minerals in the native sediment. This along with the possibility of two leaks with different compositions may be the cause of the complicated ratio versus depth distribution. The first wave starts at 20.7 meters (67.9 feet) bgs and ends at 25.8 (84.8 feet) bgs, the second wave starts at 27.1 meters (89 feet) bgs and ends at 31 meters (101.7 feet) bgs, and the third wave starts at 34.7 meters (113.8 feet) bgs and ends somewhere between 39.7 and 42.1 meters (130.1 and 138.2 feet) bgs where the tank leak chromium plume stops. Because the chromium is reacting with the sediment and being removed from solution, the ratio is high in the shallow sediment and drops to lower values as the nitrate continues to migrate but the chromium in the porewater drops. The deepest two samples show the chromium to nitrate ratio is 0, again suggesting the borehole intercepted the entire chromium plume. The chromium reduction reactions have been investigated/delineated by the science and technology activities led by John Zachara (see Appendix D in the field investigation report).^(a)

The sodium to nitrate ratio shows the same type of behavior as the chromium-to-nitrate ratio but there are only two waves, where the ratio starts out with a high value and drops to a low value versus depth. Again, a plausible explanation is that the sodium is reactive while the nitrate migrates with little interaction with the sediment. The sodium reactions are ion exchange processes.

The molybdenum to nitrate and molybdenum to technetium-99 ratios are high at the first indication of large tank leak contamination, 20.7 meters (67.9 feet) bgs, and below 25.9 and 27.1 meters (85 to 89 feet) bgs the ratios drop to ~ 0 . This suggests that molybdenum is removed from the porewater in the shallow sediment in the Hanford formation H1 coarse unit and the upper portion of Hanford formation H2 laminated sand. The nitrate and technetium-99 are less reactive and have traveled deeper into the H2 and PPlz units. This causes the molybdenum to mobile constituent ratios to decrease with depth. The selenium to technetium-99 ratio below 24.6 meters (80.6 feet) bgs is fairly stable suggesting that both contaminants are not interacting with the sediment and traveling with the mobile constituents in the plume. Above 24.6 meters (80.6 feet) bgs for most of the samples, neither the technetium-99 nor selenium were present at high enough concentrations to be quantified. The arsenic to technetium-99 ratio

(a) *Draft Field Investigation Report for Waste Management Area S-SX*. RPP-7884, Draft, Volume 2, Appendix D, CH2M HILL Hanford Group, Inc., Richland, Washington.

between 20.7 and 25.8 meters (67.9 and 84.8 feet) bgs is higher and more variable than the ratio at deeper depths that remains fairly constant at a value 0.006 $\mu\text{g/pCi}$. Because we are uncertain about our arsenic data and we do not see a large amount of excess arsenic in the acid leachates (to be discussed later), we are not certain whether there is any information in this ratio to address arsenic mobility in the redox tank leak fluids.

The chloride to nitrate ratio is constant at ~ 0.01 for all depths below 24.6 meters (80.6 feet bgs). Above this depth, the ratio is larger and variable. For the first sample at the base of the tank, but 2.4 meters (8 feet) away from the tank wall, where there is little nitrate, the ratio is 0.25. We interpret the chloride-to-nitrate ratio in the porewater as suggesting that both constituents are unreactive with the sediment.

The uranium to nitrate or uranium-to-technetium-99 ratios show a higher value in the shallow sediment (above 23.3 meters [76.4 feet] bgs) than all the deeper sediment where the ratio is very low. This suggests that uranium leaking from the tanks is rapidly sequestered in the vadose zone sediment and removed from the pore fluids. There is a small amount of natural uranium in the sediment that is water leached, but it is miniscule compared to the nitrate and technetium-99 that is present in the porewaters throughout the vadose zone profile that was sampled.

The ratio of technetium 99 to nitrate, though not as constant as it was at well 299-W23-19, is much lower than the ratio in the groundwater below the SX Tank Farm. The ratio in the groundwater is 100 pCi/mg, a value much higher than the range shown in Table 4.11 (0.02 to 0.48 pCi/mg). This would suggest that if tank SX-108 were the source of the groundwater contamination, much more technetium-99 should be in the groundwater or that there is some mechanism in the deeper sediment that preferentially removes technetium-99 from the pore fluids. Conversely, it is much more plausible that the source of the contamination in the groundwater under SX Tank Farm is the fluids lost from tank SX-115.

4.2.3 Radionuclide Content in Vadose Zone Sediment

The sediment cores from 41-09-39 and the SX-108 slant borehole were very radioactive. The radioanalytical analyses performed on the sediment from the slant borehole included direct gamma energy analysis, tritium analysis by distillation of tritium out of the sediment and condensation on special targets, and strong acid digestion followed by wet chemical separation of strontium-90 and the actinides. The technetium-99 content of the UFA extracts, water extracts, and strong acid extracts was analyzed by ICP-MS. The iodine-129 content of selected water extracts was analyzed by ICP-MS.

The radionuclide content of the sediment is shown in Tables 4.12 to 4.14. The cesium-137 concentrations in the vadose zone sediment are plotted in Figure 4.6 along with the spectral gamma logging data. The logging data below about 27.4 meters (90 vertical feet) bgs is biased high by the contamination on the inside of the casing because of the loss of sample 02. Above 27.4 meters

Table 4.12. Gamma Energy Analysis of Vadose Zone Sediment

Sample	Depth (ft) ^(a)	¹³⁷ Cs	± Uncertainty	⁴⁰ K	± Uncertainty
		pCi/g		pCi/g	
Hanford Formation H1a Sand Unit					
1A	55.1	3.06E+06	8.55E+04	<3.88E+03	
Hanford Formation H1 Coarse Sand/Gravel Unit					
3BA	67.9	1.94E+07	5.37E+05	<1.45E+04	
4B	71.5	8.16E+06	2.27E+05	<7.66E+03	
4A	72.2	1.38E+06	3.94E+04	<7.21E+03	
Hanford Formation H2 Fine Laminated Sand Unit					
5B	75.7	3.78E+06	1.05E+05	<6.40E+03	
5A	76.4	6.52E+06	1.81E+05	<2.59E+04	
6B	79.9	3.63E+07	1.64E+06	<4.17E+04	
6A	80.6	5.31E+07	2.41E+06	<6.29E+04	
7B	84.1	8.06E+06	2.26E+05	<4.16E+04	
7A	84.8	2.14E+07	5.97E+05	<5.20E+04	
7A1	84.6	9.57E+07	4.34E+06		
8B	88.3	5.03E+06	1.41E+05	<9.86E+03	
8A	89.0	5.55E+05	1.69E+04	<1.22E+03	
9B	92.5	1.29E+04	1.91E+02	1.23E+01	3.19E+00
9A	93.1	1.71E+02	3.28E+00	2.49E+01	4.40E+00
10B	96.6	6.31E+02	1.00E+01	1.55E+01	1.45E+00
10A	97.3	4.51E+02	7.23E+00	1.82E+01	1.52E+00
11B	101	1.19E+04	1.86E+02	<2.46E+01	
11A	101.7	9.12E+02	1.46E+01	2.73E+01	3.55E+00
12B	104.9	7.81E+02	1.23E+01	2.20E+01	2.82E+00
12A	105.6	3.37E+02	5.50E+00	2.66E+01	3.58E+00
13B	113.1	5.82E+03	8.95E+01	2.01E+01	3.08E+00
13A	113.8	5.21E+02	8.12E+00	1.64E+01	1.83E+00
14B	121.3	1.16E+03	1.78E+01	1.98E+01	3.37E+00
14A	122.0	8.37E+02	2.40E+01	3.01E+01	2.70E+00
Plio-Pleistocene Fine-Grained Mud Unit (PPlz)					
15B	129.4	5.31E+02	8.65E+00	2.53E+01	5.50E+00
15A	130.1	5.92E+02	9.78E+00	2.47E+01	1.66E+00
16B	137.5	4.62E+03	7.13E+01	2.57E+01	4.11E+00
16A	138.2	9.79E+01	2.09E+00	2.52E+01	1.94E+00
17B	144	7.43E+02	1.17E+01	2.05E+01	5.16E+00
17A	144.6	1.75E+02	3.08E+00	2.58E+01	3.25E+00
(a) Multiply by 0.3048 to convert to meters.					

Table 4.13. Strontium-90 and Tritium Contents of Vadose Zone Sediment

Sample ID	Depth (ft bgs) ^(a)	⁹⁰ Sr pCi/g	± Uncertainty	³ H pCi/g	± Uncertainty
Hanford Formation H1a Sand Unit					
1A	55.1	9.08	1.91	22.1	1.8
Hanford Formation H1 Coarse Sand/Gravel Unit					
3BA	67.9	0.45	1.69	4.3	1.3
4A	72.2	ND	-	2.11	1.1
Hanford Formation H2 Fine Laminated Sand Unit					
5A	76.4	49.1	3.84	12.9	1.7
6A	80.6	11.4	1.92	2.68	1.0
7A	84.8	61.4	6.99	84.4	3.3
8A	89.0	1.85	1.70	103	3.3
9A	93.1	ND	-	124	4.1
10A	97.3	ND	-	111	3.8
11A	101.7	0.08	1.68	116	3.9
12A	105.6	1.82	1.70	150	4.7
13A	113.8	ND	-	175	5.4
14A	122.0	ND	-	114	4.0
Plio-Pleistocene Fine-Grained Mud Unit [PPlz]					
15A	130.1	154	25.39	127	3.9
16A	138.2	ND	-	5.71	1.3
17A	144.6	30	2.84	1.74	1.1
(a) Multiply by 0.3048 to convert to meters. ND = Not determined.					

(90 vertical feet) bgs, the formation sediment contains so much cesium-137 that the casing contamination does not impact the field gamma logging results. The logging data show that sample 02, which was lost, was quite radioactive as corroborated by the high dose rate found on the essentially empty sampler upon opening in the laboratory. The cesium-137 activity versus depth shows the multiple peak signature found for most of the other contaminants. However, the depths for the maximum cesium-137 concentrations are much shallower in the profile suggesting that cesium-137 is more reactive with the sediment than the sodium, trace metals such as chromium, and technetium-99. Using the more complete field spectral gamma log, the maximum concentrations of cesium-137 found in two major peaks in the sediment are between 5 and 9 x 10⁷ pCi/g between 18 and 18.9 meters (59 and 62 feet) and between 24.6 and 25.8 meters (80.6 and 84.6 feet) bgs, respectively. The bulk of the contamination resides at the contact between the H1a and the H1 coarse-grained sediment and in the upper portion of the laminated fine sand (H2 unit), respectively. Below 28.3 meters (93 feet) bgs, still within the H2 unit, the cesium-137 activity

Table 4.14. Technetium-99 and Uranium-238 Content in Sediment (based on

8 M Nitric Acid Extracts) and in Water Extracts

Sample ID	Depth ft ^(a)	⁹⁹ Tc pCi/g soil	⁹⁹ Tc(Water) pCi/g soil	²³⁸ U μg/g soil	²³⁸ U pCi/g soil	²³⁸ U(water) pCi/g soil
01A	55.1	<85.3	<17.0	0.48	0.16	5.21E-04
01A dup	55.1	<84.8	<17.0	0.42	0.14	4.21E-04
02A		NS	NS	NS	NS	NS
03A	67.9	(8.15)	(3.46)	0.65	0.22	1.30E-03
04A	72.2	<82.9	(1.70)	0.54	0.18	1.95E-03
05A	76.4	(8.54)	(10.18)	0.77	0.26	1.55E-03
06A	80.6	(46.73)	40.7	0.78	0.26	4.04E-04
07A	84.8	926	1,018	0.72	0.24	2.98E-02
08A	89	2,116	2,856	0.80	0.27	8.74E-04
09A	93.1	4,238	3,955	0.68	0.23	3.70E-04
10A	97.3	4,546	4,534	0.67	0.23	3.53E-04
11A	101.7	4,666	4,540	0.73	0.24	(6.73E-05)
12A	105.6	534	595	1.38	0.46	(1.68E-04)
13A	113.8	7,502	7,400	6.15	2.07	3.44E-04
14A	122	7,779	7,028	0.95	0.32	(2.27E-04)
14A dup	122	7,241	7,737	0.94	0.32	(0.00E+00)
15A	130.1	10,306	11,512	0.96	0.32	4.04E-04
16A	138.2	1,742	1,445	1.18	0.40	4.70E-04
17A	144.6	857	551	1.13	0.38	3.36E-04

(a) Multiply by 0.3048 to convert to meters.
NS = No sample available.

is 10,000 times less concentrated, though the cesium-137 activity does not drop to background values before the end of the borehole in the PPlz unit. Thus, we did not find the maximum depth of cesium-137 penetration in this borehole.

There were no other manmade gamma emitters found in the sediment and the only other gamma-emitting nuclide that was detected was natural potassium-40, which aids in picking the contact between the various lithologies.

The strontium-90 and helium-3 content of the vadose zone sediment is shown in Table 4.13. There is no indication that the vadose zone sediment in this borehole contains significant amounts of strontium-90 that creates a well-defined plume, but there is detectable strontium-90 in most of the samples. The maximum concentration observed was 154 pCi/g at 39.6 meters (130 feet) bgs, which is near the depth of

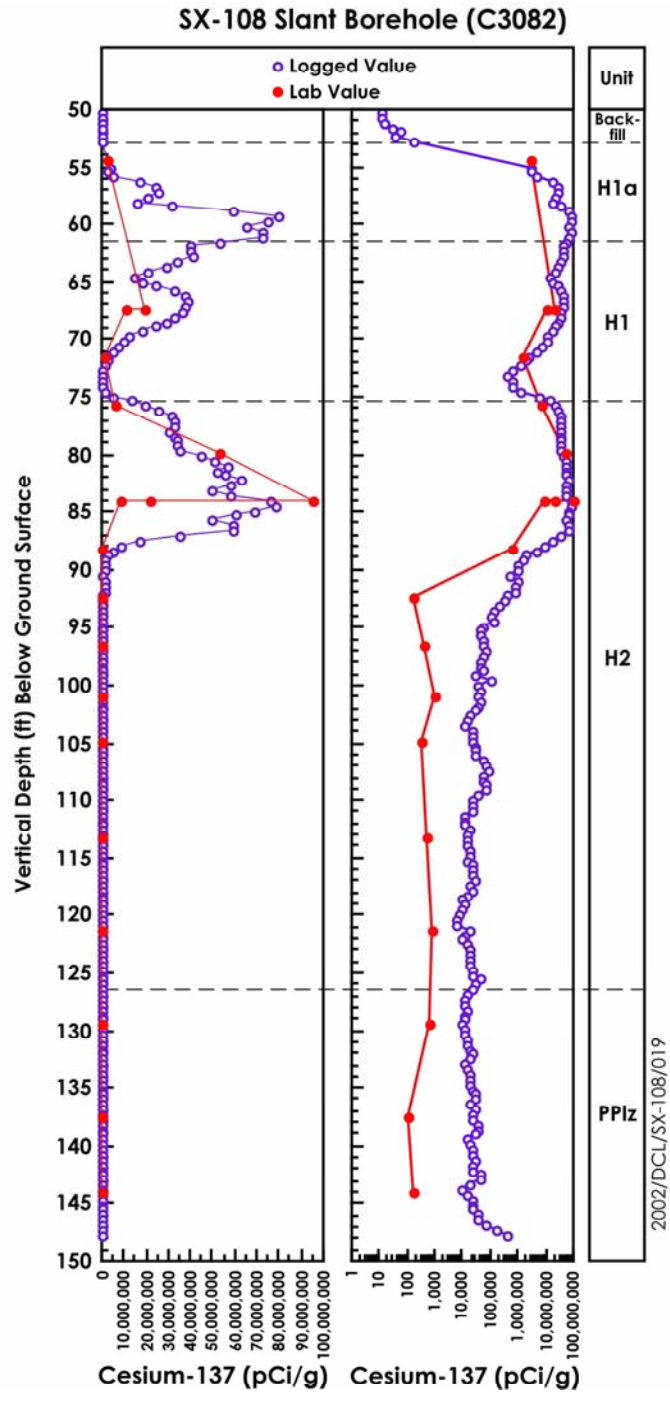


Figure 4.6. Cesium-137 in Vadose Sediment (pCi/g) Plotted with Linear and Log Scale

the deeper stable porewater strontium peak that has been attributed to ion exchange displaced divalent cations. The most consistent region of strontium-90 activity is found between 23.1 and 25.6 meters (76 and 84 feet) bgs within the top of the H2 fine-sand unit.

A small amount of tritium is present between 25.9 and 39.6 meters (85 and 130 feet) bgs at the slant borehole. The activities range from 80 to 130 pCi/g. The deepest two samples within the PPlz unit show very low tritium activities suggesting that the tank leak plume has almost dissipated in the upper PPlz unit. However, because we have observed at least two plume peaks for most constituents, it is possible that the deeper tritium plume is below the maximum depth sampled at the slant borehole. Given the understanding that tritium is generally nonreactive and travels with the other mobile constituents, we would expect it to be present as deep as there is elevated nitrate and technetium-99. Based on the data shown in Table 4.13, the leading edge of the tritium seems to be shallower than the leading edge of the technetium-99 and nitrate. Perhaps the complicated evaporation/condensation cycling of water predicted by detailed heat modeling by the Science and Technology Program explains the different tritium distribution than other mobile contaminants.

Assuming that the 8 M nitric acid leach dissolves all the technetium-99 and uranium from the sediment, Table 4.14 shows the total amount of these radionuclides in the vadose zone sediment. Because technetium-99 has been shown to be readily water extractable, we show both the acid extractable and water extractable in Table 4.14. There is excellent agreement between the technetium-99 extracted by the strong acid and the water (Figure 4.7). As discussed in Section 4.2.2, the elevated total technetium-99 in the vadose zone sediment starts at ~24.4 meters (~80 feet) bgs. The vertical distribution of technetium-99 shows a two-lobed vertical distribution. The largest concentration is found at 39.6 meters (130 feet) bgs with 10^4 pCi/g of dry sediment. The shallower peak occurs at 31 meters (101.7 feet) bgs with a maximum of 4.7×10^3 pCi/g. On a sediment basis, the shape of the technetium-99 distribution differs from the porewater distribution because of varying moisture content in the sediment. The technetium-99 in the porewaters is more concentrated in the shallower depths, likely because of desiccation by the high-heat load near the tank. The majority of the technetium-99 is spread throughout the H2 and PPlz units. There are small amounts of technetium-99 at the total depth penetrated by the slant borehole.

The uranium content of the sediment does not appear to be significantly elevated compared to values found in nearby Resource Conservation and Recovery Act (RCRA) clean boreholes (see Serne et al. 2002c). There does appear to be one sample at 34.7 meters (113.8 feet) bgs that has more uranium than the other samples, but the value is not significantly greater than some natural sediment. It is also apparent from Figure 4.8 that very little of the uranium that is acid leachable is also water leachable.

Table 4.15 lists some data for water-leachable iodine-129 that was obtained using the ICP-MS instrument. At the concentrations used to calibrate the instrument, we believe that there is no significant interference from xenon-129. The iodine-129 measurements were difficult to obtain due in part to a memory effect. Iodine-129 in standards and samples tends to hang up in the sample introduction system (tubing and spray chamber), but we are fairly certain that iodine-129 is present. After correction for

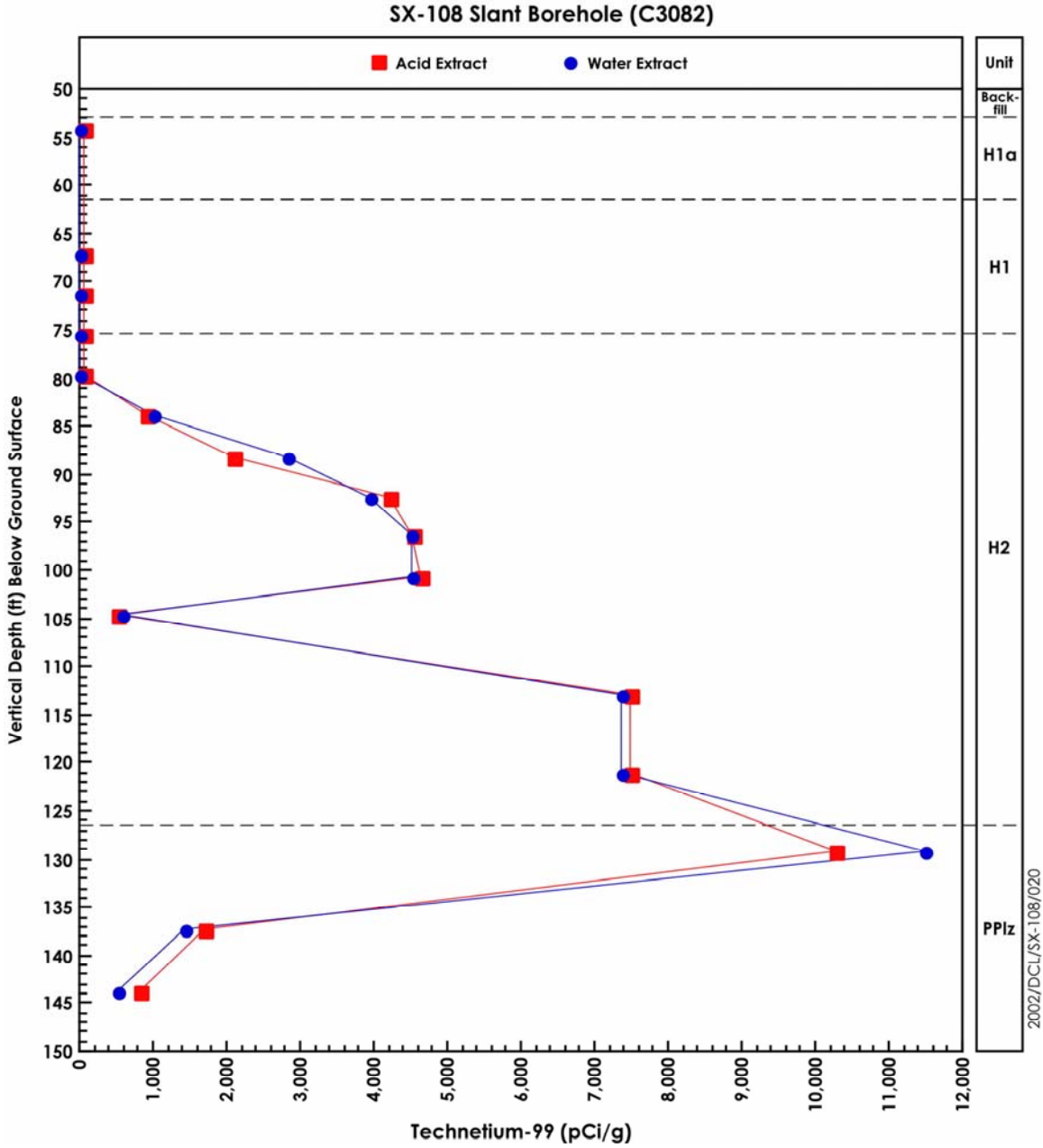


Figure 4.7. Concentration of Technetium-99 in Slant Borehole Sediment that is Water or Acid Extractable

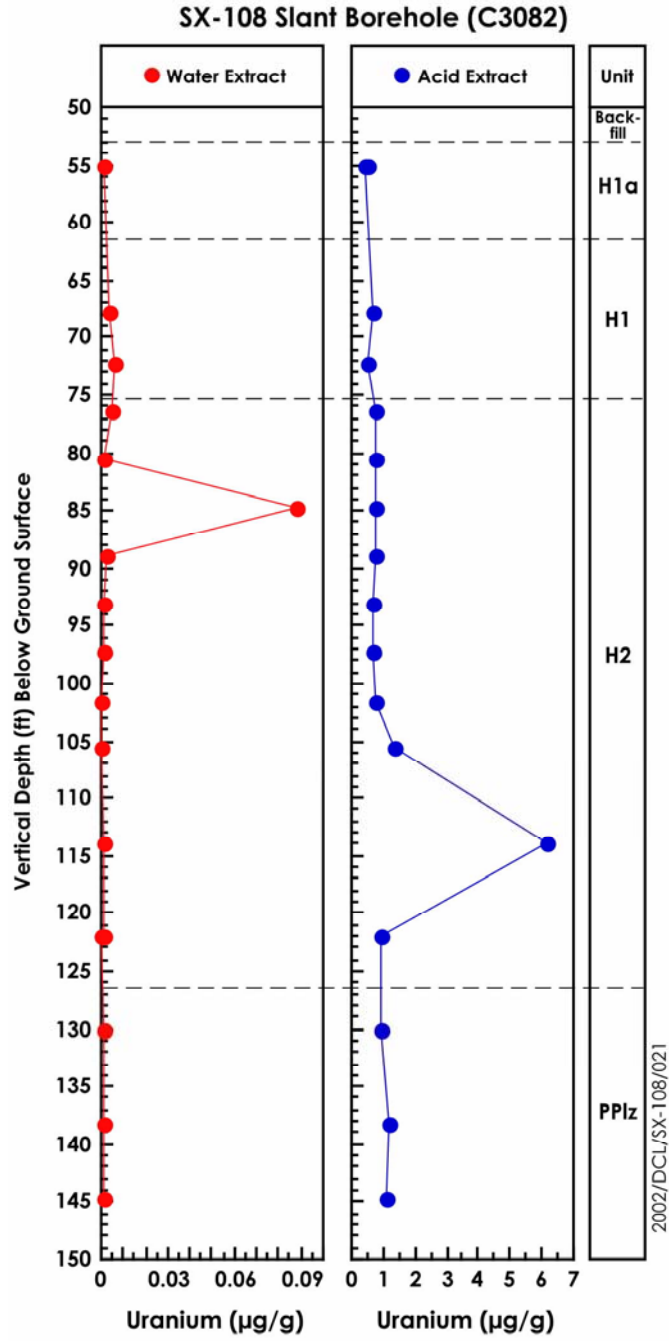


Figure 4.8. Concentration of Uranium in Slant Borehole Sediment that is Water or Acid Extractable

Table 4.15. Iodine-129 Content in Dilution-Corrected Water Extracts for Selected Slant Borehole Sediment

Sample ID	Vertical Depth (ft) ^(a)	Dilution Factor	¹²⁹ I		
			Conc $\mu\text{g/L}$	pCi/L 1:1	pCi/L Porewater
06A	80.6	27.18	8.9	1571.7	42,720
08A	89	16.61	12.6	2216.3	36,813
14A	122	8.69	12.2	2154.5	18,723
15A	130.1	5.74	18.5	3267.1	18,753

(a) Multiply by 0.3048 to convert to meters.

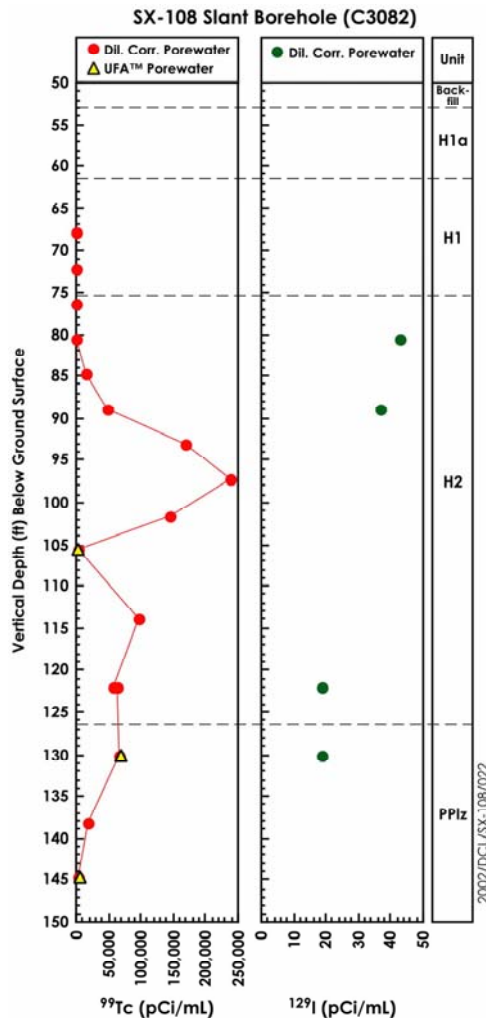


Figure 4.9. Comparison of Technetium-99 and Iodine-129 in Dilution-Corrected Porewaters

extract dilution, the calculated porewater concentrations are not very different for the four samples analyzed. The data are plotted versus the porewater technetium-99 concentrations in Figure 4.9. The iodine-129 activities are 1000 to 4000 times less than the technetium-99 values and not enough iodine-129 data was obtained to determine whether there is any plume present. We did not attempt to measure iodine-129 in the acid extracts because iodine-129 is known to volatilize in a strong acid environment such that we expected the acid extracts to lose iodine-129 during the extraction.

4.2.4 Total Carbon, Calcium Carbonate, and Organic Carbon Content of Vadose Zone Sediment

Table 4.16 shows the total carbon, inorganic carbon, and organic carbon contents of the vadose zone sediment at selected depths. The inorganic carbon was also converted to the equivalent calcium carbonate content. The sediment in the H1a and H1 units is relatively low in carbonate and shows a fairly uniform distribution. The H2 unit shows a variable distribution with the lower portion containing higher concentrations of carbonate. Sample 12A, which is the fine-grained lens, did not absorb much tank liquor

Table 4.16. Carbon Content in Vadose Sediment from Slant Borehole

Sample ID	Depth (ft bgs) ^(a)	Total Carbon % wt	Inorganic Carbon % wt	IC as CaCO ₃ % wt	Organic Carbon % wt
Hanford Formation H1a Sand Unit					
01A	54.48	0.16	0.14	1.17	0.02
01A Dup	54.48	0.16	0.13	1.12	0.03
Hanford Formation H1 Coarse Sand/Gravel Unit					
03A	67.27	0.18	0.12	1.01	0.05
04A	71.51	0.19	0.16	1.33	0.03
Hanford Formation H2 Fine Laminated Sand Unit					
05A	75.73	0.27	0.23	1.92	0.04
06A	79.94	0.23	0.21	1.72	0.02
07A	84.13	0.29	0.25	2.12	0.03
08A	88.32	0.24	0.20	1.67	0.04
09A	92.48	0.22	0.20	1.68	0.02
10A	96.64	0.22	0.20	1.66	0.02
11A	101.04	0.23	0.20	1.65	0.03
12A	104.92	0.52	0.48	4.02	0.03
13A	113.14	0.34	0.22	1.81	0.12
14A	121.3	0.39	0.37	3.04	0.02
14A Dup	121.3	0.42	0.36	3.01	0.06
Plio-Pleistocene Fine-Grained Mud Unit [PPlz]					
15A	129.44	0.33	0.27	2.23	0.07
16A	137.54	0.35	0.31	2.59	0.04
17A	143.99	0.39	0.31	2.60	0.07

(a) Multiply by 0.3048 to convert to meters.

and shows the highest carbonate content of all the samples obtained. The very bottom of the H2 unit and the fine-grained PPlz has a bit more calcium carbonate than the shallower Hanford fine-grained sands. The organic content in all the samples is low, and there is no variation in the vertical distribution.

4.2.5 8 M Nitric Acid Extractable Amounts of Selected Elements

The amount of material that was extractable from the vadose zone sediment into 8 M nitric acid is shown in Tables 4.17 and 4.18. Prior to gaining access to an x-ray fluorescence unit that can determine the total composition of the sediment directly, we had no accurate method to determine the total elemental composition of the contaminated sediment. As described in Serne et al. (2002a), we tried total fusion digestion of sediment as well as 8 M nitric acid. Neither technique works well for Hanford vadose zone sediment. The total fusion dilutes the acid-extract solution too much to get useful data for most trace metals and based on the x-ray fluorescence analyses, the 8 M nitric acid extraction dissolves only a few percent to at best 50% of various constituents.

The 8 M nitric acid extraction is a protocol used by the U.S. Environmental Protection Agency to estimate the maximum concentrations of regulated metals in contaminated sediment that would be biologically available. We subjected aliquots of contaminated sediment from the slant borehole to the acid extraction to search for obvious signs of elevated concentrations of elements from leaked tank fluids.

Compared to nearby clean boreholes, 299-W22-50 and 299-W22-48 (see Serne et al. 2002c), the concentration of some constituents that are acid extractable appear elevated for some constituents in some of the lithologic units. Tables 4.17 and 4.18 show in gray shading the lithologic units and the range for each constituent found in the uncontaminated sediment. Acid extracts data for the slant borehole sediment that exceed the comparable values in the clean boreholes by at least 10 times are highlighted in yellow and bold red type. Constituents that consistently are acid extractable from the slant borehole sediment at higher than background values are shown in red type.

The acid-extractable sodium values are consistently higher than background in the slant borehole sediment throughout the whole profile. From about 24.4 to 39.6 meters (80 to 130 feet) bgs, the acid-extractable sodium is at least 10 times the natural sediment acid-extractable quantities, except sample 12A, which was the sample in the fine-grained lens that appears to have been relatively impermeable to imbibing the tank liquor.

The acid-leachable sulfur, which is thought to be present solely as sulfate, also is elevated in the whole profile, except for the coarse-grained H1 unit that has been shown to contain high sulfate naturally in some of the uncontaminated samples from the two RCRA boreholes. Many of the major cations including calcium, barium, iron, potassium, magnesium, manganese, strontium, and titanium, show higher acid-extractable quantities than the uncontaminated sediment. The data in Tables 4.6 and 4.17 suggest that the alkali and alkaline earth cations are both within the porewater and on the sediment exchange sites in the leading edge of the massive sodium plume. These cations are essentially being

Table 4.17. Acid-Extractable Major Element Content of the Vadose Sediment from Slant Borehole

Sample ID	Depth (ft) ^(a)	Al µg/g soil	Na µg/g soil	K µg/g soil	Ca µg/g soil	Mg µg/g soil	Sr µg/g soil
H1a		“6,000-10,250”	“180-425”	“1,400-1,500”	“8,000-11,000”	“4,500-5,500”	“30-50”
01A	55.1	9,610	(1,020)	1,842	8,143	5,376	(37.3)
01A Dup	55.1	8,539	(907)	1,527	7,212	4,555	(33.7)
H1		“3,300-6,300”	“250-350”	“450-1,130”	“5,000-1,400”	“2,200-4,300”	“18-33”
03A	67.9	7,931	1,693	1,304	7,835	4,969	(29.0)
04A	72.2	7,017	1,518	1,047	8,239	4,787	(25.6)
H2		“5,400-16,300”	“150-270”	“1,200-1,700”	“6,680-13,350”	“4,000-7,800”	“25-47”
05A	76.4	9,896	1,412	2,368	9,464	5,989	(28.3)
06A	80.6	9,164	6,007	2,066	8,884	5,274	(29.1)
07A	84.8	13,542	23,758	2,352	10,245	6,342	(40.5)
08A	89	10,144	15,016	2,342	9,698	6,158	(35.0)
09A	93.1	10,586	10,647	2,354	8,922	5,815	(33.9)
10A	97.3	9,972	9,392	2,077	8,943	5,833	(36.4)
11A	101.7	10,401	2,340	2,277	11,186	6,248	56.0
12A	105.6	19,420	(491)	3,364	17,999	9,301	(50.4)
13A	113.8	14,258	11,135	3,241	10,931	7,512	(48.2)
14A	122	12,664	10,038	2,595	14,823	7,019	(47.7)
14A Dup	122	12,657	9,633	2,550	14,713	6,878	(48.3)
PPlz		“6,200-9,935”	“185-250”	“1,900-2,000”	“11,000”	“5,000-7,000”	“35-40”
15A	130.1	18,049	15,962	2,601	14,076	8,259	66.1
16A	138.2	13,549	(641)	2,404	14,153	7,411	55.5
17A	144.6	15,568	(471)	2,828	15,287	8,615	59.8

(a) Multiply by 0.3048 to convert to meters.

Table 4.17. (cont)

Sample ID	Depth (ft) ^(a)	Ba µg/g soil	Fe wt%	Mn µg/g soil	Zn µg/g soil	Ni µg/g soil	Ti µg/g soil	Si µg/g soil	P µg/g soil	S µg/g soil
H1a		“80-120”	“1.2-2.6%”	“275-450”	“33-48”	“7-11”	“500-1,800”	“18-60”	“400-900”	“45-75”
01A	55.1	91.6	2.01	363	44.4	15.4	1.23E+03	(1.69E+01)	6.31E+02	2.00E+02
01A Dup	55.1	82.5	8.50	835	52.3	103	1.24E+03	(5.35E+00)	5.45E+02	2.10E+02
H1		“40-75”	“0.9-1.5%”	“120-300”	“18-48”	“4-9”	“450-790”	“10-40”	“530-830”	“40-230”
03A	67.9	74.6	1.96	288	38.1	(11.6)	1.27E+03	(1.63E+01)	8.07E+02	2.10E+02
04A	72.2	62.5	1.93	282	37.2	(10.8)	1.32E+03	(1.76E+01)	8.45E+02	2.25E+02
H2		“60-125”	“1.0-2.1%”	“240-412”	“29-49”	“5-17”	“330-870”	“4-86”	“360-560”	“26-50”
05A	76.4	88.6	1.79	336	45.1	13.7	8.70E+02	(1.02E+01)	5.79E+02	2.26E+02
06A	80.6	92.5	1.70	301	38.5	(11.4)	7.61E+02	(9.53E+00)	5.48E+02	2.29E+02
07A	84.8	97.1	2.42	430	51.9	15.6	1.19E+03	(5.68E+00)	7.14E+02	4.71E+02
08A	89	77.4	1.78	337	44.4	15.3	8.01E+02	(7.36E+00)	6.44E+02	4.17E+02
09A	93.1	90.0	1.72	327	42.8	13.2	9.56E+02	(9.16E+00)	5.14E+02	3.96E+02
10A	97.3	89.5	1.72	327	39.8	13.9	9.55E+02	(8.44E+00)	5.15E+02	2.98E+02
11A	101.7	108	1.82	350	44.0	13.8	9.24E+02	(7.41E+00)	5.46E+02	2.66E+02
12A	105.6	149	2.67	565	69.0	17.6	8.23E+02	(8.80E+00)	6.86E+02	3.81E+02
13A	113.8	135	2.44	476	59.4	18.8	1.14E+03	(6.35E+00)	6.35E+02	3.36E+02
14A	122	103	2.00	339	53.5	14.8	8.87E+02	(7.82E+00)	6.50E+02	4.27E+02
14A Dup	122	104	1.96	341	51.2	14.3	8.94E+02	(7.33E+00)	6.18E+02	4.24E+02
PPlz		“100-110”	“1.4-1.6%”	“270-300”	“45-55”	“13-16”	“450-500”	“7.5-13”	“450-860”	“27-32”
15A	130.1	172	3.72	575	71.3	(12.2)	1.72E+03	(3.89E+00)	7.31E+02	5.05E+02
16A	138.2	131	2.28	363	56.7	16.7	9.31E+02	(9.34E+00)	6.45E+02	2.92E+02
17A	144.6	131	2.49	426	63.6	20.2	1.06E+03	(9.79E+00)	7.49E+02	3.23E+02

(a) Multiply by 0.3048 to convert to meters.

Table 4.18. Acid-Extractable Trace Element Content of the Vadose Sediment from Slant Borehole

Sample ID	Depth (ft) ^(a)	Cr ^(b) µg/g soil	Cr µg/g soil	Co ^(b) µg/g soil	Cu ^(b) µg/g soil	As µg/g soil	Se µg/g soil	Mo µg/g soil	Ag µg/g soil	Cd µg/g soil	Pb ^(b) µg/g soil	Pb µg/g soil
H1a		“8.5-10.5”		“6-12”	“7-11”	“unk”	“0.2-0.3”	“0.05-0.1”	“0.03-0.06”	“0.07-0.09”	“4-6”	
01A	55.1	89.0	(85.1)	10.5	11.2	(2.68)	(0.13)	0.48	0.06	0.07	502	(457)
01A Dup	55.1	165	(136)	15.2	241	(6.69)	(0.18)	6.35	0.20	0.07	678	(602)
H1		“3-8”		“5-14”	“7-10”	“unk”	“0.2-0.4”	“0.05-0.12”	“0.03-0.05”	“0.04-0.06”	“1.5-4.1”	
03A	67.9	125	(124)	9.32	13.7	(1.82)	(0.23)	2.12	0.04	0.07	19.23	21.1
04A	72.2	121	(121)	9.15	(9.70)	(2.45)	(0.25)	0.98	0.05	0.07	(4.64)	5.85
H2		“9-20”		“5-9”	“8-13”	“unk”	“0.1-0.3”	“0.07-0.1”	“0.04-0.06”	“0.06-0.14”	“2-10”	
05A	76.4	223	(220)	8.69	(9.20)	(4.83)	(0.19)	1.47	0.03	0.09	18.97	19.72
06A	80.6	641	(581)	7.83	(9.98)	(4.29)	(0.19)	12.6	0.03	0.09	7.81	(9.59)
07A	84.8	1228	(1105)	12.7	12.3	(4.90)	0.27	5.47	0.06	0.11	6.62	7.19
08A	89	1465	(1291)	9.17	(10.3)	(5.07)	0.29	10.2	0.05	0.12	6.32	7.50
09A	93.1	823	(699)	8.83	(9.09)	(4.39)	0.27	(0.44)	0.06	0.08	8.78	9.52
10A	97.3	561	(495)	8.55	(9.93)	(4.21)	0.36	(0.42)	0.06	0.12	(5.81)	6.55
11A	101.7	30.1	31.85	9.22	(9.55)	(4.35)	0.29	(0.56)	0.05	0.08	(5.34)	6.60
12A	105.6	23.8	24.88	13.2	18.9	(10.8)	0.29	(0.28)	0.09	0.16	15.0	16.2
13A	113.8	681	(599)	11.8	29.3	(5.61)	0.42	(2.74)	0.08	0.12	75.3	75.7
14A	122	452	(396)	10.3	15.2	(6.05)	0.43	(0.86)	0.07	0.13	8.42	9.19
14A Dup	122	430	(382)	10.0	14.0	(5.87)	0.54	(0.80)	0.06	0.13	8.89	9.65
PPlz		“4-16”		“8-18”	“13-18”	“unk”	“0.1-0.2”	“0.06-0.08”	“0.06-0.07”	“0.11-0.13”	“8-10”	
15A	130.1	411	(369)	15.4	25.5	(3.76)	0.65	(0.63)	0.08	0.15	7.78	10.9
16A	138.2	22.4	24.44	11.3	15.9	(3.24)	0.26	(0.56)	0.07	0.17	8.67	10.5
17A	144.6	32.2	34.34	12.7	21.4	(6.32)	0.33	(1.59)	0.08	0.16	9.19	10.5

(a) Multiply by 0.3048 to convert to meters.
(b) unk = Arsenic data for clean sediment has not been obtained so we have no baseline concentration.

pushed ahead of the high sodium porewater plume. It is less clear why the iron, manganese, and titanium acid extracts are elevated. One plausible explanation is that they represent alteration products and amorphous precipitates from the tank liquor that cannot be detected in the x-ray diffraction analyses to be discussed. The x-ray diffraction measurements can see only crystalline material that is present in substantial concentrations (a few weight percent of the bulk sediment).

There are a few other trends worth mentioning. There appears to be a small amount of excess acid-extractable aluminum in the coarse-grained H1 unit at the slant borehole between 20.7 to 21.9 meters (68 to 72 feet) bgs. Whether this is an artifact of our rather small data set or is caused by mineralogic differences, we cannot determine at this time. However, there are also small increases in the water-extractable aluminum (see Table 4.6) in the shallow sediment under tank SX-108 that could also be caused by the presence of extractable amorphous alteration products. Sample 12A, which appears to have not been in contact with tank liquor, shows relatively high acid-leachable barium, calcium, magnesium, and strontium, perhaps because sodium has not had the opportunity to exchange them off the sediment. There appears to be higher acid-extractable phosphorous in most of the H2 unit sediment. We have not been able to determine if these data are real and reflect phosphate or if the data are some spectral interference caused by the complicated matrix. We also have not been able to conclusively prove that ICP measurements of phosphorous in the water extracts are providing real values. If the phosphorous values, especially in water extracts, are real, they are not in agreement with the phosphorous being present as phosphate. Between 32 and 34.4 meters (105 and 113 feet) bgs, both iron and manganese appear to be elevated in the acid extract compared with the rest of the H2 samples. The acid extract of the sample 1A duplicate appears to be contaminated with some metal material from either the drilling operation or sampler opening.

Sample 12A shows very high iron, manganese, nickel, copper, and molybdenum concentrations in the acid extract compared to the separate sample 1A.

Table 4.18 shows similar acid extract comparisons for the trace metals in the slant borehole vadose zone sediment compared to values extracted from the ostensibly uncontaminated sediment from nearby RCRA boreholes. The complete slant borehole vadose zone region that was sampled shows elevated chromium and molybdenum. For chromium, there are two regions with acid-extractable concentrations that are at least 10 times higher than the uncontaminated sediment background values: between 16.8 and 29.6 meters (55 and 97 feet) bgs and between 34.7 and 39.6 meters (113.8 and 130 feet) bgs. The molybdenum acid-extractable values in these two regions also are often elevated by more than 10 times the background values. There appears to be elevated lead in the shallow H1a unit and a few samples in the H2 unit. The water extract data also suggests some elevated lead levels in the sediment that we speculate is from the tank liquor. The data suggest that lead in the tank liquor is sequestered rapidly in the sediment under the tank.

Table 4.18 shows that there is excellent agreement between the ICP and the ICP-MS analyses for chromium and lead that were present in high enough concentrations to be measured by both techniques.

Figures in Appendix C compare the amount of the element that was water extractable versus the amount that was acid extractable. For most elements (aluminum, arsenic, potassium, cadmium, calcium,

iron, lead, magnesium, manganese, silver, strontium, and zinc), the amount that is water extractable is just a fraction of the acid extractable. For the constituents chromium, molybdenum, selenium, and sodium, the amounts that are water leachable represent up to 75%, 30%, 40%, and >80%, respectively. The comparison of water leachable versus acid leachable gives a qualitative estimate of the mobility of a species. More discussion is found in Section 5.0.

4.2.6 Sediment Total Oxide Composition

Several samples of the bulk vadose zone sediment from the slant borehole were crushed and analyzed with x-ray fluorescence to obtain the complete composition of the sediment. Additional aliquots of the same sediment were subjected to particle size analysis and the sand, silt, and clay separates were retained. The clay separate was also analyzed by x-ray fluorescence to allow total oxide composition to be calculated. The total oxide composition of both the bulk- and clay-size separates was used to aid in the quantification of mineralogy that will be discussed later.

The total elemental oxide composition for the bulk sediment is shown in Table 4.19 and for the clay-size material in Table 4.20. Using two types of x-ray fluorescence instruments, we were able to analyze for all natural elements from sodium through uranium. We lack capability for measuring the concentrations of only carbon, beryllium, boron, fluorine, lithium, and nitrogen. However, we did analyze the carbon content of the bulk sediment as discussed in Section 4.2.4 so that component is available. We also assumed that the water-leachable nitrate contents of the sediment could be used to estimate the total nitrogen content of the sediment. The beryllium, boron, fluorine, and lithium content of the sediment likely is small; therefore, we should be able to calculate the oxide mass of the sediment and come close to 100% mass balance. We have assumed that the iron present in the sediment is all iron (III) oxide though there may be some reduced (ferrous oxides) iron also present.

The mass balances for the bulk sediment vary from 87 to 103%. The missing mass balance for sample 14A in the H2 unit (the one with only 87% recovery) is caused by a low silica value and perhaps low alumina value. As found for uncontaminated sediment from nearby boreholes, the Hanford formation sediment is dominated by silica and alumina. Calcium, carbonate, iron, magnesium, potassium, sodium, and titanium make up most of the rest of the oxides. We do not have a large database of elemental compositions but when compared to the two clean RCRA boreholes (see Serne et al. 2002c), the contaminated sediment at the slant borehole shows significantly higher nitrate, sodium oxide, and chromium oxide contents in the H2 unit. The nitrate and sodium oxide also are elevated in the PPlz unit. Conversely, the contaminated sediment in the entire profile shows slightly lower values for aluminum, magnesium, and silicon oxides. A few oxides (iron, sulfur, titanium, and vanadium) also appear to be a bit elevated in the PPlz sediment at the slant borehole compared to uncontaminated sediment, but again our database is sparse. The elevated chromium, nitrate, and sodium oxide contents are caused by the tank liquor that percolated through the vadose zone sediment. The other differences are not as easy to explain based on tank liquor interacting with the sediment.

Table 4.19. Total Composition of the Vadose Zone Sediment from Slant Borehole Percent Weight as Oxides

ID	3A	6A	7A	8A	9A	11A	13A	14A	15A
----	----	----	----	----	----	-----	-----	-----	-----

Depth (ft) ^(a)	67.9	80.6	84.8	89.0	93.1	101.7	113.8	122.0	130.1
Unit	H1	H2	H2	H2	H2	H2	H2	H2	PPlz
CO ₂	0.64	0.83	1.05	0.87	0.81	0.85	1.24	1.43	1.23
N ₂ O ₅	0.0	2.0	8.1	6.9	4.0	1.7	3.9	4.0	6.0
Na ₂ O	2.75	3.38	5.89	6.27	4.3	2.66	4.68	2.87	3.44
MgO	2.17	2.12	2.09	2.22	1.91	2.3	2.37	1.71	2.01
Al ₂ O ₃	12.8	11.3	12.1	11.5	11.5	11.1	12	9.7	11.3
SiO ₂	66.4	62.5	61.2	63.2	64.6	62.4	66.1	56.2	57.6
P ₂ O ₅	<0.30	<0.27	<0.25	<0.22	<0.33	<0.25	<0.22	<0.27	<0.32
SO ₃	0.09	0.09	0.17	0.08	0.13	0.1	0.08	0.11	0.18
Cl	<0.03	<0.06	<0.04	<0.05	<0.08	<0.08	<0.09	<0.08	<0.06
K ₂ O	1.86	2.41	2.14	2.41	2.56	2.49	2.65	2.3	1.87
CaO	4.39	3.04	3.43	3.34	3.09	3.34	3.19	3.6	3.64
TiO ₂	0.95	0.61	0.86	0.75	0.59	0.6	0.69	0.69	1.06
V ₂ O ₅	0.02	0.01	0.02	0.02	0.01	0.01	0.01	0.01	0.03
Cr ₂ O ₃	0.03	0.13	0.18	0.29	0.19	0.01	0.13	0.07	0.08
MnO	0.09	0.05	0.08	0.07	0.06	0.07	0.08	0.06	0.09
Fe ₂ O ₃	5.81	3.7	5.1	4.51	3.67	3.99	4.58	4.01	7.05
SrO	0.05	0.04	0.04	0.04	0.04	0.04	0.04	0.04	0.03
BaO	0.1	0.09	0.08	0.08	0.11	0.09	0.09	0.08	0.07
Total	98.16	92.35	102.56	102.58	97.55	91.71	101.81	86.85	95.71
(a) Multiply by 0.3048 to convert to meters.									

The mass balance for the clay-size separates in these samples, shown in Table 4.20 use the bulk sediment total carbon contents. However, we believe that the clay fraction may contain more carbon from the presence of fine-grained calcite. Thus, the mass balances shown are likely slightly lower than the true values. Conversely, we assume that all the nitrate was dissolved out of the clay fraction during the water rinsing and hydrometer separation steps. The clay-size material consistently has higher concentrations of aluminum, iron, and magnesium and lower concentrations of calcium, silicon, and sodium than the bulk sediment. This undoubtedly reflects the difference in mineral content with the bulk sample containing higher concentrations of quartz and feldspars than the clay-size material. Conversely, the clay separates contain higher concentrations of iron hydrous oxides and aluminosilicates.

Table 4.20. Total Composition of the Clay-Sized Fraction of Sediment from Slant Borehole Percent Weight as Oxides

ID	1A	1A-Dup	3A	6A	7A	8A	9A	13A	14A	15A
Depth (ft) ^(a)	55.1	55.1	67.9	80.6	84.8	89.0	93.1	113.8	122.0	130.1
Unit	H1a	H1a	H1	H2	H2	H2	H2	H2	H2	PPlz
CO ₂	0.585	0.593	0.64	0.83	1.05	0.87	0.81	1.24	1.43	1.23
Na ₂ O	2.91	2.75	4.27	1.97	2.08	2.49	2.64	2.7	1.37	1.64
MgO	3.12	2.95	3.07	2.77	3.05	3.27	3.38	3.6	2.8	2.88
Al ₂ O ₃	19.5	18.8	21.6	20	21.9	21.2	21.5	22.4	18.5	19.6
SiO ₂	56.8	55.4	61.1	53.4	56.2	55.6	58.2	62.1	60.7	58.2
P ₂ O ₅	<0.77	<0.77	<0.32	<0.27	<0.34	<0.31	<0.48	<0.40	<0.42	<0.50
SO ₃	0.13	0.12	0.1	0.1	0.13	0.1	0.09	0.09	0.07	0.08
Cl	<0.04	<0.04	<0.05	<0.05	<0.06	<0.06	<0.05	<0.04	<0.04	<0.03
K ₂ O	2.01	1.91	2.52	2.83	2.63	2.93	2.93	3	2.12	2.26
CaO	3.24	3.07	3.32	1.78	2.6	1.86	1.77	2.07	1.64	2.43
TiO ₂	1.06	0.99	0.9	0.8	0.92	0.86	0.76	0.89	0.63	0.93
V ₂ O ₅	0.02	0.02	0.02	0.01	0.02	0.02	0.01	0.02	0.01	0.01
Cr ₂ O ₃	0.06	0.06	0.09	0.3	0.68	0.63	0.22	0.12	0.08	0.04
Fe ₂ O ₃	8.01	7.47	6.71	6.77	7.64	7.38	7.1	7.49	6.59	8.35
SrO	0.02	0.02	0.03	0.02	0.02	0.02	0.02	0.02	0.01	0.02
BaO	0.11	0.11	0.11	0.17	0.11	0.07	0.10	0.11	0.10	0.10
Total	97.58	94.26	104.48	91.75	99.03	97.30	99.53	105.85	96.05	97.77
(a) Multiply by 0.3048 to convert to meters. The carbon content of the clay separates was not measured so the bulk values were used as an estimate.										

The clay-size material for samples 7A and 8A contain high concentrations of chromium compared to the bulk sediment, whereas the shallower clay-size samples contain lower concentrations of chromium and deeper samples contain about the same amount of chromium. The reason for the changing ratios of chromium between the bulk and clay-size material is not easily explained.

The acid extraction dissolves a portion of the total elemental composition of the vadose zone sediment. Because the x-ray fluorescence data appear to give a good mass balance, we conclude that x-ray fluorescence does in fact give an accurate measurement of the total elemental composition. Thus, we can estimate the percentage of the total elemental composition that dissolves in 8 M nitric acid. Table 4.21 lists the percentages of the total sample that the acid does dissolve.

In general, for the uncontaminated sediment from both RCRA boreholes (see Serne et al. 2002c), the acid removes only 1 to 10% of the total mass of alkali metals (sodium, potassium), about 25% of the

Table 4.21. Percentage of Elements Extracted by 8 M Nitric Acid

Element	03A	06A	07A	08A	09A	11A	13A	14A	15A
	Acid/Total								
Na	8.3%	23.9%	54.4%	32.3%	33.4%	11.9%	32.1%	47.1%	62.6%
Mg	37.9%	41.2%	50.3%	46.0%	50.6%	44.9%	52.5%	68.1%	68.3%
Al	11.4%	13.7%	21.0%	15.2%	16.8%	14.6%	19.7%	25.3%	30.4%
Si	<1%	<1%	<1%	<1%	<1%	<1%	<1%	<1%	<1%
K	8.1%	9.9%	13.0%	11.4%	10.8%	10.7%	14.2%	13.0%	16.7%
Ca	22.8%	38.6%	40.5%	39.3%	38.8%	43.9%	45.9%	54.1%	52.1%
Cr	55.4%	67.1%	94.7%	69.8%	59.1%	54.4%	73.1%	80.0%	76.1%
Mn	42.2%	72.6%	73.3%	61.5%	66.8%	69.1%	81.2%	71.3%	78.2%
Fe	48.0%	67.6%	68.5%	56.6%	67.4%	66.2%	75.9%	68.5%	76.2%
Co	>17.3%	>19.1%	>23.1%	11.9%	>21.0%	>21.0%	17.6%	>23.3%	26.2%
Ni	76.0%	81.4%	94.6%	65.8%	84.7%	84.6%	70.4%	84.0%	50.7%
Cu	83.8%	63.5%	74.6%	52.7%	54.1%	52.2%	138.8%	75.0%	79.3%
Zn	64.7%	73.7%	85.5%	75.6%	84.8%	72.5%	89.9%	85.4%	84.6%
As	>60.7%	82.5%	63.7%	63.4%	91.6%	108.8%	71.6%	82.9%	50.1%
Se	>11.3%	>9.7%	>12.2%	>15.1%	>13.5%	>14.6%	>19.9%	>22.6%	32.6%
Sr	7.6%	8.9%	11.5%	9.4%	9.5%	15.7%	12.3%	15.9%	25.7%
Mo	12.7%	37.3%	>39.0%	59.7%	>4.4%	>4.3%	33.8%	>7.2%	4.9%
Ag	>0.3%	0.1%	>0.3%	>0.3%	>0.3%	>0.2%	0.5%	>0.4%	0.4%
Ba	8.3%	11.2%	13.1%	10.8%	9.5%	13.7%	16.7%	13.6%	28.0%
Pb	95.7%	52.8%	61.7%	44.5%	70.3%	35.8%	411%	58.5%	93.7%
U	>13%	>15%	>12%	>16%	>14%	>12%	>108%	>17%	6%
Cd	>0.4%	>0.5%	>0.7%	>0.8%	>0.4%	>0.3%	>0.8%	>0.6%	0.7%

major alkaline earth metals (magnesium, calcium); and less (about 10 to 15%) of the minor alkaline earths (strontium, barium); very little of the silicon, about 15% of the aluminum and titanium; about 40 to 60% of the iron and manganese; and 25 to 70% of the various trace metals. For the contaminated sediment from the slant borehole, the acid dissolution efficiency for sodium is much higher because the total sodium is dominated by sodium nitrate salts, not structural sodium in the primary minerals. Between 32 and 54% of the sodium is extracted by acid from the slant borehole sediment samples that have the highest total sodium and highest water-extractable sodium (7A, 8A, 9A, and 13A). The deeper samples, 14A and 15A, have lower (but still elevated above background sediment) total sodium contents and moderate water-soluble sodium concentrations but the highest percent acid-extractable values (~50 to 60%) found. This suggests that the slant borehole sediment in the lower H2 and upper PPlz units still have considerable amounts of sodium from the tank liquor that is not fixed in primary minerals and clays. The acid-leachable potassium percentages in the slant borehole sediment are not significantly larger than for the uncontaminated sediment and the total potassium content of the contaminated sediment is not larger than in the uncontaminated sediment. Thus, we conclude that the tank liquor contains relatively

low concentrations of potassium and the potassium that is pushed off exchange sites in the sediment (shown in the water-extractable data) is small in relation to the potassium present in primary minerals.

The percentage of the total alkaline earth elements that is acid extractable is about twice as high in the contaminated sediment likely because the contribution from displaced ion exchange sites is large enough compared to the calcium and magnesium in primary minerals to increase the acid-extractable portion. In general, the percentage of the minor alkaline earth cations (barium and strontium) that is acid extractable in the slant borehole sediment is no different than for uncontaminated sediment. This is consistent because the mass of minor alkaline earth elements that are displaced from ion exchange sites is small, and the tank liquors did not contain high enough concentrations of these minor elements to change the acid dissolution percentages of the primary minerals that contain the majority of the barium and strontium.

The percentage of aluminum that is acid extractable in the contaminated sediment from the slant borehole does not differ from uncontaminated sediment, except perhaps in the two deeper samples where the percentage is about twice the average of 15%. It is unclear if this is an indication of the formation of amorphous alteration products containing aluminum from the interaction of the tank liquors with sediment. The x-ray diffraction results to be discussed below and limited scanning electron microscopy characterization (performed by the Science and Technology Program; reported in the field investigation report^(a)) of particles from the lower H2 and upper PPLz zone do not suggest any signs of alteration. Therefore the higher percentage aluminum that was extracted by the acid in the two deepest samples analyzed may be coincidental.

The percentage of the total iron and manganese that is acid extractable is about 10% higher (absolute value) than percentages extracted from uncontaminated sediment. Again, it is not clear whether there are any geochemical or mineral weathering implications to this observation.

In general, the percentage of the total sediment trace metal concentrations that is acid extractable from the highly contaminated slant borehole sediment is slightly higher than for the uncontaminated sediment. We would have expected that the chromium percentage would be much higher for the contaminated sediment than for comparable uncontaminated sediment, but the increase is not striking despite the fact that the total chromium content of the contaminated sediment is significantly elevated over uncontaminated sediment. The percentage of the total lead that is extractable from sample 13A suggests that lead contamination from the shielding in the samplers is present in some of the extracts. This is based on the acid leach containing four times greater amounts of lead than the total in the sediment sample that was used to perform x-ray fluorescence measurements. Somehow, lead contamination was present in the aliquot of sediment from sleeve 13A that was acid extracted, or lead contamination was introduced during the acid digest. The discrepancy is not instrumental analytical error because the lead was present in both ICP and ICP-MS measurements (see Table 4.18).

In conclusion, the manmade sodium and perhaps a percentage of the elevated trace metals concentrations are more readily acid extractable from the highly contaminated slant borehole sediment compared to uncontaminated sediment. Except for the sodium results, we expected there to be a larger

(a) *Draft Field Investigation Report for Waste Management Area S-SX*. RPP-7884, Draft, Volume 2, Appendix D, CH2M HILL Hanford Group, Inc., Richland, Washington.

increase than was observed. This unexpected lack of dramatic differences for the contaminated sediment suggests that the comparison of percentages of the total composition of any element that is acid extractable is not a very sensitive indicator of the presence of tank liquors in the vadose zone sediment. More discussions on looking for alteration products are found in the mineralogy section below.

4.2.7 Particle Size Measurements on Vadose Zone Sediment

The wet sieving/hydrometer method was used to determine the particle size distributions of several samples from the slant borehole. The wet sieving and hydrometer particle size information are shown in Tables 4.22 to 4.24 and Figures 4.10 to 4.12. Table 4.22 shows the details on the wet sieving that quantifies gravel and sand nicely. Table 4.23 shows the wet sieving data converted to calculate the modified Folk/Wentworth sediment classification used at Hanford (Fecht and Price 1977), particle size divisions, and the modified Folk sediment classification. Here we show that the H1 unit has enough gravel to be considered a slight gravelly muddy sand. The Hanford formation H2 unit has a few finer grained lenses that are sandy mud as opposed to the muddy sand based on the ratio of sand to mud dropping below 1:1. The PPlz zone is considered a sandy mud. Table 4.24 shows the combined wet sieving and hydrometer data.

Table 4.22. Particle Size Distribution (Wet Sieve) Percent Weight

ID	Sieve #	Gravel			Sand					Mud
		Fine Pebble	Very Fine Pebble	Very Coarse	Coarse	Medium	Fine		Very Fine	Silt & Clay
		5	10	18	35	60	70	120	230	Pan
Depth (ft) ^(a)	>4 mm	2-4 mm	1-2 mm	0.5-1.0 mm	0.25-0.5 mm	0.21-0.25 mm	0.125-0.21 mm	0.0625-0.125 mm	<0.0625 mm	
1A	55.1	0.00%	1.07%	2.42%	6.61%	18.7%	8.9%	23.8%	6.65%	31.8%
3AB	67.9	1.81%	4.65%	11.5%	17.5%	12.4%	2.3%	7.26%	6.70%	36.0%
6A	80.6	0.00%	0.00%	0.24%	3.40%	14.6%	4.56%	16.0%	25.6%	35.6%
7A	84.8	0.00%	0.01%	0.57%	1.04%	4.80%	3.96%	22.8%	17.8%	49.0%
8A	89	0.00%	0.03%	0.10%	0.48%	3.16%	1.30%	28.4%	15.9%	50.7%
9A	93.1	0.00%	0.29%	1.00%	3.26%	16.3%	5.9%	25.5%	8.9%	38.9%
11A	101.7	0.00%	0.00%	0.01%	0.93%	11.92%	5.65%	24.01%	21.13%	36.36%
13A	113.8	0.00%	0.03%	0.27%	0.99%	9.08%	6.82%	24.44%	8.43%	49.94%
14A	122	0.00%	0.04%	0.08%	0.17%	1.37%	0.73%	19.7%	21.8%	56.0%
15A	130.1	0.00%	0.01%	0.03%	0.46%	2.83%	1.16%	12.4%	23.5%	59.6%

(a) Multiply by 0.3048 to convert to meters.

Table 4.23. Folk-Wentworth Sediment Classification

ID	Depth (ft) ^(a)	% Gravel	% Sand	% Mud	Sand:Mud Ratio	Modified Folk Sediment CLASS	Unit
1A	55.1	1.07%	67.1%	31.8%	2.11	mS	H1a
3AB	67.9	6.47%	57.5%	36.0%	1.60	(g)mS	H1
6A	80.6	0.00%	64.4%	35.6%	1.81	mS	H2
7A	84.8	0.01%	50.9%	49.0%	1.04	mS	H2
8A	89	0.03%	49.3%	50.7%	0.97	sM	H2
9A	93.1	0.29%	60.8%	38.9%	1.57	mS	H2
11A	101.7	0.00%	63.6%	36.4%	1.75	mS	H2
13A	113.8	0.03%	50.0%	49.9%	1.00	ms	H2
14A	122	0.04%	43.9%	56.0%	0.78	sM	H2
15A	130.1	0.01%	40.4%	59.6%	0.68	sM	PPlz

(a) Multiply by 0.3048 to convert to meters.
mS = muddy sand.
sM = sandy mud.

Table 4.24. Particle Size Distribution Based on Combined Wet Sieve/Hydrometer Methods

ID	Depth (ft) ^(a)	% Gravel	% Sand	%Silt	%Clay	Silt to Clay
1A	55.1	1.07	67.1	24.8	“~7”	3.5
3AB	67.9	6.47	57.5	25.8	“~10.2”	2.5
6A	80.6	0.00	64.4	24.6	“~11”	2.2
7A	84.8	0.01	50.9	37.0	“~12”	3.1
8A	89	0.03	49.3	39.0	“~11.7”	3.3
9A	93.1	0.29	60.8	30.4	“~8.5”	3.6
11A	101.7	0.00	63.6	28.0	“~8.4”	3.3
13A	113.8	0.03	50.0	36.0	“~13.9”	2.6
14A	122	0.04	43.9	42.7	“~13.3”	3.2
15A	130.1	0.01	40.4	42.9	“~16.7”	2.6

(a) Multiply by 0.3048 to convert to meters.
Silt % is calculated as remainder after subtracting gravel, sand, and clay from total.

Besides the hydrometer estimate of clay-size particles, we physically separated the clay material from the silt by performing numerous resuspensions of the slurry and decanting off the clays after the silts had settled. The clay material was then used for mineralogy characterization. An aliquot of the final clay slurry was weighed and taken to dryness to determine the amount of clay that had been separated. This number was averaged with the hydrometer estimate to give the clay mass distribution shown in

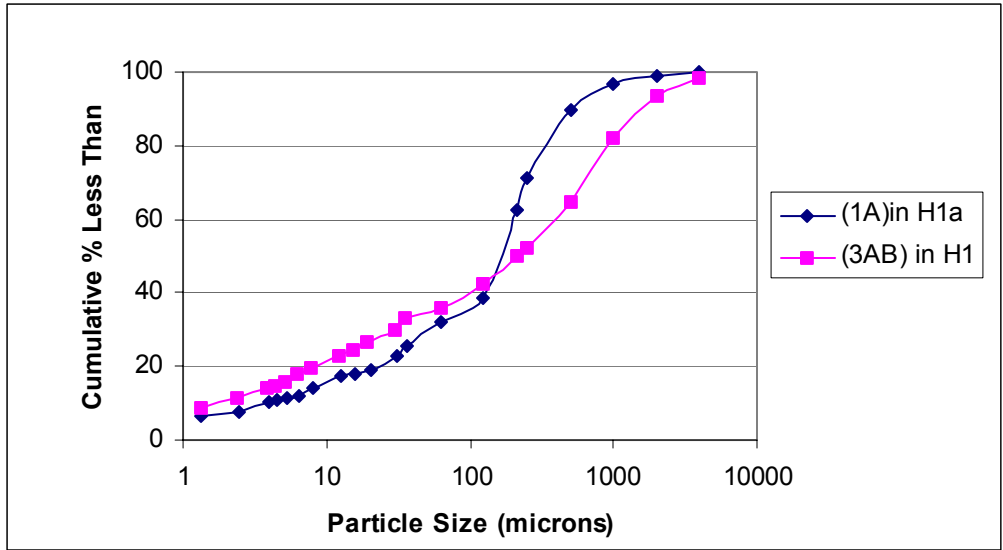


Figure 4.10. Particle Size Distribution of Slant Borehole Samples from H1a and H1 Units

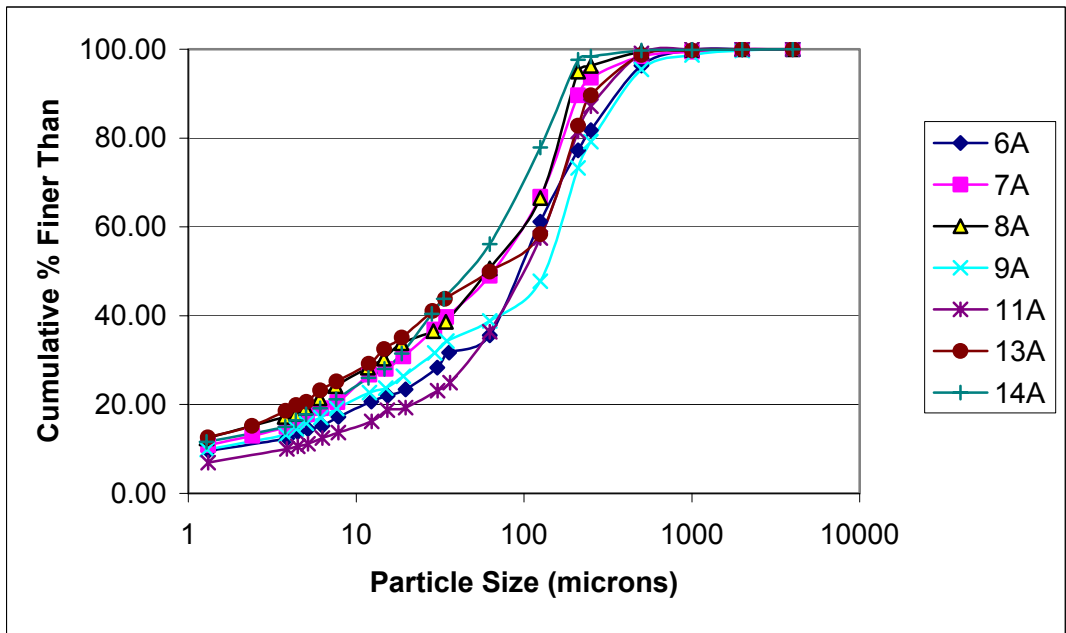


Figure 4.11. Particle Size Distribution of Slant Borehole Samples from H2 Unit

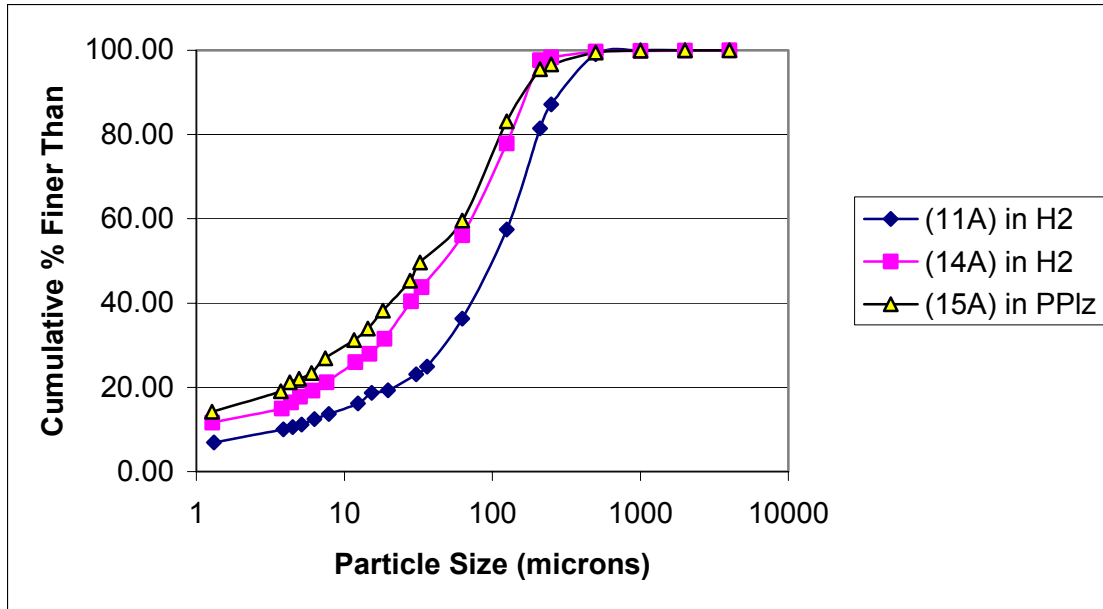


Figure 4.12. Particle Size Distribution of Slant Borehole Samples from PPlz versus Range in H2 Unit

Table 4.24. The silt mass distribution in Table 4.24 is the remainder after subtracting out the gravel, sand, and clay content from the total mass. Note that most of the mud fraction is actual silt, with silt-to-clay ratios ranging between 2.5 and 3.6.

Figure 4.10 shows the particle size distribution of sample 1A in the H1a fine-grained unit and sample 3AB in the slightly gravelly muddy sand unit H1. Figure 4.11 shows the variation in particle size distribution for the seven H2 unit sediment samples that were characterized. Finally, Figure 4.12 shows the one sample of PPlz plotted with the finest and coarsest samples of the H2 unit for comparison. One can see that the finest grained samples of the H2 are very similar in grain size to the top of the fine-grained PPlz unit represented by sample 15A. We did not measure the particle size of the next two deeper samples. Because the borehole did not penetrate the whole PPlz unit, we cannot show explicitly that the PPlz unit in general is finer grained than the H2 unit at this borehole. However, based on other nearby boreholes, we believe that the PPlz under SX-108 is finer grained than the H2 unit.

4.2.8 Particle Density of Bulk Sediment

The particle density for each of the samples that were wet sieved is shown in Table 4.25. The values are similar to those of uncontaminated sediment from the same lithologic facies (see Serne et al. 2002c).

Table 4.25. Particle Density of Bulk Sediment from Slant Borehole

ID	Depth (ft bgs) ^(a)	Facies	Ps
1A	55.1	H1a	2.704
3AB	67.9	H1	2.738
6A	80.6	H2	2.700
7A	84.8	H2	2.735
8A	89	H2	2.745
9A	93.1	H2	2.743
13A	113.8	H2	2.714
14A	122	H2	2.748
15A	130.1	PPlz	2.748

(a) Multiply by 0.3048 to convert to meters.
Ps = Particle density.

Table 4.26. Semiquantitative Mineral Composition for Bulk Samples (wt%)

Sample ID	Depth ^(a)	Geologic Unit	Quartz	K-Feldspar	Plagioclase	Calcite	Total
3A	67.9	H1	50	15	30	5	~100
6A	80.6	H2	40	25	35	5	~105
7A	84.8	H2	35	20	10	15	~80
8A	89.0	H2	30	5	20	15	~70
9A	93.1	H2	40	20	60	5	~125
11A	101.7	H2	45	5	20	5	~75
13A	113.8	H2	55	10	35	5	~105
14A	122.0	H2	50	10	20	5	~85
15A	130.1	PPlz	40	5	10	10	~65

(a) Depth in vertical feet (multiply by 0.3048 to convert to meters).

4.2.9 Mineralogy

X-ray diffraction analyses of the bulk samples from nine depths (Table 4.26) in the slant borehole indicate that the sediment is mostly quartz (~30 to 60%) and feldspar (~15 to 80%), with lesser amounts of calcite, amphibole, mica, chlorite, and smectite. Plagioclase feldspar is 1 to 4 times more abundant than potassium feldspar, with the exception of sample 7A (25.8 meters [84.8 feet] bgs), which has more potassium feldspar than plagioclase feldspar. Additionally, x-ray diffraction tracings from most samples showed evidence of the sodium nitrate mineral, nitratine. Identification of nitratine is based on the

primary peak at 3.035 Å. Chemistry of the 1:1 water extracts (Section 4.2.2) from these samples showed large amounts of sodium and nitrate (~3.0 to 15 M), so it is not unexpected that solid sodium nitrate is present.

Recoveries for semiquantification ranged from a low of 65 wt% (sample 15A) to a high of 125 wt% (sample 9A). Sample 9A has an excessive amount of plagioclase feldspar that could be the result of poor random packing of the powdered sample into the x-ray diffraction holder. Examples of x-ray diffractograms of the bulk sediment are presented in Appendix D.

The clay fraction (<2 micron) in all the samples characterized (see Table 4.27) is dominated by four clay minerals: illite (10 Å), smectite (15 Å), chlorite (14.1 Å), and kaolinite (7 Å) with minor amounts of quartz (3.34 Å), feldspar (3.18 Å), amphibole (8.4 Å), and calcite (3.03 Å). When solvated with ethylene glycol, the smectite reflection expanded up to 17 Å, leaving the chlorite (14.1 Å) visible (Appendix D). Chlorite, illite, and kaolinite are unaffected by ethylene glycol solvation and their characteristic peaks remain constant. Illite identification is based on the 10 Å and 5.0 Å reflections. Chlorites were identified by the 14.0 Å and 4.75 Å reflections. In some cases, the chlorite 4.75 Å reflection appeared to have a double component, which indicates two different types of chlorites present in the samples (see samples 3A and 6A, Appendix D). Kaolinite, although harder to identify in the presence of chlorite, is confirmed by the split in the ~3.54 Å peak. All depths showed evidence of kaolinite except depth 3A (20.7 meters [67.9 feet]). Examples of x-ray diffractograms of the oriented clay sediment saturated with magnesium (II) and ethylene glycol solvated are presented in Appendix D.

The clay fraction from samples 3A, 6A, and 7A were reanalyzed by x-ray diffraction at a slower scan rate to allow for better characterization of the trace mineral phases possibly present as the result of the tank leak. These samples were scanned from 2 to 45 degrees 2θ at a 0.04 step size and an 18 second

Table 4.27. Semiquantitative Analysis of the Clay Fraction from Slant Borehole (wt%)

Sample ID	Depth (ft) ^(a)	Geologic Unit	Quartz	Feld.	Smectite	Illite	Chlorite	Kaolinite	% Total
1A	55.1	H1a	5	5	10	15	15	5	~55
3A	67.9	H1	10	5	5	10	15	ND	~45
6A	80.6	H2	10	5	10	30	20	5	~80
7A	84.8	H2	5	5	20	20	20	5	~75
8A	89.0	H2	5	5	15	25	30	5	~85
9A	93.1	H2	10	5	15	25	30	10	~95
13A	113.8	H2	10	5	10	25	25	5	~80
14A	122.0	H2	5	5	10	15	10	5	~50
15A	130.1	H2	10	5	10	10	5	5	~50

(a) Depth in vertical feet (multiply by 0.3048 to convert to meters).
 ND = Not detected.

dwelt time. Examples of the x-ray diffraction tracings are presented in Appendix D. Trace amounts of laumontite (9.08 Å) were detected in all three samples. The zeolite, laumontite, is known to be present in

the natural uncontaminated Hanford sediment and is not thought to be a weathering product resulting from the interaction of tank liquor with the sediment. No evidence of mineral alteration or precipitation resulting from the interaction of the tank liquor with the sediment was observed based on the x-ray diffraction measurements. However, scanning electron microscopy scans of some of the samples by scientists suggests that there is evidence of caustic attack on sample 3A.

The semiquantitative abundances of minerals in the clay fraction is given in Table 4.27. Overall, smectite, illite, and chlorite are the dominant minerals in the clay fraction with 25 to 70 wt%. Smectites range in concentrations from as high as 20 wt% (sample 7A depth 25.8 meters [84.8 feet]) to as low as 5 wt%; illite occurred between ~10 and 30 wt%. Chlorite concentrations were as low as 5 wt% (sample 15A 39.7 meters, [130.1 feet] bgs) and as high as 30 wt% (6A 24.6 meters, [80.6 feet] bgs). Minor amounts of kaolinite (~10 wt%) were detected at all depths, but one (3A 20.7 meters, [67.9 feet] bgs). Quartz and feldspar made up ~10 to 15 wt% of the clay fraction. Amphibole was identified in the clay fraction in minor amounts; however, it was not quantified. Nitratine was not found in the clay fractions. This is not surprising because the clay particles were washed repeatedly during the phase separation process so that readily dissolved salts should not be present. Total mass balance for the clay fractions ranged from a low of 55% to a high of 95%. The low recoveries obtained for samples 1A, 3A, 14A, and 15A are probably the result of the clay substrate peeling and curling prior to the x-ray diffraction analysis. Quantitative analysis is considered good if errors amount to $\pm 10\%$ of the amounts present for major constituents and $\pm 20\%$ for minerals whose concentrations are less than 20% (Reynolds and Reynolds 1989).

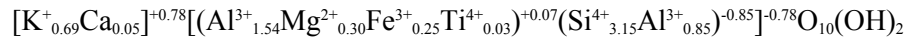
X-ray fluorescence analysis on the <2 micron fraction was conducted on all nine samples plus a duplicate for sample 1A (labeled 1A-2). The results, converted to oxides, are presented in Section 4.2.6, Table 4.20. Overall, approximately 53 to 62 wt% of the clay fraction consists of silicon oxide, followed by lesser amounts of aluminum oxide (~18 to 23 wt%) and iron oxide (~6.5 to 8.5 wt%). The clay fraction contains between 6 and 11 wt% of the total iron oxide in the bulk sample, with most depths having <7.8 wt% iron oxide. Iron oxides were detected in trace amounts during the transmission electron microscopy (TEM) analysis of the clay fraction, which suggests that most of the iron in the <2 micron fraction is incorporated into clay mineral structures (smectites, chlorites, and illites) and in the amphibole. Chromium oxide concentrations were elevated in samples 6A through 9A, peaking in samples 7A and 8A, with values of 0.68 and 0.63 wt%, respectively. We could not find discrete chromium bearing crystalline phases in the x-ray diffraction patterns.

Additional information on illite concentrations was obtained using the x-ray fluorescence data from the clay fraction. Using potassium oxide data derived from x-ray fluorescence analysis, (assuming all potassium resides in the illite structure), the potassium was converted into weight percent illite. Concentrations of illite in the individual clay fractions (beginning with the shallowest sample 1A) were 15, 10, 30, 20, 25, 25, 25, 15, and 10 wt%. The illite concentrations determined by x-ray diffraction for samples 3A and 15A are about 50% low compared to the results from the x-ray fluorescence data, otherwise the results for both x-ray diffraction and x-ray fluorescence are in good agreement.

TEM analysis of illites from samples 3A, 7A, and 15A show large, angular, platy particles typical of the weathered micas occurring in uncontaminated Hanford sediment. Illites exhibited distinct, sharp edges and were observed to be the largest size particles in the clay fraction. Figure 4.13 is a typical illite

from sample 3A. Additionally, some illites appeared to be very thin and were often serving as substrates for other minerals. Figure 4.14 is an example of two thin platy illites from sample 7A.

Using data generated by TEM analyses of ~45 illites from samples 3A, 7A, and 15A and assuming all iron as Fe³⁺, an average structural formula was calculated:



As in muscovite, most of the layer charge for the illite originates in the tetrahedral sheet (-0.85), with a slight positive contribution from the octahedral sheet (+0.07), resulting in a 2:1 layer charge of -0.78. The interlayer charge of +0.78 balances the charge on the 2:1 silicate structure.

Energy dispersive x-ray analysis of the individual illites showed little variation in the silicon and aluminum content. Potassium values ranged between 0.36 to 0.96 per O₁₀(OH)₂, with 77% of the particles having potassium concentrations between 0.6 and 0.85 atoms per O₁₀(OH)₂. Large differences were noted in the iron (III) and magnesium (II) contents. Iron values ranged between 0.01 and 1.29 atoms per O₁₀(OH)₂. Ten percent of these illites had iron (III) concentrations >1 atoms per O₁₀(OH)₂.



Figure 4.13. Typical Illite Particle from Sample 3A (~1.5 microns)

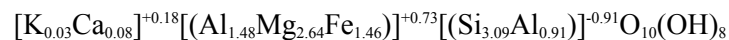


Figure 4.14. Two Thin Platy Illites Surrounded by Smaller Particles of Feldspar, Quartz, and Amphibole

and 82% had iron (III) concentrations <0.3 atoms per $O_{10}(OH)_2$. Octahedral magnesium (II) concentrations ranged between 0.00 and 1.29 atoms per $O_{10}(OH)_2$ with 80% of the particles having magnesium (II) values <0.4 atoms per $O_{10}(OH)_2$. Traces of titanium (IV) were detected in most of the illites.

Chlorite particles common in the clay fraction from samples 3A, 7A, and 15A had a similar morphology. However, the chlorites analyzed by TEM with energy dispersive x-ray spectroscopy showed a significant variability in the concentrations of iron (III) and magnesium (II). The chlorites ranged between a magnesium-rich chamosite to an iron-rich chlinoclore, with most individual grains residing somewhere in between.

Figure 4.15 shows a TEM photo of chlorite in sample 7A. A structural formula developed from five average chlorites analyzed by TEM from sample 7A gives the following:



The structural formula shows the negative charge in the tetrahedral sheet, originating from the substitution of aluminum (III) for silicon (IV), is balanced by the inclusion of the trivalent cation, aluminum (III), and divalent cations, magnesium (II) and iron (II) into the octahedral sheets. The total

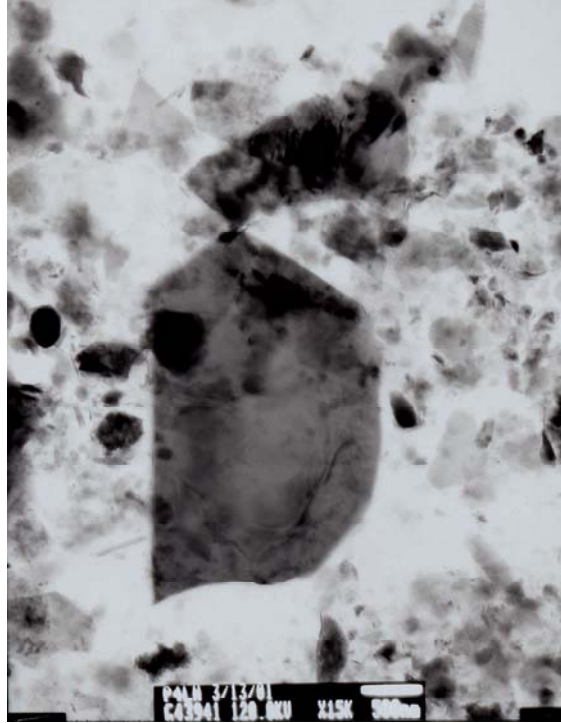


Figure 4.15. Typical Chlorite Grain from Sample 7A
(~2.5 microns long)

number of cations occupying octahedral sites is 5.60 per $O_{10}(OH)_8$. TEM analysis of the individual chlorite grains showed iron (II) concentrations ranged from a low of 0.81 to a high of 1.72 atoms per $O_{10}(OH)_8$ and Mg^{2+} ranged from 2.27 to 2.87 atoms per $O_{10}(OH)_8$. Small amounts of potassium and calcium were included in the structural formula, but are most likely from fine illite grains that could not be separated from the chlorite morphology of the illite in TEM images, with both minerals being thin and platy.

The chlorites examined from samples 3A and 15A appeared similar to chlorites characterized in sample 7A and to chlorites characterized by earlier reports on the Hanford sediment (Serne 2002a, b, c).

Smectite particles in samples 7A (25.8 meters [84.8 feet] bgs) and 15A (39.7 meters [130.1 feet] bgs) were characterized by TEM. Large flaky aggregates of smaller smectites were easily identified from the other clay minerals (Figure 4.16). These aggregates tend to project thin films of individual smectites out from the dense center of the aggregates incorporating smaller particles such as illites and iron oxides. A typical smectite aggregate exhibiting thin films from sample 15A is shown in Figure 4.17.

The following structural formula was developed from data collected on 16 smectites (samples 7A and 15A):

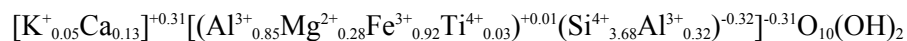




Figure 4.16. Thick Delicate Smectite Laths Curled up to Appear Dense



Figure 4.17. Typical Dense Smectite Aggregate from Sample 15A (~1 micron)

The tetrahedral sheet has minor substitution of aluminum (III) for silicon (IV), which creates a small negative charge. This negative charge is balanced by the +0.01 charge on the octahedral sheet and by the interlayer cation charge of +0.31. Iron concentrations in the octahedral sites varied between 0.52 and 1.57 atoms per $O_{10}(OH)_2$. The interlayer cation, calcium²⁺, ranged from a low of 0.03 to a high of 0.33 atoms per $O_{10}(OH)_2$. Potassium concentrations, which ranged between below-detectable-limits to as high as 0.12 atoms per $O_{10}(OH)_2$, were assigned to the interlayer position and possibly represent minor amounts of illite/smectite mixed layering. Trace amounts of titanium (IV) were also detected in most smectites examined.

The clay mineral kaolinite was identified by the x-ray diffraction analysis, but not by the TEM analysis. Kaolinite particles typically appear similar to illite particles and can be difficult to identify by TEM. Additionally, minerals such as sepiolite, apatite, iron oxide, sodium-plagioclase, amphibole, and anatase were detected in trace amounts during TEM analysis.

Mineral assemblages and structural formulas were similar to data reported earlier on uncontaminated sediment from the Hanford Site (Serne et al. 2002c). No evidence of caustic tank liquor reacting with the sediment to alter the mineral phases or properties was observed by x-ray diffraction or TEM analysis.

5.0 Contaminant Migration Potential and Comparison of Contaminant Contents at the SX-108 Slant Borehole to Borehole 41-09-39

In this section, we summarize and interpret the contaminant distributions found at the SX-108 slant borehole and compare the distributions with those at borehole 41-09-39 at the SX-109 tank leak. Further, we compare and contrast the potential for future migration of the contaminants.

5.1 Quantification of Desorption Potential for Major Contaminants in Slant Borehole

Desorption potential is an important parameter, because it shows the tendency of the sediment to give up contaminants as recharge passes through the layer of contaminants to the groundwater. This then provides a means of future contaminant potential to the groundwater at the SX Tank Farm.

Using the direct gamma energy analyses for cesium-137 and the acid extracts for the other constituents and the water extracts for all, we calculated in situ desorption K_d values for several constituents. The calculation relies on knowledge that the total gamma energy analysis and acid extracts give the total quantity of contaminant in the sample obtained from coring. That is, the value includes any material precipitated/adsorbed onto the sediment plus material in the porewater. The 1:1 water extracts can be used to calculate the amount of material that was in the porewater (this assumes that the water extraction does not also remove material that was precipitated/adsorbed on the sediment). For constituents that are moderately to strongly adsorbed, there is little need to subtract the small amount of mass in the porewater from the total measured by direct gamma energy analysis or acid extraction. Thus, the desorption K_d is simply the ratio of the amount of material in the acid extract/direct gamma energy analysis to the amount in the dilution-corrected water extract with both values based on 1 gram and 1 milliliter of sediment and porewater, respectively. For constituents that show little interaction with the sediment (e.g., technetium-99), one must subtract the portion in the porewater from the total found in the acid extract to determine the amount associated with the sediment. This difference is then ratioed against the amount in the porewater to obtain the desorption K_d .

Table 5.1 shows desorption K_d values for key constituents that are present in the tank liquor. The values represent desorption tendencies after 40 years of interaction. It is often observed that desorption K_d values are larger than those for adsorption of contaminants onto sediment. Conversely, the 1:1 water extracts may overestimate the porewater concentrations of some of the contaminants, such that the denominator in the ratio is larger than it should be. This would lead to the values in Table 5.1 being biased low. We cannot determine what the correct K_d values should be for the original adsorption process that controlled the original distribution of contaminants within the sediment. We can state that the values shown in Table 5.1 represent the desorption tendencies for the contaminants today and in the

Table 5.1. In Situ K_d Values for Contaminants Desorbing from Slant Borehole Vadose Zone Sediment

ID	Depth (ft bgs) ^(a)	Lith. Unit	K _d Values (mL/g)						
			¹³⁷ Cs	⁹⁹ Tc	U	Cr	As	Se	Mo
01A	55.1	H1a	230.3	indeterm	13	423	3.02	indeterm	1.53
01A-dup	55.1	H1a		indeterm	14	749	8.34	0.11	18.26
03A	67.9	H1	25.7	0.04	5	4.26	1.44	indeterm	0.16
04A	72.2	H2	72.9	indeterm	3	4.32	0.64	indeterm	0.42
05A	76.4	H2	99.3	-0.01	8	2.92	2.68	1.26	0.44
06A	80.6	H2	2.3	0.01	24	0.01	16	0.11	0.06
07A	84.8	H2	4.2	-0.01	0	0.18	2.37	0.21	0.00
08A	89	H2	24.8	-0.02	18	0.05	10	0.06	0.19
09A	93.1	H2	6.5	0.00	14	0.01	3.38	0.02	0.04
10A	97.3	H2	10.2	0.00	12	0.01	2.49	0.02	0.46
11A	101.7	H2	>49.7	0.00	114	1.04	5.74	0.04	3.01
12A	105.6	H2	>120.7	-0.02	588	24.1	461	7.52	4.72
13A	113.8	H2	>46.5	0.00	459	0.04	10	0.06	0.79
14A	122	H2	307.4	0.01	168	0.06	14	0.10	3.21
14A-dup	122	H2		-0.01	132	0.03	13	0.12	3.36
15A	130.1	PPlz	>136.7	-0.02	139	0.04	8.32	0.10	7.84
16A	138.2	PPlz	>13.9	0.02	63	84.9	39	0.55	3.02
17A	144.6	PPlz	35.6	0.11	223	1864	303	4.58	15.7

(a) Multiply by 0.3048 to convert to meters.

future as recharge water or sluicing fluids that might escape mixes with the contaminated vadose zone sediment. For future desorption processes, the values in Table 5.1 may be biased low and are thus, conservative estimates of future migration potentials.

As can be seen, the cesium-137 data show a highly variable K_d value ranging from a low of 2.3 to a high of 307 mL/g. Much of the variability can be correlated to the major cation composition of the porewater, especially the sodium concentration. From 24.6 to 29.7 meters (80.6 to 97.3 feet) bgs, the cesium-137 K_d is relatively low because the sodium concentration in the porewater varies from 6.6 to 17 M. Aside from sample 13A that has a moderate K_d value of ~≥50 and sample 8A where the K_d is 25 mL/g, the cesium-137 K_d values are below 10 mL/g when the sodium concentration in the porewater is above 5 M. See Figure 4.3 for the cation distributions in the porewaters.

The technetium-99 desorption data are consistently near zero, meaning that the technetium-99 is not interacting with the sediment down to the very deepest sample obtained. For sample 17A, there appears to be a slight interaction of the technetium-99 with the sediment. This may be caused by sample heterogeneity and measurement of the two extracts, acid and water, on two different aliquots of sediment. The overall data set suggests that technetium-99 is not interacting with the sediment and will travel at the same speed as water that is slowly percolating through the vadose zone.

Aside from sample 7A, uranium shows significant resistance to water leaching/desorption. The uranium in the sediment does not appear to be elevated significantly over values for natural sediment. Thus, the uranium in the vadose zone probably is mostly natural and, thus, resistant to water leaching.

The chromium content in the slant borehole sediment is very elevated in many of the samples. There are two zones where the chromium desorption K_d values are quite low, 24.6 to 31 meters (80.6 to 101.7 feet) and 34.7 to 42.1 meters (113.8 to 138.2 feet) bgs. There is one sample, 12A, between these two zones that has been shown to have little signature of tank fluids. If this sample is excluded, the two relatively mobile chromium plumes would coalesce into one from 24.6 to 42.1 meters (80.6 to 138.2 feet) bgs. It is quite dramatic that chromium migration abruptly stopped somewhere between 39.6 and 42.1 meters (130 and 138 feet) bgs, but technetium-99 has migrated deeper. Despite the science and technology findings that approximately one-third of the chromium appears to be reduced via heterogeneous reaction dissolution of ferrous containing minerals, the chromium desorption K_d values are still <1 mL/g in the entire zone where the bulk of the tank fluid currently resides. Below the zone of elevated chromium, the chromium K_d value is quite large (≥ 100 mL/g). Beneath the tank bottom between 20.7 to 23.3 meters (67.9 and 76.4 feet) bgs, there is elevated total chromium in the sediment, and the apparent desorption K_d ranges from 3 to 5 mL/g. This is likely the zone where most of the chromium reduction occurred by the caustic-induced dissolution of ferrous-bearing minerals mechanism described in the Science and Technology Program activities.

Based on Table 5.1, we would conclude that selenium is slightly more interactive with the sediment than technetium-99, but more detailed fission product isotope signature work by scientists suggests that tank liquor containing selenium is just as mobile as technetium-99. We conclude that the acid extractions may be dissolving enough natural selenium from the sediment to skew the in situ desorption K_d calculations. By dissolving natural selenium, we overestimate the amount of selenium bound to the sediment and, thus, overestimate the K_d value. The molybdenum data in Table 5.1 suggest that in the lower portion of the profile molybdenum is more interactive than chromium. The Science and Technology Program, using more sophisticated measurements of isotope signature, also suggests molybdenum is more interactive and likely more prone to reduction when ferrous ions are released from the dissolution of sediment by caustic tank fluids. Our data suggest that the in situ desorption K_d values for molybdenum in the shallower sediment (above 24.6 meters [80.6 feet] bgs) are smaller than the chromium values and thus molybdenum would be more mobile in this zone. This is a disagreement with Science and Technology Program conclusions, and we defer to their more elegant analyses. In the depth zones 24.6 to 31 meters [80.6 to 101.7 feet] and 32.2 to 39.7 meters [105.6 to 130.1 feet] bgs, our molybdenum in situ desorption K_d values are higher than the chromium values in agreement with the Science and Technology Program interpretations.

5.2 Comparison of Porewater Composition in Boreholes 41-09-39 and 299-W23-19

In this section, we compare the dilution-corrected porewater and actual porewater obtained by ultracentrifugation between the two boreholes. The first observation is that the vadose zone sediment under tank SX-108 between 16.8 to 21.8 meters (55 to 71.5 feet) and 26.8 to 30.8 meters (88 to 101 feet)

bgs is drier (i.e., has lower moisture contents) than comparable sediment from borehole 41-09-39. Thus, moisture content measurements do indicate that the heat/temperature environment below tank SX-108 was higher. In fact, temperature measurements of the slant borehole casing (shown in Figure 2.9) show that the temperature is still elevated and significantly higher than temperatures measured several years earlier at borehole 41-09-39. The moisture contents in the shallow sediment from the slant borehole ranged from 1.9 to 6.5% by weight. The moisture content for borehole 41-09-39 samples from the same depths (or more correctly from the same lithologies) ranged from 4 to 12% by weight. Thus, the dilution corrections for the drier sediment at the slant borehole are significantly larger than the values for borehole 41-09-39 extracts.

Table 5.2 shows the pH of the uncorrected water extracts and the dilution-corrected electrical conductivity for samples from the two boreholes. Borehole 41-09-39 was sampled twice within the backfill so that baseline conditions could be established. The slant borehole beneath tank SX-108 was not sampled until the H1a unit was found, just below the backfill. At the 41-09-39 borehole that was ~3 meters (~10 feet) from the side of tank SX-109, the backfill and the H1a unit appear to be relatively uncontaminated. The sediment pH is normal and the electrical conductivity is about the same as for uncontaminated sediment. The only constituent that appears to be elevated above background is nitrate. At the slant borehole at tank SX-108, the H1a unit sediment (based on the only sample obtained [1A]) shows high pH and elevated electrical conductivity. Thus, the impact of tank fluid is seen closer to the bottom of the tank at SX-108 than at SX-109. The sample 1A at the slant borehole is about 2.4 meters (8 feet) from the edge of the tank, so it is not that much closer to the tank edge than borehole 41-09-39.

The H1 coarse-grained sediment at both boreholes shows a high pH (compared to uncontaminated sediment) and elevated electrical conductivity. Because only one sample was obtained in the H1 unit at the slant borehole, the effects of the leaking tank liquor cannot be described in detail under tank SX-108 within this unit. However, there is no doubt that effects from the tank liquor impacted this unit. Within this unit at borehole 41-09-39, the nitrate concentration in porewater is 1.5 M.

At both boreholes, the fine-laminated sands underneath the coarse H1 unit contain the bulk of the tank liquor salts. At borehole 41-09-39, the pH is normal suggesting that most of the caustic components have reacted in shallow sediment or the sediment closer to the tank. At SX-108 slant borehole, the pH is still elevated down to at least 25.6 meters (84 vertical feet) bgs. At 26.8 meters (88 feet) bgs to the final depth of the borehole, the sediment pH is normal. Thus, it would appear that caustic reactions reached a deeper depth under tank SX-108.

Table 5.2. Comparison of the pH and Electrical Conductivity in Porewaters from the Two Boreholes

Lithology	Vertical Depth (ft) ^(a)	Slant SX-108 Sample ID	1:1 pH	Pore EC mS/cm	Depth (ft bgs) ^(a)	Sidewall 41-09-39 Sample ID	1:1 pH	Pore EC mS/cm
BckFil					25.5	15A/B/C	8.39	2.3
					44.5	14A/B/C	8.52	2.6
H1a	55.1	01A	9.16	9.34	56.5	13A/B/C	8.31	1.8
	61.5				61.5	12A/B/C	8.61	2.8
H1	67.9	03AB	9.58	25.85	65	11A/B	9.18	19.1
					66	11C	9.76	9.5
					69.5	10A/B/C	9.18	17.2
					74.5	9A/B/C	9.6	13.9
					79.5	8A/B/C	9.55	16.1
H1					82.5	7A/B/C	8.70	98.7
H2	71.51	04A	9.54	9.57				
	75.73	05A	9.78	14.21				
	79.94	06A	8	454.2				
	84.13	07A	9.55	1166.5				
	88.32	08A	7.83	1771.6	90	6A/B	8.33	408.0
	92.48	09A	7.88	1009.3				
	96.64	10A	8.23	1337.7	95.5	3A/B/C	7.93	521.1
	101.04	11A	8.38	592.8	102.5	5A/B/C	8.01	402.9
	104.92	12A	8.02	11.04	108.5	4A/B/C	8.07	470.7
	113.14	13A	7.99	398.4	112	2B/C	8.12	524.4
H2	121.3	14A	7.82	262.8				
PPlz	129.44	15A	7.45	229.7	127.4	1A/B/C	7.92	130.8
						extension		
					131.7	1B	8.06	36.2
	137.54	16A	7.24	77.16	135.9	3A	8.34	3.3
					138	4B	8.61	1.8
					138.7	4A	8.63	1.1
					141.5	5A	8.97	1.7
	143.99	17A	7.22	17.63	144.1	6C	8.29	3.1
					144.7	6B	8.5	3.0
					146.4	7C	8.41	2.1
					148.3	8C	8.71	3.2
PPlz					149.9	8B	8.71	2.0

(a) Multiply by 0.3048 to convert to meters.
EC = Electrical conductivity.

Table 5.3. Comparison of the Anion Concentrations in Porewaters from the Two Boreholes

Lithology	Depth (ft bgs) ^(a)	Slant SX-108 ID	Dilution Corrected Porewater mg/L				Depth (ft bgs) ^(a)	41-09-39 ID	Dilution-Corrected Porewater mg/L			
			Nitrate	Nitrite	Chloride	Sulfate			Nitrate	Nitrite	Chloride	Sulfate
BckFil							25.5	15A/B/C	161	3.18	<4.0	20.9
							44.5	14A/B/C	152	3.0	10.7	190.9
H1a	55.1	1A	161	<2.31	40.7	462	56.5	13A/B/C	81	1.6	5.2	17.2
	55.1	1A-Dup	140	<2.31	29.4	405	61.5	12A/B/C	102	2.0	6.3	40.0
H1							65.5	11A/B	618	5.5	10.9	243.9
							66	11C	333	4.9	4.9	122.1
	67.9	3AB	1,072	13.1	125	801	69.5	10A/B/C	767	5.9	8.8	198.7
	72.2	4A	851	11.2	54.7	415	74.5	09A/B/C	857	5.0	10.5	350.6
							79.5	08A/B/C	3,464	13.1	31.2	483.3
H1							82.5	07A/B/C	33,746	976.4	357.5	3,999
H2	76.4	5A	1,984	7.3	83.8	584						
	80.6	6A	319,225	ND	<272	1,926						
	84.8	7A	755,649	ND	421	9,833						
	89	8A	659,796	1,453	1,383	9,412	90	06A/B	273,614	1355.0	2,992	2,642
	93.1	9A	972,499	2,429	5,213	24,092	95.5	03A/B/C	416,332	363.7	4,074	3,308
	97.3	10A	994,113	3,088	6,713	14,465						
	101.7	11A	302,677	318	4,121	1,486	102.5	05A/B/C	304,385	1279.2	1,903	1,904
	105.6	12A	7,191	<46.9	109	147	108.5	04A/B/C	353,773	1084.2	2,990	3,215
	113.8	13A	297,334	970	2,846	3,923	112	02B/C	401,733	1297.2	4,212	4,576
	122	14A	186,815	402	1,624	2,945						
H2	122	14A-Dup	201,786	267	1,773	3,246						

Table 5.3. (cont)

Lithology	Depth (ft bgs) ^(a)	Slant S-X108 ID	Dilution Corrected Porewater mg/L				Depth (ft bgs) ^(a)	41-09-39 ID	Dilution-Corrected Porewater mg/L			
			Nitrate	Nitrite	Chloride	Sulfate			Nitrate	Nitrite	Chloride	Sulfate
PPlz							127.4	01A/B/C	10,1213	226.2	612.7	579.5
	130.1	15A	198,485	198	1,903	2,908		extension				
							134.2	2B	1,929.3			
							134.7	2A	1,591.9			
							135.2	3B	2,447.1			
							135.9	3A	1,219.4			
	138.2	16A	55,822	<133	749	151	138	4B	198.7			
							140.3	5C	65.4			
							140.9	5B	28.5			
							141.5	5A	101.9			
	144.6	17A	12,155	<5.08	176	59.1	144.1	6C	502.3			
							144.7	6B	464.2			
							146.4	7C	318.6			
PPlz							152.8	9A	170.2			

(a) Multiply by 0.3048 to convert to meters.

Table 5.4. Comparison of the Cation Concentrations in Porewaters from the Two Boreholes

Lithology	Depth (ft bgs) ^(a)	Slant SX-108 ID	Ca mg/L	K mg/L	Mg mg/L	Na mg/L	Sr µg/L	Depth (ft bgs) ^(a)	Sidewall 41-09-39 ID	Ca mg/L	K mg/L	Mg mg/L	Na mg/L	Sr µg/L
BckFil								25.5	15A/B/C	114.4	78.8	13.8	364	655.6
								44.5	14A/B/C	69.9	80.8	7.8	488	567.9
H1a	55.1	1A	28.23	(77)	(5.7)	2,378	(259)	56.5	13A/B/C	139.8	46.3	12.6	270	226.5
	55.1	1A-Dup	25.51	(82)	(5.3)	2,344	<23,130	61.5	12A/B/C	28.4	20.3	2.5	629	330.2
H1								65.5	11A/B	23.7	36.1	9.4	2,572	743.4
								66	11C	17.9	50.0	36.6	4,005	966.3
	67.9	3AB	(34.97)	(131)	27.18	6,829	(265)	69.5	10A/B/C	19.4	82.2	23.1	4,031	795.4
	72.2	4A	(32.95)	(86)	(16.9)	7,195	<36,150	74.5	9A/B/C	9.7	45.9	1.2	3,259	910.1
								79.5	8A/B/C	6.6	38.9	0.7	3,953	536.3
H1								82.5	7A/B/C	263.2	190.7	25.8	24,290	5,452.0
H2	76.4	5A	(17.97)	(43)	(4.8)	5,716	<21,360							
	80.6	6A	1,647.9	703	101	153,069	(8,131)							
	84.8	7A	39.59	1339	(3.3)	345,472	(2,794)							
	89	8A	1966	2961	118	305,019	31,612	90	6A/B	1,385	2,039	70	109,958	26,152
	93.1	9A	4303	4388	151	370,034	45,684	95.5	3A/B/C	12,389	1,639	251	129,715	191,563
	97.3	10A	1821.3	3604	128	391,103	(36,890)							
	101.7	11A	37905	1358	3143	65,257	421,747	102.5	5A/B/C	5,412	1,230	232	103,364	97,387
	105.6	12A	1309	87	213	691	7,485	108.5	4A/B/C	3,743	971	144	127,148	72,986
	113.8	13A	1583	1001	137	110,749	23,332	112	2B/C	5,557	996	291	139,061	104,987
	122	14A	1678	566	163	68,587	27,027							
H2	122	14A-Dup	1855	611	175	73,859	29,976							

Table 5.4. (cont)

Lithology	Depth (ft bgs) ^(a)	Slant SX-108 ID	Ca mg/L	K mg/L	Mg mg/L	Na mg/L	Sr μg/L	Depth (ft bgs) ^(a)	Sidewall 41-09-39 ID	Ca mg/L	K mg/L	Mg mg/L	Na mg/L	Sr μg/L
PPlz								127.4	1A/B/C	13,481	606	1,469	15,184	107,202
	130.1	15A	2555	555	270	70,723	37,277		extension					
								134.2	2B	327	35.7	85.5	207.5	1,459
								134.7	2A	341	25.5	82.0	133.7	1,544
								135.2	3B	387	151.2	101.4	362.3	1,758
								135.9	3A	290	79.3	60.5	172.9	1,035
	138.2	16A	10030	348	2,259	4,404	64,992	138	4B	166	67.2	33.0	122.5	497
								140.9	5B	168	51.0	24.7	109.3	539
								141.5	5A	185	24.6	33.7	140.4	728
								144.1	6C	219	62.7	79.4	218.2	1,126
	144.6	17A	2169	113	593	649	11,816	144.7	6B	217	49.8	78.2	212.7	967
								146.4	7C	135	33.2	48.9	177.9	708
PPlz								152.8	9A	74	32.8	25.7	115.6	355

(a) Multiply by 0.3048 to convert to meters.

Table 5.5. Comparison of the Metal Concentrations in Porewaters from the Two Boreholes

Lithology	Depth (ft bgs) ^(a)	Slant SX-108 ID	Al µg/L	Fe µg/L	Si mg/L	Mn µg/L	Cr mg/L	Depth (ft bgs) ^(a)	Sidewall 41-09-39 ID	Al µg/L	Fe µg/L	Si mg/L	Mn µg/L	Cr mg/L
BckFil								25.5	15A/B/C	10,299	6,254	264.9	55.4	0.006
								44.5	14A/B/C	6,883	1,682	173.3	6.8	0.034
H1a	55.1	1A	16,351	16,197	420	(585)	(0.21)	56.5	13A/B/C	3,157	1,559	58.2	311.9	0.022
	55.1	1A-Dup	15,702	14,623	398	(526)	(0.22)	61.5	12A/B/C	4,362	375	58.4	42.9	0.064
H1								65.5	11A/B	31,461	43,041	301.0	876.0	6.5
								66	11C	108,143	169,650	700.0	2,366.8	6.5
	67.9	3AB	66,585	67,342	734	(1,349)	(29)	69.5	10A/B/C	70,543	97,865	550.7	1,788.2	116.3
	72.2	4A	50,399	56,108	865	(882)	27.8	74.5	9A/B/C	12,559	2,160	242.2	968.6	79.3
								79.5	8A/B/C	7,020	231	49.4	467.2	6.7
H1								82.5	7A/B/C	5,741	209	82.8	595.0	8,874.2
H2	76.4	5A	26,641	29,374	367	(375)	75.1							
	80.6	6A	10,769	9,997	(193)	<1,359	13,150							
	84.8	7A	85,98	8,481	170.3	<810	5,018							
	89	8A	(3,405)	(3,397)	(99)	<831	13,782	90	6A/B	3,607	399	29	488	6,943
	93.1	9A	(4,924)	(5,271)	(225)	<2,128	21,817	95.5	3A/B/C	2,856	780	46	635	3,308
	97.3	10A	(11,869)	(12,356)	(295)	<2,617	20,838							
	101.7	11A	<7,945	<7,945	(285)	1,813	28.1	102.5	5A/B/C	1,893	729	36	481	5,073
	105.6	12A	(929)	(929)	66	(91)	1.0	108.5	4A/B/C	2,208	631	40	417	4,012
	113.8	13A	(2,006)	(2,124)	(102)	<669	5,766	112	2B/C	6,131	758	60	613	2,153
	122	14A	(1,297)	(1,297)	(74)	<435	2,588							
H2	122	14A-Dup	(1,146)	(1,125)	(71)	<419	2,913							

Table 5.5. (cont)

Lithology	Depth (ft bgs) ^(a)	Slant SX-108 ID	Al µg/L	Fe µg/L	Si mg/L	Mn µg/L	Cr mg/L	Depth (ft bgs) ^(a)	Sidewall 41-09-39 ID	Al µg/L	Fe µg/L	Si mg/L	Mn µg/L	Cr mg/L
PPlz								127.4	1A/B/C	3,951	293	41	815	0.09
	130.1	15A	(370)	(357)	82	<287	1931		extension					
								134.2	2B	<500	<500	30.6	<500	<0.01
								134.7	2A	<500	<500	35.7	<500	<0.01
								135.2	3B	<500	<500	53.6	405.6	<0.01
								135.9	3A	<500	<500	31.3	443.4	<0.01
	138.2	16A	(577)	(577)	164	2287	0.26	138	4B	<500	<500	44.3	<500	<0.01
								140.9	5B	<500	<500	36.2	<500	<0.01
								141.5	5A	<500	<500	65.5	<500	<0.01
								144.1	6C	606.2	<500	106.5	<500	<0.01
	144.6	17A	(412)	(412)	60	541	0.02	144.7	6B	<500	<500	109.3	<500	<0.01
								146.4	7C	531	<500	126.6	<500	<0.01
PPlz								152.8	9A	1205.3	<500	69.8	<500	<0.01

(a) Multiply by 0.3048 to convert to meters.

The maximum electrical conductivity found in the porewater at borehole 41-09-39 within the H2 sands reached 525 mS/cm, and at the slant borehole, the maximum electrical conductivity in the porewater reached 1772 mS/cm. Table 5.3 through 5.5 show the anion, major cations, and selected metals in the two porewaters.

The upper 1.5 to 1.8 meters (5 to 6 feet) of PPlz sediment at borehole 41-09-39 shows effects of the more mobile contaminants from the tank leak(s). At the slant borehole, all three samples obtained in the PPlz sediment show the presence of many constituents from tank leaks. The tank leak plume, thus, has migrated deeper under tank SX-108 than it has to the side of tank SX-109 at borehole 41-09-39. Based on the nitrate profile at borehole 41-09-39 (shown in Table 5.3 and in Serne et al. 2002a), we estimate that the leading edge of the plume under tank SX-108 should extend between another 1.5 to 3 meters (5 and 10 feet) deeper than the bottom of the slant borehole. This would put the plume's leading edge near the bottom of the PPlz unit near its contact with the PPlc unit.

The anion distributions in the porewaters from the vadose zone sediment from both boreholes (shown in Table 5.3) suggest that the bulk of the leaked liquor still resides in the H2 unit and the upper portion of the PPlz unit. At borehole 41-09-39, the porewaters in the H2 unit range from 273 to 416 g/L nitrate, 0.4 to 1.4 g/L nitrite, 2 to 4.2 g/L chloride, and 2 to 4.6 g/L sulfate. Under tank SX-108, the highly contaminated porewaters in the H2 sediment range from 300 to 994 g/L nitrate, 0.3 to 3 g/L nitrite, 1.4 to 6.7 g/L chloride, and 2 to 24 g/L sulfate.

Similar porewater anion concentrations in the upper portion of the PPlz sediment are 101 g/L nitrate, 0.25 g/L nitrite, 0.6 g/L chloride, and 0.6 g/L sulfate for the one highly contaminated sample at borehole 41-09-39 and 200 g/L nitrate, 0.2 g/L nitrite, 2 g/L chloride, and 3 g/L sulfate for the slant borehole under tank SX-108.

The cation distributions (see Table 5.4) in the porewaters are controlled by the ion exchange reactions between the sediment (containing mostly calcium and magnesium on the exchange sites) and the concentrated sodium nitrate tank liquor. We also are interested in monitoring the aluminum, iron, manganese, and silicon contents (see Table 5.5) in the waters in hopes of observing signs of the reaction of the caustic tank liquors with the sediment that leads to sediment weathering. Relative to the H1a sand unit, the backfill at borehole 41-09-39 appears to water extract higher amounts of aluminum, iron, potassium, silicon, and strontium. This might have been caused by all the mechanical disturbances during excavation/stockpiling and coarse screening of the larger particles before use as backfill. The one sample of H1a sediment obtained from the slant borehole shows ~10 times higher sodium and silicon in the porewater than found at borehole 41-09-39. We suspect that this finding is explained by the presence of some tank liquor (high sodium) and caustic neutralization reactions that leave more soluble amorphous silicon phases in the sediment. It is interesting that elevated water-leachable aluminum is not found in this sample because the tank liquor purportedly had tenths to molar concentrations of soluble aluminum.

The water extracts (porewaters after dilution correction) from both boreholes in the H1 coarse unit at ~20.1 to 21.9 meters (~66 to 72 feet) bgs show elevated aluminum, iron, and silicon and low calcium and magnesium concentrations. The first three constituents might be indicative of the caustic reactions

between the tank liquor and the sediment. The low calcium and magnesium undoubtedly indicate the removal of these alkaline earth cations from the exchange sites by the high sodium in the leaking fluid.

The porewater from the top of the H2 laminated sand unit at the slant borehole 22.9 meters (75 feet) bgs shows elevated concentrations of aluminum. This, again, may be indicative of the alkaline attack on the sediment. At borehole 41-09-39, the very top of the H2 unit was not sampled; however, the pH at borehole 41-09-39 shows no indication of being high in the H2 unit, so we would not expect much water-extractable aluminum. Most all of the porewaters from the H2 unit at the slant borehole show elevated potassium and sodium concentrations and lower silicon concentrations than porewaters from the shallower H1 unit. For some of these constituents, there are similar but less pronounced trends at borehole 41-09-39. At both boreholes near the bottom of the H2 unit, the porewaters show elevated calcium, magnesium, and strontium that were displaced by the sodium.

The porewaters from the PPlz sediment at both boreholes show lower (compared to the H1 and H2 porewaters) aluminum, iron, and potassium concentrations. There is still elevated sodium in the porewaters at top of the PPlz at each borehole but water-leachable sodium drops significantly within 6 and 1.5 meters (20 and 5 feet) of the top of the PPlz at the slant and 41-09-39 boreholes, respectively. It appears that the bulk of the tank liquor's leading edge is still within the PPlz sediment. At the slant borehole, there still is evidence of enriched calcium in some of the porewaters from the tank liquor ion exchange reactions with the sediment supporting this.

The maximum concentrations of common components in the porewaters from both boreholes as a function of lithology are shown in Table 5.6. Along with simulated tank liquors, the solutions in Table 5.6 could be used to perform laboratory experiments to further study the fate of contaminants in vadose zone sediment. The values in Table 5.6 are the maximum concentrations observed within each lithologic unit and are not internally charge balanced. There is also some inorganic carbon/alkalinity in the porewaters that is difficult to quantify using water extracts because they overestimate the true values presumably because of dissolution of small amounts of calcite in the sediment. Alkalinity titrations of 1:1 sediment-to-water extracts also significantly overestimate the true porewater concentrations when they are corrected for dilution. It appears that the true alkalinity value of vadose porewaters is similar to the uncorrected 1:1 sediment-to-water extract value. The alkalinity or bicarbonate concentrations are a minor component when compared to the sodium, nitrate, and in some cases, calcium and chromate concentrations in the dilution-corrected water extracts (~ vadose zone porewaters).

Because we obtained only two samples from the slant borehole within the H1 unit, we cannot estimate the maximum concentrations of the pore fluid in the H1 unit at the slant borehole. The samples obtained are not as saline as the porewater from the lower portion of H1 at borehole 41-09-39. Thus, we expect that more affected sediment exists at the bottom of the H1 unit at the slant borehole, but it was not sampled. On the other hand, the hypersaline plume beneath tank SX-108 may have traveled below the H1 unit or been diluted by the convection cells that may have been active from the complicated heat profile. If we have, in fact, measured the maximum porewater composition for the H1 unit under tank SX-108, then it is not very saline and, thus, cesium-137 that is sequestered in the H1 unit would not be easily desorbed by fluids percolating through this unit. Further, if we have identified the porewater composition in the H1 unit below tank SX-108, the greater than signs in Table 5.6 can be removed.

As can be seen, the maximum concentrations in the porewater from the slant borehole for the H2 laminated sands is approximated by ~16 to 17 M sodium nitrate. At room temperature, this is supersaturated. However, at the temperature of the leak, the Science and Technology Program suggests that this hypersaline composition is reasonable (Dr. Peter Lichtner, Los Alamos National Laboratory). We did find measurable amounts of precipitated sodium nitrate (nitratine) in the bulk sediment from sample 7A in the H2. There were also equivocal signs of nitratine in the x-ray diffraction patterns of samples in the H1 and upper PPlz zones of the slant borehole that likely formed during the transit and

Table 5.6. Comparison of the Maximum Concentration of Porewaters from Various Lithologies in the Two Boreholes

Constituent	Lithology Borehole	H1 SX-108	H1 41-09-39	H2 SX-108	H2 41-09-39	PPlz (top) SX-108	PPlz (top) 41-09-39	PPlz (bottom) SX-108	PPlz (bottom) 41-09-39
Grams per Liter in Porewater (Maximum Values)									
Na		>7.0	24	391	139	71	15	0.6	0.2
Ca		>0.04	0.3	38	12.4	10	13.5	2	0.1
Mg		>0.03	0.04	3.1	0.3	2.2	1.5	0.6	0.07
K		>0.1	0.2	4.4	2	0.6	0.6	0.1	0.05
NO ₃		>1.1	34	994	416	200	100	12	0.4
NO ₂		>0.01	1	3.1	1.3	0.2	0.3	0	0
SO ₄		>0.8	4	24	4.6	2.9	0.6	0.06	0.1
Cl		>0.1	0.4	6.7	1.4	1.9	2.4	0.2	0.3
CrO ₄		>0.07	19.85	48.63	15.39	4.24	0	0	0
Porewater Maximum Molarity of Main Constituents									
Na		>0.304	1.04	17	6.04	3.09	0.652	0.026	0.009
Ca		>0.001	0.01	0.95	0.31	0.25	0.338	0.05	0.003
Mg		>0.001	0.00	0.13	0.01	0.09	0.062	0.025	0.003
K		>0.003	0.01	0.11	0.05	0.02	0.015	0.003	0.001
NO ₃		>0.018	0.55	16	6.71	3.23	1.613	0.194	0.006
NO ₂		>0.000	0.02	0.07	0.03	0.00	0.007	0	0
SO ₄		>0.008	0.04	0.25	0.05	0.03	0.006	0.001	0.001
Cl		>0.003	0.01	0.19	0.04	0.05	0.068	0.006	0.008
CrO ₄		>0.001	0.17	0.42	0.13	0.04	0	0	0

storage (under refrigeration) at the laboratory prior to subsampling. However, aside from sample 7A, the nitratine indications could also be attributed to calcite that is known to be present in most of the samples.

The maximum concentration of the porewater in the H2 unit of 41-09-39 is between 6 and 7 M sodium nitrate. The data in Tables 5.2 through 5.6 suggest that the fluids in the vadose zone pores under tank SX-108 are about 2 to 2.5 times more saline than fluids along the east side of tank SX-109. The

hypersaline plume also extends deeper into the PPlz sediment under tank SX-108 than along the side of tank SX-109. The difference in concentration may reflect concentration by thermal heating under tank SX-108, or perhaps the two boreholes are not reflecting a common leak. That is, the boreholes may have intercepted separate leaks from tanks SX-108 and SX-109 that had different concentrations of redox waste. There is no doubt that the two tanks contained similar reprocessing waste, but the absolute concentrations of the salts in the two tanks at the time of the leaks may have varied. The difference in vertical distribution of the plumes relative to absolute and lithology (note the Hanford formation beds slope downward from tanks SX-108 to SX-109) may reflect differences in the volume and rate of leaking.

Figures 5.1 through 5.3 show the water-extractable calcium, chromium, and sodium from the sediment from both 41-09-39 and the slant borehole under tank SX-108 in micrograms of constituent per gram of oven-dried sediment. When plotted on this basis, the peak concentrations are quite similar. The differences shown in Table 5.6 are caused by the drier state of the slant borehole sediment compared to the sediment in the core from borehole 41-09-39. That is, if we assume that the water-extractable species were truly present in the existing porewater, then the concentrations of chemicals in the slant borehole porewater are significantly higher because there is less porewater.

Table 5.7 and Figures 5.4 and 5.5 present comparisons between the total cesium-137 and technetium-99 contents in the sediment at the two boreholes versus lithology. Because we do not have continuous core at either borehole and the fact that the geologic units dip to the southwest, the comparisons are subject to interpretation. However, continuous spectral gamma logging allows more detailed comparisons for the cesium-137 distribution versus depth and lithology. The cesium-137 concentration in the sediment in the fine sand H1a unit below the SX-108 tank is one to two orders of magnitude larger than at borehole 41-09-39, which is about 16.8 meters (55 feet) to the west. In the upper portion of the coarse-grained H1 unit, the cesium-137 concentration in the sediment below the SX-108 tank is also one to three orders of magnitude larger than the 41-09-39 sediment, but in the lower half of the H1 unit, the sediment from borehole 41-09-39 is 2 to 10 times more concentrated than below tank SX-108. In the upper portion of the Hanford fine laminated sand (H2) unit, the sediment under tank SX-108 has much higher concentrations than sediment from borehole 41-09-39. In the lower portion of the H2 unit, there are similar concentrations of cesium-137 in the sediment; however, the cesium-137 in borehole 41-09-39 is effected by push down of cesium-137 during the original pile driving of the closed-end casing. The push down affect is more pronounced in the upper PPlz . Within the formation, we believe that low concentrations of cesium-137 are found deeper in the PPlz unit under tank SX-108 than at borehole 41-09-39. Similarly, much more cesium-137 is found in the H2 unit under tank SX-108 than in the H2 unit sediment at 41-09-39.

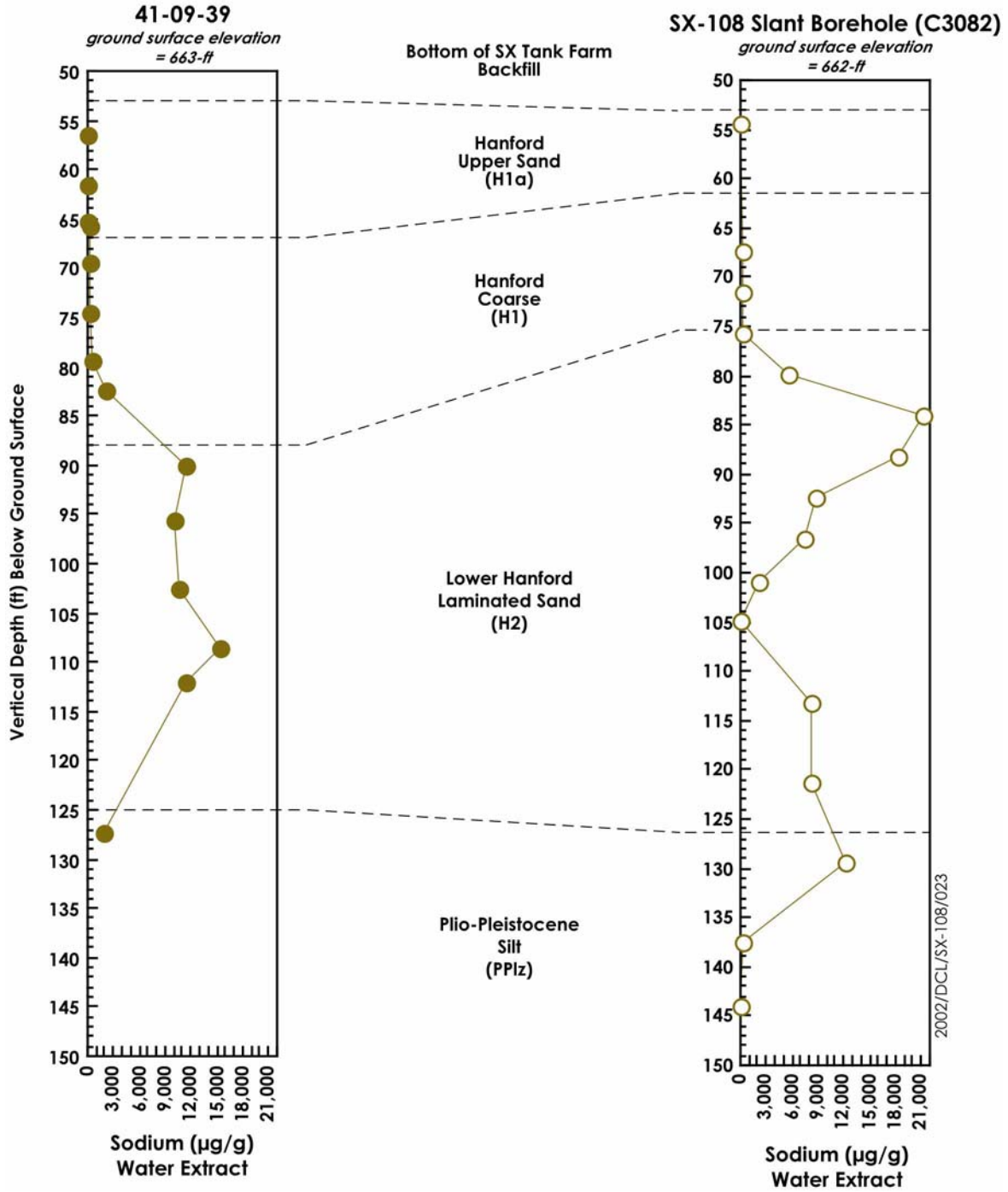


Figure 5.1. Comparison of Water-Extractable Sodium for the Two Contaminated SX Boreholes

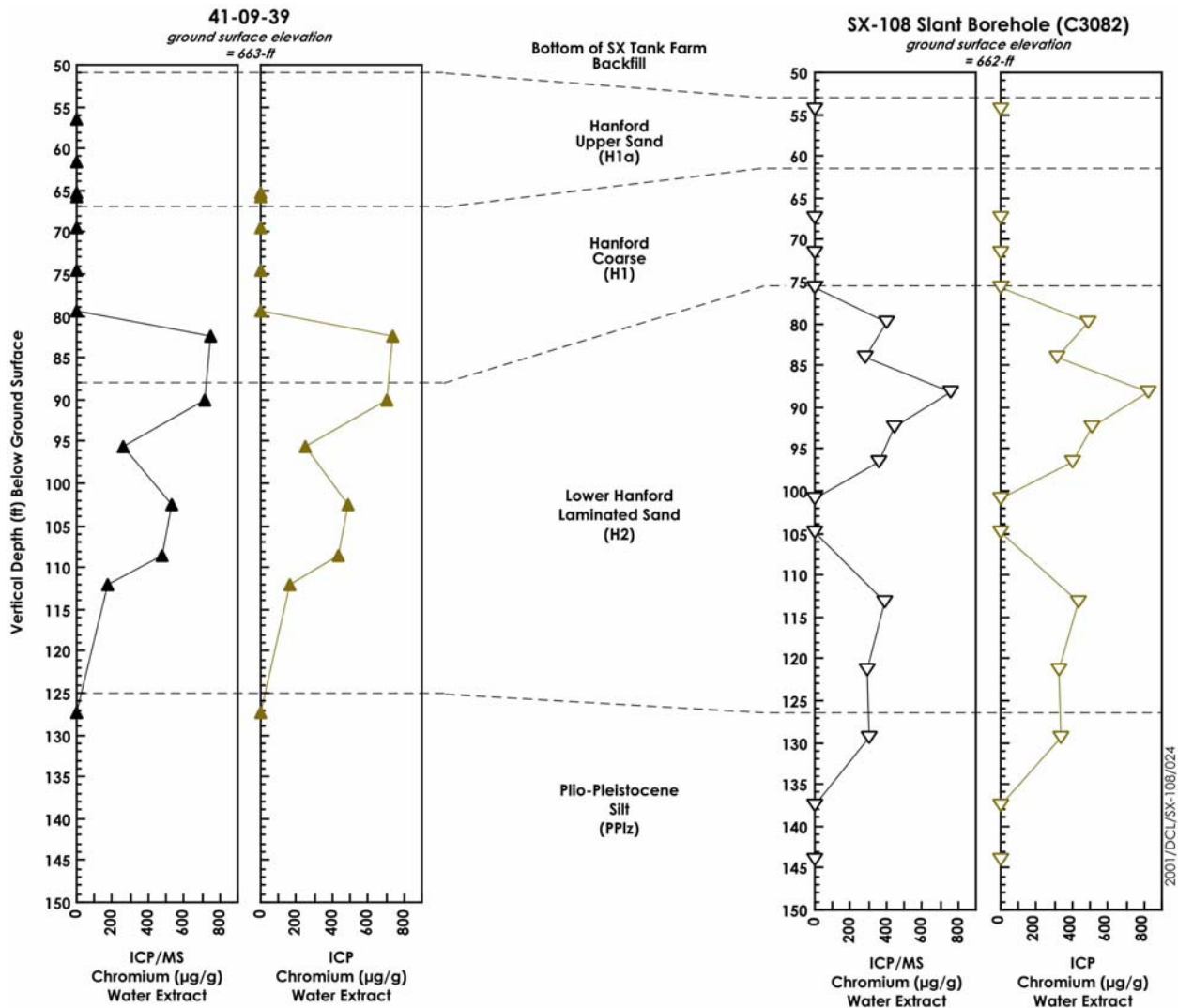


Figure 5.2. Comparison of Water-Extractable Chromium for the Two Contaminated SX Boreholes

The technetium-99 concentrations in the two boreholes are plotted in Figure 5.5. There is an indication that technetium-99 is present in the H1a unit in the sediment from the slant borehole and there is very little present in this unit at borehole 41-09-39 (Table 5.7). There is also very little technetium-99 in the coarse H1 sediment in the slant borehole sediment; but in the lower portion of the H1 sediment sampled at 41-09-39, there are measurable concentrations. Both boreholes show very high concentrations of technetium-99 in the H2 unit. The technetium-99 concentrations per gram of sediment in the H2 unit at borehole 41-09-39 is slightly larger than under tank SX-108. The vertical distribution of technetium-99 at borehole 41-09-39 peaks about two-thirds of the way into the unit. At the slant borehole, the technetium-99 concentrations in the sediment peak in the PPlz sediment near 39.6 meters (130 feet) bgs, about 6.1 meters (20 feet) deeper than at borehole 41-09-39. There is very little

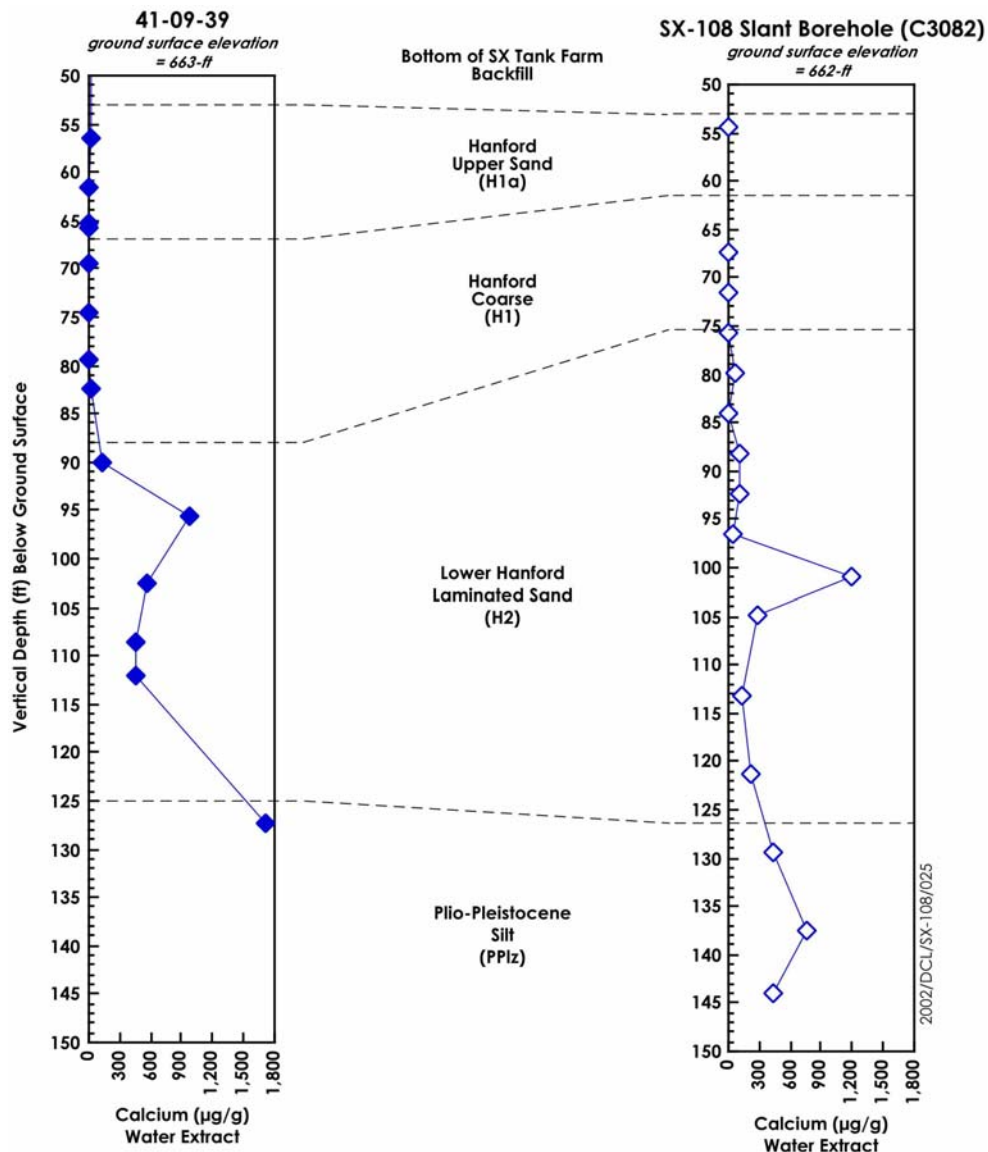


Figure 5.3. Comparison of Water-Extractable Calcium for the Two Contaminated SX Boreholes

technetium-99 in the PPlz unit at borehole 41-09-39. Thus, both vertical profiles suggest that these contaminants have traveled deeper into the sediment under tank SX-108 than at the nearby borehole 41-09-39.

Table 5.7. Comparison of the Radionuclide Content in Sediment from the Two Boreholes

Lithology	Depth (ft bgs) ^(a)	Slant SX-108 ID	¹³⁷ Cs pCi/g	⁹⁹ Tc pCi/g	Depth (ft bgs) ^(a)	Sidewall 41-09-39 ID	¹³⁷ Cs pCi/g	⁹⁹ Tc pCi/g	Ratio Slant to 41-09-39	
									¹³⁷ Cs	⁹⁹ Tc
BckFil					25.5	15A/B/C	5.943E+02	<19.95	--	--
					44.5	14A/B/C	1.097E+03	(5.96)	--	--
H1a	55.1	1A	3.06E+06	<85	56.5	13A/B/C	2.743E+04	30.32	112	--
						12A/B/C	1.275E+05	10.44	24	--
H1					65.5	11A/B	5.944E+05	25.59	33	--
					66	11C	3.908E+06	(13.00)	5	--
	67.9	3AB	1.94E+07	(8.15)	69.5	10A/B/C	8.988E+03	(25.24)	2158	0.32
	72.2	4A	1.38E+06	<82.9	74.5	9A/B/C	2.235E+06	(35.61)	0.62	0.23
					79.5	8A/B/C	2.569E+06	2,527	0.54	0.04
H1					82.5	7A/B/C	1.730E+07	1,079	0.08	0.09
H2	76.4	5A	6.52E+06	(8.54)					--	0.01
	80.6	6A	5.31E+07	(46.73)					--	0.04
	84.8	7A	2.14E+07	926					--	0.86
	89	8A	5.55E+05	2116	90	6A/B	4.379E+04	3,241	13	0.65
	93.1	9A	1.71E+02	4238	95.5	3A/B/C	3.661E+04	7,597	0.00	0.56
	97.3	10A	4.51E+02	4546					0.01	0.60
	101.7	11A	9.12E+02	4666	102.5	5A/B/C	1.586E+06	12,979	0.00	0.36
	105.6	12A	3.37E+02	534	108.5	4A/B/C	3.355E+05	13,766	0.00	0.04
	113.8	13A	5.21E+02	7502	112	2B/C	1.432E+03	9,840	0.36	0.76
H2	122	14A	8.37E+02	7510					0.58	0.76
PPlz					127.4	1A/B/C	4.199E+03	405	0.14	25
	130.1	15A	5.92E+02	10306		extension				
					134.2					
					134.7	2AB	1.29E+03	NA	0.46	--
					135.2					
					135.9	3AB	3.90E+03	NA	0.15	--
	138.2	16A	9.79E+01	1742	138					
					140.9					
					141.5					
					144.1					
	144.6	17A	1.75E+02	857	144.7					
					146.4					
PPlz					152.8	10AB	<0.02	NA	8,750	--

(a) Multiply by 0.3048 to convert to meters.

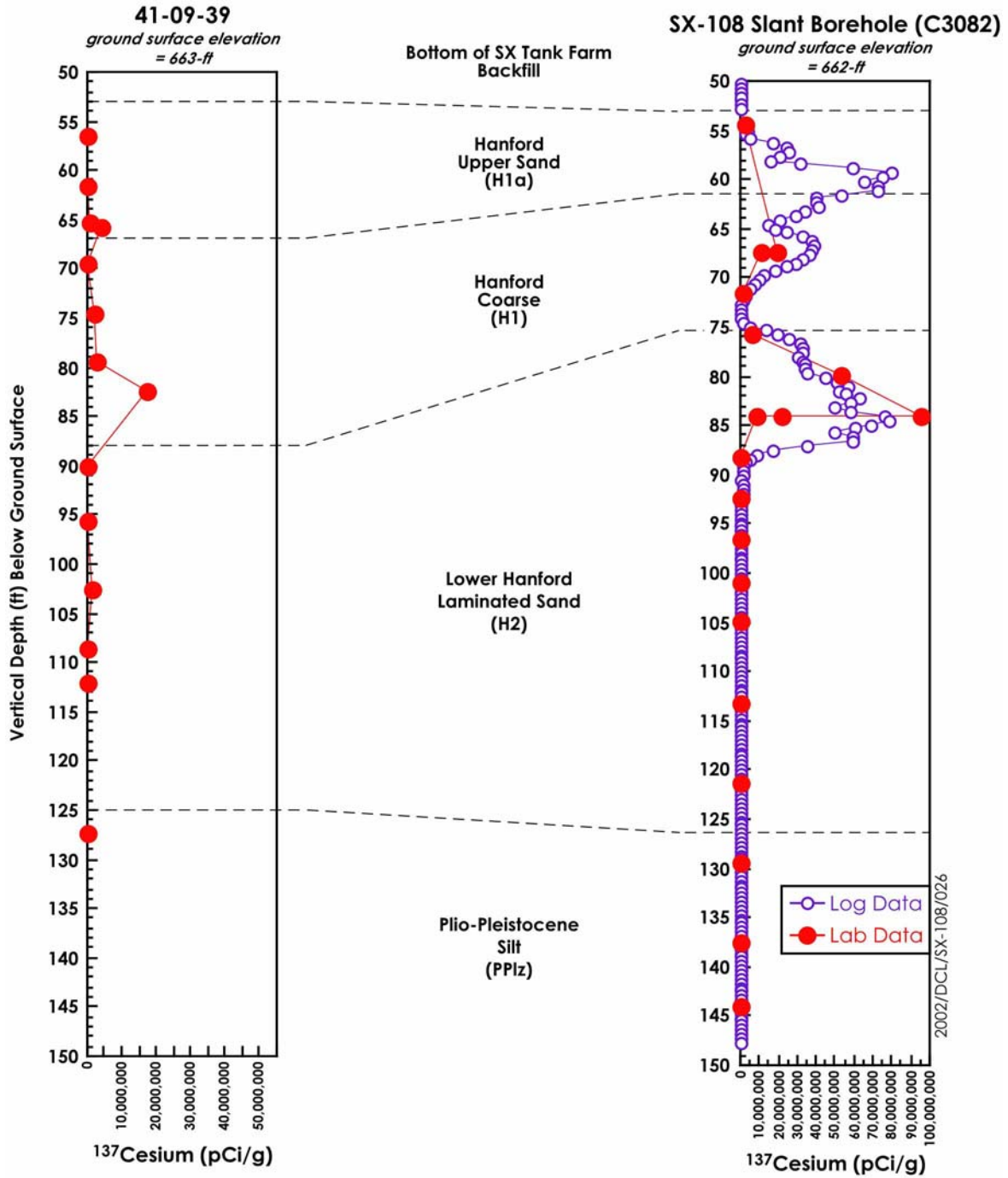


Figure 5.4. Comparison of Cesium-137 Content in the Sediment from the Two SX Boreholes

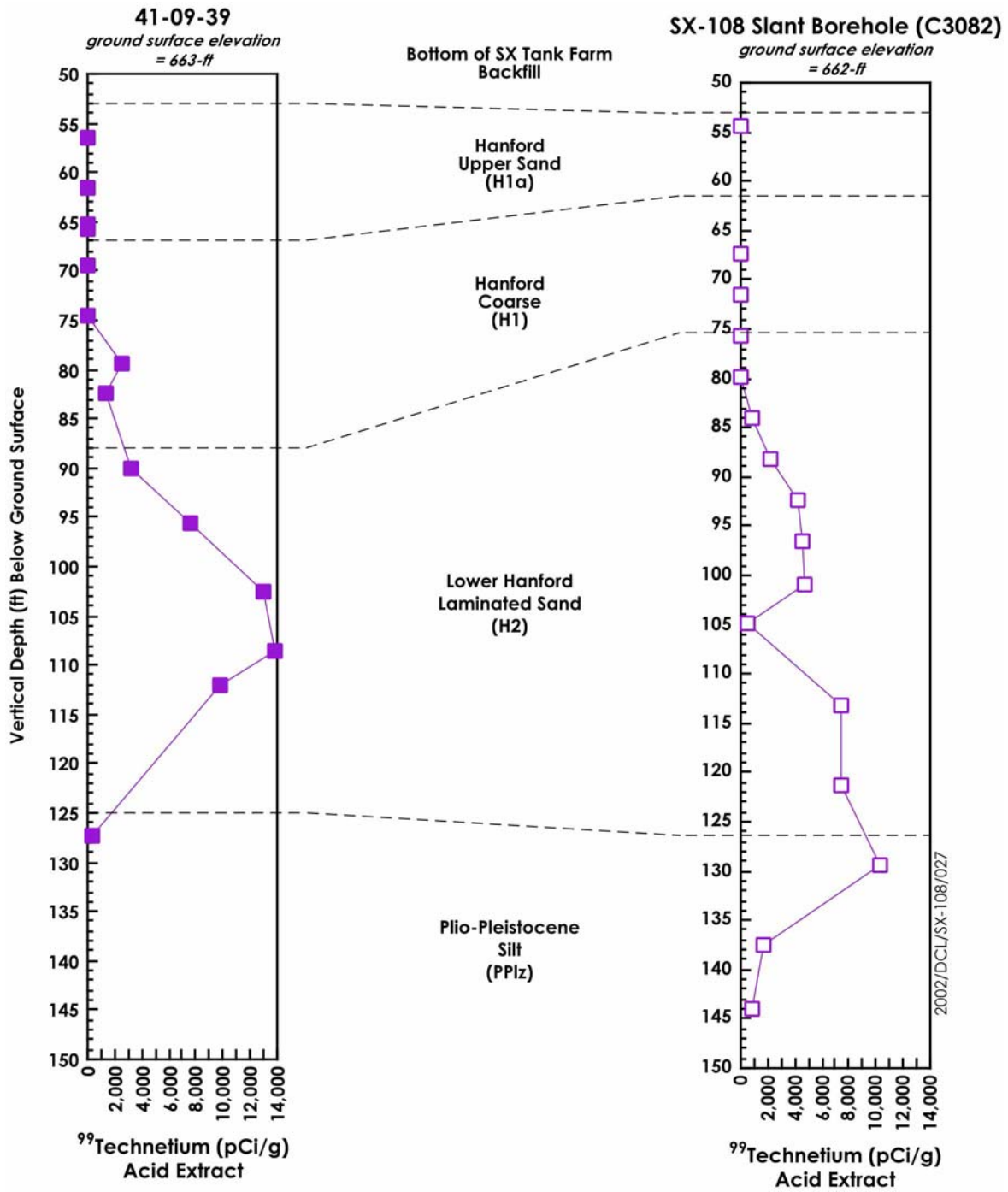


Figure 5.5. Comparison of Technetium-99 Content in the Sediment from the Two SX Boreholes

6.0 Summary and Conclusions

In this section, we present summary information on our interpretation of the significance of the slant borehole sediment characterization data. Conclusions are included to aid in making decisions on what interim actions and future studies are needed to make current and future tank farm operations less likely to unfavorably impact the environment.

6.1 Conceptual Model of the Geology at the Slant Borehole

Borehole SX-108 intersected three primary stratigraphic units: 1) backfill (not sampled), 2) the Hanford formation, and 3) the top of the upper Plio-Pleistocene (PPlz) unit. The backfill appears to extend to a depth of about 16.1 meters (53 feet) bgs where it is in contact with the Hanford formation. This contact depth is supported by an increase in blow counts and an increase in moisture content (as indicated in the neutron-neutron moisture log; see Figure 2.9). The next 2.6 vertical meters (8.4 vertical feet) are interpreted to correlate with the upper fine sand and mud sequence of the Hanford formation, H1a unit. The location of the H1a/H1 contact (at 18.7 meters [61.5 feet] bgs) is supported by a slight increase in the blow counts and a sharp decrease in the neutron-neutron moisture log. Only one split-spoon sample, S0070-01, was collected from the H1a upper fine sand and mud sequence.

Below H1a lies the 4.3-meter (14-foot)-thick middle coarse sand and gravel sequence (H1 unit) extending to a vertical depth of approximately 22.9 meters (75.3 feet) bgs. This contact between H1 and H2 is supported by a sharp decrease in blow counts and an increase in the neutron-neutron moisture log, which is further substantiated by an increase in the gravimetric moisture content of samples collected below this contact. Two split-spoon samples, S0070-03 and S0070-04, were recovered from the H1 coarse unit. A third sample, S0070-02, was attempted but the sample was not retained by of the sampler during retrieval.

The lower fine sand and mud Hanford sequence, the Hanford formation H2 unit, is estimated to be approximately 15.6 meters (51.1 feet) thick, extending to a vertical depth of approximately 38.5 meters (126.4 feet) bgs. The H2/PPlz contact at this depth is supported by a slight increase in the blow counts and a sharp increase in the neutron-neutron moisture log, which is further substantiated by an increase in the gravimetric moisture content of samples collected below this contact. Ten split-spoon samples (S0070-5 through S0070-14) were collected throughout the H2 horizon. These samples were collected from vertical distances of approximately 6.9 to 21 meters (22.8 to 68.8) feet directly beneath tank SX-108. The Hanford formation H2 unit represented by these samples is composed of stratified sand, muddy sand, and mud, and can be further broken down into three subunits on the basis of texture (grain size), moisture content, blow counts, and gamma contamination.

The upper portion of the Hanford formation H2 unit beneath tank SX-108 is composed of mostly interstratified medium to fine sand with occasional muddy very fine sand and/or mud strata. The middle portion of the H2 unit appears to be dominated by interstratified sand deposits often exhibiting an upward grading texture ranging from medium sand at the bottom to fine to very fine sand with some mud (silt) at

the top. Samples from the lower portion of the H2 unit suggest that the lower deposits are composed of highly stratified fine to very fine sand and mud to muddy very fine sand. The fine-grained strata can be further described as massive to very finely laminated and well compacted. The coarse-grained strata within the lower portion of the H2 unit are described as friable with no obvious internal structure.

The contact between the Hanford formation and the PPlz unit is interpreted to occur at a depth of 38.5 meters (126.4 feet) bgs. Approximately 5.6 vertical meters (18.5 vertical feet) of the upper PPlz unit was penetrated. The lower contact of this unit was not encountered. Three split-spoon samples (S0070-15 through -17) were collected from this horizon. Visual examination of these samples suggests that the upper portion of the PPlz sequence consists of interstratified mud and muddy very fine sand, with occasional very fine sand. Based on actual particle size analyses (described in Section 4.2.7), the PPlz zone is considered a sandy mud. However, the finest-grained samples of the H2 are very similar in grain size to the top of the fine-grained PPlz unit represented by sample 15A. We did not measure the particle size of the next two deeper samples and because the borehole did not penetrate the whole PPlz unit, we cannot show explicitly that the PPlz unit, in general, is finer grained than the H2 unit at this borehole. But based on other nearby boreholes, we believe that the PPlz under tank SX-108 is finer grained than the H2 unit.

Based on the overall regional geology of the tank farm, the Hanford formation units dip toward the southwest. Two Ringold facies (Wood Island subunit E and Taylor Flat), two Plio-Pleistocene facies (carbonate [PPlc] and bottom of the mud/fine sand [PPlz]) were not penetrated by the borehole).

We estimate, based on historical well level measurements, that the peak water elevation beneath the nearby tank SX-109 was approximately 146.2 meters (479.7 feet mean sea level). This occurred in 1976 and places the water table approximately 55 to 56 meters (182 feet) bgs or 40 meters (132 feet) beneath the bottom of the tank. A secondary water table maximum occurred in 1984, just before the 216-U-10 pond was decommissioned. At this time, the water table was estimated to have been almost as high as it was in 1976. In December 1997, the water table was encountered at a depth of approximately 64.5 meters (211.5 feet) in borehole 41-09-39. Thus, the water table has dropped an estimated 8 to 9 meters (28.5 feet) since 1984. An examination of the hydrographs since about 1988 suggests that the water level is dropping at a rate of 0.5 to 0.6 meters per year (1.5 to 1.9 feet per year).

In general, the slightly dipping sediment layers likely cause anisotropy in water movement. The vertical distribution of cesium-137 based on borehole gamma logging within the SX Tank Farm suggests that much of the tank fluid that leaked from tanks SX-108, SX-109, SX-111, and SX-112 traveled down dip (toward the southwest) within the coarse-grained Hanford formation H1 unit that is found between 18.7 and 22.9 meters (61.5 and 75.3 feet) bgs below tank SX-108. At the slant borehole under tank SX-108, there is an interesting fine-grained lens in the H2 unit at 32.2 meters (105.6 feet) bgs that was not greatly affected by the hypersaline tank liquors. This sample was mostly bypassed by the migrating plume under the tank. This region of limited interaction with tank liquor has made it difficult to fully interpret the vertical distribution of contaminants under tank SX-108.

6.2 Vertical Extent of Contamination

The following describes measurements of various parameters that help us determine the extent of vertical migration of the tank leak plume. We used several parameters including chromium, electrical conductivity, nitrate, pH, sodium, and technetium-99 concentrations in water extracts for our main indicators to determine the leading edge of the tank leak plume. The concentrations of acid-extractable or directly measured constituents in the sediment were used to delineate the total inventory of constituents within the plume. In many cases, the water-extractable and acid/total concentrations were similar, signifying that the most mobile constituents do remain in the vadose zone porewater and hardly interact with the sediment. The vertical distribution of many parameters also was evaluated so that we could distinguish sediment that had been affected/altered by drilling and sampling artifacts as opposed to actual tank liquor.

Based on evaluating all these measurements, we are confident that the vertical extent of tank leak contamination at the slant borehole was not penetrated because the borehole was stopped at ~44.2 meters (~145 feet) bgs and many of the mobile constituents were still present at elevated concentrations compared to natural background. We do not claim that the information from one borehole can be extrapolated across the entire tank farm. However, when we couple the data from the slant borehole, the nearby 41-09-39, the historical gamma logging of the nearby dry wells, and detailed geologic lithology models, a defensible picture, to be presented in the field investigation report,^(a) is anticipated.

The moisture content is a direct measure of the mass of fluid in the vadose zone sediment. One would logically assume that wetter than normal conditions would represent the existence of leaked tank liquor. However, temperature measurements at the wall of the slant borehole casing, previous in-tank temperature measurements, and thermal modeling performed by the Science and Technology Program suggest that complicated convection cells of water vapor and liquid water were active under tank SX-108. Moisture readings obtained from most of the vadose zone samples collected below the tank bottom from 16.8 to 21.8 meters (55 to 71.5 feet) and 26.8 to 30.8 meters (88 to 101 feet) bgs are drier (have lower moisture contents) than the comparable sediment from borehole 41-09-39. We, thus, do not consider moisture content to be indicative of the vertical migration of tank liquor beneath tank SX-108.

The second parameter measured was the pH of water extracts of the vadose zone sediment. We anticipated that the highly caustic tank liquor would alter the sediment pH dramatically. At the slant borehole under tank SX-108, the H1a unit sediment (based on the only sample obtained, 1A) shows high pH and elevated electrical conductivity. In contrast, there was no indication that the H1a sediment at borehole 41-09-39 was affected by tank fluids. Thus, the effect of tank fluid is seen in shallower sediment at tank SX-108 than at tank SX-109. The sample 1A at the slant borehole is about 2.4 meters (8 feet) from the edge of the tank, so it is not closer to the tank edge than borehole 41-09-39 is to the edge of tank SX-109. This difference in zone of pH alteration may indicate that borehole 41-09-39 is up dip from tank SX-109 but down dip from tank SX-108 and that the contamination observed at borehole 41-09-39 is from the leak(s) at tank SX-108. If this hypothesis is true, there was extensive horizontal migration of leaked tank liquor from SX-108 down dip toward SX-109 within the coarse H1 sediment and

(a) *Draft Field Investigation Report for Waste Management Area S-SX*. RPP-7884, Draft, Volume 2, Appendix D, CH2M HILL Hanford Group, Inc., Richland, Washington.

perhaps deeper H2 sediment. If this were true, then we would not expect the sediment in the shallower H1a unit at 41-09-39 to have altered pH, as is the finding. At the slant borehole, the tank liquor would have to percolate through the shallow H1a unit to get into the coarse high permeability H1 unit. The zone of pH alteration could then be observed in the H1 sediment down dip from tank SX-108 all the way to borehole 41-09-39.

The H1 coarse-grained sediment at both SX boreholes shows high pH (compared to uncontaminated sediment) and elevated electrical conductivity. Because only one sample was obtained in the H1 unit at the slant borehole, the effects of the tank leak liquor cannot be described in detail under tank SX-108 within this sediment unit. However, there is no doubt that tank liquor impacted this sediment unit at both boreholes.

At both boreholes, the fine laminated sands (H2) underneath the coarse H1 unit contain the bulk of the tank liquor salts. At borehole 41-09-39, the pH is normal suggesting that most of the caustic components have reacted in shallower sediment or the sediment closer to the tank. Alternatively, if the contamination at borehole 41-09-39 is from leaks at tank SX-108, then the fluid that contaminated sediment in the H2 unit at borehole 41-09-39 may have reacted closer to tank SX-108 and lost all its caustic nature before arriving where borehole 41-09-39 penetrated. At SX-108 slant borehole, the pH is still elevated down to at least 25.6 vertical meters (84 vertical feet) bgs. This depth is about 2.7 meters (9 feet) into the H2 unit. At 26.8 meters (88 feet) bgs (still within the H2 unit) to the final depth of the borehole, the slant borehole sediment pH is normal. Thus, caustic reactions reached a deeper depth under tank SX-108 than at borehole 41-09-39. The sediment extracted from the slant borehole from 16.8 meters (55 feet) bgs down to a vertical depth of 25.6 meters (84 feet) bgs (includes H1a, H1, and part of H2 units) have elevated pH values that range from 9.2 to 9.8, except one sample that has a pH of 8. This is the same elevated pH range found at borehole 41-09-39 between 19.8 and 24.4 meters (65 and 80 feet) bgs, which is all within H1. If the fluids that affected the sediment at borehole 41-09-39 had traveled from below tank SX-108, we might expect the pH range at tank SX-108 to reach higher pH values, but this was not the case. We speculate that the main controls on sediment pH must not be sensitive to the distance traveled and might be more sensitive to time of reaction.

The observed pH values are not nearly as high as would be expected for sediment completely saturated with tank liquor. As described in Serne et al. (1998), the pH can quickly reach values of >13 when simulated tank liquor reacts with Hanford sediment. One plausible explanation for the lower than expected pH is that the pH re-neutralizes with time from the slow dissolution of alumino-silicates. Likewise, it is also possible for the tank liquor to react with carbon dioxide in the vadose zone air filled porosity such that the initial pH excursion to high values is muted over time.

The third parameter that was assessed to estimate the vertical extent of the leak plume was dilution-corrected electrical conductivity for water extracts. The electrical conductivity results suggest that the tank leak fluid dominates the porewater at the slant borehole down to a depth of 39.3 meters (129 feet) bgs, about 1.5 meters (5 feet) into the PPlz sediment. The electrical conductivity of the two deeper samples within the PPlz sediment does not drop to natural background levels, but is significantly lower than all the samples shallower in the profile. Thus, the leading edge of the plume is below the total depth sampled, but the bulk of the salt is still above 39.3 (129 feet) bgs.

Nitrate was the fourth parameter that was measured to define the vertical extent of contamination. Nitrate is perhaps the most sensitive chemical marker of tank leaks migrating through the vadose sediment. The nitrate concentration in tank liquor from tank SX-108 at the temperature present at the time of the leak has been calculated to be as high as 16 to 18 M (~1,000,000 ppm), but the porewater in deep vadose zone sediment in the semiarid region where the Hanford Site is located is not expected to contain more than several parts per million to perhaps a few tens of parts per million nitrate. The difference between the background nitrate baseline and the full-strength tank liquor is at least 10^5 . Therefore, adding about 0.001% tank liquor into existing porewater should be readily measurable above the natural background. Thus, the 1:1 water-extract nitrate data should be quite useful to trace the vertical extent of the tank leak plume.

There are obvious indications of high nitrate concentrations in the slant borehole sediment throughout all the samples to the total vertical depth of the borehole, ~44.2 meters (~145 feet) bgs. Based on the nitrate profile at borehole 41-09-39, which does show the whole extent of the plume, we suggest that the leading edge of the tank-leak plume beneath tank SX-108 may have stopped at the contact of the PPlz and PPlc units near 45.7 meters (150 feet) bgs. This estimate does not consider any complications from the convection cells that may have transported water vapor and recondensed water under tank SX-108 as indicated by the Science and Technology Program Study.

The fifth indicator species used was sodium in the water extract. Sodium is the dominant cation in tank liquor and like nitrate is present at over 10 M concentrations. Water extract sodium data for the slant borehole sediment suggest that tank fluid has severely affected the vadose zone sediment to a depth of at least 39.7 meters (130.5 feet) bgs (1.2 meters [4 feet] into the PPlz unit) and moderately affected the sediment to the total vertical depth of the borehole.

There also appears to be at least one if not two ion-exchange fronts where sodium displaces the native calcium, magnesium, and potassium from the sediment surface sites resulting in the elevated calcium, magnesium, and potassium in the water extracts of the deeper sediment. There is obvious low water leachable calcium, magnesium, and potassium in samples at shallow depths of 20.7 to 24.4 or 25.9 meters (68 to 80 or 85 feet) bgs caused by the displacement and subsequent transport deeper by the tank fluids and recharge since the leak(s). The sediment at 32.2 meters (105.6 feet) bgs (sample 12A) appears to be affected very little by the tank fluid or the ion exchange reactions. This sample appears to have been bypassed by the percolating tank liquor probably because of lower permeability.

Finally, the water extracts (porewaters after dilution correction) from both boreholes in the H1 coarse unit at ~20.1 meters (~66 feet) bgs show elevated aluminum, iron, and silicon and low calcium and magnesium concentrations. The first three constituents might be indicative of the caustic weathering/precipitation reactions between the tank liquor and the sediment. As just mentioned, the low calcium and magnesium undoubtedly indicate the removal of these alkaline earth cations from the exchange sites by the high sodium in the leaking fluid. The porewater from the top of the H2 laminated sand unit, at the slant borehole (22.9 meters [75 feet] bgs) shows elevated concentrations of aluminum. This again may indicate an alkaline attack on the sediment. Most all of the porewaters from the H2 unit at the slant borehole show elevated iron, potassium, and sodium and lower silicon concentrations than

porewaters from the shallower H1 unit. We expected to find more significant changes in aluminum, iron, and pH, in both the water extracts and sediment themselves, but the zone of caustic alteration is either small or has been muted by continued weathering since the leaks began.

The traditional sampling of Hanford sediment focuses on determining the total concentration of radionuclides in the sediment. For the most part, the highly radioactive samples in the sediment from the slant borehole were found between 16.8 and 25.9 meters (55 and 85 feet) bgs (cesium-137) and 25.9 to 42.1 meters (85 to 138 feet) bgs (technetium-99).

Using the more complete field spectral gamma log, the maximum concentrations of cesium-137 found in two major peaks in the sediment are between 5 and 9×10^7 pCi/g between 17.1 and 19.3 meters (56 to 63 feet) and between 24.6 to 25.8 meters (80.6 to 84.6 feet) bgs, respectively. The bulk of the contamination resides at or near the contact between the H1a and the H1 coarse-grained sediment and in the upper portion of the laminated fine sand (H2 unit), respectively. Below 28.3 meters (93 feet) bgs, still within the H2 unit, the cesium-137 activity is 10,000 times less concentrated, though the cesium-137 activity does not drop to background values before the end of the borehole in the PPlz unit. Thus, we did not find the maximum depth of cesium-137 penetration in this borehole.

The technetium-99 data show that there are significant concentrations of technetium-99 between the depths of approximately 25.9 to 42.1 meters (85 to 138 feet) bgs. The leading edge of the technetium-99 plume appears to reach 42.1 meters (138 feet) bgs, though even the deepest sample at 44 meters (144.5 feet) bgs is slightly elevated in technetium-99. Strontium-90 activities (>10 pCi/g) in the sediment are found sporadically in the slant borehole samples. Between 23.2 and 25.9 meters (76 and 85 feet) bgs, the strontium-90 activity is between 11 and 61 pCi/g, and there are two other hits at 39.6 and 44.1 meters (130 and 144.6 feet) bgs. The latter two elevated strontium-90 activities are associated with higher stable strontium in the water extracts suggesting that the sodium ion exchange process is affecting the strontium-90 distribution. Compared to the cesium-137 distributions, there is very little strontium-90 in the sediment suggesting that strontium-90 is not mobile in the fluid from the Reduction Oxidation (REDOX) Plant that leaked from the SX tanks. Strontium is not considered very soluble in most single-shell tank environments and has been found to reside predominately in precipitates in the sludge at the bottom of the tanks.

In summary, the moisture content, pH, chromium(VI) (discussed in Section 6.3), and cesium-137 profiles do not identify the leading edge of the plume. The profiles of more mobile constituents, such as electrical conductivity and sodium, suggest that the leading edge of the hypersaline plume resides about 1.5 meters (5 feet) into the fine-grained PPlz unit at ~ 39.6 meters (~ 130 feet) bgs. The most mobile constituent profiles, such as nitrate and technetium-99, suggest that the leading edge of the plume was not found because the borehole did not penetrate far enough. Based on the complete plume identification at borehole 41-09-39, we speculate that the nitrate and technetium-99 activities would return to near background values at the contact of the PPlz and PPlc units at ~ 45.7 meters (~ 150 feet) bgs.

The majority of the borehole 41-09-39 plume still resides in the shallower coarse-grained H1 unit. The plume under tank SX-108 resides predominately in the H1 and upper H2 units. Compared to the plume from tank SX-115 leaks that predominately resides in the PPlz unit, the center mass of the tank

SX-108 plume traveled deeper than the plume at borehole 41-09-39 but shallower than the plume at tank SX-115. The leading edge of the tank leak plume is within the PPlz unit below tank SX-108; we did not find the maximum vertical extent. However, we do speculate that the plume does not extend into the Ringold sediment below the PPlc carbonate rich zone.

6.3 Controlling Geochemical Processes Based on Characterization

The more detailed characterization activities of the cores from the slant borehole added insight to the processes that control the observed vertical distribution of contaminants and to their migration potential in the future. The first key finding was that the 1:1 sediment-to-water extracts give a good estimate of the porewater chemistry in the vadose zone sediment. We extracted porewater from three samples of the slant borehole vadose zone sediment using high-speed centrifugation. The chemical composition of the actual porewater was found to be fairly well estimated by dilution correcting the 1:1 water extracts. Because it is much easier to obtain a water extract of the vadose zone sediment, this finding is important to understanding the porewater chemistry throughout the vadose zone plumes under disposal facilities and leaking tanks. Constituents that showed the best agreement include electrical conductivity, nitrate, sodium, chromium, and technetium.

The porewaters in the sediment from the cores in the three Hanford formation units (H1a, H1, and H2) were dominated by sodium and nitrate. At the slant borehole, the most concentrated porewater was in the H2 unit and was essentially 16 to 17 M sodium nitrate with 1 M concentrations of calcium, 0.5 M chromate, and several tenths molar chloride, magnesium, potassium, and sulfate. This extremely hypersaline composition is about three times higher in all constituents as found in the H2 porewater at borehole 41-09-39. The slant borehole vadose zone porewater in the upper region of the PPlz zone was 3 M sodium nitrate with a few tenths molar calcium and magnesium, and a few hundredths molar chloride, chromate, potassium, and sulfate. Only one sediment sample was obtained from the slant borehole in the coarse-grained H1 unit where tank liquor was present. Based on the fact that the composition of borehole 41-09-39 porewater from sediment in the H2 unit is about three times less saline, we took the most saline porewater in the H1 unit of borehole 41-09-39 and multiplied by three to get an estimate of the concentration of the slant borehole H1 porewater composition. This gives the H1 unit under the slant borehole concentrations estimated to be at least 3 M sodium nitrate with 0.5 M chromate. We do not know whether the heat induced convection cells would significantly alter this estimate.

The nitrite distribution suggests that once it leaked into the sediment, oxidation converts the nitrite to nitrate because the ratio of nitrite to nitrate is much lower in the vadose zone porewaters than the values within the tanks.

Based on both water and strong acid extracts, there is elevated chromium, molybdenum, technetium-99, and to a lesser extent selenium, in the region where electrical conductivity, sodium, and nitrate show the presence of tank fluids. There may also be elevated arsenic values but the inductively coupled plasma-mass spectroscopy (ICP-MS) data may be biased by an argon-chloride complex species that has the same mass as arsenic.

In the first sediment sample obtained from the slant borehole (at the base of the tank), there is evidence of elevated lead in both the acid extract and water extracts. There is also a faint indication that acid-extractable copper is elevated in some of the sediment samples. There is no indication that cadmium, cobalt, or silver is elevated in acid or water extracts from the slant borehole sediment.

Based on both the water or acid extract concentrations (per gram of sediment), the first significant sign of elevated technetium-99 is at 24.6 meters (80.6 feet) bgs, and this shallower high concentration plume peaks at 31 meters (101.7 feet) bgs. A second plume of technetium-99 starts at 34.7 meters (113.8 feet) bgs, and peaks at 39.7 meters (130.1 feet) bgs but extends to the bottom of the borehole. If the sample 12A that was bypassed by the tank fluids is ignored, the technetium-99 profile is one large plume with a maximum at 39.7 meters (130.1 feet) bgs. If we look solely at the dilution-corrected water extract data (porewater only), the technetium-99 profile is somewhat different. The highest porewater concentration is at 29.7 meters (97.3 feet) bgs because the moisture content of this sample is very low. Although on a mass-of-sediment basis the water extractable technetium-99 is quite high, below 34.7 meters (113.8 feet) bgs this sediment is much wetter, which leads to lower porewater concentrations.

The water-extractable selenium profile is quite similar to the technetium-99 profile, suggesting that selenium is also quite mobile and not interacting with the sediment. However, the acid-extractable selenium distribution suggests that only the sediment between 34.5 and 39.7 meters (113.2 and 130.1 feet) bgs has elevated total selenium. The percentage of the acid-leachable selenium that is water leachable is between 45 and 60% for most of the profile. This is a lower percentage than for technetium-99. The Science and Technology Program took several of our water and acid extracts and used wet chemical separation techniques to isolate and concentrate several fission products from the bulk matrix. They then measured the various selenium isotopes and separated the fission-produced selenium from the natural selenium to better study the fission-produced fraction. Our data do not allow us to easily separate the fission only components from the naturally present portions. Thus, we find that a slightly lower percentage of the acid extractable selenium is water soluble because we include a mix of fission-produced and naturally present selenium. The naturally present selenium is undoubtedly held more tightly in the sediment, thus giving the appearance that selenium is less water leachable than technetium-99, which is all waste related and has no natural (more tightly bound) fraction.

The chromium concentration in the sediment is dominated by tank waste throughout the whole profile, based on the elevated acid-leachable chromium contents. From 16.8 to 29.7 meters (55.1 to 97.3 feet) and 34.7 to 39.7 meters (113.8 to 130.1 feet) bgs the acid-leachable chromium contents are over 20 times larger than chromium contents that are acid leachable from uncontaminated sediment. The porewater chromium shows sharp increases starting at 20.7 meters (67.9 feet) bgs. There are peaks in the porewater chromium at 24.6, 28.4 and 34.7 meters (80.6, 93.1, and 113.8 feet) bgs. The water-leachable chromium (per gram of dry soil), that ignores water content in the pores, suggests that the elevated chromium vertical distribution starts at 24.6 meters (80.6 feet) bgs and has two peaks at 22.1 and 34.7 meters (89 and 113.8 feet) bgs. The water-leachable chromium is elevated down to 42.1 meters (138.2 feet) bgs. The water-leachable chromium and the porewater profiles suggest that chromium is not as mobile as technetium-99. This is true also at the two other boreholes within the SX Tank Farm. The Science and Technology Program identified a caustic catalyzed reaction where ferrous bearing minerals are dissolved by the caustic and the iron (II) released to the pore fluids reduces chromium(VI) to

chromium(III) that coprecipitates with the oxidized iron to form ferric(chromic) hydroxides. In the zones where the chromium is highly elevated and water leachable, between 52 and 75% of the acid-extractable chromium is water leachable. Right below the tank, down to 23.2 meters (76 feet) bgs, less than 2% of the chromium that is acid extractable is also water extractable. This signifies that within the shallowest zone where there is chromium that leaked from the tank, the binding mechanism is much stronger. Below 39.7 meters (130.1 feet) bgs, the percentage of the acid-extractable chromium that is also water extractable is <0.1%. In this deeper region, the acid-extractable chromium is at least equally a mixture of natural chromium and tank-derived chromium. It is obvious that natural chromium in the Hanford sediment is not water soluble and likely all chromium(III).

Molybdenum distribution, based on acid extraction, is significantly elevated down to a depth of 27.1 meters (89 feet) bgs and also around 34.7 meters (113.8 feet) bgs. The water extractable molybdenum between 24.6 and 28.4 meters (80.6 and 93.1 feet) bgs is greater than 25% of the acid-extractable molybdenum while for shallower depths and deeper depths the percentage of molybdenum that is water leachable is generally less than 10% of the acid extractable. The water-leachable, and to some extent the acid-leachable, molybdenum profiles suggest that molybdenum is less mobile than chromium. The molybdenum distribution in the porewaters shows one significantly elevated plume that starts at 23.3 meters (76.4 feet), peaks at 24.6 meters (80.6 feet), and dies off at 29.7 meters (97.3 feet) bgs. There may also be a smaller molybdenum plume that peaks at 20.7 meters (67.9 feet) bgs. Because the tank fluids do not contain such high concentrations of molybdenum as chromium(VI), our analyses are less clear than the isotope fingerprinting performed by the Science and Technology Program. The Science and Technology Program isotope fingerprinting that focuses on fission product contributions more clearly found that tank-derived molybdenum was less mobile than the chromium that left the tank as chromium(VI). More discussion of this fingerprint showing that the fluid in the vadose zone is tank related will occur in the field investigation report.^(a)

The elements arsenic, cadmium, cobalt, nickel, ruthenium, silver, uranium, and zinc (data not shown because all analyses were below detection limit) did not leach into water or acid at high enough concentrations to show any tank fluid-enhanced concentrations were affecting the sediment. There does appear to be some elevated lead in the water extract and definitely in the acid extract from the first sample obtained from the slant borehole. This suggests that lead is the least mobile metal that is present in the tank fluids and it becomes bound very near the bottom of the tank.

The water-extractable cations suggest that an ion-exchange process dominates the porewater/sediment interactions in the slant borehole zone where tank fluid passed by or currently exists. The leading edge of the tank leak plume is enriched in alkaline earth cations that were displaced from the native sediment exchange sites. There appears to be two ion exchange fronts present in the slant borehole profile but the fact that the hole is slanted and the presence of the bypassed zone at about 32 meters (105 feet) bgs may be complicating our suggestion that there could have been two leak events that produced two separate plumes.

(a) *Draft Field Investigation Report for Waste Management Area S-SX*. RPP-7884, Draft, Volume 2, Appendix D, CH2M HILL Hanford Group, Inc., Richland, Washington.

The sodium water-extractable/calculated porewater composition shows a distribution that differs from the divalent cations. Elevated sodium porewater concentration starts at 23.3 meters (76.4 feet) bgs, but the first peak occurs at 29.7 meters (97.3 feet) bgs with a concentration of 391 g/L. The sodium peak concentration is 1.3 meters (4.4 feet) shallower than the divalent cation peaks. The second peak for the monovalent cations is 7.4 meters (24.4 feet) shallower than the depth for second peak in the divalent cations. The ion exchange reactions, especially for the borehole 299-W23-19 near tank SX-115, have been modeled by the Science and Technology Program funded by the Vadose Zone/Groundwater/Columbia River Integration program. They have shown that the separation between the peaks of the divalent and monovalent cations increases as the concentration of the sodium in the invading tank liquor decreases. Thus, the greater separation in the peaks for the deeper plume at the slant borehole agrees with the hypothesis that the first leak was more dilute than the second leak. This could occur if the amount of in-tank concentration from self-boiling was significantly different prior to the separate leak events. Again, there are other plausible scenarios that could be the cause of the bimodal distribution of water-leachable cations in the slant borehole vadose zone sediment such that there may not have been two leak events.

Based on the acid and water leach profiles at both borehole 41-09-39 and the slant borehole, we suggest that there is little indication that the sediment contains significant amounts of leachable technetium-99 or other mobile constituents much deeper than the vertical extent of the slant borehole. We speculate that the leak(s) at tank SX-108 have not penetrated below the top of the PPlc unit. The bulk of the technetium-99 mass is found between 25.9 and 42.1 meters (85 and 138.2 feet) bgs, in the H2 and upper half of the PPlz unit. Very little technetium-99 activity was found below 42.1 meters (138.2 feet) bgs to the bottom of the borehole at ~44.2 meters (~145 feet) bgs. As mentioned, the chromium does not migrate as fast as the technetium-99 and though its leading edge (based on porewater concentrations and water-extractable chromium per gram of sediment) is also found near 42.1 meters (138.2 feet) bgs, the acid-extractable center of mass is located in the shallower plume between 23.2 and 30.8 meters (76 and 101 feet) bgs. The bulk of the water-leachable chromium has been confirmed as chromium(VI)(chromate) by its distinct yellow color and by ion chromatography.

The differing technetium-99 and selenium versus chromium and molybdenum migration observation is being studied by several investigators within the Environmental Management Science Program and the Science and Technology Program and some results will be discussed in the field investigation report.^(a)

In summary, we have identified common ion exchange and heterogeneous (solid phase-liquid solute) redox reactions as two mechanisms that are influencing the distribution of contaminants in the vadose zone sediment. There may have been two separate leak events below tank SX-108 with the earlier plume being less concentrated than the later leak.

(a) *Draft Field Investigation Report for Waste Management Area S-SX*. RPP-7884, Draft, Volume 2, Appendix D, CH2M HILL Hanford Group, Inc., Richland, Washington.

6.4 Estimates of Sorption-Desorption Values

In this section, we discuss our measurement and data synthesis used to quantify the adsorption-desorption values for the major contaminants found in the sediment at the slant borehole. We estimated the K_d for various contaminants using one method. By combining the data from the dilution-corrected 1:1 water extracts, which represent the porewater, with the activities measured on the sediment, we can get a semiquantitative sense of what the desorption K_d is. For a contaminant that has very little water-soluble mass, such as cesium-137, the K_d can be approximated as the amount of mass in the total sample per gram of dry sediment divided by the amount of mass in the porewater per milliliter. For a contaminant that is quite soluble in the water extract (about equivalent to saying that the contaminant resides mainly in the porewater within the sediment), one needs to subtract the amount that was water extractable from the total amount present in the moist sediment sample to obtain a value for the amount that would remain on the solid at equilibrium with the pore fluid.

Using these measured distributions, the in situ desorption K_d for cesium-137 is highly variable from a low of 2.3 to a high of 307 mL/g. In the sediment where the estimated porewater composition was >10 M sodium nitrate (between 24.4 and 29.6 meters [80 and 97 feet] bgs), the in situ desorption K_d varied between 2 and 10 mL/g. Much of the variability is correlatable to the major cation composition of the porewater, especially the sodium concentration. Aside from sample 13A that has a moderate K_d value of ~50 and sample 8A where the K_d is 25 mL/g, the cesium-137 K_d values are below 10 mL/g when the sodium concentration in the porewater is above 5 M. Above and below 24.4 and 29.6 meters (80 and 97 feet) bgs, cesium-137 in situ desorption K_d is larger because the pore fluids do not contain high sodium concentrations that compete for adsorption sites.

The technetium-99 desorption data are consistently near zero, meaning that the technetium-99 is not interacting with the sediment, down to the very deepest sample obtained. For sample 17A, there appears to be a slight interaction of the technetium-99 with the sediment. This may be caused by sample heterogeneity and analytical measurement uncertainties for the two extracts, acid and water, which were performed on two different aliquots of sediment. The overall data set suggests that technetium-99 is not interacting with the sediment and will travel at the same speed as water that is slowly percolating through the vadose zone. The technetium in situ desorption K_d data are consistent with a wealth of literature that finds essentially no technetium adsorption onto Hanford Site sediment from less saline waters (Kaplan and Serne 1995, 2000).

Aside from sample 7A, uranium shows significant resistance to water leaching/desorption. The uranium in the sediment does not appear to be elevated significantly over values for natural sediment. Thus, the uranium in the vadose zone is likely mostly natural and thus resistant to water leaching.

The chromium content in the slant borehole sediment is very elevated in most of the samples. There are two zones where the chromium desorption K_d values are quite low, 24.6 to 31 meters (80.6 to 101.7 feet) and 34.7 to 42.1 meters (113.8 to 138.2 feet) bgs, respectively. There is one sample between these two zones, 12A, which has been shown to have little signature of tank fluids. If this sample is excluded, the two relatively mobile chromium plumes would coalesce into one from 24.6 to 42.1 meters (80.6 to 138.2 feet) bgs. It is quite dramatic that chromium migration abruptly stopped somewhere

between 39.7 and 42.1 meters (130 and 138 feet) bgs, but technetium-99 has migrated deeper. Despite the findings that approximately one-third of the chromium appears to get reduced via caustic dissolution of ferrous containing minerals, the chromium desorption K_d values are still <1 mL/g in the entire zone where the bulk of the tank fluid currently resides.^(a) Below the zone of elevated chromium, the chromium K_d value is quite large (>100 mL/g). Between the tank bottom and 24.4 meters (80 feet) bgs, there is elevated total chromium in the sediment and the apparent desorption K_d ranges from 3 to 5 mL/g. This is likely the zone where most of the chromium reduction occurred by the caustic-induced dissolution of ferrous-bearing minerals. Deeper in the profile, there was no or much less caustic attack to release the iron (II) ions that cause the chromium(VI) reduction. Any chromium that reached the deeper depths would exhibit less retardation.

Based on the in situ desorption K_d presented in Table 5.1, we would conclude that selenium is slightly more interactive with the sediment than technetium-99. However, more detailed fission product isotope signature work by the Science and Technology Program suggests that tank liquor bearing selenium is just as mobile as technetium-99. We conclude that our acid extractions were dissolving enough natural selenium from the sediment to skew the in situ desorption K_d calculations. By dissolving natural selenium, we overestimate the amount of tank-leak selenium bound to the sediment and, thus, overestimate the K_d value for the manmade selenium. The molybdenum data in Table 5.1 suggest that molybdenum in the deeper sediment is more interactive with the sediment than chromium. The Science and Technology Program using more sophisticated isotope signature measurements also suggests molybdenum is more interactive, likely more prone to reduction when ferrous ions are released from the dissolution of sediment by caustic tank fluids. Our data suggest that the in situ desorption K_d values for molybdenum in the shallower sediment (above 28.3 meters [93 feet] bgs) are smaller than the chromium values and thus molybdenum would be more mobile in this zone. This is in disagreement with the Science and Technology Program, and we defer to their more elegant analyses.

A second method of determining K_d values would be laboratory batch tests. Batch adsorption tests were contemplated for the slant borehole sediment but the contaminant profiles, in situ K_d s, and porewater compositions were so similar to the data from borehole 41-09-39 that additional batch K_d desorption tests were not deemed necessary (see the report on batch desorption tests at borehole 41-09-39 for more discussion; Serne et al. 2002a). Further, some desorption work was performed by the Science and Technology Program and their results will be combined with the data herein to present a detailed data package in the field investigation report.^(a)

None of the data collected from borehole 41-09-39 or the slant borehole under tank SX-108 can be interpreted to suggest that cesium-137 can travel through Hanford formation sediment without adsorbing to some degree. Albeit, the data and tests performed to date do not address elevated temperature or colloidal transport. These two drivers are not expected to significantly change our conclusion that

(a) *Draft Field Investigation Report for Waste Management Area S-SX*. RPP-7884, Draft, Volume 2, Appendix D, CH2M HILL Hanford Group, Inc., Richland, Washington.

(a) *Draft Field Investigation Report for Waste Management Area S-SX*. RPP-7884, Draft, Volume 2, Appendix D, CH2M HILL Hanford Group, Inc., Richland, Washington.

cesium-137 will be adequately retarded once it is separated from the high sodium porewater plume. The temperature effect on adsorption reactions is not well studied but the few available studies suggest only small effects (see Ames et al. 1982 for cesium-137 adsorption onto basalt and smectite clay weathering products).

Another technique to estimate mobility is to compare the ratio of cesium-137 to technetium-99 activity in the borehole sediment. Slant borehole sediment from 20.7 to 24.6 meters (67.9 to 80.6 feet) bgs has a cesium-137 to technetium-99 activity ratio >10,000. Johnson and Chou (1998) suggest that the ratio in SX tank liquors would be 10,000. Therefore, the shallow sediment from the slant borehole between 20.7 to 24.6 meters (67.9 and 80.6 feet) bgs either adsorbed cesium-137 relative to technetium-99 or the tank liquor has been flushed from the shallow sediment so that the ratio is greater than it is within the tank supernate. Between the depths of 27.1 meters (89 feet) bgs and the bottom of the slant borehole, the cesium-137 to technetium-99 decreases from 100 to about 0.1, which suggests that cesium-137 gets removed from the tank fluid by adsorption reactions and technetium-99 continues to migrate deeper into the sediment with the mobile constituents in the tank liquor plume.

Based on comparing the depth of penetration of various contaminants and comparing the percentages that are water leachable, we can state that chromium and molybdenum migrate faster than cesium-137 but slower than nitrate, selenium, and technetium-99. In other waste disposal situations at Hanford, oxidized chromium in reactor cooling water (low ionic strength and neutral pH) appears to migrate similarly to nitrate and technetium-99. All of these observations, based on directly measuring sediment or their water and acid extracts, suggest that nitrate, selenium, and technetium-99 migrate with no measurable retardation, while chromium, molybdenum, and sodium migrate with a small amount of retardation, and cesium-137 and lead migrate with moderate to strong retardation.

6.5 Other Characterization Observations

The ratio of one ostensibly mobile species to others in the porewaters can be used to determine relative mobilities. If the absolute concentrations of co-migrating species are changed solely by dilution with existing porewater, then the ratio of the two should remain constant. Unlike similar ratio discussions for the other two contaminated boreholes (41-09-39 and 299-W23-19; see Serne et al. 2002a, b), the ratios for the porewaters in the slant borehole are not constant. It would appear that there are some complicating processes occurring at the slant borehole compared to the other two boreholes. Perhaps the fact that the slant borehole is not a vertical borehole that conceivably allows one to follow systematically the expected vertical recharge is part of the problem. The possibility of two distinct leak events that caused additional irregular mixing between the two plumes or dynamic convection currents driven by the time varying head load under the tank makes this ratio approach difficult. Sample 12A is also adding complexity because it is a thin lens of fine-grained sediment that appears to be isolated from having imbibed much of the tank liquor. It is similar to an isolated pocket of sediment that the tank liquor flowed around instead of through. Despite these complications the following observations are offered.

The ratio of technetium-99 to nitrate, though not as constant as it was at borehole 299-W23-19 (Serne et al. 2002b), is much lower than the ratio in the groundwater below the SX Tank Farm. The ratio in the groundwater is 100 pCi/mg, a value much higher than the range found for the slant borehole porewaters (0.02 to 0.48 pCi/mg). This would suggest that if tank SX-108 were the source of the groundwater

contamination, much more nitrate or less technetium-99 should be in the groundwater. Alternatively there would have to be some mechanism in the deeper sediment that preferentially removes technetium-99 from the pore fluids. Conversely, it is much more plausible that the source of the contamination in the groundwater under the SX Tank Farm is the fluids lost from tank SX-115 that show a technetium-99 to nitrate ratio closer to 100 in the vadose zone porewater.

In general, the percentage of the total sediment trace metal concentrations that is acid extractable from the contaminated sediment is slightly higher than for the uncontaminated sediment. We would have expected that the chromium percentage would be measurably higher for the contaminated sediment but the increase is not striking despite the fact that the total chromium content of the contaminated sediment is significantly elevated over uncontaminated sediment. The percentage of the total lead that is extractable from several of the samples suggests that lead contamination from the shielding in the samplers is present in some of the extracts. For example, the concentration of lead in sample 13A that acid leached is 4 times greater than the total in the sample that was used in perform the x-ray fluorescence measurements. Somehow lead contamination was present in the aliquot that was acid extracted or lead contamination was introduced before the acid digest was measured by both ICP and ICP-MS (see Table 4.18).

The manmade sodium, and perhaps a percentage of the trace metals, show a higher percentage of the total concentrations are acid extractable from the highly contaminated slant borehole sediment compared to uncontaminated sediment. Except for the sodium results, we expected there to be a larger increase than was observed for the contaminated sediment suggesting that the comparison of percentages of the total composition of any element that is acid extractable is not a very sensitive indicator of the presence of tank liquors or its reaction products with vadose zone sediment. More on alteration products is found in the mineralogy section.

As part of our characterization, the contaminated sediment parameters that can control contaminant migration were measured. Key parameters that were measured on the slant borehole sediment include the calcium carbonate content, particle size distribution, and bulk and clay-size mineralogy.

Particle size measurements showed that the H1 unit does have enough gravel to be considered a gravelly muddy sand. The Hanford formation H2 unit has a few finer grained lenses that are sandy mud. The PPlz zone is considered a sandy mud.

The finest grained samples of the H2 unit are very similar in grain size to the top of the fine-grained PPlz unit represented by sample 15A. Because the borehole did not penetrate the whole PPlz unit, we cannot show explicitly that the PPlz unit is finer grained in general than the H2 unit at this borehole; but based on other nearby boreholes, we believe that the PPlz under tank SX-108 is finer grained than the H2 unit.

X-ray diffraction analyses of the bulk samples from nine depths in the slant borehole indicate that the sediment is mostly quartz (~30 to 60%) and feldspar (~15 to 80%), with lesser amounts of calcite, amphibole, mica, chlorite, and smectite. X-ray diffraction tracings from several of the bulk samples showed evidence of the sodium nitrate mineral, nitratine. Chemistry of the 1:1 water extracts from these

samples showed large amounts of sodium and nitrate (~3.0 to 15 M), so it is not unexpected that solid sodium nitrate is present in the dried samples.

The clay fraction (<2 micron) in all the samples characterized is dominated by four clay minerals: illite, smectite, chlorite, and kaolinite with minor amounts of quartz, feldspar, amphibole, and calcite. Overall, smectite, illite, and chlorite are the dominant minerals in the clay fraction. Smectites range in concentrations from as high as 20 wt% to as low as 5 wt%; illite occurred between ~10 and 30 wt%. Chlorite concentrations were as low as 5 wt% and as high as 30 wt%. Minor amounts of kaolinite (~10 wt%) were detected at all depths, but one (3A, 20.7 meters [67.9 feet] bgs). Quartz and feldspar made up ~10 to 15 wt% of the clay fraction. Amphibole was identified in the clay fraction in minor amounts. Nitrate was not found in the clay fractions. This is not surprising because the clay particles were washed repeatedly during their collection.

The presence of illites as the dominant clay-size mineral is fortuitous because illites are strong adsorbers of cesium-137 and can irreversibly adsorb cesium-137 within interlayer sites.

Trace amounts of laumontite (9.08 Å) were detected in three samples (3A, 6A, and 7A). The zeolite, laumontite, is known to be present in the natural uncontaminated Hanford formation sediment and is not thought to be a weathering product resulting from the interaction of tank liquor with the sediment. No evidence of mineral alteration or precipitation resulting from the interaction of the tank liquor with the sediment was observed based on the x-ray diffraction measurements. However, scanning electron microscopy scans of some of the samples by the Science and Technology Program suggest that there is evidence of caustic attack on sample 3A.

7.0 References

Ames LL, JE McGarrah, BA Walker, and PF Salter. 1982. "Sorpton of uranium and cesium by Hanford basalts and associated secondary smectite." *Chem. Geol.* 35:205-225.

ASA - American Society of Agronomy. 1986a. "Hydrometer Method." Chapter 15-5 in *Methods of Soil Analysis-Part 1, 2nd edition of Physical and Mineralogical Methods*, SSSA Book Series no. 5, A Klute (ed.), pp. 404-408. Soil Science Society of America, Madison, Wisconsin.

ASA - American Society of Agronomy. 1986b. "Pynchnometer Method." Chapter 14-3 in *Methods of Soil Analysis-Part 1, 2nd edition of Physical and Mineralogical Methods*, SSSA Book Series no. 5, A Klute (ed.), pp. 378-379. Soil Science Society of America, Madison, Wisconsin.

ASA - American Society of Agronomy. 1996a. "Cation exchange capacity and exchange coefficients." In *Methods of Soil Analysis-Part 3, Chemical Methods*, SSSA Book Series no. 5, DL Sparks et al. (eds.), pp. 1220-1222. Soil Science Society of America, Madison, Wisconsin.

ASA - American Society of Agronomy. 1996b. "Elemental Analysis by XRF Spectroscopy." Chapter 7 in *Methods of Soil Analysis-Part 3, Chemical Methods*, SSSA Book Series 5, DL Sparks (ed.), pp. 161-223. Soil Science Society of America, Madison, Wisconsin.

ASTM D422-63 (R1972). 1986. "Standard method for particle size analysis soils." *Annual Book of ASTM Standards*. American Society for Testing and Materials, Philadelphia, Pennsylvania.

ASTM D4129-88. 1988. "Standard test method for total and organic carbon in water by high temperature oxidation and by coulometric detection." American Society for Testing and Materials, West Conshohocken, Pennsylvania.

ASTM D2488-93. 1993. "Standard practice for description and identification of soils (visual-manual procedure)." American Society for Testing and Materials, West Conshohocken, Pennsylvania.

ASTM D2216-98. 1998. "Test method for laboratory determination of water (moisture) content of soil and rock." American Society for Testing and Materials, West Conshohocken, Pennsylvania.

Bjornstad BN. 1990. *Geohydrology of the 218-W-5 burial ground, 200 West Area, Hanford Site*. PNL-7336, Pacific Northwest Laboratory, Richland, Washington.

Brindley GW and G Brown (eds.). 1980. "Crystal structures of clay minerals and their x-ray identification." *Monograph No. 5*, Mineralogical Society, London.

DOE. 1988. *Consultation draft site characterization plan*. DOE/RL-0164, 9 volumes, U.S. Department of Energy, Richland Operations Office, Richland, Washington.

DOE. 1999. *Phase I RCRA facility investigation/corrective measures study work plan for the SST Waste Management Areas*. DOE/RL-99-36, Rev. 0, U.S. Department of Energy, Richland Operations Office, Richland, Washington.

Drever JI. 1973. "The preparation of oriented clay mineral specimens for X-ray diffraction analysis by a filter-membrane peel technique." *Amer. Minerl.* 58:553-554.

EPA Method 300.0A. 1984. *Test method for the determination of inorganic anions in water by ion chromatography*. EPA-600/4-84-017, U.S. Environmental Protection Agency, Washington, D.C.

EPA. 1986. *Test methods for evaluating solid waste: physical/chemical methods, SW-846, Third Edition*. U.S. Environmental Protection Agency, Office of Solid Waste and Emergency Response, Washington, D.C., available online <http://www.epa.gov/epaoswer/hazwaste/test/sw846.htm>

EPA Method 3050B. 2000a. "Acid Digestion of Sediments, Sludges, and Soils." *Test methods for evaluating solid waste, physical/chemical methods*. EPA publication SW-846, available online <http://www.epa.gov/epaoswer/hazwaste/test/sw846.htm>

EPA Method 6010B. 2000b. "Inductively Coupled Plasma-Atomic Emission Spectrometry." *Test methods for evaluating solid waste, physical/chemical methods*. EPA publication SW-846, available online <http://www.epa.gov/epaoswer/hazwaste/test/sw846.htm>

EPA Method 6020. 2000c. "Inductively Coupled Plasma-Mass Spectrometry." *Test methods for evaluating solid waste, physical/chemical methods*. EPA publication SW-846, available online <http://www.epa.gov/epaoswer/hazwaste/test/sw846.htm>

Fecht KR and WH Price. 1977. *Granulometric data 241-SX tank farm monitoring well sediment*. RHO-LD-18, Rockwell Hanford Operations, Richland, Washington.

Folk RL. 1968. *Petrology of sedimentary rocks*. Hemphill, Austin, Texas.

Gardner MG and KD Reynolds. 2000. *SX-108 slant borehole completion report*. RPP-6917, Rev. 0, Office of River Protection, Richland, Washington.

Jackson ML. 1969. *Soil chemical analysis – advanced course – 2nd Edition*. Department of Soil Science, University of Wisconsin, Madison.

Johnson V and CJ Chou. 1998. *Results of phase I groundwater quality assessment for single-shell tank Waste Management Areas S-SX at the Hanford Site*. PNNL-11810, Pacific Northwest National Laboratory, Richland, Washington.

Johnson V and CJ Chou. 1999. *Addendum to the RCRA assessment report for single-shell tank Waste Management Areas S-SX at the Hanford Site*. PNNL-11810 Addendum 1, Pacific Northwest National Laboratory, Richland, Washington.

Johnson VG, TE Jones, SP Reidel, and MI Wood. 1999. *Subsurface conditions description for the S-SX Waste Management Area*. HNF-4936, Rev. 0, Lockheed Martin Hanford Corporation, Richland, Washington.

Kaplan DI and RJ Serne. 1995. *Distribution coefficient values describing iodine, neptunium, selenium, technetium, and uranium sorption to Hanford sediment*. PNL-10379, Supplement 1, Pacific Northwest Laboratory, Richland, Washington.

Kaplan DI and RJ Serne. 2000. *Geochemical data package for the Hanford immobilized low-activity tank waste performance assessment (ILAW-PA)*. PNNL-13037 Rev.1, Pacific Northwest National Laboratory, Richland, Washington.

Lindsey KA, SE Kos, and KD Reynolds. 2000. *Vadose zone geology of boreholes 299-W22-50 and 299-W23-19 S-SX Waste Management Area Hanford Site, south-central Washington*. RPP-6149 Rev. 0, Daniel B. Stephens & Associates, Richland, Washington.

Newman ACD (ed.). 1987. *Chemistry of clays and clay minerals*. Monograph No 6, Mineralogical Society, London.

PNL - Pacific Northwest Laboratory. 1990. *Procedures for groundwater investigations*. PNL-MA-567-DO-1, Pacific Northwest Laboratory, Richland, Washington.

PNNL - Pacific Northwest National Laboratory. 1997. *Gamma energy analysis operation and instrument verification using the Genie2000™ support software*. PNNL-RRL-01, Pacific Northwest National Laboratory, Richland, Washington.

PNNL - Pacific Northwest National Laboratory. 1998. *Inductively coupled plasma mass spectrometric (ICP-MS) analysis*. PNNL-AGG-415, Pacific Northwest National Laboratory, Richland, Washington.

Price WH and KR Fecht. 1976. *Geology of the 241-SX tank farm*. ARH-LD-134, Atlantic Richfield Hanford Company, Richland, Washington.

Reynolds DM and RC Reynolds, Jr. 1989. *X-ray diffraction and the identification and analysis of clay minerals*. Oxford University Press, New York.

Rhoades JD. 1996. "Salinity: Electrical conductivity and total dissolved solids." In *Methods of Soil Analysis Part 3*, JM Bigham (ed.), pp. 417-435. American Society of Agronomy, Madison, Wisconsin.

Serne RJ, JM Zachara, and DS Burke. 1998. *Chemical information on tank supernatants, Cs adsorption from tank liquids onto Hanford sediment, and field observations of Cs migration from past tank leaks*. PNNL-11495, Pacific Northwest National Laboratory, Richland, Washington.

Serne RJ, GV Last, GW Gee, HT Schaef, DC Lanigan, CW Lindemeier, RE Clayton, VL LeGore, RD Orr, MJ O'Hara, CF Brown, DS Burke, AT Owen, IV Kutnyakov, and TC Wilson. 2002a. *Characterization of Vadose Zone Sediment: Borehole 41-09-39 in the S-SX Waste Management Area*. PNNL-13757-3, Pacific Northwest National Laboratory, Richland, Washington.

Serne RJ, HT Schaef, BN Bjornstad, DC Lanigan, GW Gee, CW Lindemeier, RE Clayton, VL LeGore, MJ O'Hara, CF Brown, RD Orr, GV Last, IV Kutnyakov, DS Burke, TC Wilson and BA Williams. 2002b. *Characterization of Vadose Zone Sediment: Borehole 299-W23-19 [SX-115] in the S-SX Waste Management Area*. PNNL-13757-2, Pacific Northwest National Laboratory, Richland, Washington.

Serne RJ, HT Schaef, BN Bjornstad, BA Williams, DC Lanigan, DG Horton, RE Clayton, VL LeGore, MJ O'Hara, CF Brown, KE Parker, IV Kutnyakov, JN Serne, AV Mitroshkov, GV Last, SC Smith, CW Lindemeier, JM Zachara, and DS Burke. 2002c. *Characterization of Vadose Zone Sediment: Uncontaminated RCRA Borehole Core Samples and Composite Samples*. PNNL-13757-1, Pacific Northwest National Laboratory, Richland, Washington.

Sobczyk SM 2000. *Subsurface interpretation of the SX tank farm Hanford Site, Washington based on gamma-ray logging*. Nez Perce Tribe Environmental Restoration Waste Management Program, Lapwai, Idaho.

Tallman AM, KR Fecht, MC Marratt, and GV Last. 1979. *Geology of the separations areas, Hanford Site, south-central Washington*. RHO-ST-23, Rockwell Hanford Operations, Richland, Washington.

U.S. Geological Survey. Revised 9/2001. "Alkalinity and Acid Neutralizing Capacity." *National Field Manual for the Collection of Water-Quality Data*. Available online at <http://water.usgs.gov/owq/FieldManual/Chapter6/6.6-contents.html>

Wentworth CK 1922. "A grade scale and class terms for clastic sediment." *Journal of Geology* 30:377-392.

WMTS. 2000a. *Description of work: demonstration of slant borehole installation and sampling methods*. WMTS-DOW-001, Rev. 0, Waste Management Technical Services, Richland, Washington.

WMTS. 2000b. *Description of work: slant borehole demonstration summary report*. WMTS-DOW-002, Rev. 0, Waste Management Technical Services, Richland, Washington.

WMTS. 2000c. *Description of work: slant borehole installation beneath 241-SX-108*. WMTS-DOW-003, Rev. 0, Waste Management Technical Services, Richland, Washington.

Wood MI, TE Jones, R Schalla, BN Bjornstad, and FN Hodges. 2001. *Subsurface conditions description of the T-TX-TY Waste Management Area*. RPP-7123, Rev. 0, CH2M HILL Hanford Group, Inc., Richland, Washington.

Appendix A

Core Descriptions

DAILY BOREHOLE LOG

Pacific Northwest National Laboratory

Boring/Well No SX-1DB Slenhole Depth 28.2-99.2 ^{ON} AXEL Date 7/11/00
 Location 241-SX TRXFRM Project 40165/40212

Sheet 1 of 1

Logged by G.L. PRIST ^{PRINT} Drilling Contractor NA
 Reviewed by [Signature] Driller NA

Lithologic Class. Scheme Folk/Wentworth Procedure D9781-99-EVL-01 Rev 00
 Steel Tape/E-Tape NA / NA Field Indicator Equip. 1) NR 2) NA

DEPTH MEAS. (FT)	TIME	SAMPLES		CONTAMINATION		MOIS- TURE	GRAPHIC LOG			LITHOLOGIC DESCRIPTION (particle size distribution, sorting, mineralogy, roundness, color, reaction to HCl, etc.)	H ₂ O ADDED	CASING	DRILLING COMMENTS (drilling rate, down time, blow counts, water level, drill fluid, etc.)
		TYPE	ID NUMBER	INSTR.	READING		C	Z	S				
98.1	14:20		S0070-07										
98.2													
.3			07B			D				M.F. Sand, 2.5Y 5/3. Weak-stony Reaction. Some coarser (M)			* = GEA SAMPLE O = MOISTURE SAMPLE
.4										lamination. Slight color change grinding up sand (more yellowish)			
.5													
.6													
.7													
.8			07-A	CP	1.5R(2.9)					M.F. Sand, 2.5Y 5/2. Weak-stony Rx. (HOTTEST STUFF)			
.9					0.5R(2)								
99.0			07-A1							Silt, Considered bedding/structure. (soft sed. definition compacted. 2.5Y 3/3. strong Rx.)			
.1													
.2										Med. to Fine Sand, 2.5Y 5/3. Weak-Stony Rx. Coarse to medium sand. (in shoe)			

W = Wet, M = Moist, D = Dry

1999/DCL/PROC/DBLU001

DAILY BOREHOLE LOG

Pacific Northwest National Laboratory

Boring/Well No SX-105, Slant borehole Depth 108.2-109.2 Date 7/13/00 Sheet 1 of 1

Location 241-SX Tankfarm Project 40165/40212

Logged by G.V. LAST Drilling Contractor NA
 Reviewed by [Signature] Driller _____
 Lithologic Class. Scheme Fitz/Wentworth Procedure 99-EVL-01 Rev 0
 Steel Tape/E-Tape NA Field Indicator Equip. 1) NA 2) NA Depth Control Point ↓

DEPTH ARCULE (FT.)	TIME	SAMPLES		CONTAMINATION		MOIS- TURE	GRAPHIC LOG			LITHOLOGIC DESCRIPTION (particle size distribution, sorting, mineralogy, roundness, color, reaction to HCl, etc.)	H ₂ O ADDED	CASING	DRILLING COMMENTS (drilling rate, down time, blow counts, water level, drill fluid, etc.)
		TYPE	ID NUMBER	INSTR.	READING		C	Z	S				
108.0	15:00		S0070-09										
11													
12													
13													
14													
15			CP	10 MR DQ 1/2						SAND, some silt. Disaggregated. Perhaps some slough			SLEEVE A = 100% FULL SLEEVE B = 70% FULL
16			9B	25 MC 7									* = BEN Sample O = MUDstone Sample
17													
18			CP	511-18 MR 0						SAND, Fine to Very Fine some silt at top. 2.5 P5/3. Grains determined to medium sand. Silt & Pepper texture. Strong reaction to HCl at bottom. Less strong at top of A sleeve			Samples held together very well etc. top of B sleeve. Perhaps some slough
108.0													
11			9A							- Fine to Very Fine Sand 2.5 P 5/3. Weak to strong reaction. Sharp contact at top. Finely laminated.			
12													

W = Wet, M = Moist, D = Dry

DAILY BOREHOLE LOG

Pacific Northwest National Laboratory

Boring/Well No SX-10B borehole Depth 13.2-114.2 Date 7/18/00

Location 241-SX Tankfarm Project 40165/4D212

Logged by GVL/AF Drilling Contractor NA Sheet 1 of 2

Reviewed by [Signature] Driller NA

Lithologic Class. Scheme Folk/Wentworth Procedure 7701-99-SVL-01 Rev 0

Steel Tape/E-Tape NA / NA Field Indicator Equip. 1) NA 2) NA

DEPTH ANGLE (FT)	TIME	SAMPLES		CONTAMINATION		MOIS- TURE	GRAPHIC LOG			LITHOLOGIC DESCRIPTION (particle size distribution, sorting, mineralogy, roundness, color, reaction to HCl, etc.)	H ₂ O ADDED	CASING	DRILLING COMMENTS (drilling rate, down time, blow counts, water level, drill fluid, etc.)
		TYPE	ID NUMBER	INSTR.	READING		C	Z	S				
13.2	14:35		55007-10										
.1													
.2													
.3													
.4													
.5													
.6				B	CP	0.2	D						B sleep is SD 5/8.
.7													A sleep is Full.
.8													A = GEA sample
.9													O = moisture sample.
114.0				A	sample		D						
.1													
.2													

W = Wet, M = Moist, D = Dry

DAILY BOREHOLE LOG

Pacific Northwest National Laboratory
 Boring/Well No SX-108 borehole
 Location 241-SX Tankfarm
 Depth 118.2 - 119.2 Date 1/18/50
 Project 40165/42212 Sheet 2 of 2

Logged by GVL RST Date _____
 Reviewed by [Signature] Date _____
 Lithologic Class. Scheme Folk/Wentworth Procedure DTA-97-G1-01 Rev 0
 Steel Tape/E-Tape NR / NR Field Indicator Equip. 1) NA 2) NR

Drilling Contractor NA
 Driller _____
 Rig/Method _____
 Depth Control Point _____

DEPTH AS-LOG (FT.)	SAMPLES ID NUMBER	CONTAMINATION		MOIS- TURE	GRAPHIC LOG	LITHOLOGIC DESCRIPTION (particle size distribution, sorting, mineralogy, roundness, color, reaction to HCl, etc.)	H ₂ O ADDED	CASING	DRILLING COMMENTS (drilling rate, down time, blow counts, water level, drill fluid, etc.)	
		INSTR.	READING							
118.0	55007-11									
11										
12										
13										
14										
15										
16										
17										
18										
19										
119.0										
11										
12										

W = Wet, M = Moist, D = Dry

DAILY BOREHOLE LOG

Pacific Northwest National Laboratory

Boring/Well No SX-108 SLANTHOLE Depth 123.2-124.2 Date 07/19/00 Sheet 1 of 1
 Location 241-SX TRINITY Project 48165/40212

Logged by S.V. LAST Drilling Contractor NA
 Reviewed by [Signature] Driller NA

Lithologic Class. Scheme Folk/Wentworth Procedure ZTR-32-01-01 Rev 0
 Steel Tape/E-Tape NA / NA Field Indicator Equip. 1) NA 2) NA Depth Control Point ↓

DEPTH (FT)	TIME	SAMPLES		CONTAMINATION		MOISTURE	GRAPHIC LOG			LITHOLOGIC DESCRIPTION (particle size distribution, sorting, mineralogy, roundness, color, reaction to HCl, etc.)	H ₂ O ADDED	CASING	DRILLING COMMENTS (drilling rate, down time, blow counts, water level, drill fluid, etc.)
		TYPE	ID NUMBER	INSTR.	READING		C	Z	S				
123.0	14:30	SS	50070-12										
.1													
.2													
.3													
.4													
.5													
.6													
.7													
.8													
.9													
124.0													
.1													
.2													

W = Wet, M = Moist, D = Dry

Pacific Northwest National Laboratory **DAILY BOREHOLE LOG** Boring/Well No. 5X-108 SLANT HOLE Date 7/27/08 Sheet 1 of 2
 Location 241-5X TRAILWAY Project 4D165/4D212 ANISE Depth 153.0-154.2

Logged by G.V. LAIST Drilling Contractor NA
 Reviewed by G.V. LAIST Driller NA
 Lithologic Class. Scheme Folk/Wentworth Procedure D731-99-GAL-01 Rev 0
 Steel Tape/E-Tape NA / NA Field Indicator Equip. 1) NA 2) NA

DEPTH ANGLE (FT)	TIME	SAMPLES		CONTAMINATION		MOIS- TURE	GRAPHIC LOG			LITHOLOGIC DESCRIPTION (particle size distribution, sorting, mineralogy, roundness, color, reaction to HCl, etc.)	H ₂ O ADDED	CASING	DRILLING COMMENTS (drilling rate, down time, blow counts, water level, drill fluid, etc.)
		TYPE	ID NUMBER	INSTR.	READING		C	Z	S				
153.0	14:20		550076-15										
.1													
.2													
.3			B	CP	<0.5mm	M							B sample is 100% fill.
.4													A sample is 100% fill.
.5													C= moisture sample
.6													*=GEA sample.
.7													
.8			A	CP	<0.5mm	M							
.9													
154.0													
.1													
.2													

W = Wet, M = Moist, D = Dry

Appendix B

Additional Core Photos

C3082 (SX-108 Slant Hole): Sample S0070-01B
Angle Depth: 63.2' - 63.7' Vertical Depth: 54.5' - 54.9'



2001/DCL/SX-108/053

Figure B-1. SX-108 Slant Hole Sample S0070-01B

C3082 (SX-108 Slant Hole): Sample S0070-04B
Angle Depth: 83.2' - 83.7' Vertical Depth: 71.5' - 71.9'



2001/DCL/SX-108/054

Figure B-2. SX-108 Slant Hole Sample S0070-04B

C3082 (SX-108 Slant Hole): Sample S0070-05B
Angle Depth: 88.2' - 88.7' Vertical Depth: 75.7' - 76.2'



2001/DCL/SX-108/055

Figure B-3. SX-108 Slant Hole Sample S0070-05B

C3082 (SX-108 Slant Hole): Sample S0070-05A
Angle Depth: 88.7' - 89.2' Vertical Depth: 76.2' - 76.6'



2001/DCL/SX-108/056

Figure B-4. SX-108 Slant Hole Sample S0070-05A

C3082 (SX-108 Slant Hole): Sample S0070-06B
Angle Depth: 93.2' - 93.7' Vertical Depth: 79.9' - 80.4'



2001/DCL/SX-108/057

Figure B-5. SX-108 Slant Hole Sample S0070-06B

C3082 (SX-108 Slant Hole): Sample S0070-06A
Angle Depth: 93.7' - 94.2' Vertical Depth: 80.4' - 80.8'



2001/DCL/SX-108/058

Figure B-6. SX-108 Slant Hole Sample S0070-06A

C3082 (SX-108 Slant Hole): Sample S0070-07B
Angle Depth: 98.2' - 98.7' Vertical Depth: 84.1' - 84.6'



2001/DCL/SX-108/059

Figure B-7. SX-108 Slant Hole Sample S0070-07B

C3082 (SX-108 Slant Hole): Sample S0070-08B
Angle Depth: 103.2' - 103.7' Vertical Depth: 88.3' - 88.8'



2001/DCL/SX-108/060

Figure B-8. SX-108 Slant Hole Sample S0070-08B

C3082 (SX-108 Slant Hole): Sample S0070-08A
Angle Depth: 103.7' - 104.2' Vertical Depth: 88.8' - 89.2'



2001/DCL/SX-108/061

Figure B-9. SX-108 Slant Hole Sample S0070-08A

C3082 (SX-108 Slant Hole): Sample S0070-09B
Angle Depth: 108.2' - 108.7' Vertical Depth: 92.5' - 92.9'



2001/DCL/SX-108/062

Figure B-10. SX-108 Slant Hole Sample S0070-09B

C3082 (SX-108 Slant Hole): Sample S0070-09A
Angle Depth: 108.7' - 109.2' Vertical Depth: 92.9' - 93.3'



2001/DCL/SX-108/063

Figure B-11. SX-108 Slant Hole Sample S0070-09A

C3082 (SX-108 Slant Hole): Sample S0070-10B
Angle Depth: 113.2' - 113.7' Vertical Depth: 96.6' - 97.1'



2001/DCL/SX-108/064

Figure B-12. SX-108 Slant Hole Sample S0070-10B

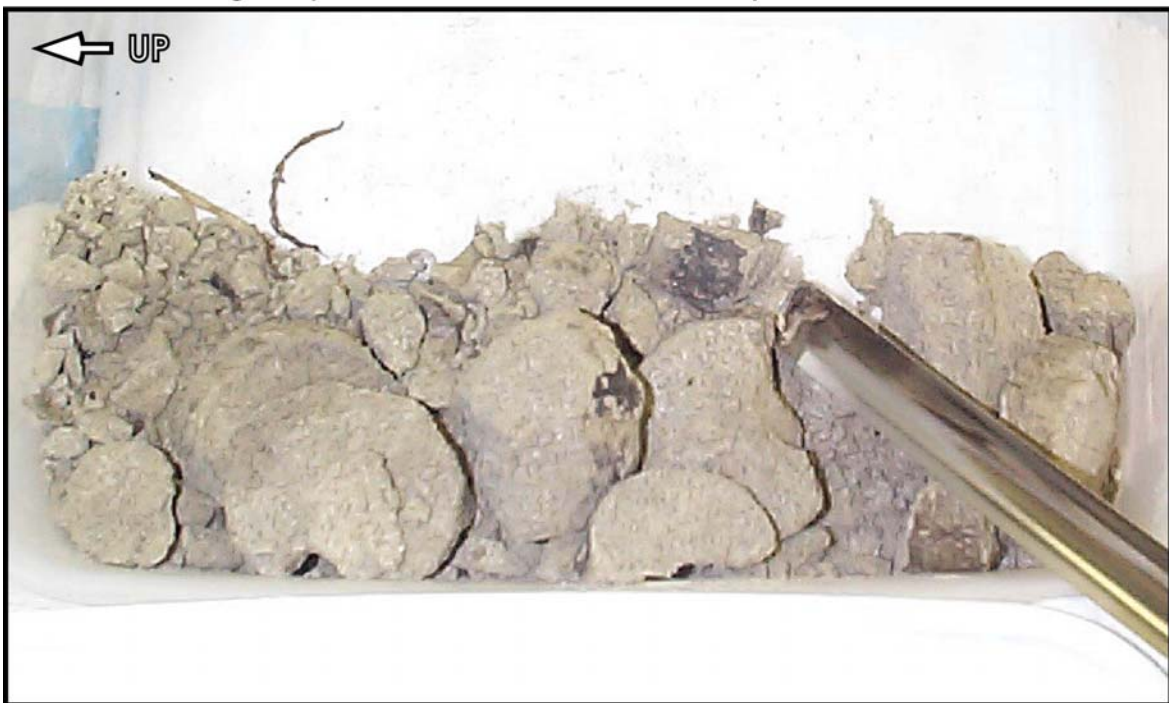
C3082 (SX-108 Slant Hole): Sample S0070-10A
Angle Depth: 113.7' - 114.2' Vertical Depth: 97.1' - 97.5'



2001/DCL/SX-108/065

Figure B-13. SX-108 Slant Hole Sample S0070-10A

C3082 (SX-108 Slant Hole): Sample S0070-11B
Angle Depth: 118.2' - 118.7' Vertical Depth: 101.0' - 101.5'



2001/DCL/SX-108/066

Figure B-14. SX-108 Slant Hole Sample S0070-11B

C3082 (SX-108 Slant Hole): Sample S0070-11A
Angle Depth: 118.7' - 119.2' Vertical Depth: 101.5' - 101.9'



2001/DCL/SX-108/067

Figure B-15. SX-108 Slant Hole Sample S0070-11A

C3082 (SX-108 Slant Hole): Sample S0070-12B
Angle Depth: 123.2' - 123.7' Vertical Depth: 104.9' - 105.4'



2001/DCL/SX-108/068

Figure B-16. SX-108 Slant Hole Sample S0070-12B

C3082 (SX-108 Slant Hole): Sample S0070-12A
Angle Depth: 123.7' - 124.2' Vertical Depth: 105.4' - 105.8'



2001/DCL/SX-108/069

Figure B-17. SX-108 Slant Hole Sample S0070-12A

C3082 (SX-108 Slant Hole): Sample S0070-13B
Angle Depth: 133.2' - 133.7' Vertical Depth: 113.1' - 113.6'



2001/DCL/SX-108/070

Figure B-18. SX-108 Slant Hole Sample S0070-13B

C3082 (SX-108 Slant Hole): Sample S0070-14B
Angle Depth: 143.2' - 143.7' Vertical Depth: 121.3' - 121.7'



2001/DCL/SX-108/071

Figure B-19. SX-108 Slant Hole Sample S0070-14B

C3082 (SX-108 Slant Hole): Sample S0070-15B
Angle Depth: 153.2' - 153.7' Vertical Depth: 129.4' - 129.9'



2001/DCL/SX-108/072

Figure B-20. SX-108 Slant Hole Sample S0070-15B

C3082 (SX-108 Slant Hole): Sample S0070-15A
Angle Depth: 153.7' - 154.2' Vertical Depth: 129.9' - 130.3'



2001/DCL/SX-108/073

Figure B-21. SX-108 Slant Hole Sample S0070-15A

C3082 (SX-108 Slant Hole): Sample S0070-16B
Angle Depth: 163.2' - 163.7' Vertical Depth: 137.5' - 138.0'



2001/DCL/SX-108/074

Figure B-22. SX-108 Slant Hole Sample S0070-16B

C3082 (SX-108 Slant Hole): Sample S0070-16A
Angle Depth: 163.7' - 164.2' Vertical Depth: 138.0' - 138.4'



2001/DCL/SX-108/075

Figure B-23. SX-108 Slant Hole Sample S0070-16A

C3082 (SX-108 Slant Hole): Sample S0070-17B
Angle Depth: 171.2' - 171.7' Vertical Depth: 144.0' - 144.4'



2001/DCL/SX-108/076

Figure B-24. SX-108 Slant Hole Sample S0070-16B

Appendix C

Comparison of Water Extractable and 8 M Nitric Acid Extractable Concentrations

In this appendix, we compare the water extractable and 8M nitric acid extractable concentrations of various constituents that were not discussed/shown in the main text. On most of the figures, the water extract concentrations as a function of vertical depth are shown in light blue print with an expanded scale at the top of the figures. That is, the amount of the constituent that was water leachable is very small compared to the concentration of acid leachable. Thus, to see any detail in the water extractable, the concentration scale needs to be expanded. The water leachable concentration is also plotted in dark blue print on the same scale as the acid leachable (plotted in red print) with the axis scale on the bottom of the figure. As can be seen, the water leachable concentration, when plotted on the same scale as the acid leachable essentially hugs the left side of the figures reflecting very little of the total mass leached into water.

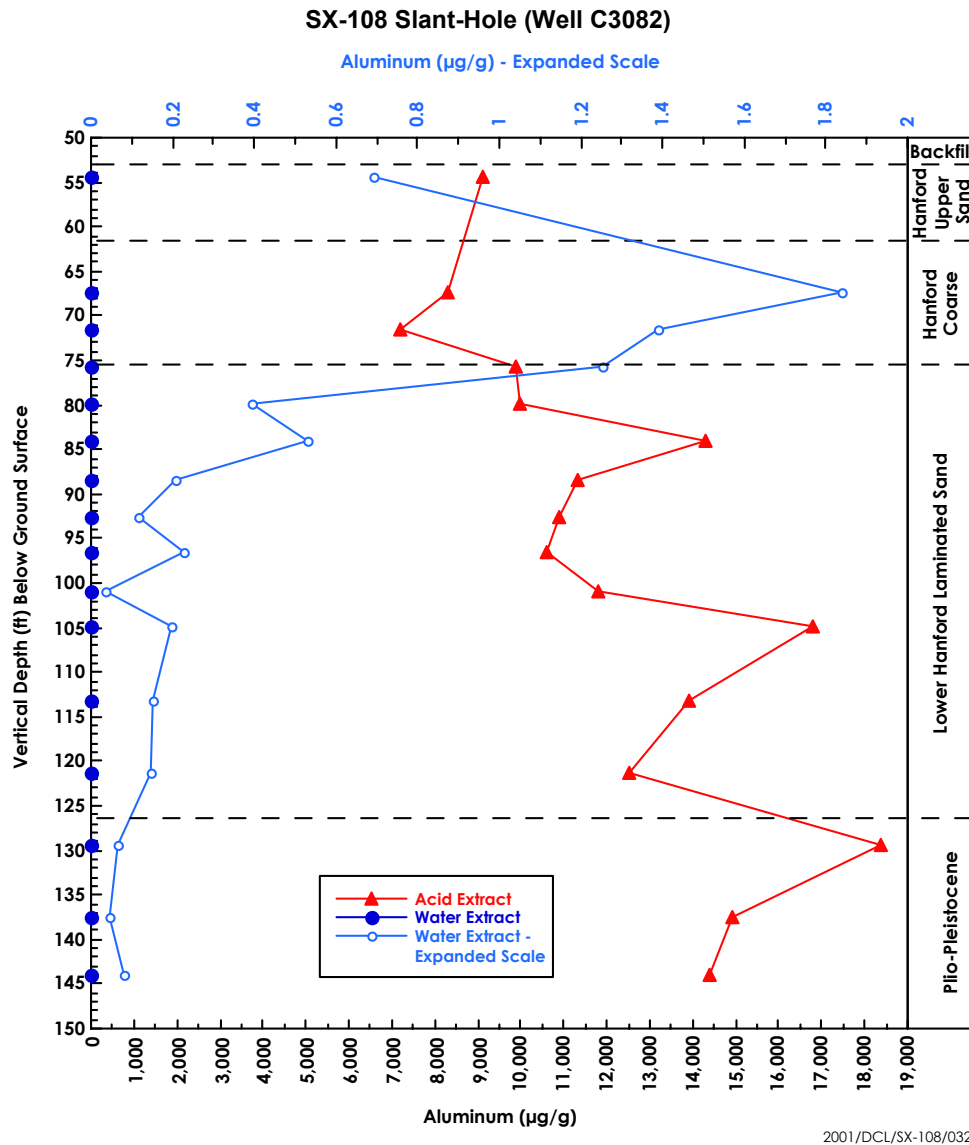


Figure C-1. Aluminum Concentrations in Acid and Water Extracts

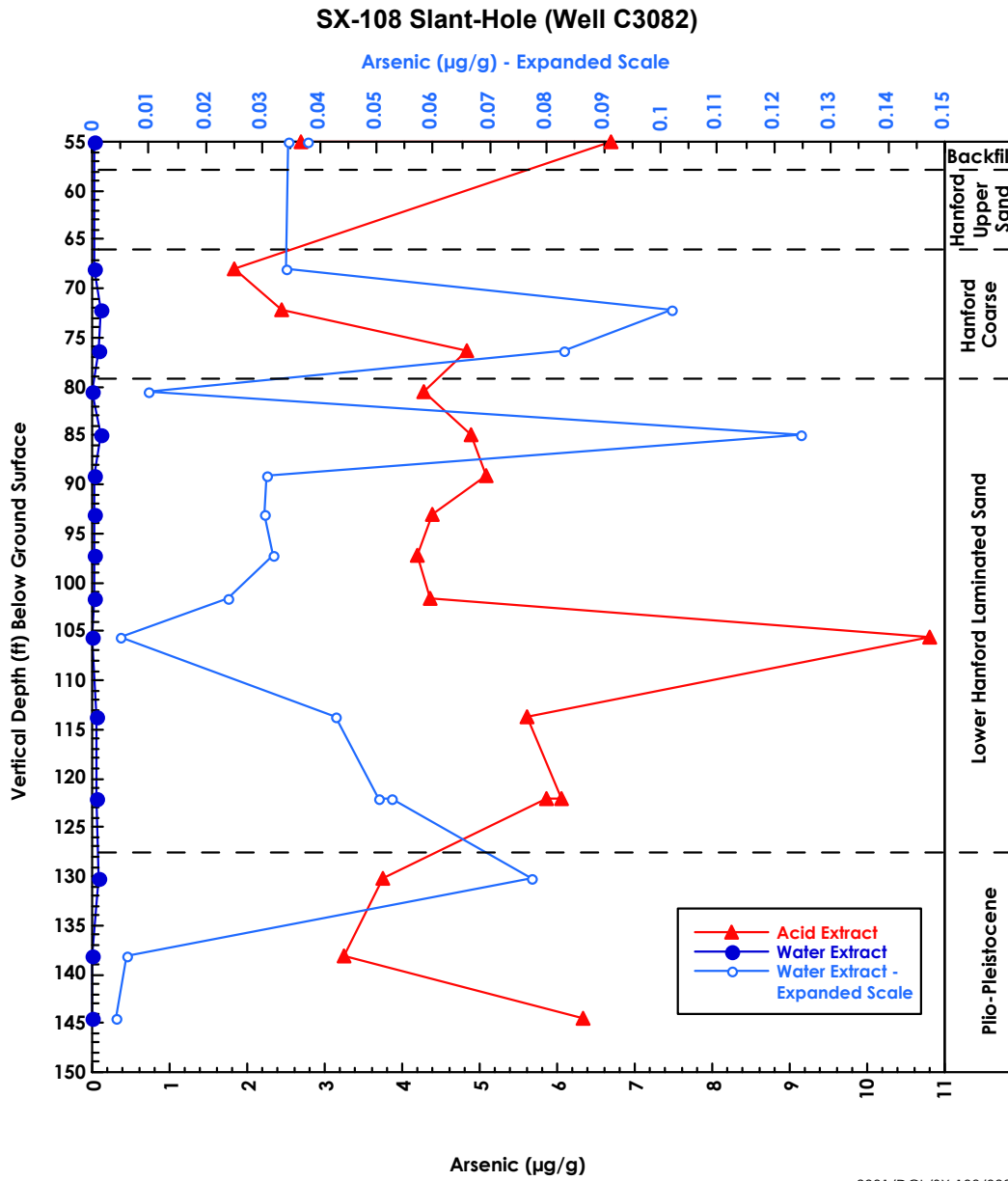
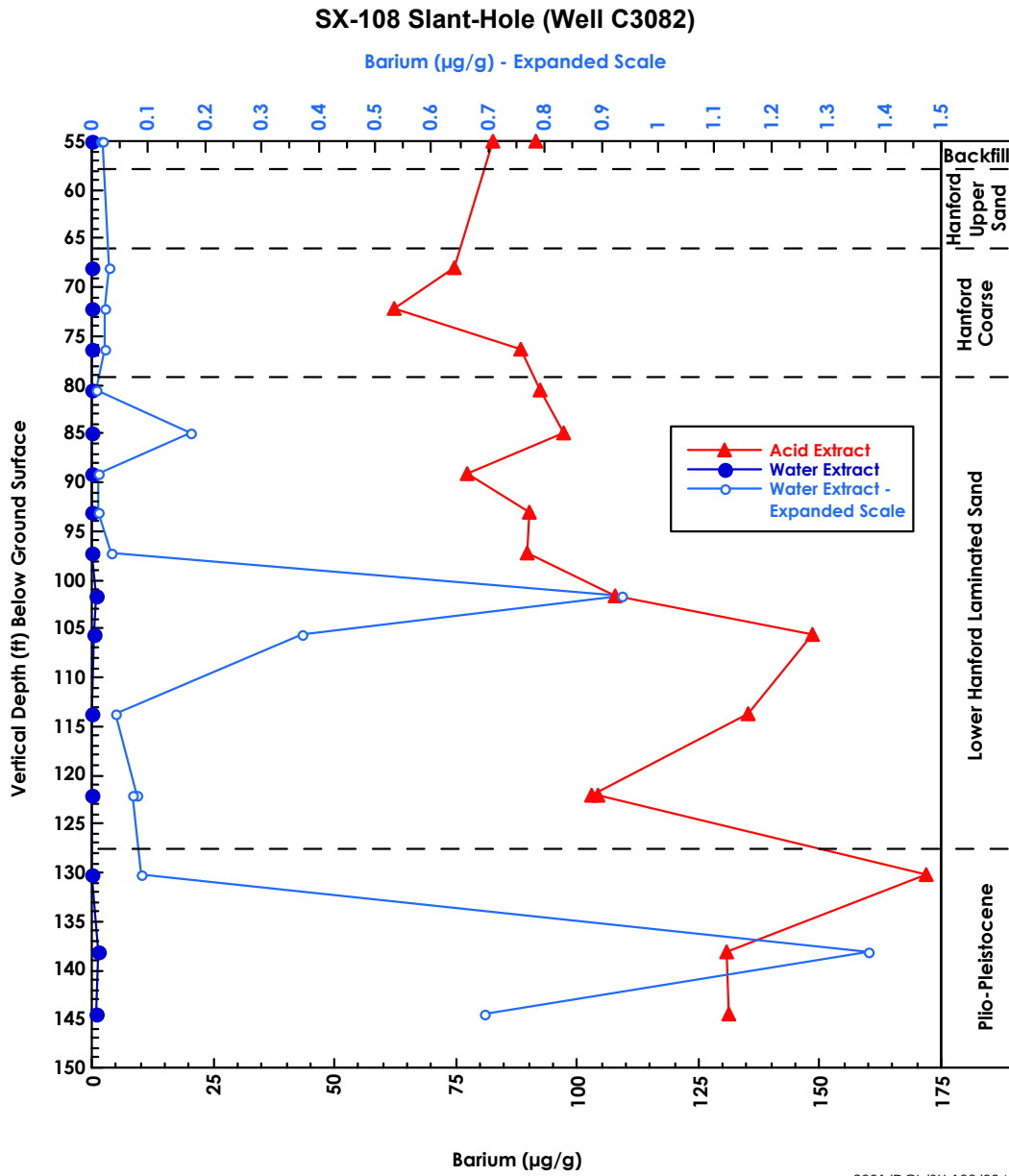


Figure C-2. Arsenic Concentrations in Acid and Water Extracts



2001/DCL/SX-108/034

Figure C-3. Barium Concentrations in Acid and Water Extracts

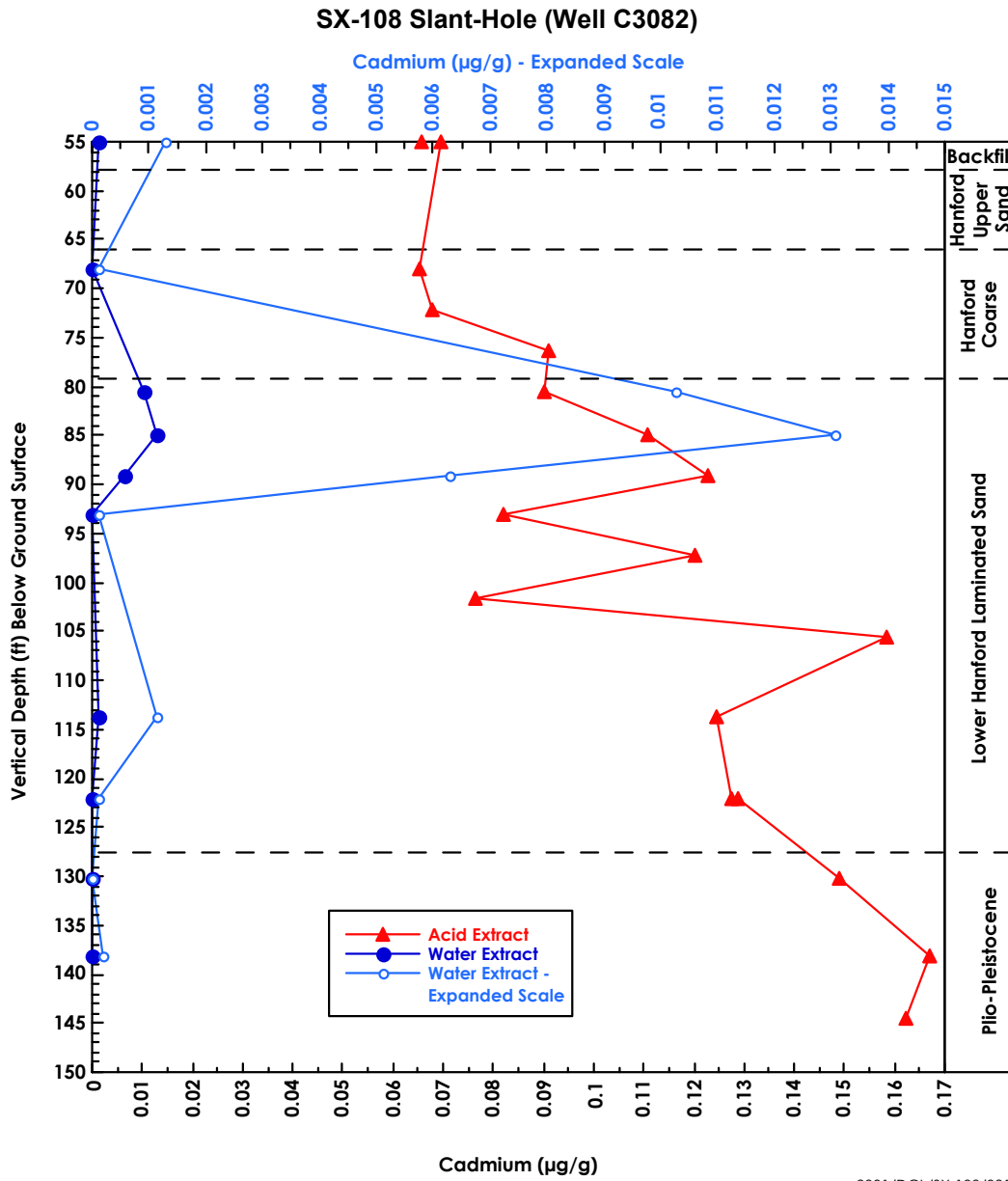


Figure C-4. Cadmium Concentrations in Acid and Water Extracts

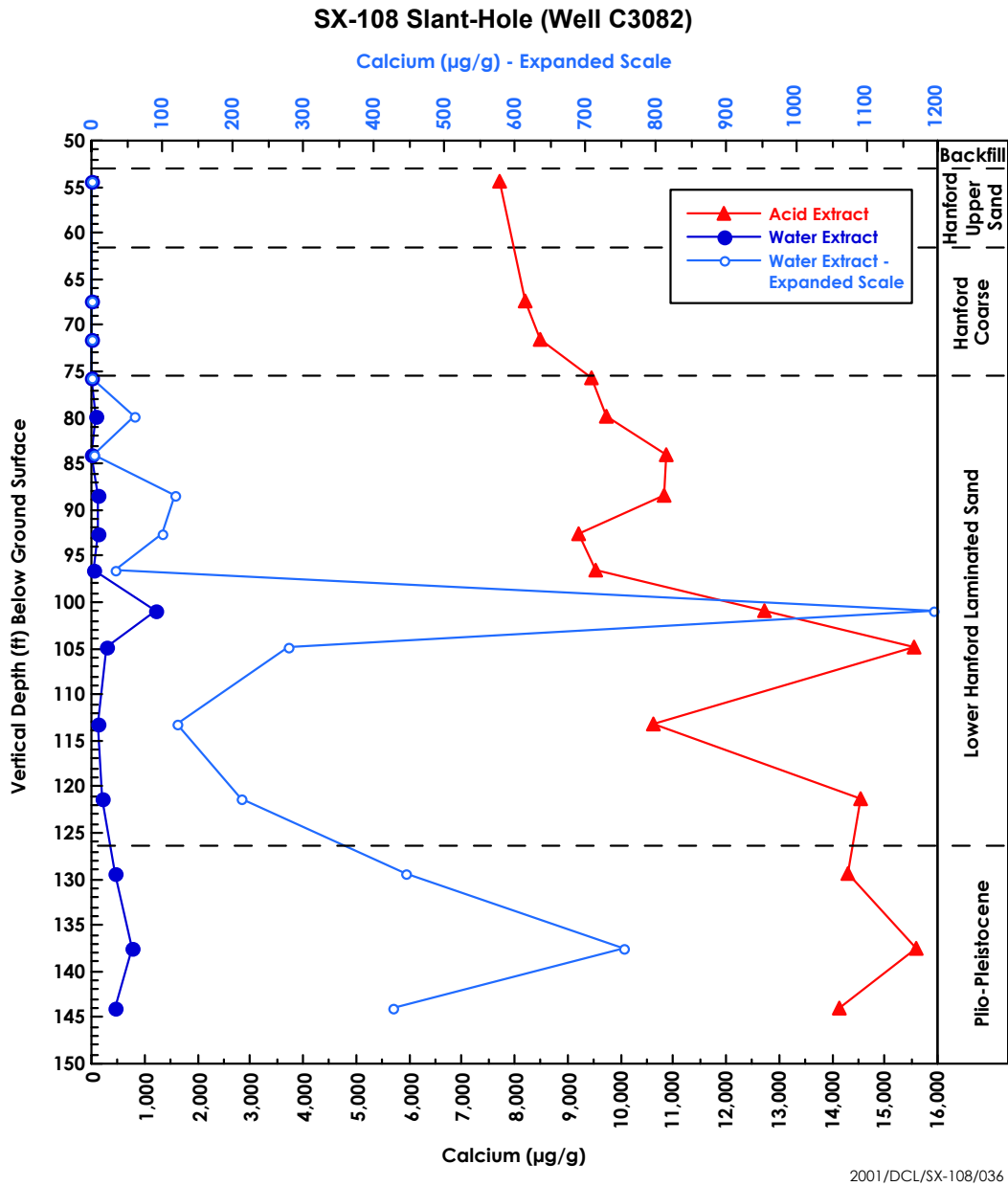


Figure C-5. Calcium Concentrations in Acid and Water Extracts

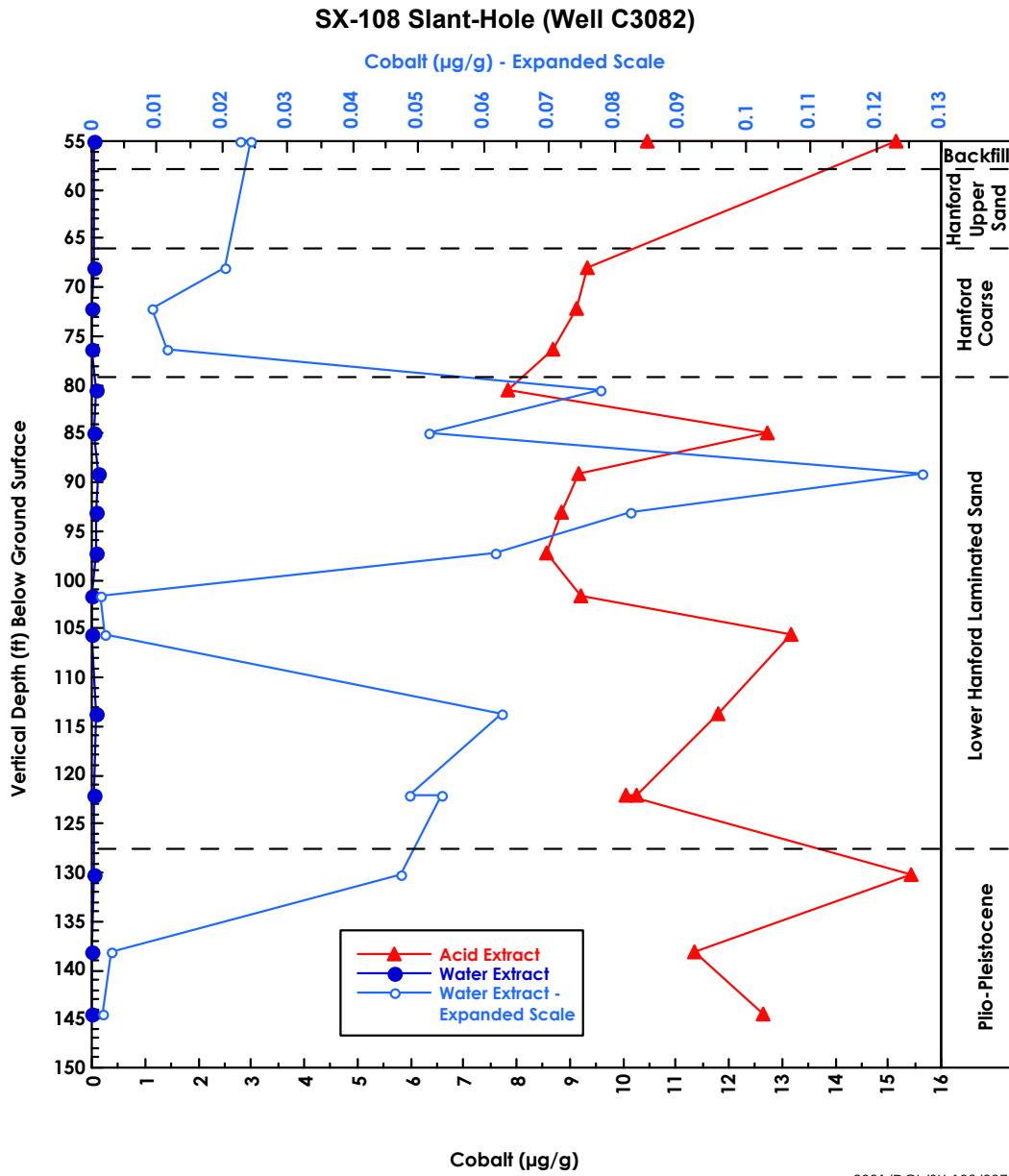


Figure C-6. Cobalt Concentrations in Acid and Water Extracts

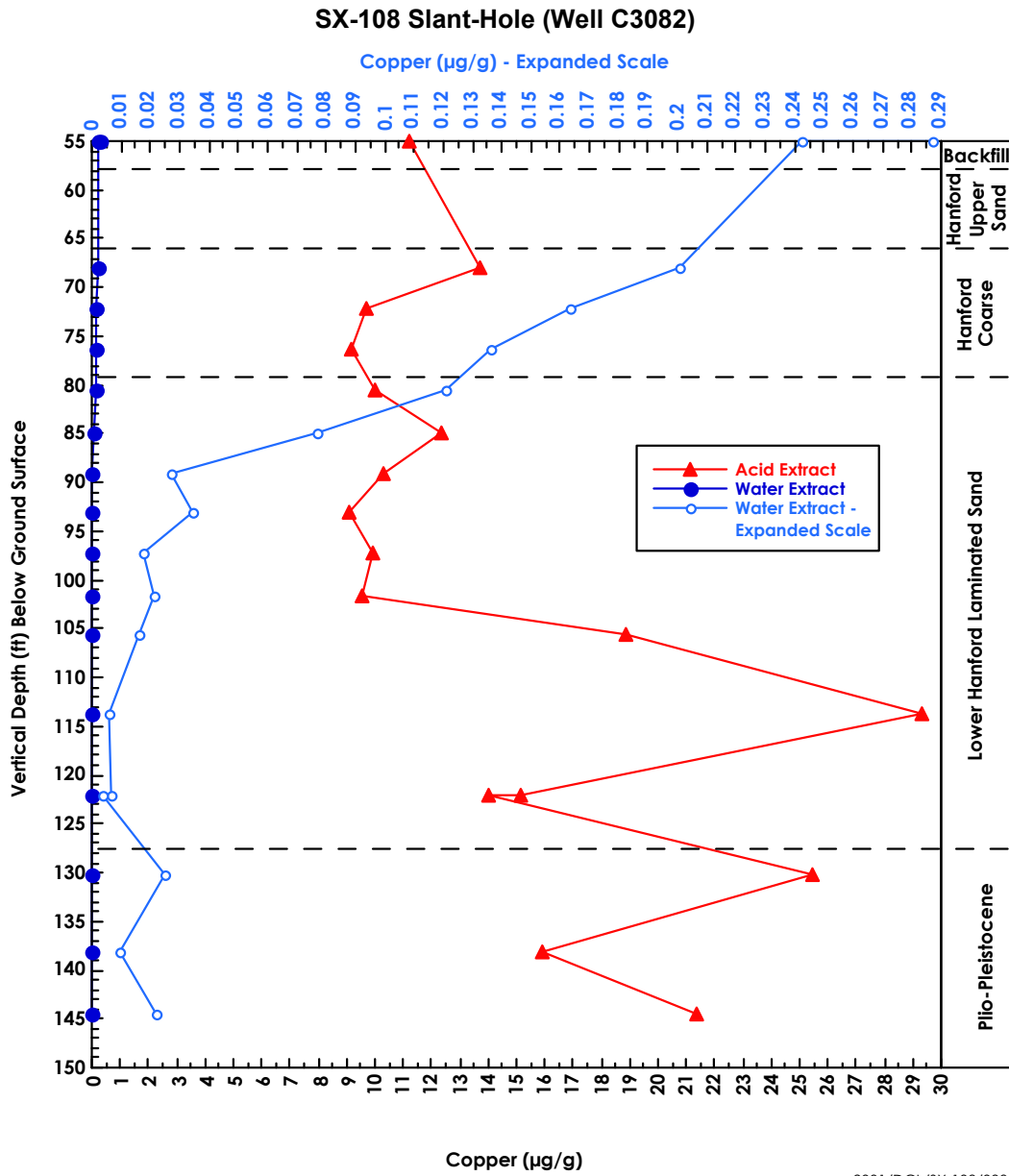


Figure C-7. Copper Concentrations in Acid and Water Extracts

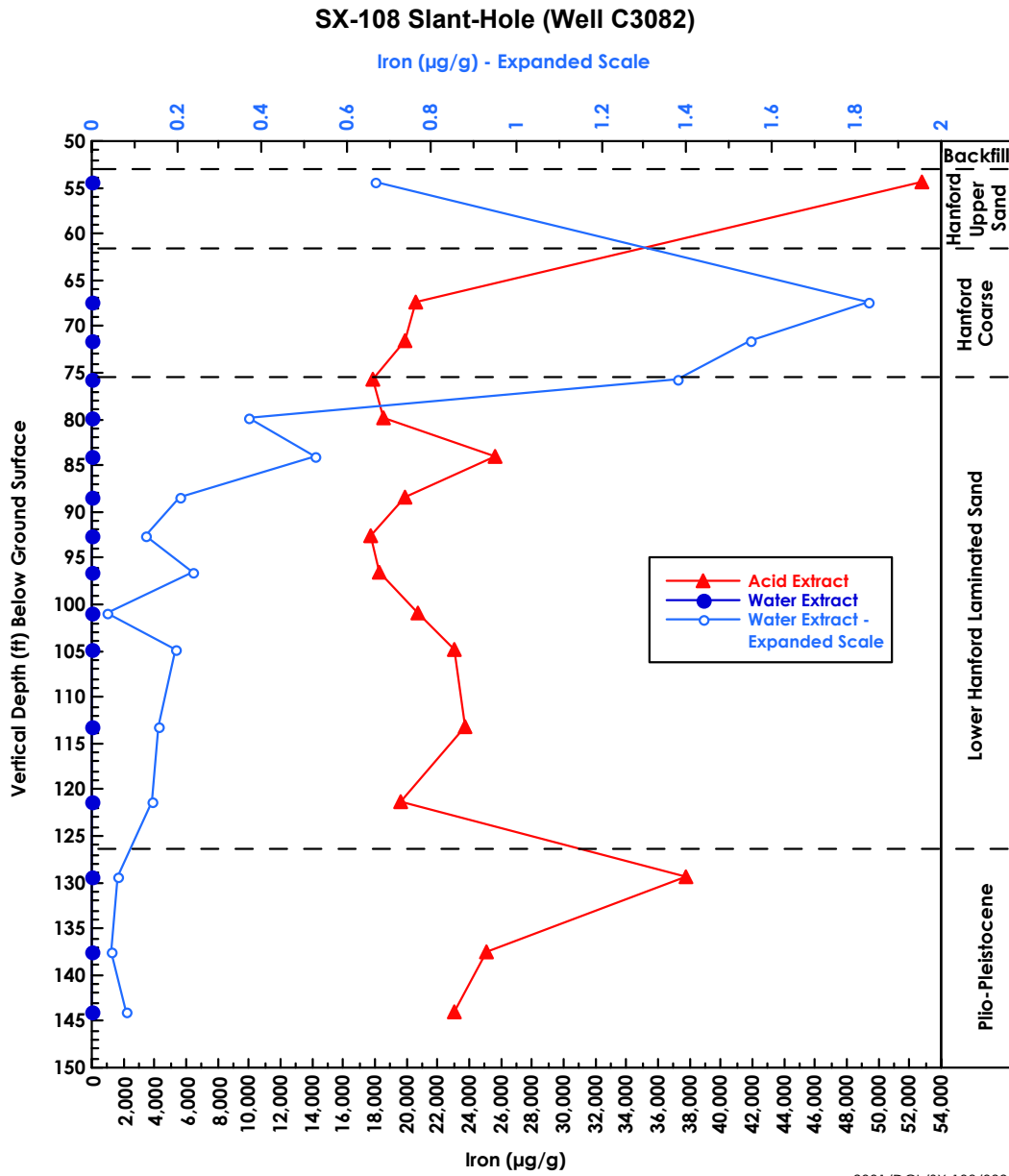
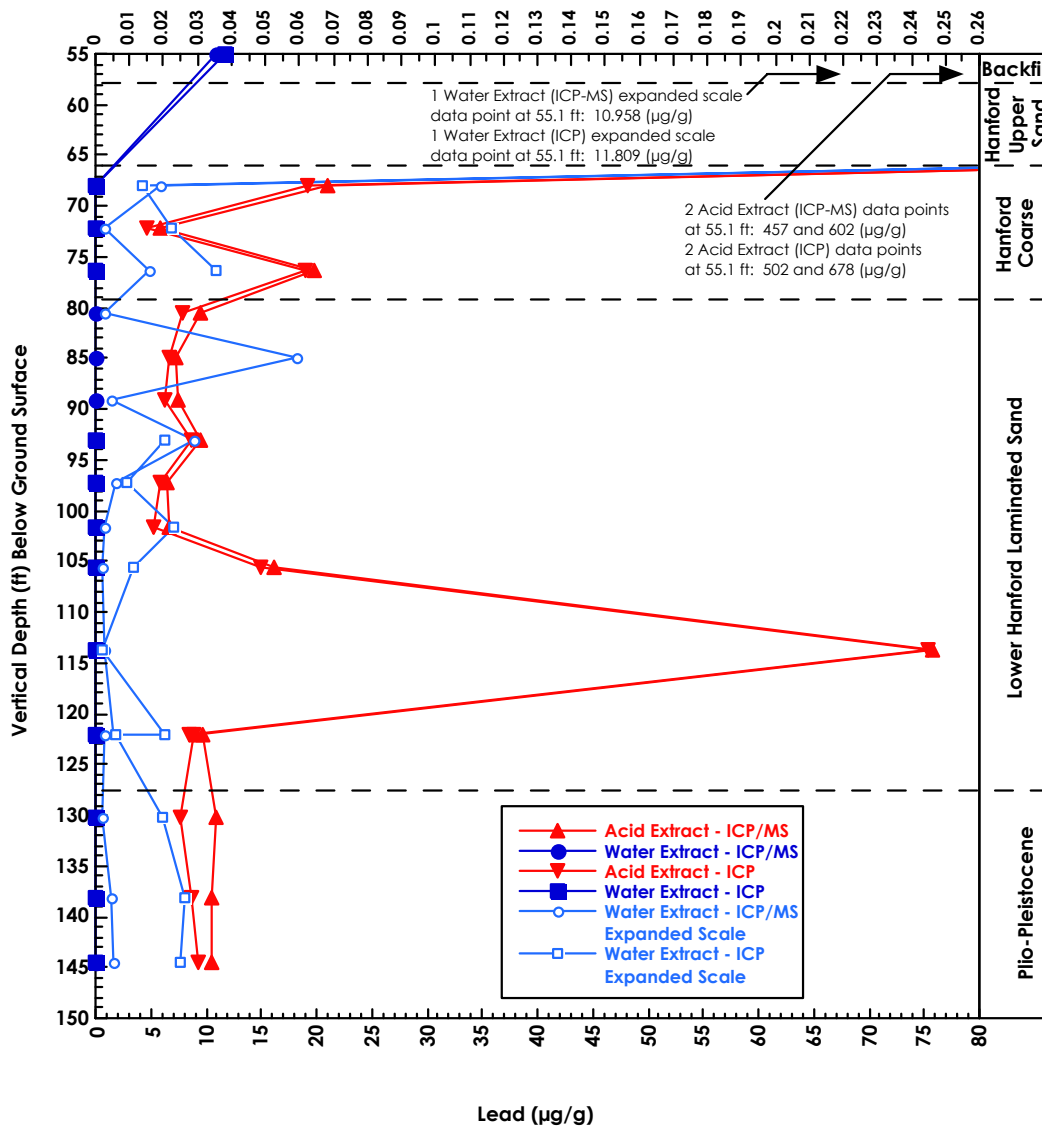


Figure C-8. Iron Concentrations in Acid and Water Extracts

SX-108 Slant-Hole (Well C3082)

Lead ($\mu\text{g/g}$) - Expanded Scale



2001/DCL/SX-108/040

Figure C-9. Lead Concentrations in Acid and Water Extracts

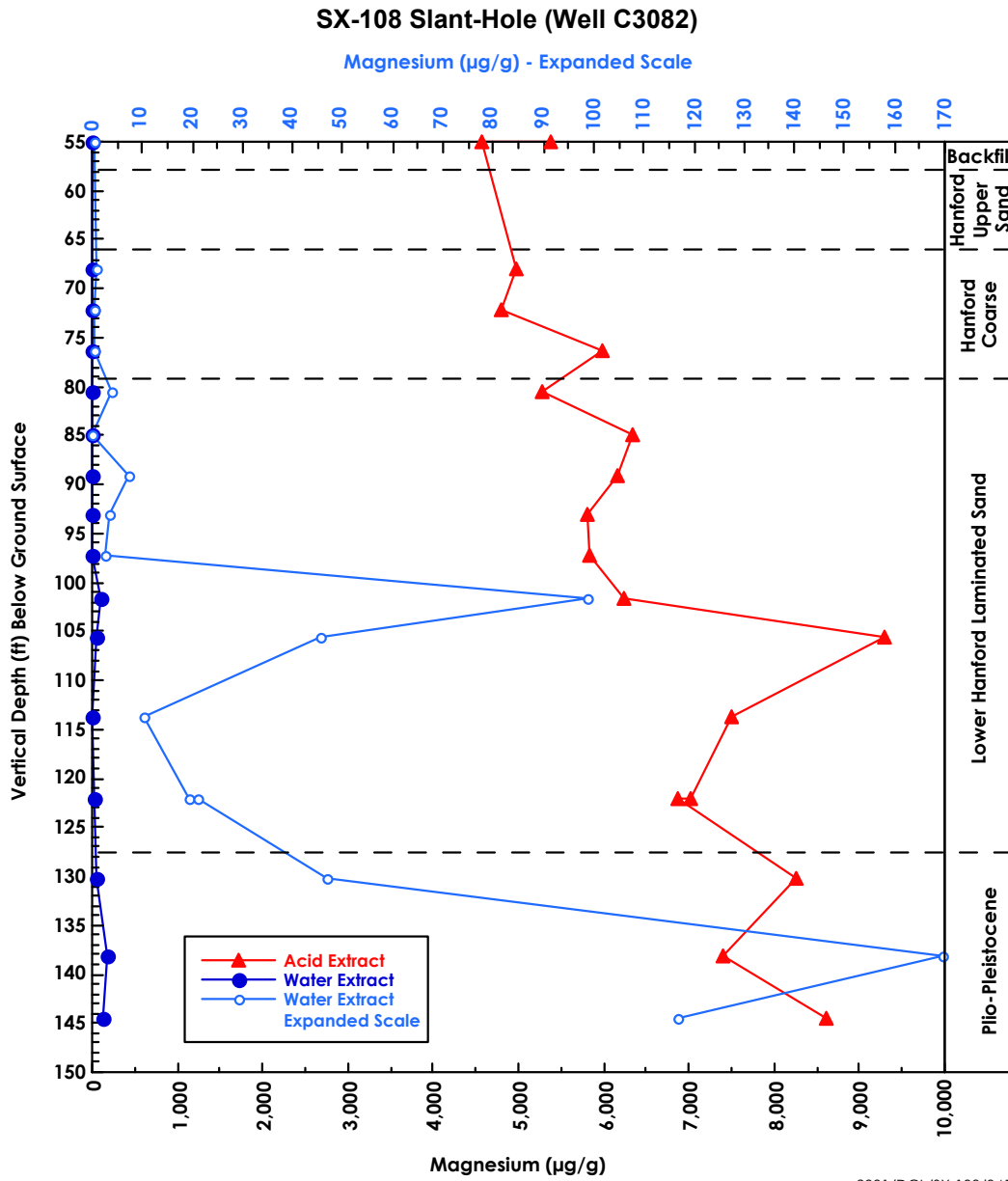


Figure C-10. Magnesium Concentrations in Acid and Water Extracts

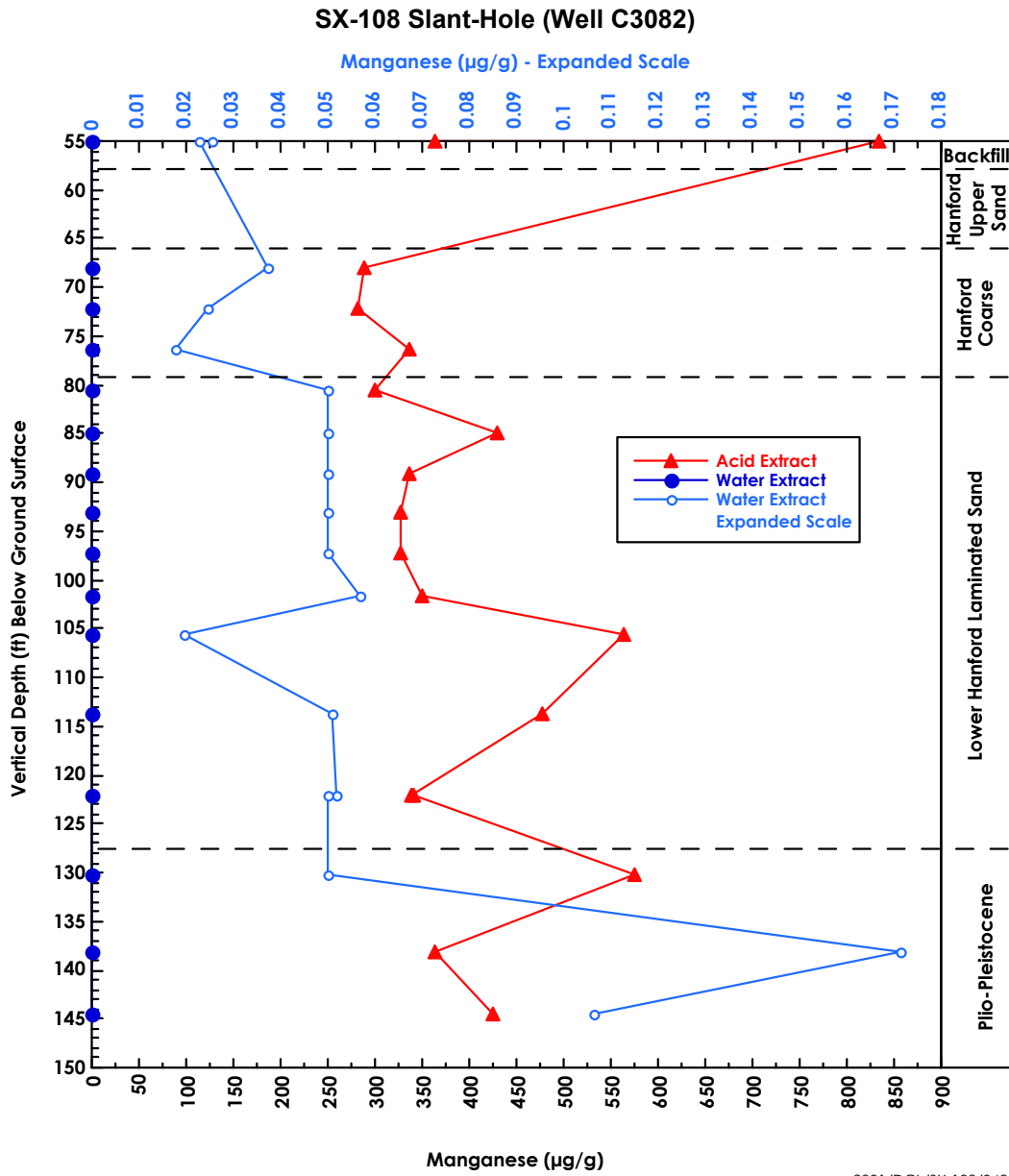


Figure C-11. Manganese Concentrations in Acid and Water Extracts

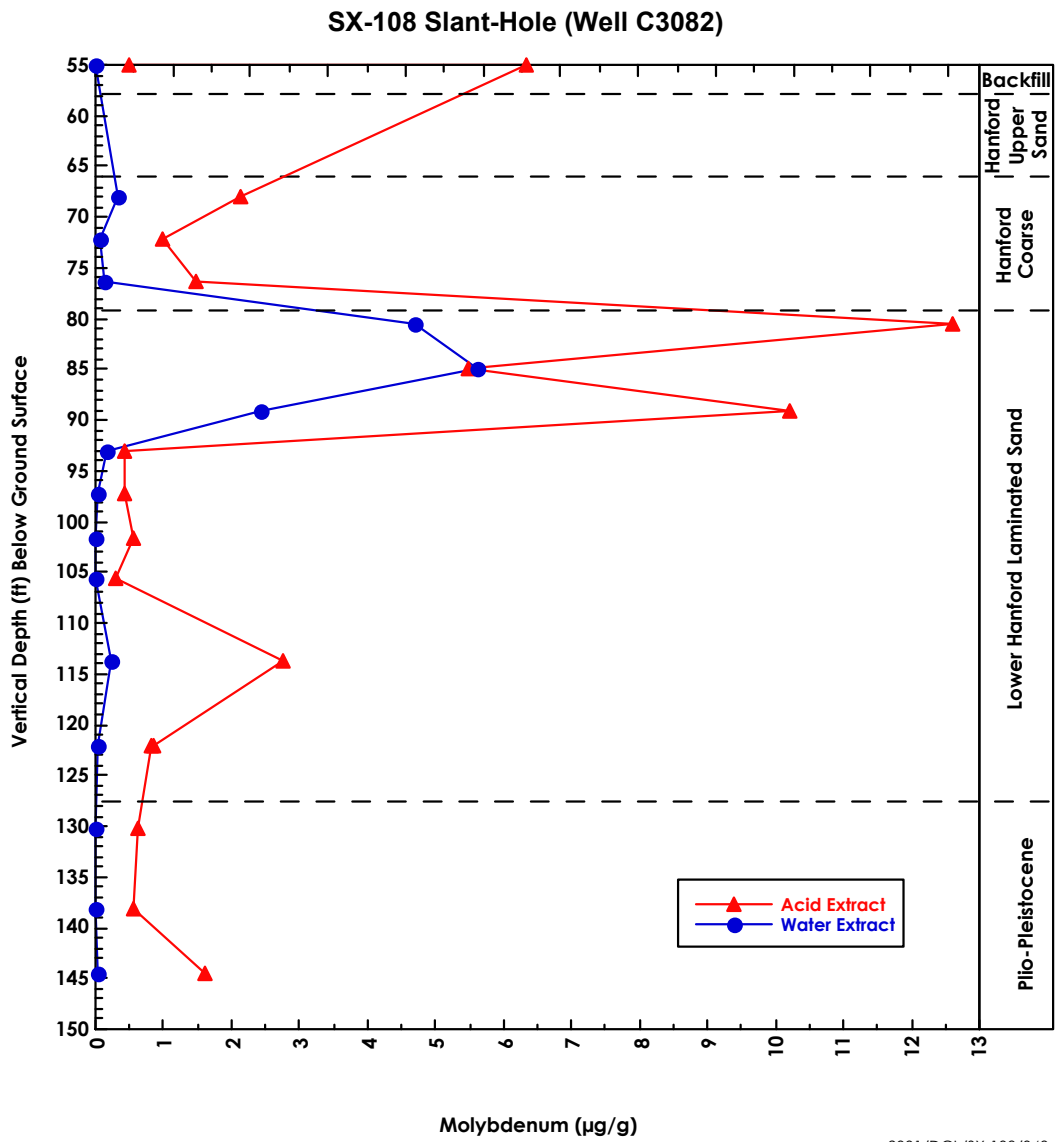


Figure C-12. Molybdenum Concentrations in Acid and Water Extracts

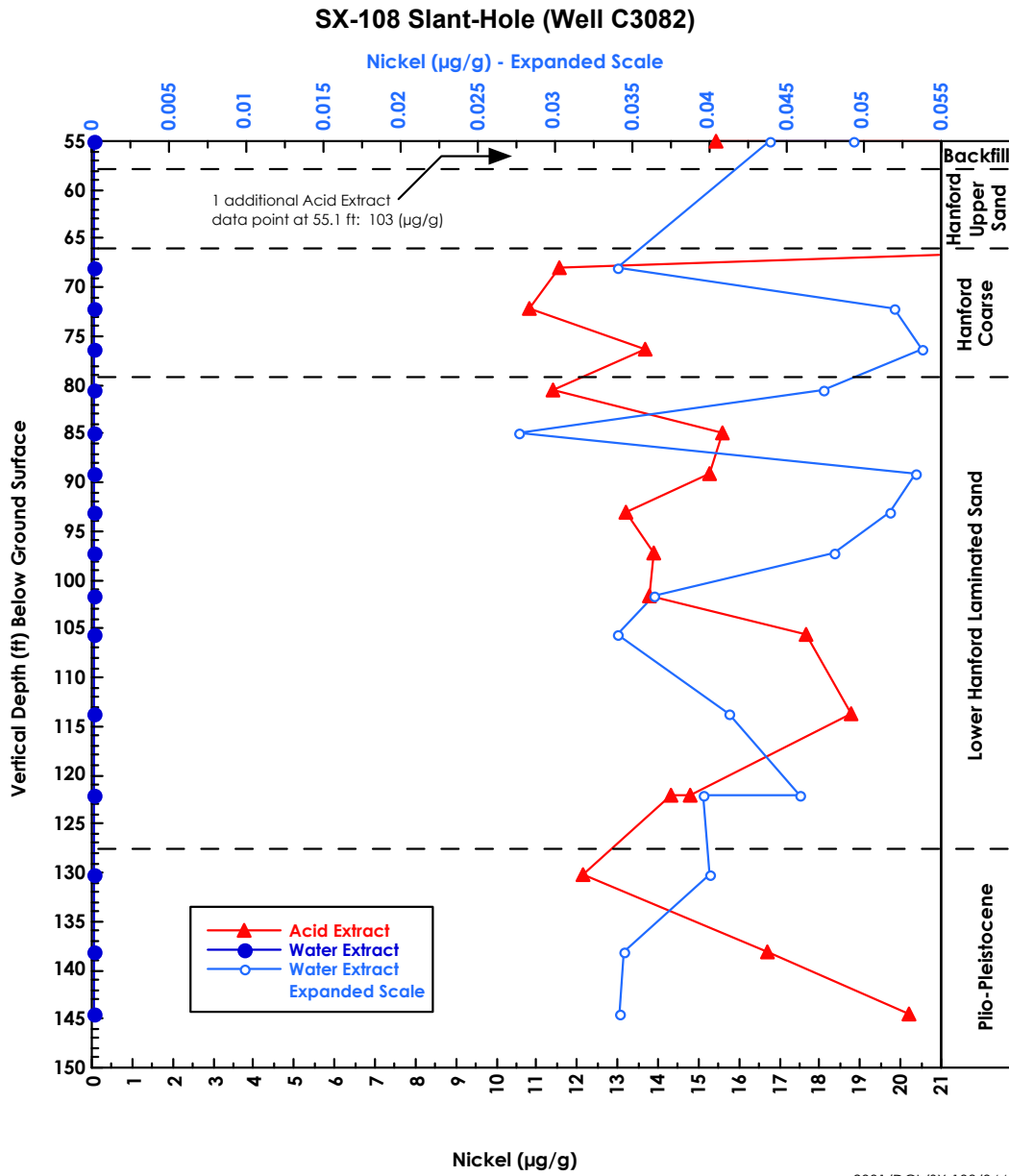
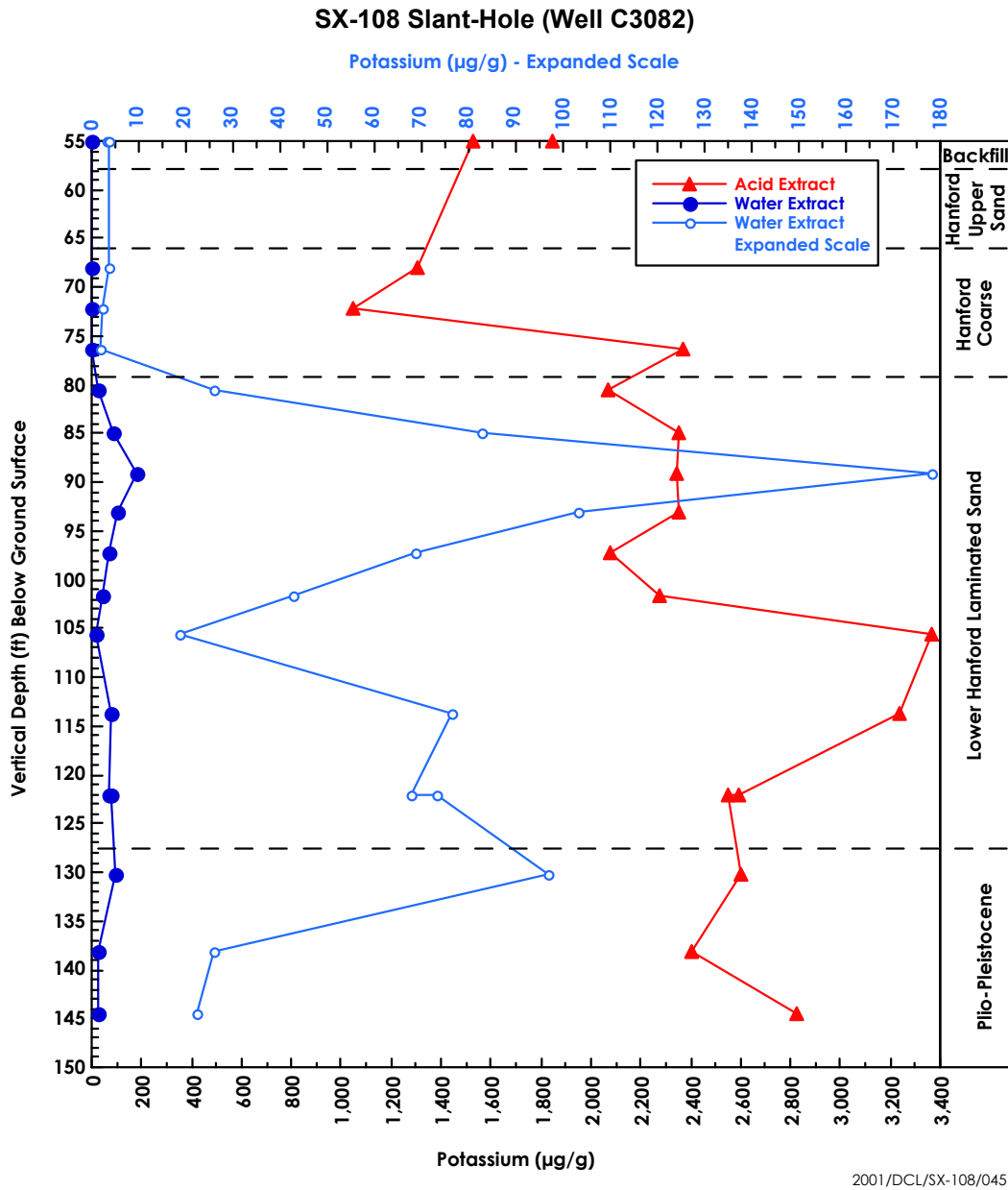
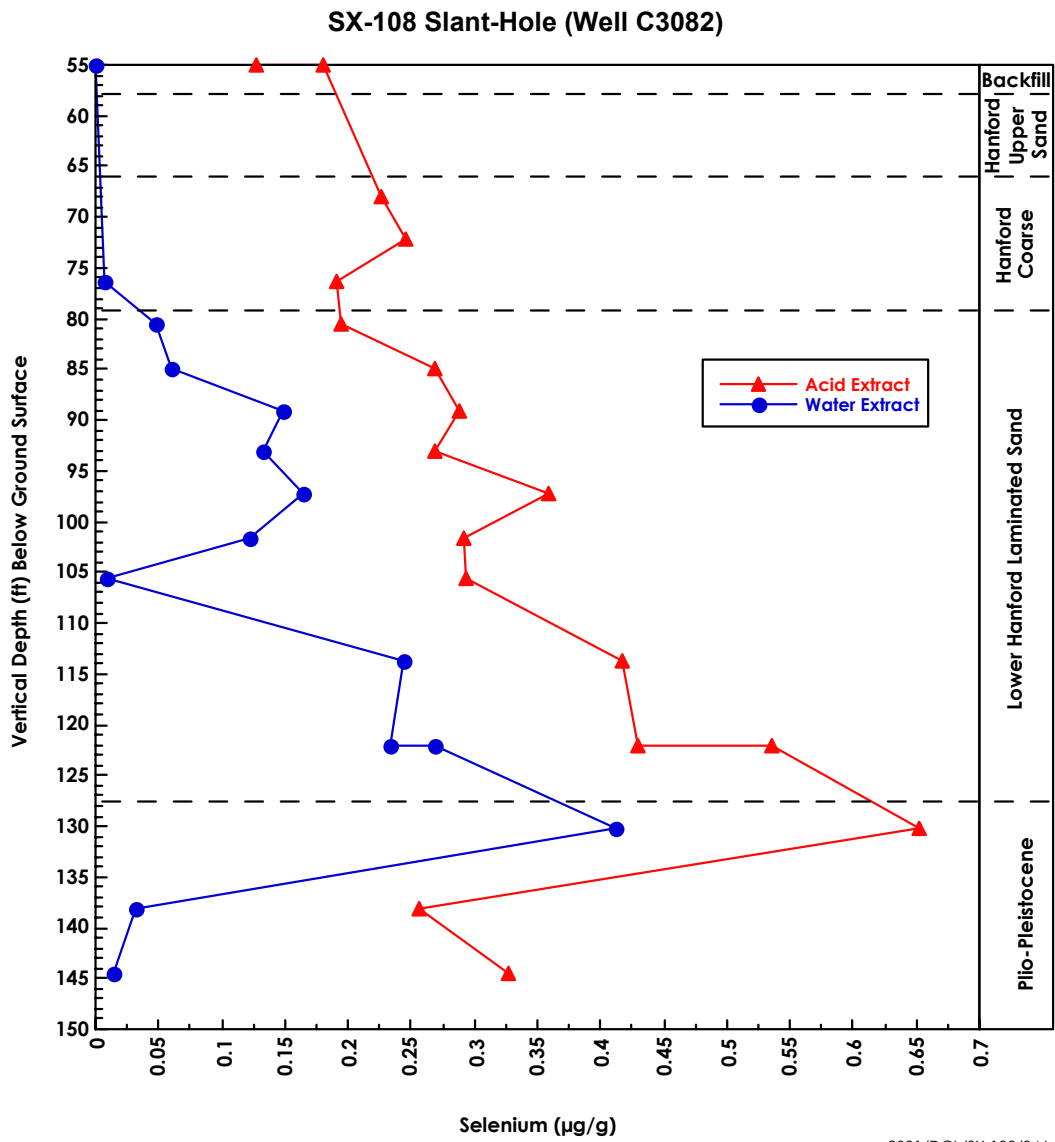


Figure C-13. Nickel Concentrations in Acid and Water Extracts





2001/DCL/SX-108/046

Figure C-15. Selenium Concentrations in Acid and Water Extracts

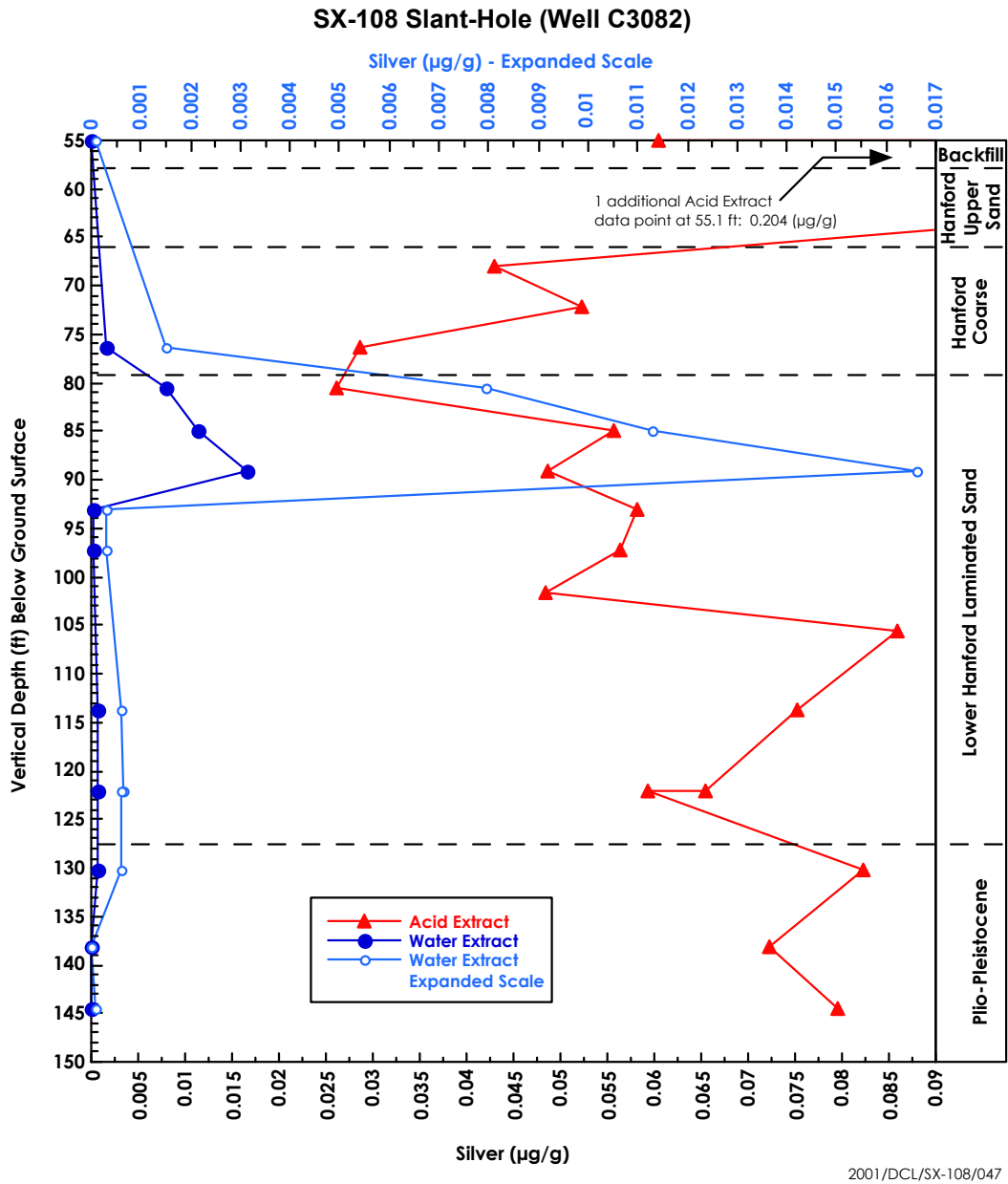
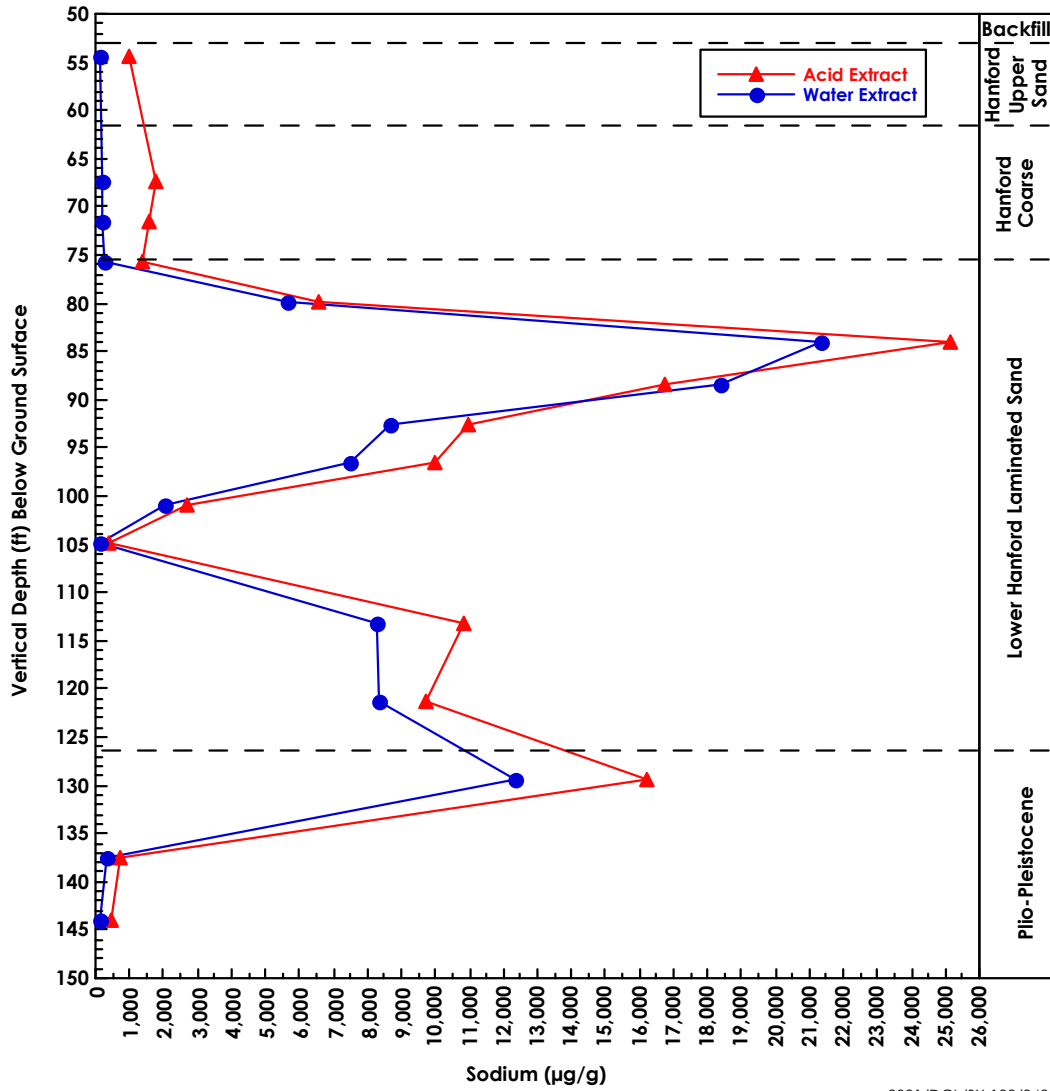


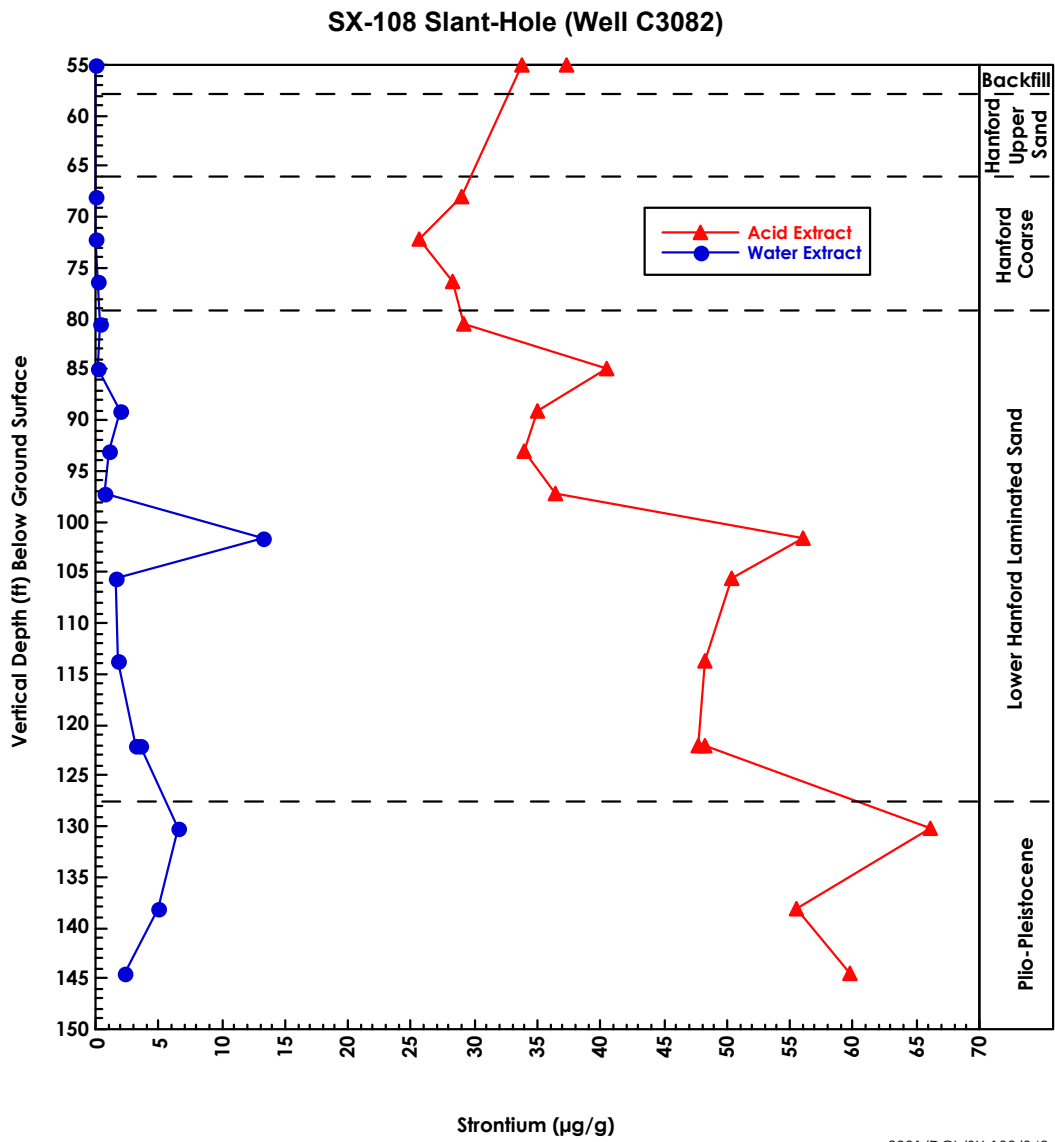
Figure C-16. Silver Concentrations in Acid and Water Extracts

SX-108 Slant-Hole (Well C3082)



2001/DCL/SX-108/048

Figure C-17. Sodium Concentrations in Acid and Water Extracts



2001/DCL/SX-108/049

Figure C-18. Strontium Concentrations in Acid and Water Extracts

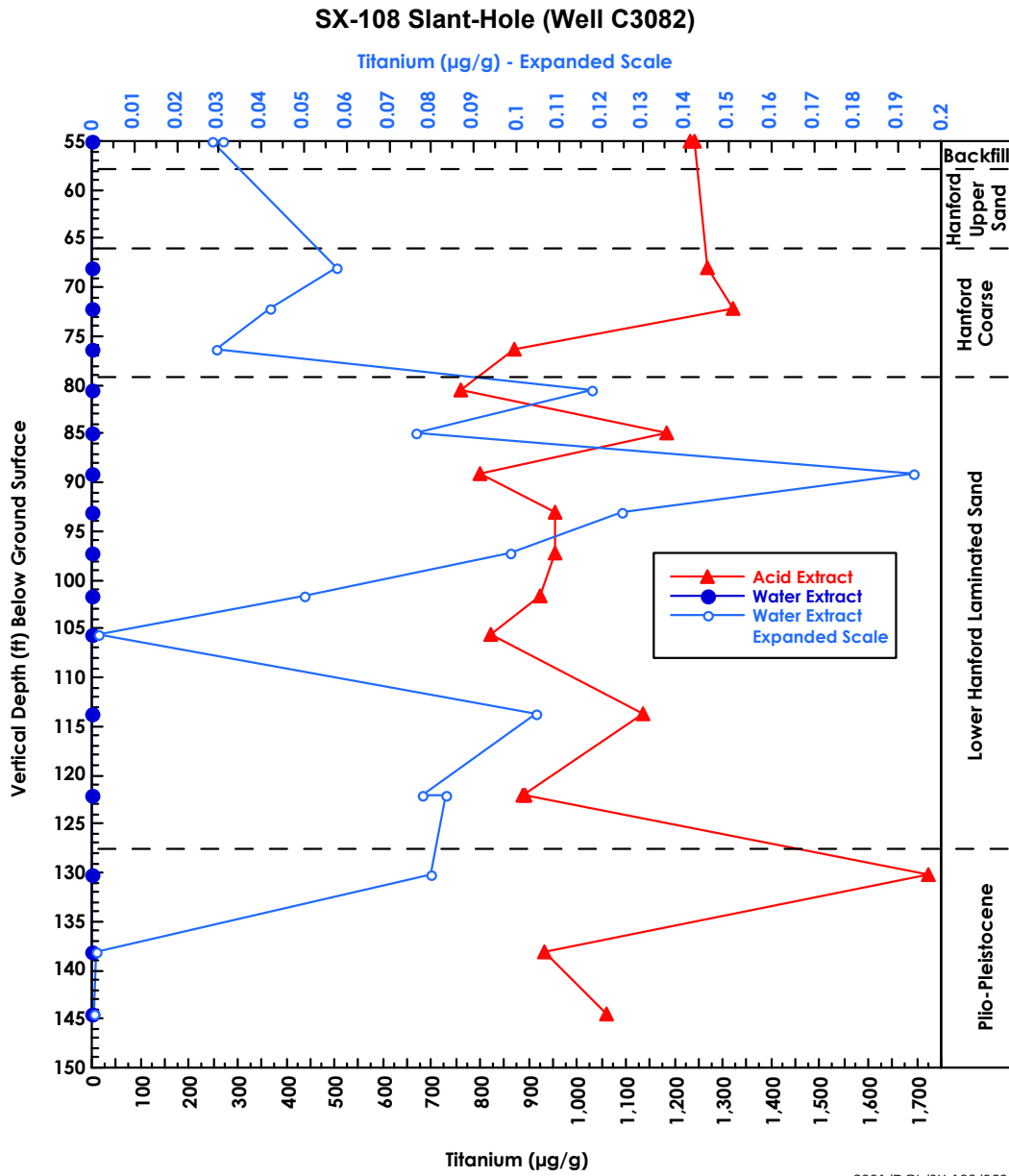


Figure C-19. Titanium Concentrations in Acid and Water Extracts

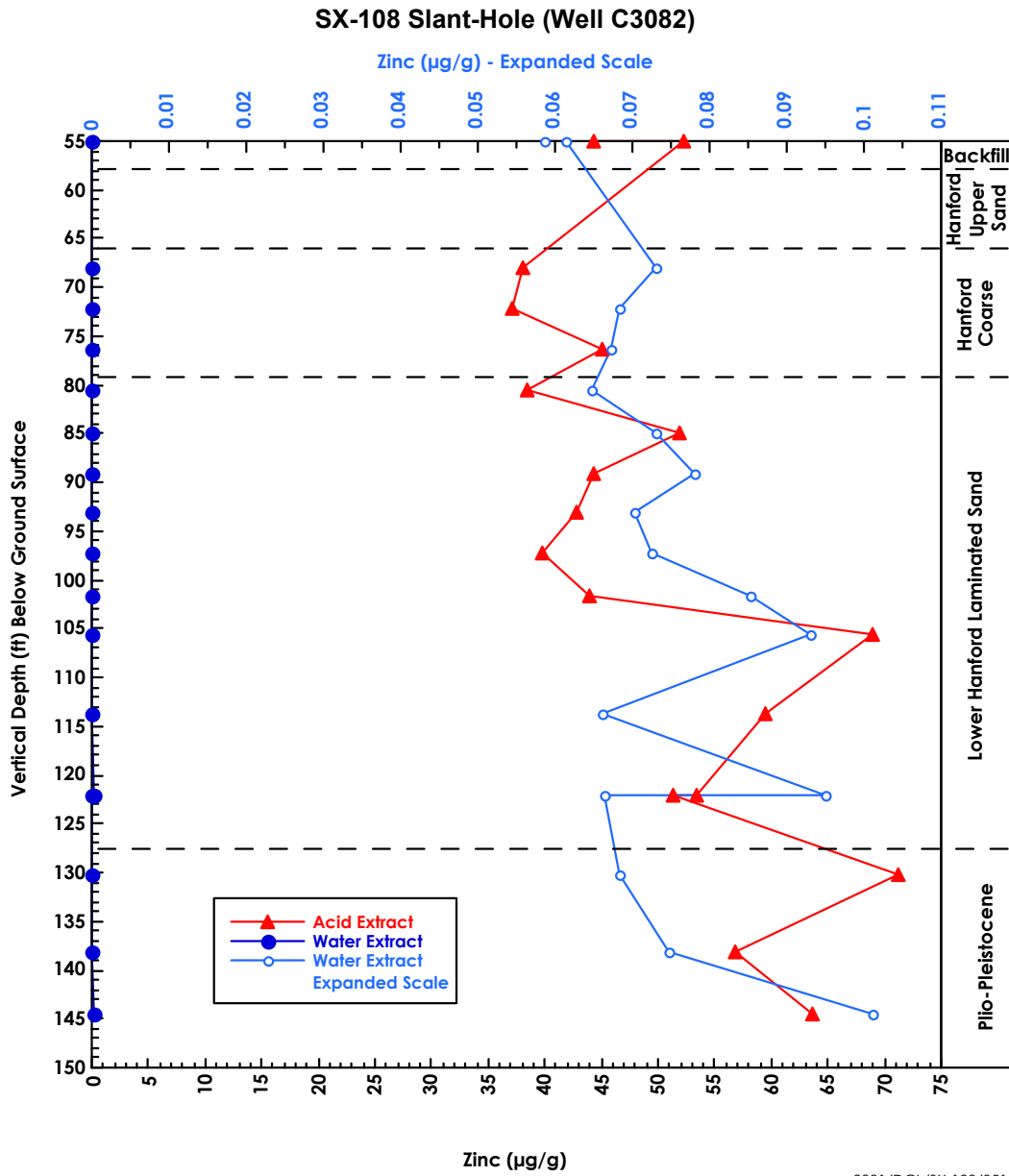


Figure C-20. Zinc Concentrations in Acid and Water Extracts

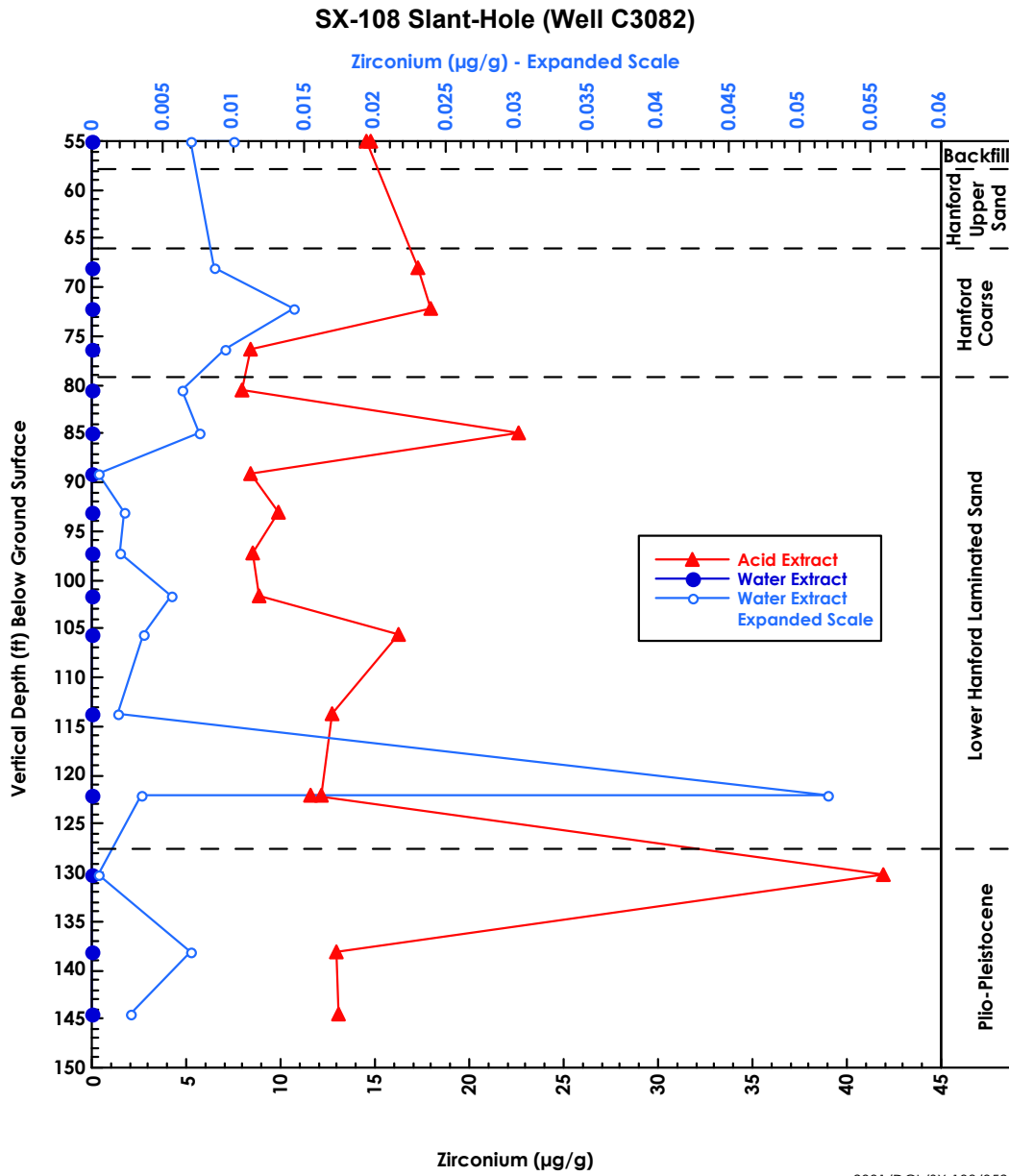
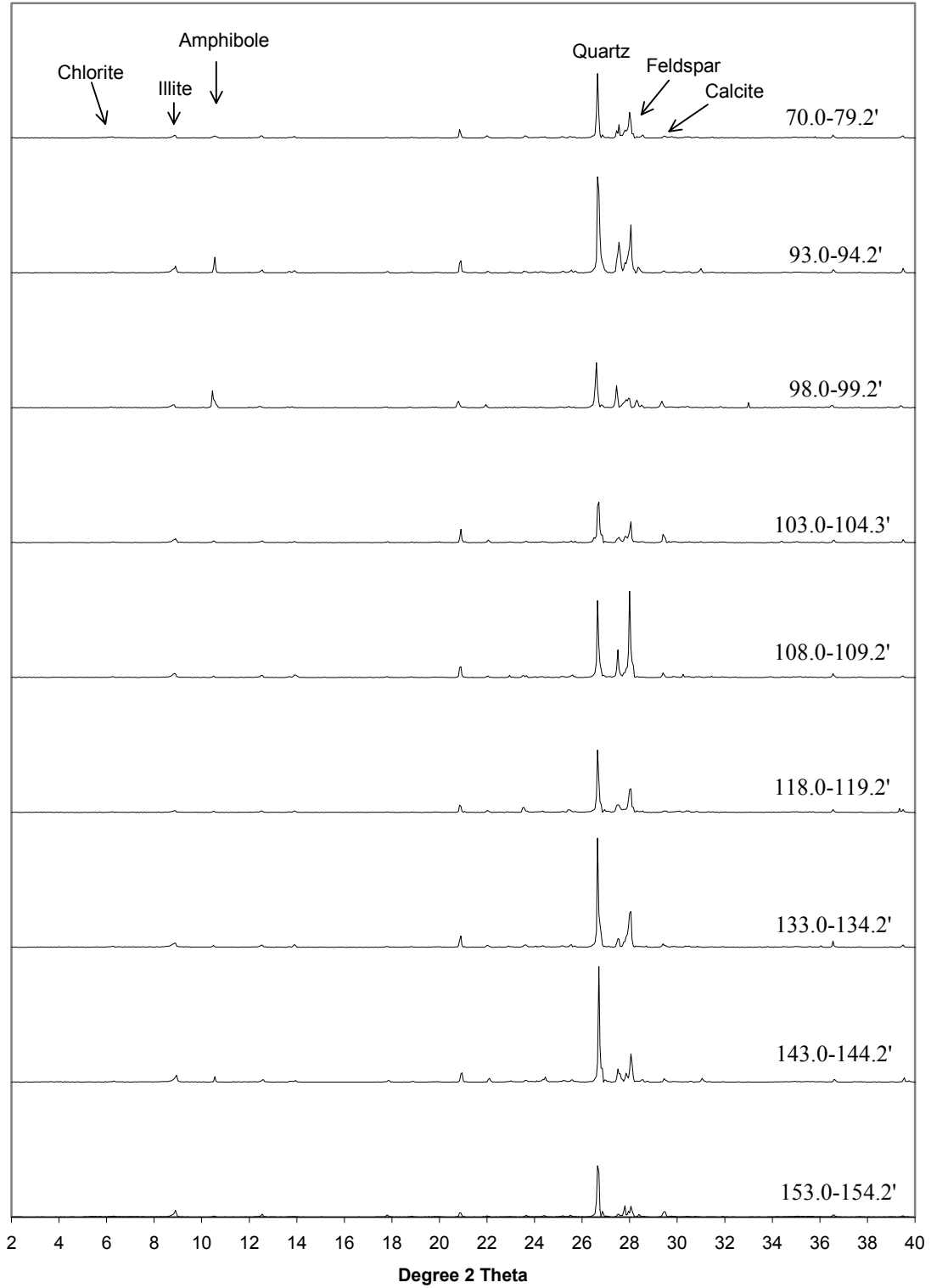


Figure C-21. Zirconium Concentrations in Acid and Water Extracts

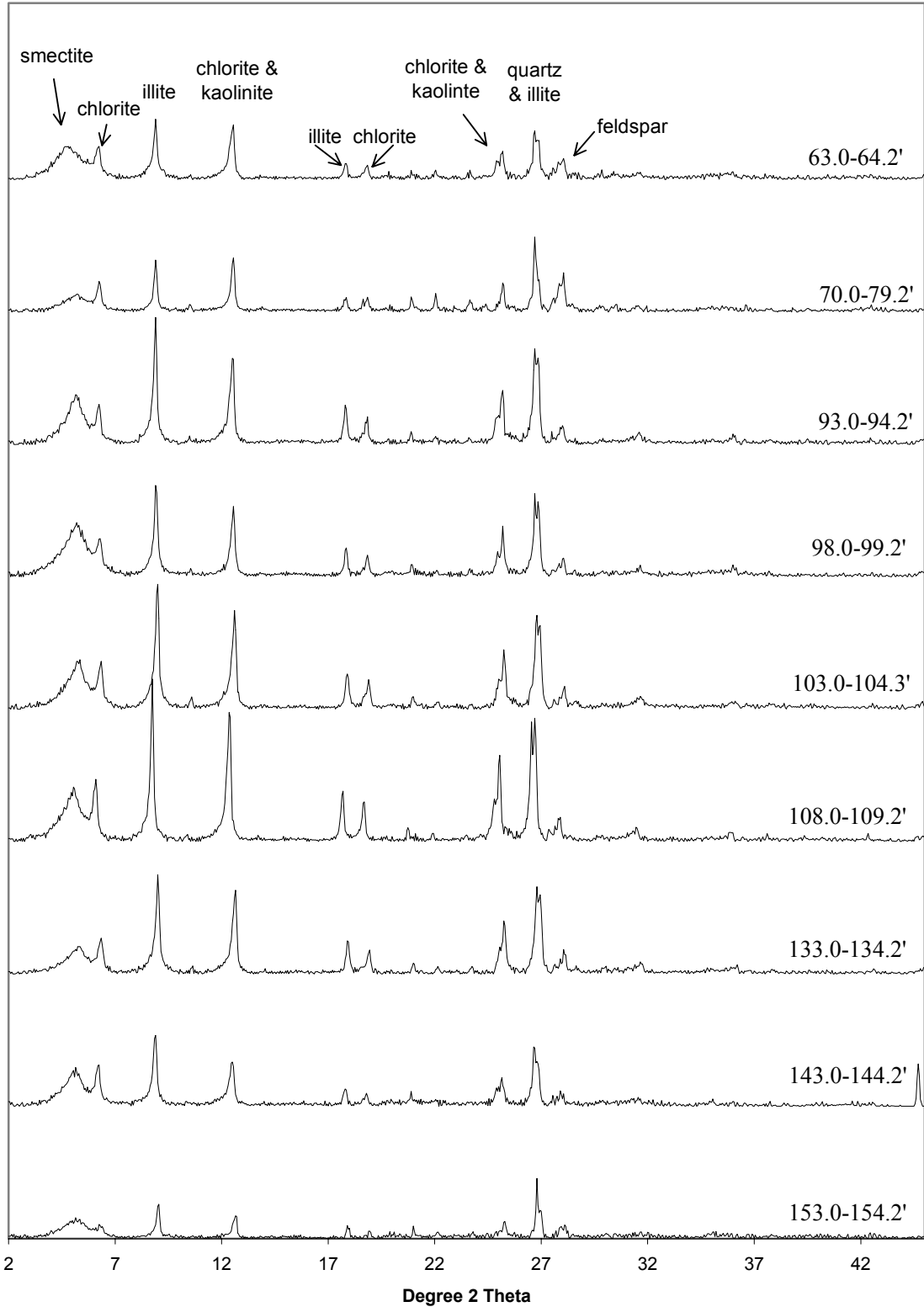
Appendix D

X-Ray Diffraction Patterns for Selected Core Samples

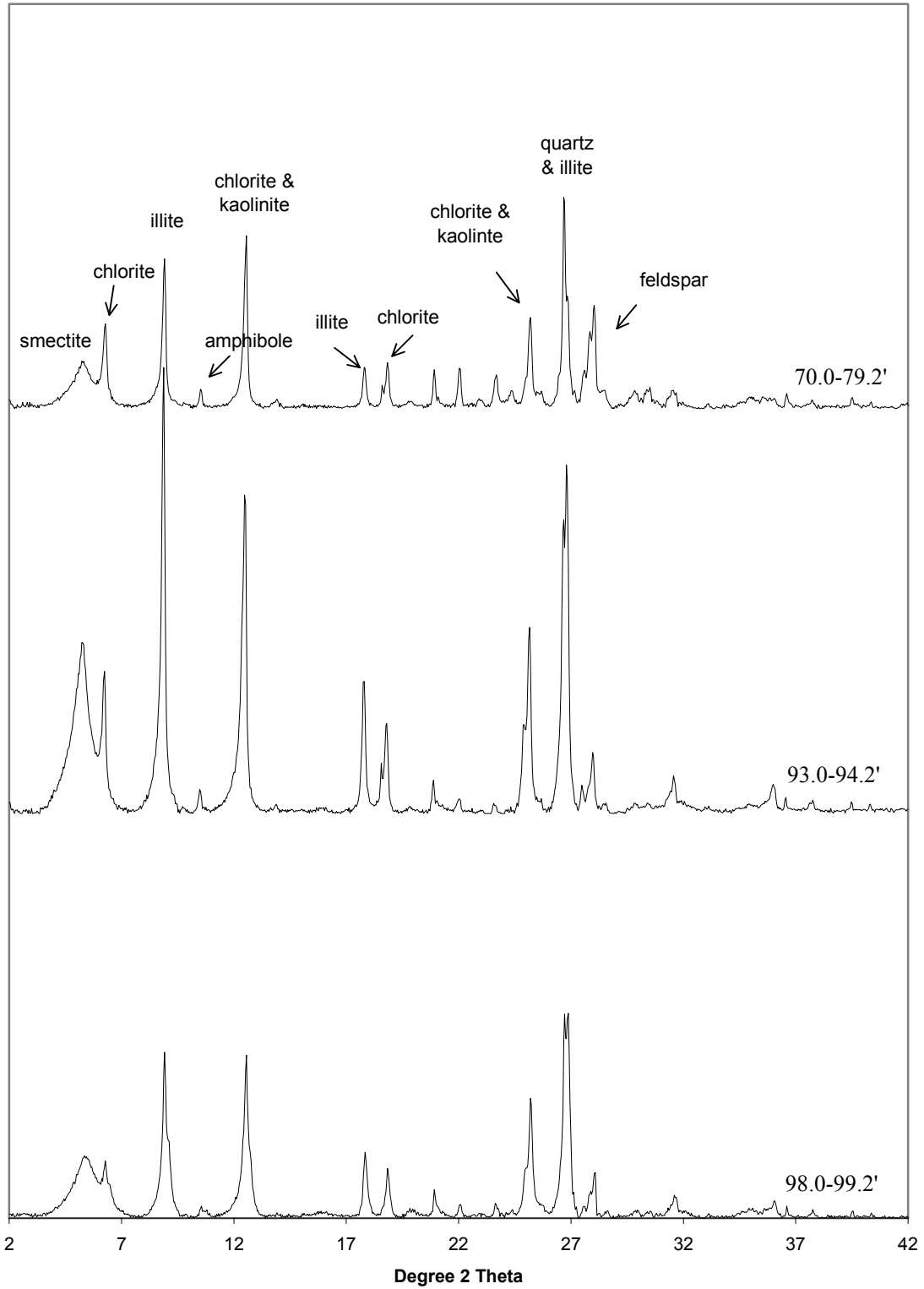
XRD Patterns of Bulk Samples From Slant Borehole
(Random Orientation Mount)



XRD Patterns of Clays From Slant Borehole
(Ca-saturated, Ethylene Glycol Solvated)



XRD Patterns of Clays From Slant Borehole
(Ca-saturated, Ethylene Glycol Solvated, 6 Hour Scan)



Distribution

<u>No. of Copies</u>		<u>No. of Copies</u>	
ONSITE			<u>Pacific Northwest National Laboratory</u>
	<u>CH2M HILL Hanford Group, Inc.</u>		R. Jeff Serne (50 CD) K6-81
			Clark W. Lindenmeier P8-37
	Anthony J. Knepp (10 CD) H0-22		George V. Last K6-81
	Fredrick M. Mann H0-22		Bruce N. Bjornstad K6-81
			Duane G. Horton K6-81
	<u>U.S. Department of Energy</u>		H. Todd Schaefer K6-81
	Robert M. Yasek H6-60		
	<u>U.S. Department of Ecology</u>		
	Joseph Caggiano B5-18		

1 hard copy and 1 CD except as noted.